A FEEDFORWARD/FEEDBACK APPROACH TO RETRIEVAL OF A TETHERED SUB-SATELLITE

by

Eric J. FLEURISSON

Ingénieur de l'Ecole Nationale Supèrieure de l'Aéronautique et de l'Espace (Sup'Aéro)
(1989)
Diplome d'Etudes Approfondies d'Automatique, Informatique et Traitement du Signal
(1989)

SUBMITTED IN PARTIAL FULFILLMENT OF
THE REQUIREMENTS FOR THE DEGREE OF

MASTER OF SCIENCE
IN AERONAUTICS AND ASTRONAUTICS

at the

MASSACHUSETTS INSTITUTE OF TECHNOLOGY

August 1990

Signature of Author _____
Department of Aeronautics and Astronautics
August, 1990

Certified by _____
Professor Andreas H. von Flotow
Thesis Supervisor

Accepted by _____
Professor Harold Y. Wachman
Chairman, Departmental Graduate Committee

A Feedforward/Feedback Approach to Retrieval of a Tethered Sub-satellite

By

Eric J. Fleurisson

Submitted to the Department of Aeronautics and Astronautics in August 1990
in partial fulfillment of the requirements for
the Degree of Master of Science in Aeronautics and Astronautics
Massachusetts Institute of Technology, Cambridge, Mass. 02139

ABSTRACT

This study presents a feedforward control scheme to retrieve a Tethered Sub-satellite System (TSS) consisting of the space shuttle and a tethered sub-satellite. An optimal retrieval trajectory is computed by determining the length acceleration history which minimizes final pitch angle, pitch rate at docking and total retrieval time. The minimization of such a cost leads to a bang-bang control which respects the positive tension constraint. A sub-optimal retrieval strategy is then developed in order to retrieve the tethered sub-satellite for all initial conditions.

The retrieval dynamics of the TSS are unstable and open loop retrieval by itself is not reasonably practical. Consequently, an LQG loop structure is designed which combines feedforward information with thruster augmented feedback stabilization. The thrusters mounted on the sub-satellite are used to stabilize the in-plane and out-of-plane dynamics along the optimal trajectory instead of along some arbitrary retrieval path. An extended Kalman filter is implemented in the loop in order to retain the non-linear nature of the dynamics in the estimation of the pitch rate and the filtering of sensor noise and thruster granularity effects.

This whole design ensures a total retrieval time included in the interval [.57 .91] orbits and a minimization of the fuel consumption compared with the previous methods, while the final docking conditions and tension constraints are met.

Thesis Supervisor: Andreas H. von Flotow
Associate Professor, Department of Aeronautics and Astronautics

To my Parents,

for their continuous support in my engineering studies.

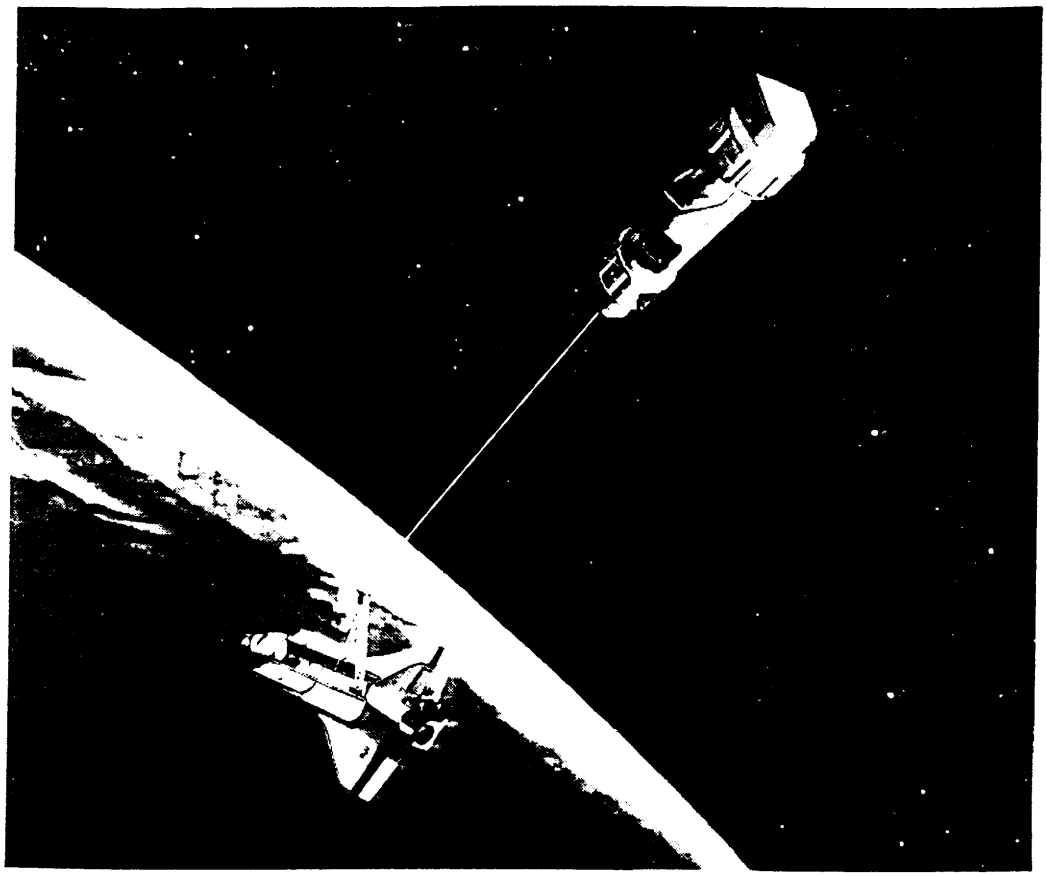

ACKNOWLEDGEMENTS

The author would like to thank Professor Andreas H. von Flotow who succeeded in making him forget about Draper Lab., if only for the duration of this project, by giving him the opportunity to work in a very challenging environment.

In addition, special thanks go to Ralf and Burt Swanson for welcoming the author to Massachusetts and for their great understanding, and to the Rotary International Foundation which made this year at MIT possible.

The author also wishes to express his sincere thanks to Mathieu Marcadal for his willingness to share his scientific expertise, and to Darryll Pines and Dave Vos for their constant support and guidance.

Finally, the author wishes not to forget "le petit blond", the inconsolable softball coach and his wife, and "l'aventurier", for their patience and support outside MIT.

TABLE OF CONTENTS

Abstract 2

Acknowledgements 5

Introduction 8

Chapter 1: The Retrieval of a Tethered Sub-satellite System, Problem Statement 10
- 1.1 The Tethered Sub-satellite System, (TSS) 10
  - 1.1.1 The Mission 10
  - 1.1.2 A Description of the System 12
- 1.2 An Overview of Previous Work 14
- 1.3 A New Approach: A Feedforward/Feedback Scheme 16

Chapter 2: Optimal Retrieval Trajectory Design 18
- 2.1 Formulation of the Optimal Control Problem 18
  - 2.1.1 The Pitch and Tether Dynamics 18
  - 2.1.2 Formulation of the Optimization Problem 23
- 2.2 Hamiltonian Analysis 24
- 2.3 Analysis of the Retrieval Dynamics, Limitations 26
  - 2.3.1 Phase Plan Analysis 26
  - 2.3.2 Investigation of the Cost Function 33
- 2.4 Numerical Solution 36
  - 2.4.1 Investigation of the Optimization Problem under Inequality Constraint 36
  - 2.4.2 The Bang-bang Solution 38
    - 2.4.2.1 Choice of the Limits of The Control 38
    - 2.4.2.2 A First Order Gradient Algorithm 39
  - 2.4.3 Numerical Results 41
  - 2.4.4 The Reduced Optimal Problem 45
    - 2.4.4.1 One Parameter Optimization 45
    - 2.4.4.2 Sensitivity Issue 49
- 2.5 A Proposed Sub-Optimal Retrieval Scheme 54
  - 2.5.1 Analysis 54
  - 2.5.2 Retrieval Scheme Statement 56
  - 2.5.3 Example of Retrieval 58

2.6 Conclusion and Future Work 60

Chapter 3: A Feedforward/Feedback Design 62
3.1 The Feedforward/Feedback Loop Structure 62
3.1.1 Introduction 62
3.1.2 The Actuators 63
3.1.3 The Sensors 64
3.1.4 The Specifications 65
3.1.5 The Closed Loop Structure 66
3.2 The System Analysis 68
3.2.1 Linearization 68
3.2.2 The Open Loop Dynamics 72
3.2.2.1 Open Loop Poles 72
3.2.2.2 Observability, Controllability, Modal Decomposition 76
3.2.2.3 Frequency Domain, Singular Value Decomposition 79
3.3 The Feedback Design 83
3.3.1 A Decoupling of Controls 83
3.3.1.1 The Pitch Dynamics 84
3.3.1.2 The Length Dynamics 85
3.3.1.3 An LTI Simulation 85
3.3.2 LQR Compensator, a Multivariable Feedback Design 92
3.4 The Estimator Design 100
3.5 LQG Simulation of the Linearized System 107
3.6 Non Linear Numerical Simulation 118
3.6.1 The Algorithm 118
3.6.2 Results 120

Chapter 4: Conclusion 129
4.1 Trajectory Design and Feedforward 129
4.2 Feedback Control 131

References 133

Appendix A: List of Figures 137
Appendix B: List of Symbols 143

INTRODUCTION

The concept of tether in space has been a subject of investigations and studies in the international scientific community for the past thirty years. Ivan Beley from the Office of Space Flight at NASA Headquarters in Washington, traces back the first published application before 1960. The Russian engineer Artsutanov suggested to deploy a tether from a geostationary satellite to the Earth surface in order to use it as a funicular between the ground and the outer space. It was only in fact the reversal of a no less "Jules Verne" idea known as the Tsiolkovskii tower. This Russian father of the propergol proposed in 1895 an equatorial tower reaching beyond geostationary altitude.

But in one decade, the critical issues which obstructed the way to real implementations of tethers in space were pointed out by the scientific community. In 1969, Collar and Flower suggested a very long tether connecting a satellite located beyond the geostationary distance with another satellite positioned at a relatively low altitude such that the center of gravity would be located at the geostationary distance. The lower satellite would involve large reduced power compared with existing geo-synchronous Intelsat satellite to transmit communication signals. However, the authors assessed that that a 0.2 mm tether of 50,000 km would be severed by micro-meteorites in about an hour. In addition, the reduction of temperature due to the passage of the system through the Earth's shadow would result in a tether length variation of about 40 km. In 1975, Pearson was among the first to analyse some of the tether dynamics and calculate that the implementation of Artsutanov's idea would require 24,000 flights of a shuttle with 30 times the payload of the present orbiter.

The first and so far unique space experiments of tether in space was performed in September and November of 1966 when Gemini XI and XII capsules were linked to an Atlas-Agena D stage. The effect on this system of gravity gradient and of an initial angular velocity were studied. The results of these experiments were consistent with the predictions of the analytical modelization. But it was not until the early 1970's that NASA decided to seriously investigate the feasibility of tether in space applications under the management of George von Tiesenhausen from the NASA Marshall Space Flight Center.

The outcome of this investigation is the Tethered Sub-satellite System (TSS) concept. The Tiesenhausen team shares the paternity of this system with Giuseppe Colombo who co-invented the Tethered Sub-satellite concept for the Italians in 1974-75. The TSS now is an official program of NASA and PSN, the Italian National Space Plan, which involves the deployment of a 20 to 130 km tether. Martin Marietta, Denver, is the prime contractor to perform the US part of the project whereas Aeritalia in Torino, Italy, is in charge of the manufacturing of the satellite module. It is this joined US/Italian project [9] which serves as a basis for this investigation of a feedforward/feedback approach to retrieval of a tethered sub-satellite.

CHAPTER 1:
THE RETRIEVAL OF THE TSS
PROBLEM STATEMENT

1.1. The Tethered Sub-satellite System, (TSS).

1.1.1. The Mission.

The TSS consists of a shuttle and a sub-satellite connected together with a tether. The joint Memorandum of Understanding signed between the United-Sates and the Italian governments plans two types of missions which will illustrate, in fact, the two main applications of this system.

The first application involves the deployment of a sub-satellite 20 km above the orbiter with an electrically conductive tether (fig 1.1). This tether, intersecting the Earth's magnetic field at orbital velocity, generates an electrical voltage in the range of 0.2 to 0.4 $V.m^{-1}$. Electrons can be generated from the orbiter with an electron gun in order to close the current loop and convert orbital energy to electrical energy . Inversely, if a current produced on the orbiter travels through this same tether, an electromagnetic force is produced which could be used for attitude keeping or maneuvering, or to boost the orbit of the shuttle. For instance, both ways could be used as an emergency system. In any case, this system opens the way to a variety of electromagnetic experiments in the space plasma. In particular, a 20 km tether would lead to a voltage of 2,000 to 4,000 V. The Shuttle instrumentation isolation and the interaction of such a differential of potential with the surrounding plasma are two issues which remain to be addressed.

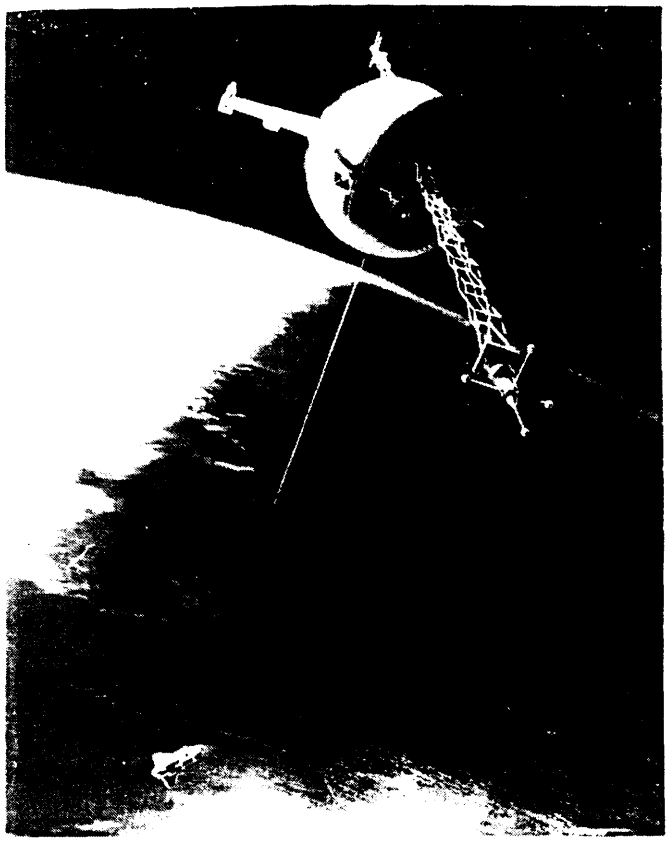

fig 1.1: Tethered electrodynamic satellite system.

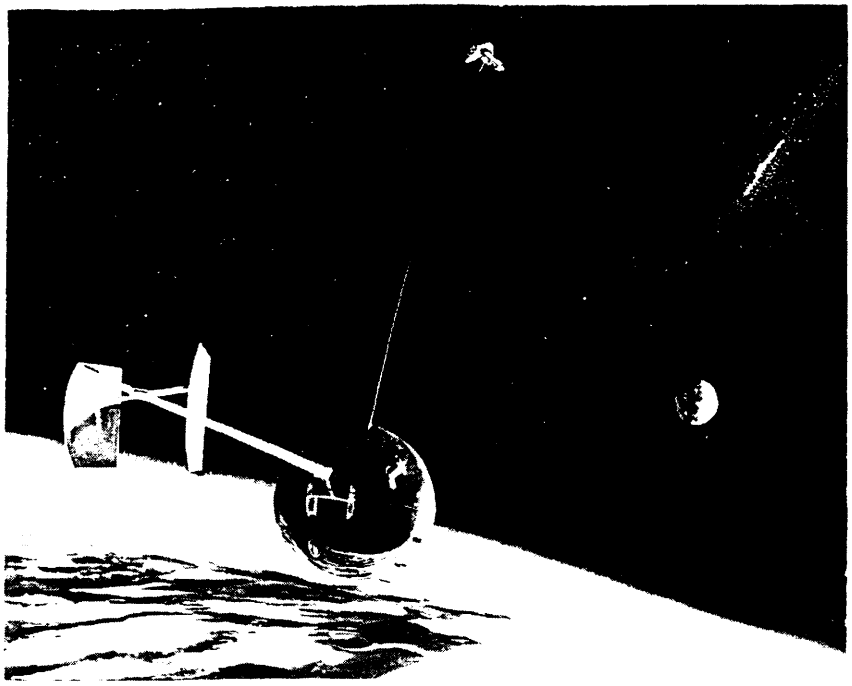

fig 1.2: Downward tethered satellite system.

If the first application is aimed at taking advantage of the tether properties, the second application uses the tether as a mean to deploy a measurement platform in the upper atmosphere and to recover it (fig 1.2). It is a unique way of gathering data on the upper atmosphere above an altitude of 60 km, the upper limit of probe-balloons, and below an altitude of 150 km, the lower limit of low orbit satellites. The applications of such a system range from upper atmosphere data collection to aerodynamic studies for reentry vehicles like orbital planes. The measurement platform must be aerodynamically stable and capable of standing high aerodynamic heating since it will fly in the upper atmosphere at hypersonic velocity. This application involves the deployment of a 130 km tether from the 200 km altitude shuttle orbit.

1.1.2. Description of the System.

The tethered sub-satellite is carried in the cargo bay of the orbiter along with the deployment and retrieval system. The tether is initially wrapped around a reel. The tether control mechanism includes a reel drive, a tensiometer, a length measurement wheel and a tachymeter.

The critical issue of the tether control is to keep the tension of the tether positive. If the tether becomes slack, the whole system is uncontrollable. This inherent property of tether dynamics imposes some constraints on the velocity of retrieval. The rate of deceleration of reeling in the tether is limited by the hard constraint: the tension must remain positive, or in other words, one cannot push with a tether. The natural force which keeps the shuttle and the sub-satellite apart is the gravity gradient. However, its intensity decreases with the length between the two spacecrafts. Consequently, the danger of having an uncontrollable system is more acute close to the orbiter. Two safeguards to this problem are planned. A tether-aligned thruster is mounted on the sub-satellite and fired at 2 N along the final two kilometers of

retrieval. However, no firing of any jet close to the shuttle is allowed by NASA. Therefore, the sub-satellite is deployed and docked at the end of a 10 m boom (front page picture).

A typical mission scenario from a control engineer point of view would be divided in three parts:

- control the deployment of the sub-satellite along an efficient trajectory,
- regulate the sub-satellite about the desired orbit for experimentations,
- retrieve the sub-satellite along a stable trajectory, keeping the tension positive.

Of the three parts of the mission, the retrieval phase is the most critical since the retrieval of a tethered sub-satellite is an inherent unstable process leading to large oscillations when the length of the tether decreases.

The first mission of the TSS was scheduled for 1987. Since then, it has constantly been postponed. The main reason is that the TSS has received a low priority in the reschedule of shuttle missions following the Challenger accident and various technical problems. But it also seems that the retrieval aspect of the tether sub-satellite has not been definitely finalized yet.

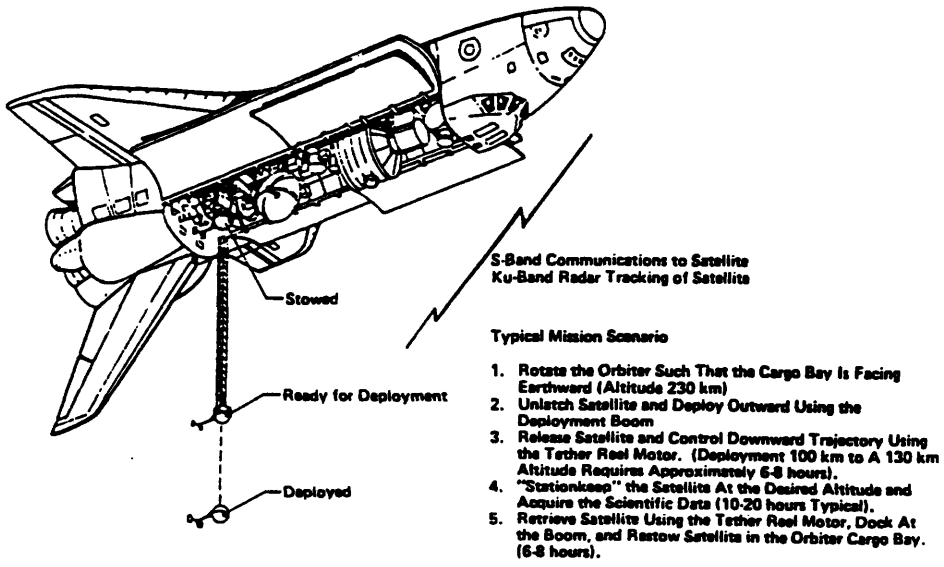

fig 1.3: The TSS system.

1.2. An Overview of Previous Work.

Since the TSS became an official NASA project, the dynamics and control of a sub-satellite suspended to the shuttle has received a considerable amount of attention from the scientific community. A survey and a compilation of the past publications on this subject was performed by Misra and Modi in 1986 [17].

The same Misra and Modi have presented a very general dynamic model which takes into account the tether vibrations and the rotational motion of both end-bodies [18],[16]. But many authors have studied the dynamics of tethers in space, including the deformation of the tether in three dimensions [12],[19],[20].

Von Flotow and Williamson have investigated the deployment aspect [13], and Lemke and Powell, the attitude control of a tethered spacecraft [15]. But it obviously is the retrieval phase which has been the subject of most control studies because of its inherent unstable dynamics.

First, the stabilization of the retrieval was attempted using the tether reel-in rate as the control. Such approaches rely on the gravity gradient torque to remove the excess angular momentum. But since the gravity gradient weakens when the tether length is reduced, this leads to very slow retrieval under 2 km. Rupp presents a tether tension linear feedback law which controls the tether swinging motion in the orbital plane and the tether stretching motion [25]. Bainum and Kumar implement an LQR regulator, exploiting the tether reel control [2]. In his PhD thesis, Boschitsch also applies linear quadratic feedback theory in order to stabilize the in-plane and out-of-plane motions, retaining the time-varying nature of the linearized equations. He observes, in particular, that the feedback gains vary significantly during the retrieval. Xu, Misra and Modi propose a non linear feedback law to control the rigid body motion of the tethered sub-satellite in the in-plane and out-of-plane motion [29]. However the tether does not seem to reach the final desired length for rapid retrievals.

The introduction of tether normal thrusters results in a significant improvement of the performances of the retrieval in terms of time and versatility. This improvement is done at the

expenses of an increase of the mass of the sub-satellite and a fuel consumption. Banerjee and Kane [3], are the firsts with Xu, Misra and Modi [28], to investigate this new approach. The latter use tether normal thrusters assumed to be proportional and a quasi-linear control law to stabilize the tethered sub-satellite during retrieval. Vadali and Kim use a combination of tension control with out-of-plane thrusting to derive a non-linear feedback control law based on the second method of Liapunov [27]. This approach leads to some very convincing results.

Pines, von Flotow and Redding [23] propose both an ad-hoc phase plane control scheme and a more rigorous sliding mode control methodology. They show that on-off firing of the orbiter thrusters in the first approach leads to a stable limit cycle for both pitch and roll dynamics, whereas the sliding mode method achieves remarkable performance for continuous thruster firing. However,since spacecraft thrusters are on-off devices, continuous thrust levels must be approximated by fast pulsing with pulse width and frequency modulation which will destroy most of the smoothness of the closed loop trajectory. The stabilization is performed along some arbitrary retrieval trajectory resulting in a non optimal fuel use.

In order to reduce the fuel consumption, the previous authors as well as Banerjee and Kane [3] recommend that thruster control be used in conjunction with tether reel-in rate control.

At last, Beletsky and Levin have gathered together most of their previous work in tether dynamics in a book now available in English [4].

All the presented control schemes so far regulate the retrieval about some arbitrary nominal path without taking into consideration the time of retrieval or the minimization of the fuel consumption. Even if they can be approximated by a second order linear oscillator for some variations, as it will be shown in the next chapter, the TSS dynamics are non linear. It seems of interest to know what the optimal path of the retrieval which minimizes the total retrieval time is, with reasonable final pitch angle and pitch rate, and to derive the non-linear length history required to follow this trajectory. Then this optimal trajectory could be tracked with a loop combining feedforward information with thruster augmented feedback. Bendinksen and

Boschitch [6] derive a non-linear length history, but in order to track a pre-defined trajectory. The cost they intend to minimize is composed of the variations of each state with respect to the states along a nominal trajectory, so that no consideration is given to the final time of retrieval. Boschitch has also designed a time varying regulator [7] which tracks a desired trajectory, but does not use thruster augmented feedback.

Therefore, it seems that it exists here a real opportunity for a new approach to the problem of retrieving a tethered sub-satellite.

1.3. A New Approach: a Feedforward/Feedback Scheme.

The addition of thrusters on the sub-satellite brings better control authority to stabilize the in-plane and out-of-plane motions of the tethered system. However, to intend to retrieve it along some arbitrary trajectories leads to an important fuel consumption [23]. On the other hand, the use of tether reel-in rate as the control is an attractive solution since it relies on the natural gravity gradient to remove excess angular momentum. A new approach would be to stabilize the retrieval with thrusters along a trajectory which would exploit the natural dynamics of the system.

This new approach requires first investigation of the possibility of computing an optimal retrieval trajectory, by minimizing a cost function, a combination of total retrieval time and final pitch angle and pitch rate. Open loop retrieval being obviously unpractical, a closed loop regulator needs then to be designed. In this feedforward scheme, the length rate history or length acceleration, depending on the control used in the cost minimization, is fed forward in the loop. The regulator commanded by the pre-computed nominal pitch angle, pitch rate and length, computes the necessary corrections to track the optimal trajectory in presence of external disturbances and modeling error (fig 1.4).

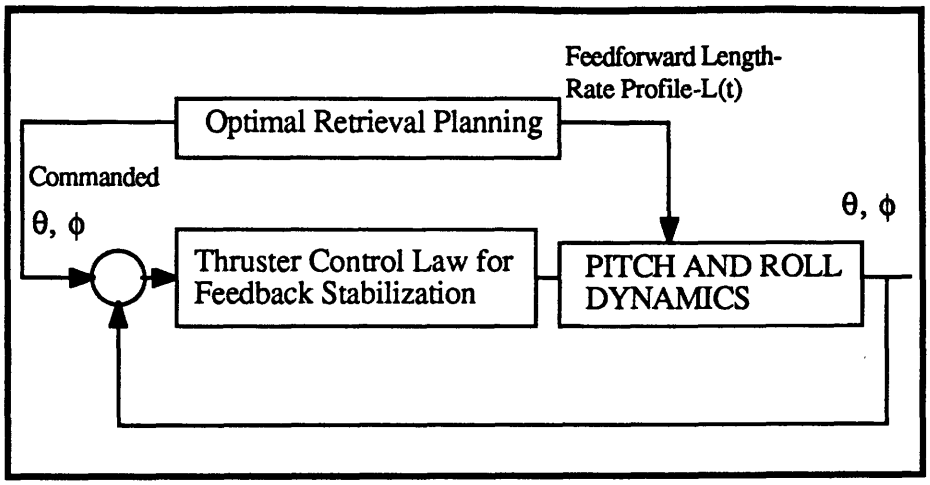

fig 1.4

This report presents a study of feasibility of this concept. Since pitch dynamics are directly driven by length changes, while roll dynamics are not, this study focuses upon length and pitch dynamics. Roll perturbations must be regulated with an independent feedback loop.

In the following chapter, the equations driving the pitch and length dynamics are derived. Then an Hamiltonian analysis is performed in order to deduce the structure of the optimal control minimizing the cost function. A study performed in the phase plan enables to deduce some inherent properties of the retrieval dynamics. These properties are used to initialize a numerical search of the optimal solution. Then a sub-optimal scheme is derived in order to retrieve the sub-satellite for any initial conditions.

A feedforward/feedback loop is designed in the third chapter to stabilize the system about the nominal retrieval trajectory computed in chapter 2. For this purpose, the system is first linearized at each step. A compensator based on a decoupling of the controls is first derived. Then an LQR regulator is designed in order to take advantage of the multicontrol nature of the system. A final non-linear simulation of the tracking of the nominal trajectory in presence of sensor noise, thruster granularity is performed with a one percent initial error. This simulation implements an extended Kalman filter in order to estimate the pitch rate and filter the sensor and plant noises.

CHAPTER 2:
OPTIMAL RETRIEVAL TRAJECTORY DESIGN

2.1. Formulation of the Optimal Control Problem.

2.1.1 Pitch Dynamics.

Simplified dynamics are used to numerically solve this optimization problem. In this entire study, the following assumptions and approximations are made: the roll angle is driven to zero by an appropriate feedback control; the Earth frame is supposed Galilean; the mass of the orbiter is assumed to be much higher than that of the sub-satellite so that the retrieval dynamics have no effect on the orbit of the shuttle. This last approximation is discussed by Bergmann [5]. The purpose of the shuttle attitude control system is to keep a specified orbit. However, its limit cycle nature may excite some tether responses.

Only the rigid body motion is retained in this model. With this assumption, it may be considered that the system is composed of a mass m, the sub-satellite, subject to the earth gravitational force $\mathbf{f}$ and connected to a point O' by an unstretchable tether of length L, unable to transmit bending modes. O' orbits about the center of the Earth O at a rotational velocity ω.

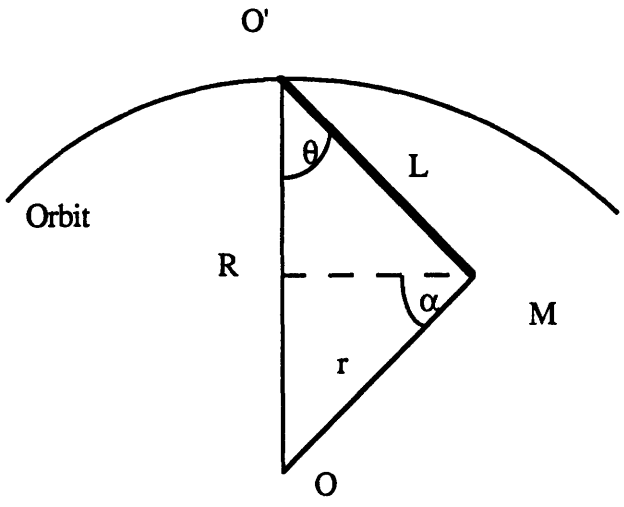

Fig 2.0

If R = OO' and r = OM, $\left(\frac{R}{r}\right)^3$ may be approximated by $1+3\frac{L}{R}\cos\theta\sin\theta$ and $\frac{L}{R}$ may be considered very small compared with one. At the first order in $\frac{L}{R}$,

$$\cos\alpha = \frac{L}{R}\sin\theta \quad \text{and} \quad \sin\alpha = \frac{R}{r}\left(1 - \frac{L}{R}\cos\theta\right).$$

The gravitational force applied to the tethered sub-satellite is equal to:

$$\underline{f} = m\,\underline{g} = m\frac{\mu}{r^3}\underline{r}.$$

Still to first order in $\frac{L}{R}$, the course of the orbiter can be approximated by a circular orbit. Since the mass of the sub-satellite is very small compared with that of the orbiter (with a factor of 10^3), the orbital rate ω is rewritten as:

$$\omega^2 = \frac{\mu}{R^3} \Rightarrow \mu = \omega^2 R^3.$$

Consequently, to first order in $\frac{L}{R}$, the gravitational torque applied on the sub-satellite with respect to O' is equal to:

$$\underline{M}_{o'} = - m L \frac{R^4}{r^3} \omega^2 \sin\theta \, \underline{z} \qquad (2.1)$$

On the other hand, the angular momentum of the sub-satellite with respect to O' is given by:

$$\underline{H}_{o'} = m\left[L^2\left(\dot{\theta} + \omega\right) - R\,\omega\,L\cos\theta\right]\underline{z} \qquad (2.2)$$

O' being in motion about the Earth frame, the Newton's law implies:

$$\dot{\underline{H}}_{o'} + \underline{O\dot{O}'} \times m\,\underline{V}_M = \underline{M}_{o'} \qquad (2.3)$$

Thus, the in-plane rigid body motion is governed by:

$$\ddot{\theta} + 2\frac{\dot{L}}{L}\left(\dot{\theta} + \omega\right) + 3\,\omega^2 \sin\theta\cos\theta = 0 \qquad (2.4)$$

which is a second order non linear differential equation.

This simple model gives several insights into the dynamics of the system. First of all, if the sub-satellite is being retrieved, $\dot{L}$ is negative. The damping coefficient is negative and the dynamics of the pitch angle are described by an unstable, non-linear, second order oscillator. The effect can be illustrated by pulling a string between two fingers. The smaller the remaining length of the string to pull is, the larger the oscillations at the tip of the string are. Secondly, if the length of the tether is constant, the equation (2.4) describes the classical dynamics of a pendulum subject to the gravitational torque without damping. However, if $\dot{L} < 0$, two competing effects on the tethered sub-satellite can be observed. First, the gravitational torque proportional to $3\,\omega^2 \sin\theta\cos\theta$ tends to restore the configuration to the local vertical. But secondly, the Coriolis acceleration proportional to $2\frac{\dot{L}}{L}\omega$ drives the sub-satellite away from the local vertical. For $4\left|\frac{\dot{L}}{L}\right|\frac{1}{3\,\omega} < 1$, an equilibrium angle can be reached given by:

$$\frac{\sin 2\theta_{eq}}{2} = - 2\frac{\dot{L}}{L}\frac{1}{3\,\omega} \qquad (2.5)$$

Consequently, the sub-satellite may be retrieved at constant but unstable equilibrium pitch angle with $\frac{\dot{L}}{L}$ constant (exponential retrieval). But it does not necessarily lead to the fastest retrieval scheme. In addition, if the Coriolis acceleration overcomes the gravity gradient, then no equilibrium is achieved and $\theta(t)$ diverges exponentially. Fig 2.2.1 and 2.2.2 show an example of divergent retrieval in the LVLH plane and phase plane. The sub-satellite ends up, in fact, wrapped about the shuttle.

In this analysis, tether deflections and deformations are not considered but only its libration. The tether is supposed to be unstretchable. The tether length is directly controlled with the reel, making the assumption that the control mechanism overpowers any friction. Either the length rate or length acceleration can be used as the command. However the retrieval is subject to the uncircumventable constraint that the tension must remain positive. If the tension is driven to zero, the tether becomes slack and the system is uncontrollable. Therefore, a tether-aligned thruster will be fired at 2N during all the retrieval as a safeguard in order to guarantee the controllability of the system.

If $\underline{\mathbf{a}}$ is the acceleration of the assumed point mass sub-satellite, $\underline{\mathbf{T}}$ the tension and $\underline{\mathbf{f}}$ the gravitational force applied on the sub-satellite, then the first Newton law implies:

$$\underline{\mathbf{a}} = \underline{\mathbf{T}} + \underline{\mathbf{f}}$$

In the orbital plane, $\underline{\mathbf{f}}$ may be approximated at the first order in $\frac{L}{R}$ as follow:

$$\underline{\mathbf{f}} = -\omega^2 R \left(\frac{R}{r}\right)^3 \begin{bmatrix} \frac{L}{R}\sin\theta \\ 1 - \frac{L}{R}\cos\theta \end{bmatrix}$$

Thus the tension is given by:

$$\frac{T}{m} = L\left[\left(\dot{\theta} + \omega\right)^2 + 3\omega^2\cos^2 - \omega^2\right] - \ddot{L} \qquad (2.6)$$

If ϕ is driven to 0 and θ is kept small, the positive tension constraint may be approximated by:

$$\ddot{L} - 3\omega^2 L < 0 \qquad (2.7)$$

In order to prevent the boom from being damaged at the impact, the final impact velocity should not be lower than -.5 $m.s^{-1}$, ie: $-.5 < \dot{L}(t_f) < 0$. This final constraint is also a safeguard in the case the sub-satellite would miss the docking point.

At this point, it appears that taking the length rate as the control will not ensure that the no-pushing constraint will be met, since the derivative of the length rate appears in the expression of equation (2.7). Therefore, it seems necessary to increase the order of the system so as to take the length acceleration as the control.

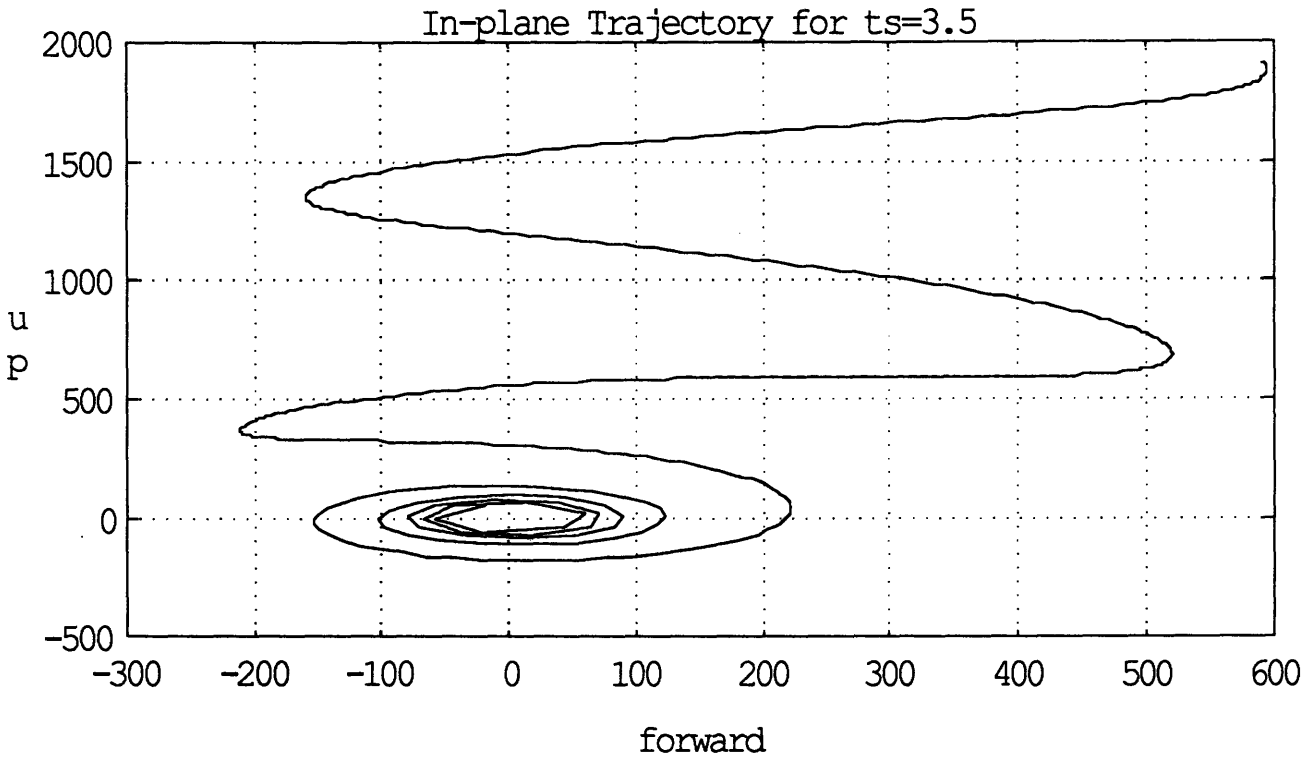

fig 2.1: Example of divergent retrieval trajectory in the LVLH plane.

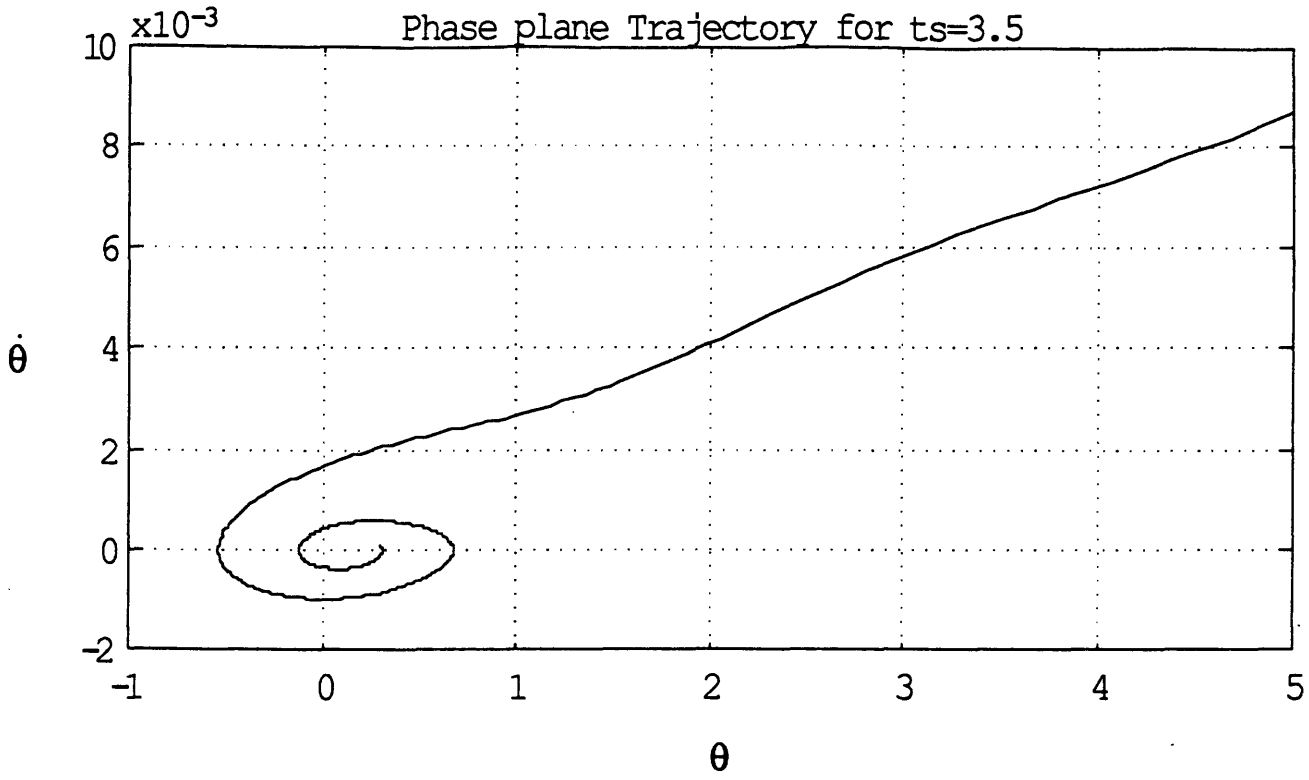

fig 2.2: Example of divergent retrieval trajectory in the phase plane.

2.1.2 Formulation of the Optimization Problem.

The goal is to retrieve the sub-satellite quickly along a reasonable retrieval trajectory. As demonstrated in § 2.1.1, the pitch angle may diverge before docking for certain conditions. Therefore, the derived non-linear control law must also minimize the final pitch angle and pitch rate in addition to the final time. This can be done by formulating a quadratic cost of the following form:

$$J = \theta^2(t_f) + \left(\frac{\dot{\theta}}{\omega}\right)^2(t_f) + \left(\frac{\omega\, t_f}{2\,\pi}\right)^2 \qquad (2.8)$$

In this cost, it is assumed that a deviation of one radian of the pitch angle is as bad as a deviation of one orbital rate of the pitch rate and as bad as an increase of the total time of

retrieval of one orbit. The roll angle ϕ is still assumed to be driven to zero. Consequently, this trajectory optimization problem can be stated as follow:

" given some initial conditions $\theta(0)$, $\dot{\theta}(0)$, $L(0)$ and $\dot{L}(0) = 0$, find the control law $u(t) = \dddot{L}(t)$ which minimizes the cost J given by equation (2.8) subject to the following constraints:

$$\ddot{\theta} + 2\frac{\dot{L}}{L}\left(\dot{\theta} + \omega\right) + 3\,\omega^2 \sin\theta \cos\theta = 0$$

$$\ddot{L} - 3\,\omega^2 L < 0$$

$$-.5 < \dot{L}(t_f) < 0$$

$L(t_f) = L_f = 10$ m , (length of the boom) ".

2.2 Hamiltonian Analysis

To assure that the impact velocity constraint be respected, it may be necessary to include the final length rate into the cost:

$$J = x_1^2(t_f) + \left(\frac{x_2}{\omega}\right)^2(t_f) + \left(\frac{\omega\, t_f}{2\,\pi}\right)^2 + \alpha\, x_4^2(t_f) \qquad (2.9)$$

$\alpha > 0$ is a penalty used to ensure that the docking velocity is inside the limits stated in § 2.1.2. The tension constraint is:

$$C(x,u) = \ddot{L} - 3\,\omega^2 L.$$

Choosing a state-space representation for the system dynamics with the state vector x defined as:

$$x^T = [x_1\ x_2\ x_3\ x_4]^T = \left[\theta\ \dot{\theta}\ L\ \dot{L}\right]^T$$

the optimal retrieval problem can be formulated according to the maximum principal in terms of the Hamiltonian:

"find the control law u(t) which maximizes:

$$H = \lambda^T f(x,u) + \mu\, C(x,u) \tag{2.10}$$

subject to: $\dot{x} = f(x,u)$,

$\dot{\lambda} = - H_x$,

$$\sum_i \left(\lambda_i(t_f) - \frac{\partial J}{\partial x_i(t_f)} \right) \delta x_i - \left(\frac{\partial J}{\partial t_f}(t_f) + H(t_f) \right) \delta t_f = 0$$

and with $\mu = 0$ if $C(x,u) < 0$ and $\mu > 0$ if $C(x,u) = 0$. μ is a Kune-Tucker coefficient ".

The system is given by:

$$\begin{aligned} \dot{x}_1 &= x_2 \\ \dot{x}_2 &= - 2 \frac{x_4}{x_3}(x_2 + \omega) - \frac{3}{2} \omega^2 \sin 2x_1 \\ \dot{x}_3 &= x_4 \\ \dot{x}_4 &= u \end{aligned} \tag{2.11}$$

Consequently, the Hamiltonian becomes:

$$H = \lambda_1 x_2 - \lambda_2 \left[2 \frac{x_4}{x_3}(x_2 + \omega) + \frac{3}{2} \omega^2 \sin 2x_1 \right] + \lambda_3 x_4 + \lambda_4 u + \mu \left(u - 3 \omega^2 x_3 \right) \tag{2.12}$$

The costates are given by:

$$\begin{aligned} \dot{\lambda}_1 &= 3 \omega^2 \lambda_2 \cos 2x_1 \\ \dot{\lambda}_2 &= - \lambda_1 + 2 \lambda_2 \frac{x_4}{x_3} \\ \dot{\lambda}_3 &= - 2 \lambda_2 \frac{x_4}{x_3^2}(x_2 + \omega) + \mu\, 3 \omega^2 \\ \dot{\lambda}_4 &= - \lambda_3 + 2 \lambda_2 \frac{x_2 + \omega}{x_3} \end{aligned} \tag{2.13}$$

and the transversality conditions give:

$$\begin{aligned} & x_1(t_f) \text{ free } \Rightarrow \lambda_1(t_f) + 2\, x_1(t_f) = 0 \\ & x_2(t_f) \text{ free } \Rightarrow \lambda_2(t_f) + \frac{2}{\omega^2} x_2(t_f) = 0 \\ & x_3(t_f) \text{ fixed } \Rightarrow x_3(t_f) - 10 = 0 \\ & x_4(t_f) \text{ free } \Rightarrow \lambda_4(t_f) + 2 \alpha\, x_4(t_f) = 0 \\ & t_f \text{ free } \Rightarrow H(t_f) - 2 \frac{\omega}{2\pi}^2 t_f = 0 \end{aligned} \tag{2.14}$$

To the five unknowns, the four initial values of the costates and the final time, correspond five terminal equalities. So this two boundary value problem is well posed.

According to the maximum principle, the control u is given by the maximization of the Hamiltonian. $H_u = \lambda_4 + \mu$ does not depend on u. The Hamiltonian is linearly dependent on the control and therefore, the structure of the control u is bang-bang as long as the constraint is not reached. On the optimal solution, the constraint is always respected. If the case tension strictly equal to zero is rejected, $\mu = 0$ and the control $u = u_{max}$ if $\lambda_4 > 0$ or $u = u_{min}$ if $\lambda_4 < 0$.

This open loop optimization problem is one of the most difficult to solve. It combines a non linear unstable dynamic with an inequality constraint and an Hamiltonian linearly dependent on the control. The solution might be a blend of bang-bang control with analytical control when the constraint is reached. The method of resolution can only be numerical and only a sub-optimal solution might be implementable in real time. The goal of this study is not to academically find the optimal trajectory but to find a reasonable family of trajectories which can be implemented in real time on orbit, even if knowing the true optimal trajectory would be of interest in the TSS program.

2.3 Analysis of the Retrieval Dynamics, Limitations.

2.3.1 Phase Plane Analysis.

In this entire study, a numerical integrator based on Bulirsh, Gragg and Stoer [24] is used.

The dynamics of θ are given by a second order differential equation. (2.4) may be rewritten as:

$$\ddot{\theta} + 2\frac{\dot{L}}{L}\dot{\theta} + 3\,\omega^2 \cos\theta \sin\theta = -2\frac{\dot{L}}{L}\omega \qquad (2.15)$$

For small angle, the previous equation may be identified with:

$$\ddot{\theta} + 2\,\delta\,\omega_n\,\dot{\theta} + 3\,\omega_n^2\,\theta = \omega_n^2\,\theta_{eq} \qquad (2.16)$$

where $\omega_n = \sqrt{3}\,\omega$, $\delta = \frac{\dot{L}}{L}\frac{1}{\sqrt{3}\,\omega}$ and $\theta_{eq} = -2\frac{\dot{L}}{L}\frac{1}{3\,\omega}$.

Since $\dot{L} < 0$ during the retrieval, δ is negative, characteristic of an unstable dynamic.

To understand which kind of retrieval path is physically realizable, it is interesting to plot the phase plane for different values of δ. At the beginning of the retrieval $\dot{L} = 0 \Rightarrow \delta = 0$. It is the classical case of a pendulum subject to gravity gradient, cf § 2.1.1. [14].

$$\ddot{\theta} + 3\,\omega^2 \cos\theta \sin\theta = 0 \qquad (2.17)$$

The phase trajectories are given by:

$$3\,\omega^2 \frac{\sin^2\theta}{2} + \frac{\dot{\theta}^2}{2} = \text{constant}$$

If $[\theta_0\ ,\ \dot{\theta}_0]$ is the initial point in the phase plane,

$$\sin^2\theta_0 + \frac{\dot{\theta}_0^2}{3\,\omega^2} \leq 1 \qquad (2.17.1)$$

must be verified to have a contained pitch angle. On the other hand, for initial conditions outside this area, the tether wraps itself about the shuttle with an increasing pitch rate since the length decreases. Thus, if such a configuration is detected, the length must be increased appropriately, or the pitch thruster will have to be fired so as to come back inside the limits defined by (2.17.1) and stabilize the oscillations. Such spinning initial conditions are not anticipated in the TSS system.

The sub-satellite oscillates with a decreasing period which converges to $\frac{2\pi}{\sqrt{3}\,\omega}$ = 3627.6 s = .5774 orbits when θ_0 diminishes. Fig 2.3 shows the period of oscillation vs θ_{max}, maximum angle of oscillations.

θ_{max} (rad)	T (orbit)
.92	.7635
.8	.6688
.6	.6184
.4	.5989
.2	.5916
$\rightarrow 0$	.5774

Fig 2.3

Making the approximation θ small, which would give $T = \frac{1}{\sqrt{3}}$, leads to some important error. However, such an approximation may be used later to get some insights in the physics of the dynamics.

When $\dot{L}$ is different from zero, the phase trajectories are divided into two parts. For $\delta > -\frac{\sqrt{3}}{4} = -.433$, a pitch equilibrium θ_{eq} exists. The phase trajectories become divergent spirals centered on θ_{eq} given by (2.5), (fig 2.4.3). There is a "splitting line" which divides the spirals between those diverging towards positive pitch angles and those diverging towards negative pitch angles. For the latest, they originate from θ_{eq}'s higher than $\frac{\pi}{2}$. If $\delta < -\frac{\sqrt{3}}{4}$, θ_{eq} disappears. The "splitting line" becomes the generator of divergent trajectories, one part diverging towards θ's > 0 and the others towards θ's < 0. As δ decreases, the splitting line flattens. Cf fig 2.4.6. Obviously, since δ is not constant in the retrieval, the true phase plane will be a blend of these phase trajectories, as L and $\dot{L}$ decrease.

These plots reveal some very important points about what is reachable. A good trajectory would end as close as possible to the point $(\theta,\dot{\theta}) = (0,0)$. This point can only be reached with a negative pitch rate. θ will decrease from approximately 1 rad to zero. In this part, the pitch rate will lie in the interval [-1.74e-3 0]. So in one way or another, a divergent branch of spiral will have to end in the lower part of the phase plane. Then the retrieval path will follow the "splitting line" and leave it on a divergent branch which goes through (0,0). If the "splitting line" is crossed, the retrieval path will irreversibly diverge towards negative θ. It means that instead of docking on the boom, the tether with the sub-satellite will end up wrapped around the orbiter. But in any case, because the dynamic is unstable, the optimal path will be very sensitive to disturbances. Therefore an open loop retrieval is unrealistic.

To sum up, the trajectory of the retrieval is very likely to follow first an expanding spiral which might lead to several periods of oscillation, depending on the initial conditions. Then, it will join the "splitting line" at about 1 rad. After having followed this line, it will leave it on a divergent path going through (0,0), ultimately reaching this point or some point around it.

All these results could also have been obtained through some hand waving, as Professor von Flotow points out in [22]. If the pitch dynamics are linearized, then:

$$\theta_{eq} = -\frac{2}{3}\frac{\dot{L}}{\omega L} = -\frac{2}{\sqrt{3}}\delta \qquad (2.18)$$

The switch from spiral phase trajectory to divergent one occurs at $\delta = -1$ in this model. At this point, θ_{eq} is joined to the point where the "splitting line" crosses the line $\dot{\theta} = 0$. This point is equal to $\frac{\sqrt{3}}{2}$ = 1.15 rad = 66.16°. Since the retrieval path can only get to this "splitting line" from above (fig 2.4.3), θ will go around 1.15 rad. Fig 2.4.3 also shows that all the previous approximations almost cancelled each other since on this plot, the "splitting line" appears at 66.2°.

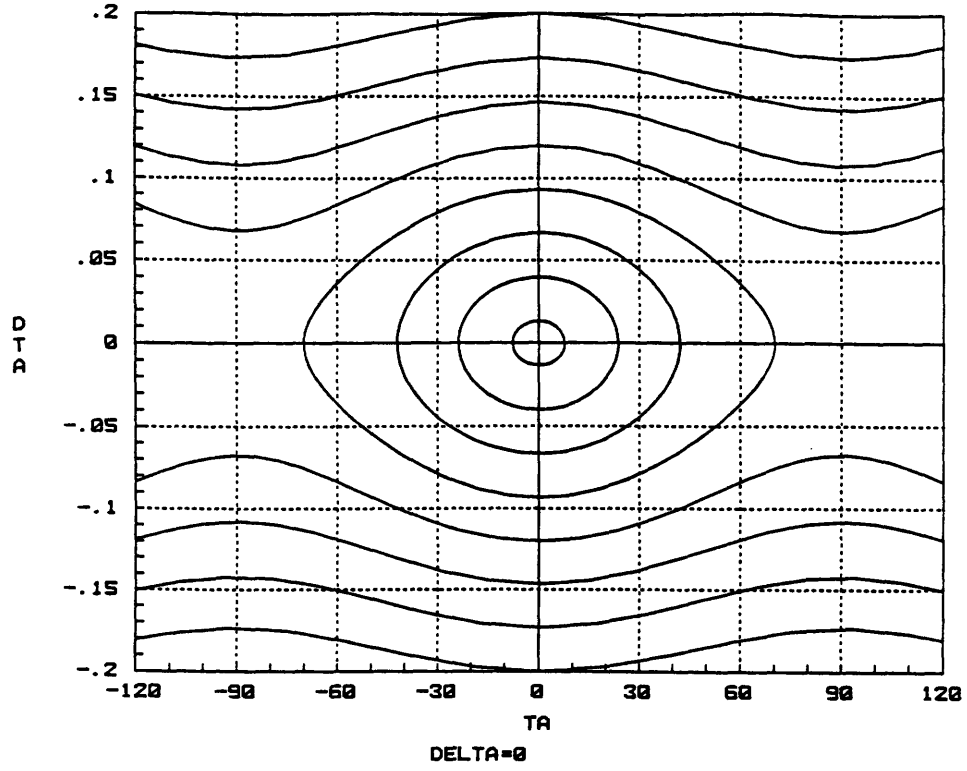

fig 2.4.1: Phase plane trajectories for $\delta = 0$.

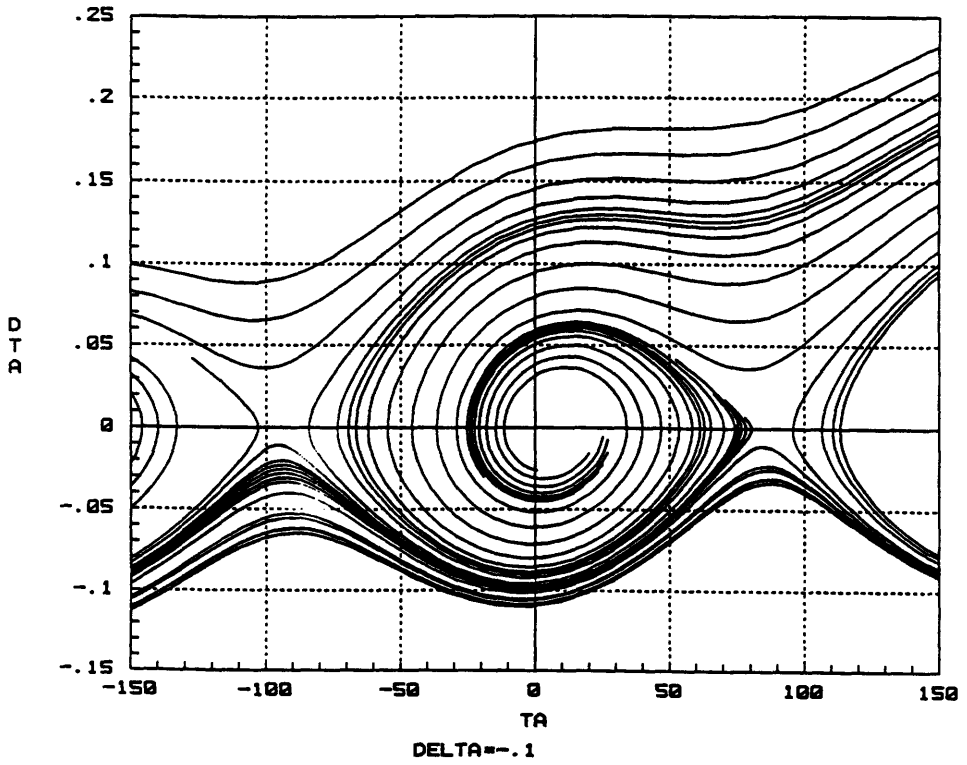

fig 2.4.2: Phase plane trajectories for $\delta = -.1$.

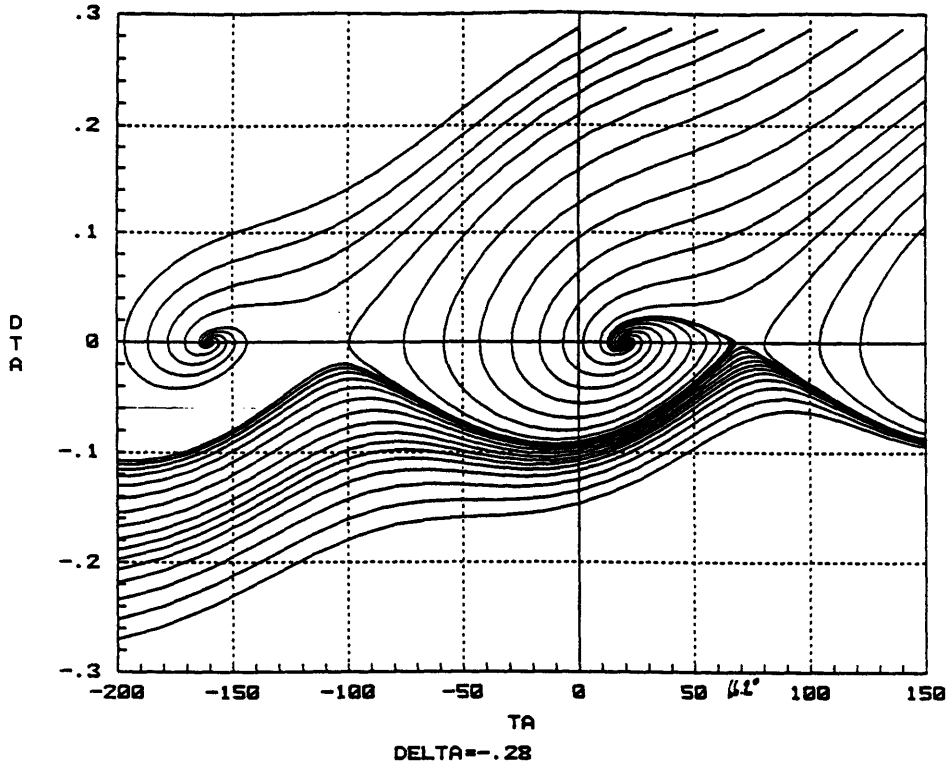

fig 2.4.3: Phase plane trajectories for $\delta = -.28$.

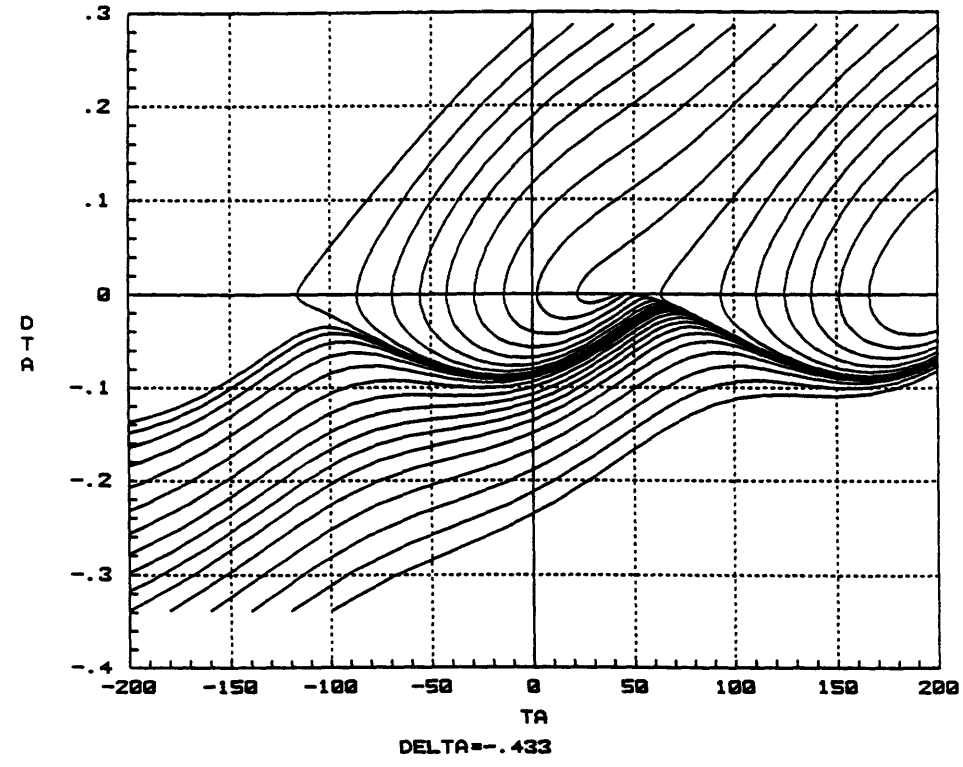

fig 2.4.4: Phase plane trajectories for $\delta = -.43$.

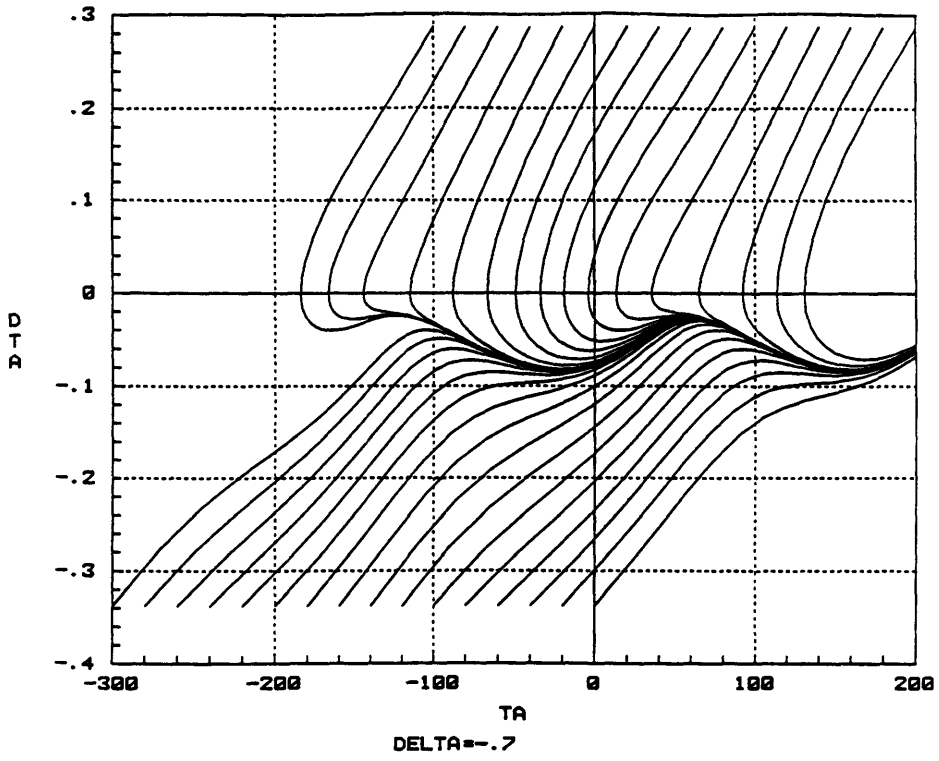

fig 2.4.5: Phase plane trajectories for $\delta = -.7$.

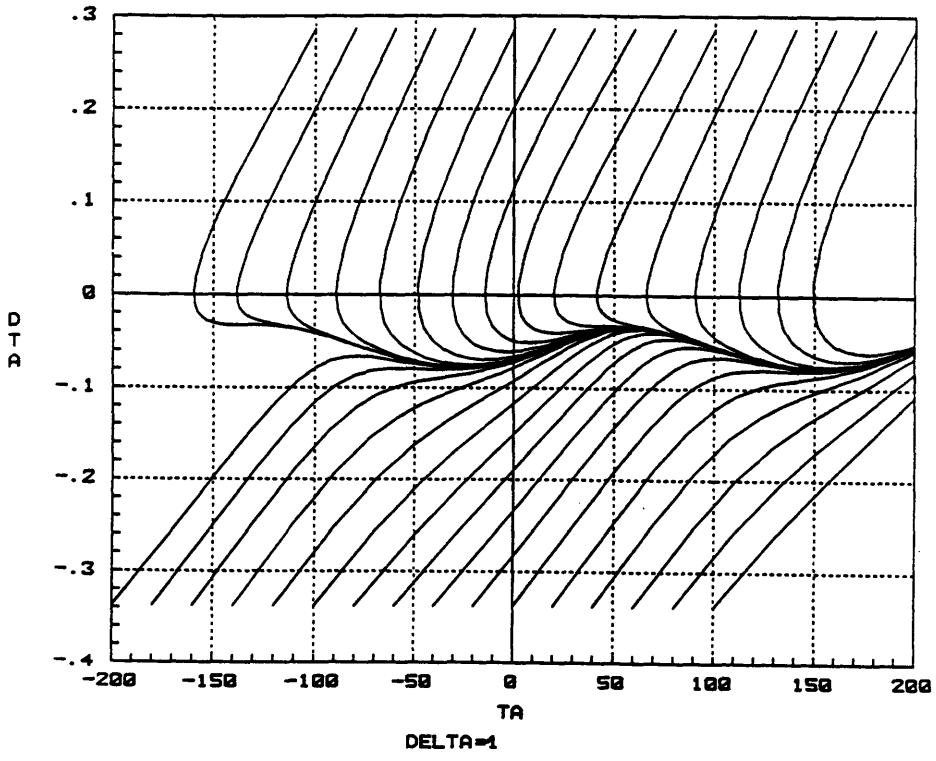

fig 2.4.6: Phase plane trajectories for $\delta = -.1$.

2.3.2 Investigation of the cost function.

Most numerical algorithms of optimization suppose that the cost is convex on the domain of possible solutions. This is due to the fact that they are unable to discern local extrema from absolute one when they converge. For this reason, Darryll Pines [22] scanned the cost function for the two parameter optimization problem, ie for constant acceleration retrieval with $\dot{L}_i$ and $\dot{L}_f$ as parameters, in order to investigate the shape of the function.

The constraints remain: $\ddot{L} - 3\omega^2 L < 0$ and $L_f > -.5$ m.s^{-1}. With the constant acceleration assumption, the no-pushing condition becomes:

$$\frac{\dot{L}_i^2 - \dot{L}_f^2}{L_f - L_i} = 6\,\omega^2 L_f \qquad (2.18)$$

Fig 2.5.1 shows the feasible region defined by these constraints in the parameter plane $(\dot{L}_i, \dot{L}_f)$. The shape of the cost function in this region with the initial conditions $\theta(0) = .3$ rad and $\dot{\theta}(0) = .1\,\omega$ rad.s^{-1} is given by fig 2.5. This three D plot of the cost function shows that peaks and valleys alternate. The valleys decrease as $\dot{L}_f$ decreases and almost follows the direction of constant retrieval time. A one parameter scanning, fig 2.6, ie constant velocity retrieval, gives the same shape of cost function. In fact, each valley corresponds to the number of encirclement the path does in the phase plane in the spiral region. A minimum time recovery corresponds to a minimum number of tours which is one. Some retrieval trajectories in the LVLH plane are given by fig 2.7 for different valleys.

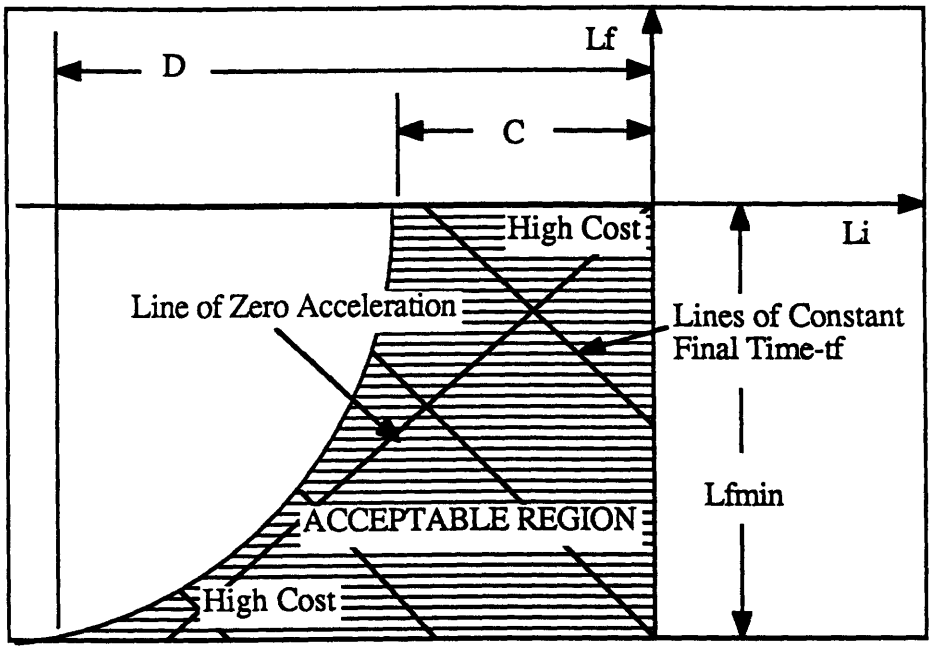

fig 2.5.1: Feasible Region in the $(\dot{L}_i,\dot{L}_f)$ plane for constant acceleration retrieval.

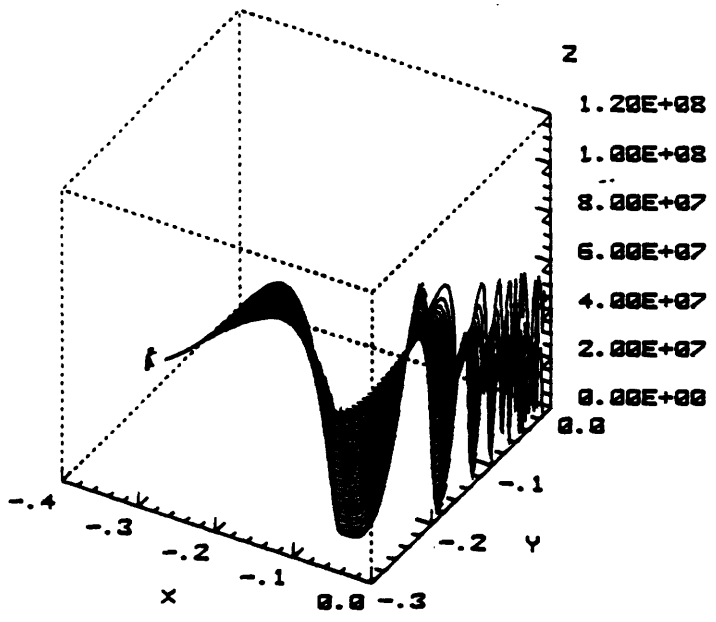

fig 2.5.2: Cost function for constant acceleration retrieval, $(\theta,\dot{\theta})_i = (.3,.1\omega)$.

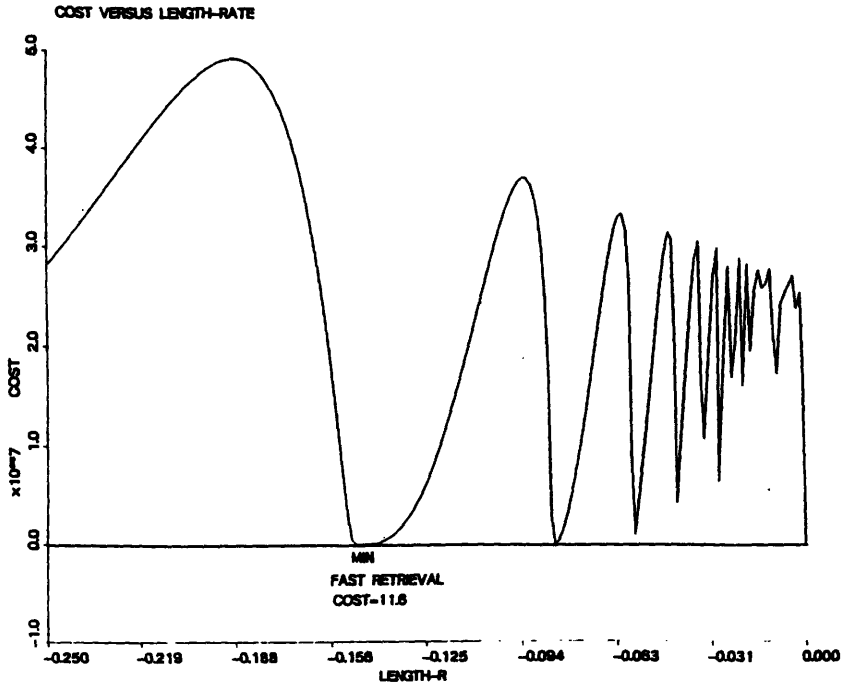

fig 2.6.1: Cost function for constant velocity retrieval $(\theta,\dot{\theta}) = (.3,.1\omega)$.

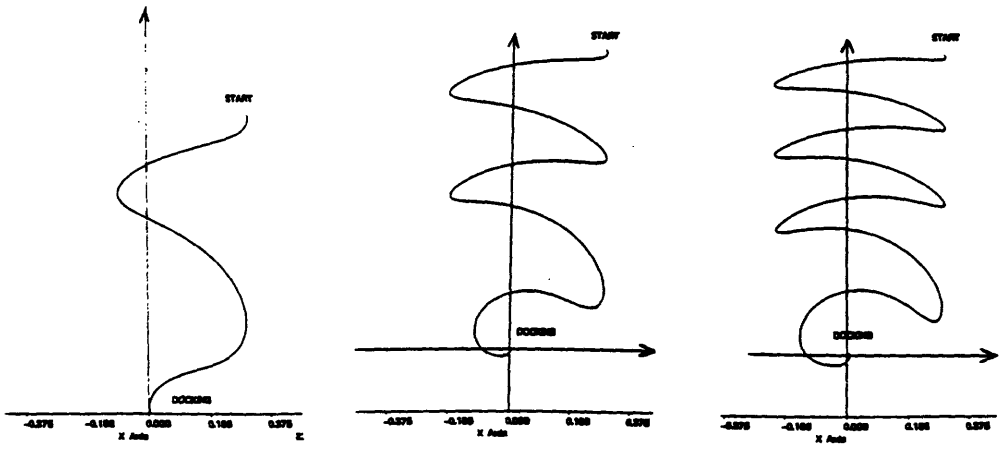

$\dot{L}$ = -.148 tf = 1.05 orb $\dot{L}$ = -.083 tf = 1.90 orb $\dot{L}$ = -.057 tf = 2.77 orb

fig 2.6.2: In-plane retrieval trajectory for different vallaies

2.4 Numerical Solution.

2.4.1 Investigation of the Optimization Problem under Inequality Constraint.

The fact that the Hamiltonian is linearly dependent on the control introduces an additional difficulty to the classical maximum principal. This problem has seven unknowns: the four initial costates, the final time, the control and μ if the constraint is reached. The transversality conditions give five equations (2.14) for the four states and the final time. If the constraint is not reached, $\mu = 0$ and u(t) is given by the sign of λ_4. The difficulty occurs when the constraint is reached. The value of μ is required to compute the costates. If the Hamiltonian is not linearly dependent on the control, the two unknowns correspond to the two following equations:

$$C(x,u) = 0$$
$$H_u = \lambda^T f_u + \mu C_u = 0$$

However, in the case of a linear optimization problem, this second equation does not hold any more. The problem becomes ill-posed unless each time the constraint is reached, the control switches from an extremum to another. Then a parameter optimization algorithm based on the Hamiltonian formulation may still be used. The parameters of optimization are the four initial costates and the final time. μ is always equal to zero and the control switches, depending on the sign of λ_4 and on the sign of C(x,u). But there is no guarantee that such an algorithm will converge since nothing proves that switching the control at t^- when the constraint starts to be violated actually prevents it from being violated at t^+.

To get the general solution, the algorithm must allow the control to drive the system on the constraint for a certain period of time. During this time, $\mu > 0$ and the control is given by $C(x,u) = 0$. For this latest solution, all the effective numerical algorithm like BNDSCO from

Oberle [21], require one to make an initial guess on the structure of the control, ie the number of times the constraint is reached.

One way to approach this initial guessing problem is to try to minimize the violation of the constraint instead of attempting to respect it. For this purpose, the cost is rewritten in:

$$J^* = J + \mu \int_{t0}^{tf} C^2(x,u)\ 1(C)\ dt$$

where $1(C) = 0$ if $C < 0$ and $1(C) = 1$ if $C > 0$ as suggested in [8] § 7.9.

μ is adjusted so as to respect the constraint $C(x,u) < 0$, increased if the constraint is violated in the numerical solution, decreased to improved the retrieval time if C is not violated. A one order gradient algorithm can be used to numerically solve this problem like in [11].

As Bryson points out in [8], this method only gives an approximate solution to the original optimization problem since the algorithm might more focus more on respecting the constraint than on actually minimizing the original cost J. However, it will give an initial guess in the structure of the optimal path, ie how many times the constraint is reached.

From then, the original optimization problem can be solved. If n is the number of times the constraint is reached, the problem becomes a 5+2n parameter optimization problem where the 2n additional parameters are the times t_i^- when the constraint is reached and the t_i^+'s when the constraint is left. The additional conditions to make the problem well posed are at t_i^-'s, $C(x,u) = 0$ and at t_i^+'s, $\mu = 0$.

The program BNDSCO developed by Oberle from the Institute for Applied Mathematics, University of Hamburg and Grimm from the DFVLR, [21] can be used to numerically solve this parametric optimization problem. This numerical code is used by Well and Hoffman

(Virginia Tech.), Calise (Georgia Tech.), Shinar (Technion)... The inputs are the first order differential equations driving the states and costates, and the equality conditions at t_0, t_i^-, t_i^+ and t_f. A solution by steepest ascent is also given by Denham and Bryson [10]. In both cases, μ is given in the interval $[t_i^-, t_i^+]$ by $H_u = \lambda^T f_u + \mu C_u = 0$. So all these solutions are excluded in the case of a linear optimization problem.

Consequently, to keep the freedom of retrieving the sub-satellite at the fringe of the constraint, the cost must be changed so as to avoid a linear optimization problem. Theoretically, for C(x,u)=0, the tether is slack and the system is uncontrollable. However C only is an approximation of the tension constraint and in addition, a thruster is planned to be fired all along the retrieval at 2N to ensure a positive tension.

2.4.2 The Bang-Bang Solution.

2.4.2.1 Choice of the Limits of the Control.

This part addresses two questions: how to deal with the tension constraint in the case of a linear optimization problem, and how many times the control switches in a bang-bang pattern.

The difficulties of solving a linear optimization problem with inequality constraints were previously discussed. Since the control is bang-bang, $u = u_{min}$ or $u = u_{max}$, the constraint can only be reached when $u = u_{max}$, which corresponds to a maximum deceleration. A program can be envisioned which would look for the maximum allowed u_{max} in the interval where $\lambda_4 > 0$. It would automatically reduce u_{max} if the constraint was violated. Would such a program converge? The maximum principal does not prove it since it supposes that u_{max} remains constant on the whole trajectory.

However $C(x,u) = \dddot{L} - 3\,\omega^2 L < 0 \Rightarrow u < 3\,\omega^2 L$ and $\forall\, t, L(t) > L_f$. So, if we take the extremely conservative approach of limiting the deceleration by the gravity gradient tension at the final length, $u_{max} = 3\,\omega^2 L_f \Rightarrow \forall\, t \in [t_0, t_f[\,, u(t) \leq u_{max} < 3\,\omega^2 L(t)$ and the constraint will never be violated except at t_f which is the docking time. If the maximum allowed deceleration is increased, there is a risk that the final pitch angle and pith rate values will be unacceptably large since they are only constrained by the minimization of the cost. A study of time of retrieval versus the maximum allowed deceleration here needs to be carried out.

The natural limitations for u_{min} are the tension and the acceleration the tether and the sub-satellite can stand. A reasonable number is $u_{min} = -.1 m.s^{-2}$. But the author here acknowledges a lack of numerical data on the system.

For $L_f = 10$ m and $\omega = .001$ rad.s^{-1}, $u_{max} = 3.10^{-5}$ m.s^{-2} and $u_{min} = -.1$ m.s^{-2}. (2.19)

At this point, the structure of the bang-bang control still needs to be defined. A two parameter search gave the optimal solution for a constant acceleration retrieval [22]. However, it is not necessarily the optimal solution when the acceleration is left free. To answer to this question, the approach described in § 2.4.1 is used. The control is decomposed in 30 parameters over the interval of retrieval and we try to minimize the cost J using a first order gradient algorithm like the one developed in [11].

2.4.2.2 A First Order Gradient Algorithm.

This algorithm is stated in §7.4 of Bryson and Ho, [8]. The advantage of it is that it does not initially fix the structure of the control. It starts with an initial guess of the control over the 30 intervals and the algorithm updates each of the steps of the parameterized control in order to converge towards the solution.

If $J = \phi[x(t_f), t_f]$ is the cost to be optimized with the final constraint $\psi[x(t_f)] = 0$, let's consider the first variation of

$$J = \phi[x(t_f), t_f] + \nu\psi[x(t_f)] + \int_{t_0}^{t_f} \lambda^T [f(x,u) - \dot{x}]\, dt$$

where ν is a Kune-Tucker parameter used to enforce the solution to meet the final conditions.

With $\delta u = -\dot{\lambda} = -f_x^T \lambda$ and $\lambda(t_f) = \phi_{x(t_f)}$,

$\dot{R} = -f_x^T R$, $R(t_f) = \psi_{x(t_f)}$ and $\forall\, t$, $R(t) = \psi_{x(t_f)}^T \varphi(t_f, t)$,

$$dJ = \left[\phi_{x(t_f)}^T \dot{x} + \nu^T \psi_{x(t_f)}^T \dot{x}\right] dt_f + \int_{t_0}^{t_f} \left[\lambda^T + \nu^T \psi_{x(t_f)}^T\right] f_u \delta u\, dt$$

By taking $\delta t_f = -K_f \left[\phi_{x(t_f)}^T \dot{x}(t_f) + \nu^T \psi_{x(t_f)}^T \dot{x}(t_f)\right]$ and $\delta u = -K_u f_u^T \left[\lambda(t) + R(t)\nu\right]$ with K_f and K_u positive definite matrices,

$$dJ = K_f \left|\phi_{x(t_f)}^T \dot{x} + \nu^T \psi_{x(t_f)}^T \dot{x}\right|^2 + K_u \int_{t_0}^{t_f} \left| f_u^T \left[\lambda(t) + R(t)\nu\right]\right|^2 dt \geq 0$$

So J decreases until $\delta t_f = \delta u = 0$, ie $dJ = 0$.

The final constraint must also be met. A δt_f and δu lead to a $d\psi$ given by:

$$d\psi = \psi_{x(t_f)}^T \dot{x}\, dt_f + \int_{t_0}^{t_f} \psi_{x(t_f)}^T \varphi(t_f, t) f_u \delta u\, dt$$

To meet the constraint $\psi[x(t_f)] = 0$, $d\psi$ is taken proportional to the residue of ψ. By reporting δt_f and δu in the previous equation, we may write:

$$\nu = A^{-1} B$$

with
$$A = K_f \psi_{x(t_f)}^T \dot{x}(t_f) \dot{x}^T(t_f)\, \psi_{x(t_f)} + K_u \int_{t_0}^{t_f} R^T(t) f_u f_u^T R(t) dt$$

$$B = d\psi - K_f\, \psi_{x(t_f)}^T \dot{x}(t_f) \dot{x}^T(t_f) \phi_{x(t_f)} - K_u \int_{t_0}^{t_f} R^T(t) f_u f_u^T \lambda(t) dt.$$

2.4.3 Numerical Results.

The algorithm is run with the following initial conditions:

$$\theta(0) = .3 \text{ rad},$$

$$\dot{\theta}(0) = .1\ \omega \text{ rad.s}^{-1},$$

$$L(0) = 2000 \text{ m},$$

$$\dot{L}(0) = 0 \text{ m.s}^{-1}. \qquad (2.20)$$

and the terminal condition is $L(t_f) = L_f = 10$ m. (2.21)

Using the results of § 2.3.2, the algorithm is initialized in the valley of the cost function corresponding to one tour in the phase plane. The initial guess on the control is taken consistent with the no pushing condition. The length rate is taken as the command in order to reduce the amount of computation by decreasing the order of the system. The true control, $\ddot{L}$, will be the derivative of the computed length rate. The tension constraint will have to be verified a posteriori.

The true retrieval starts with $\dot{L}(0) = 0$. However, in the numerical solution where $\ddot{L}$ is the control, the initial length rate $\dot{L}_i$ is let free so as not to change the nature of the optimization problem. $\dot{L}_i$ will give in fact the time of the first switch t1. If $\dot{L}_i$ turns out to be positive, it will mean that:

$$\int_0^{t_1} \ddot{L}(t)\, dt = \dot{L}_i = u_{max}\, t_1 \quad \text{or} \quad = u_{min}\, t_1 \quad \text{if } \dot{L}_i < 0.$$

Obviously, the larger $|u_{min}|$ or $|u_{max}|$ are, the smaller t_1 is.

The algorithm converges with a final cost J = 1.36 and a docking time $t_f = 1.15$ orbits, for $\dot{L}_i = -3.84\ 10^{-1}$. The final pitch angle and pitch rate are -0.19 rad and 1.31 10-5 rad.s^{-1} respectively, and the final length rate is equal to $-1.67\ 10^{-1}$.

Fig 2.7 shows that the acceleration is almost constant approximately equal to 3.10^{-5} $m.s^{-2}$. The variations are likely due to numerical noise. Consequently, for these initial conditions, the structure of the control is composed of one initial acceleration at u_{min} followed by a constant deceleration at u_{max}. Fig 2.8 shows as expected that the costate λ_4 remains positive as $u = u_{max}$.

The results of this numerical solution confirms the previous assumptions. Fig 2.9 shows that the phase trajectory actually starts with an expanding spiral and then goes to the neighborhood of $(\theta,\dot{\theta}) = (1,0)$. Then it seems to follow the "splitting line"before diverging to come close to (0,0). The target point is actually missed on this example since the final condition is the final length.

This numerical study gives us a confirmation that the control is bang-bang. By adjusting u_{max} at $3\ \omega^2 L_f$, the constraint is taken into account in a simple and effective way. It may be also deduced that for some initial conditions, the control will be an initial acceleration followed by a constant deceleration. However, further studies are necessary to deduce the structure of the control depending on the initial conditions in pitch angle and pitch rate.

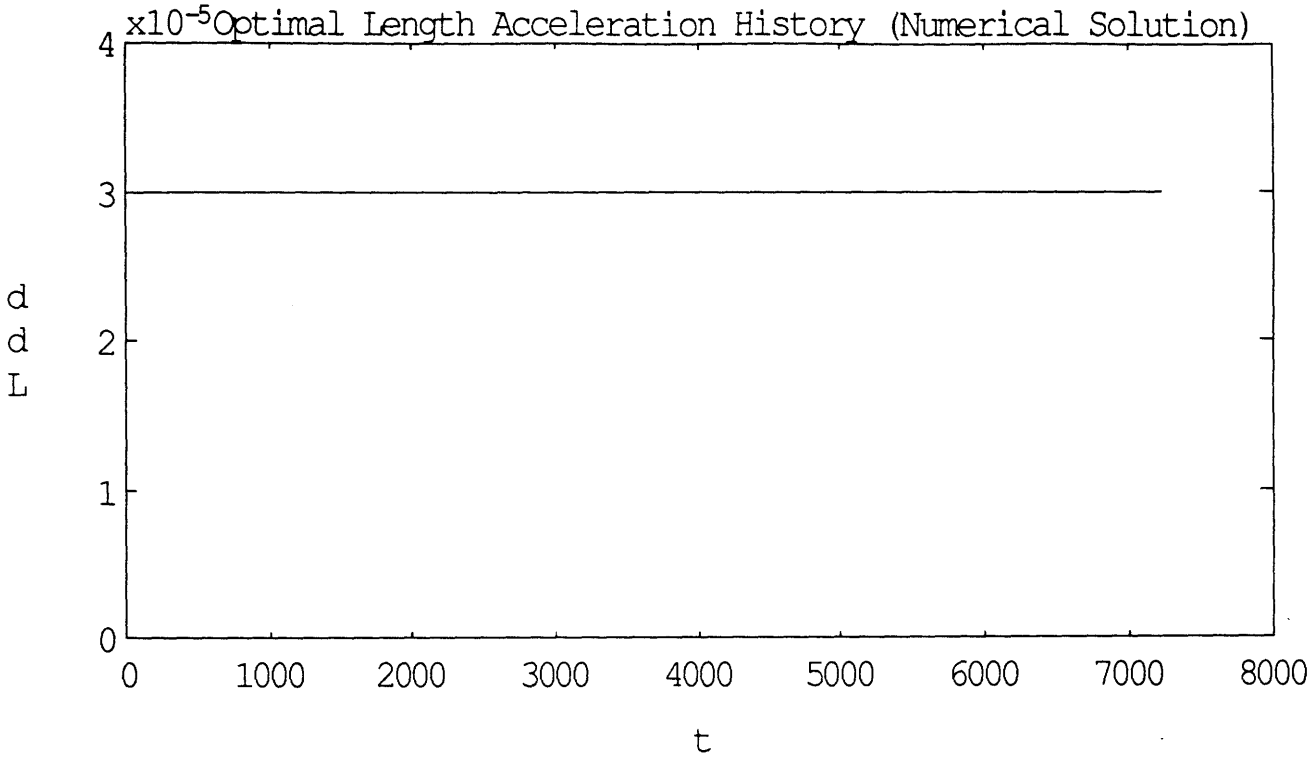

fig 2.7: Optimal retrieval acceleration, numerical solution.

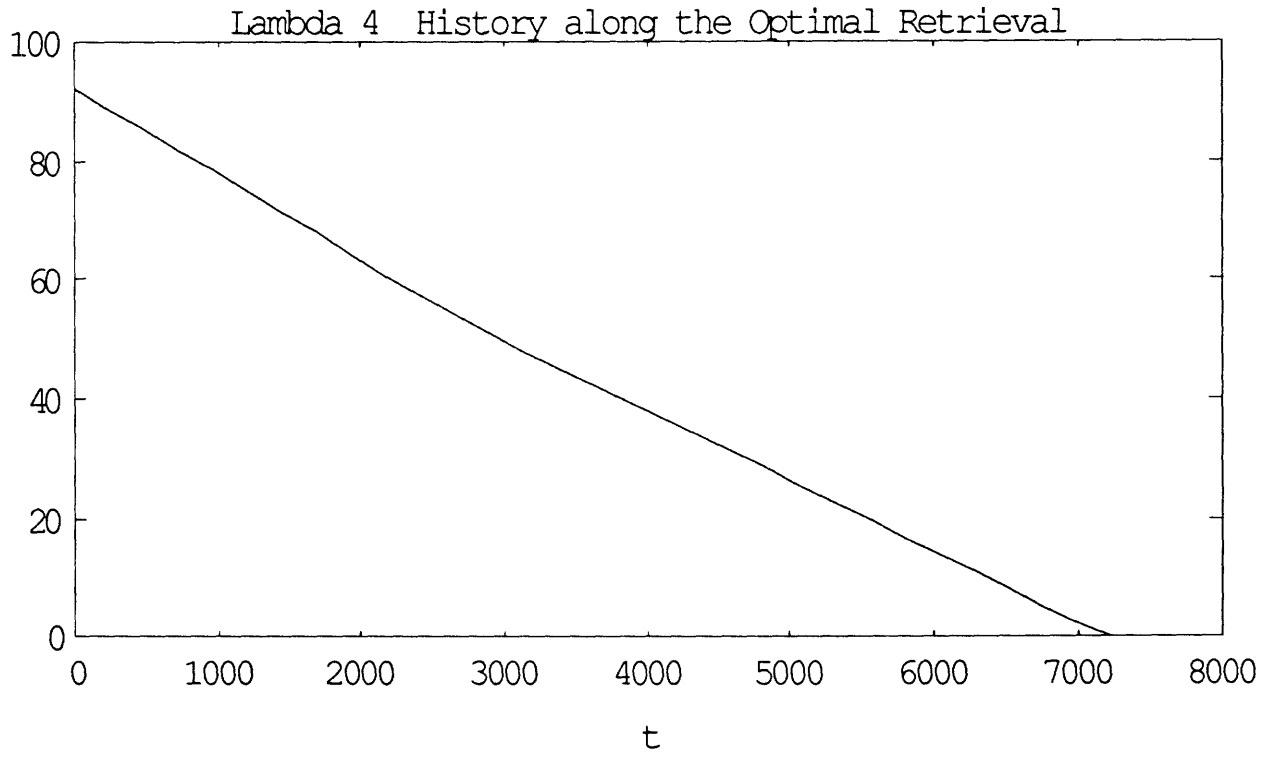

fig 2.8: Costate λ_4 history along the optimal retrieval.

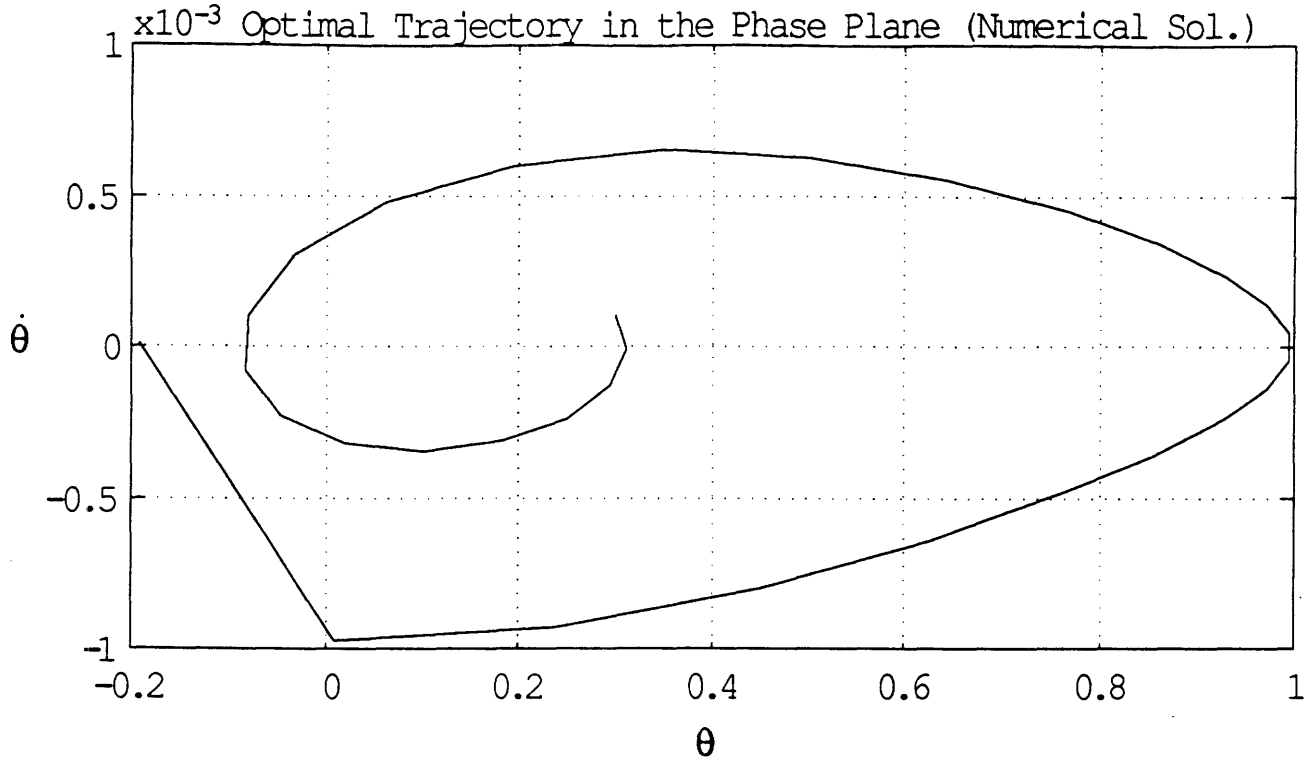

fig 2.9.1: Optimal retrieval phase trajectory.

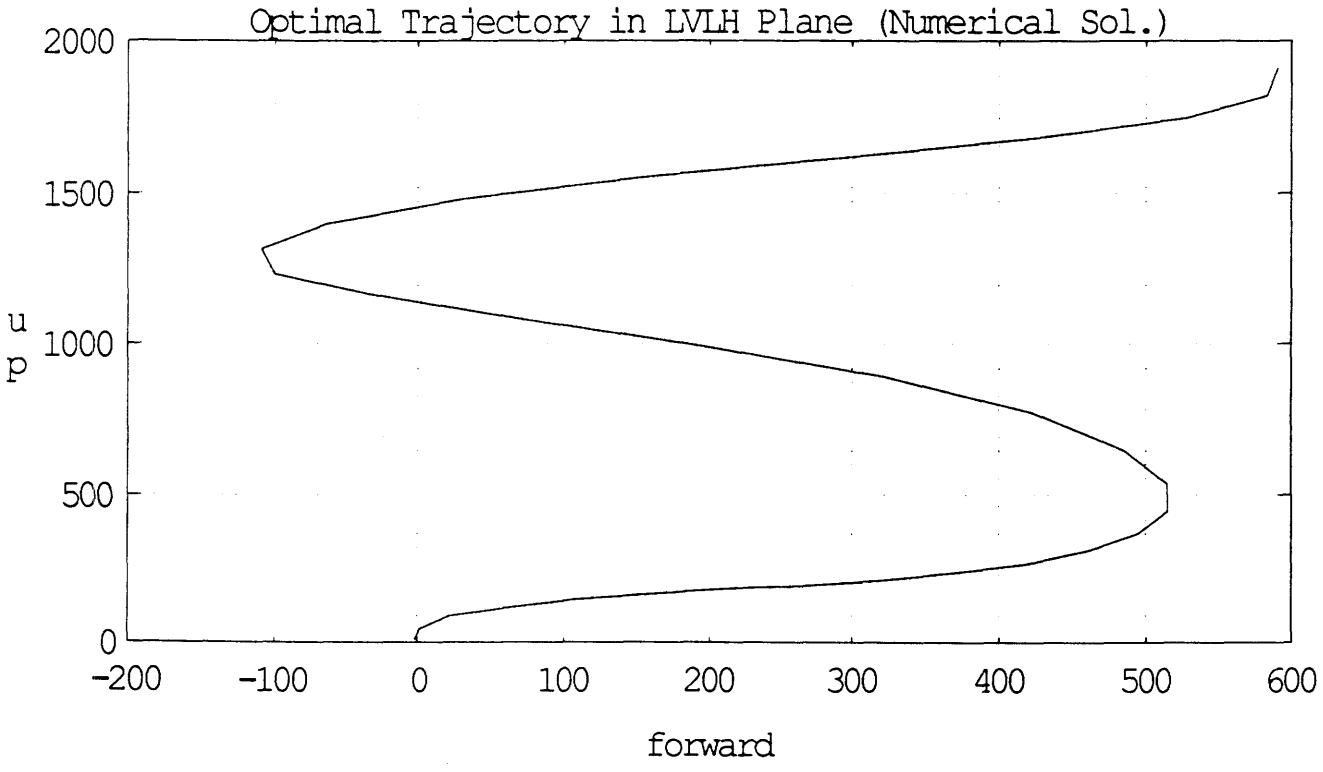

fig 2.9.2: Optimal in-plane retrieval trajectory.

2.4.4 The Reduced Optimal Problem.

2.4.4.1 One Parameter Optimization.

The Hamiltonian analysis revealed that the optimal control is bang-bang. A numerical search of the optimal solution with free initial length velocity was performed, § 2.3.3. The result of which was a constant acceleration retrieval. In the real problem, it is assumed that the initial length velocity is null. The initial length velocity found in the the numerical search could be physically produced by an initial impulse of acceleration, the area of which being equal to $\dot{L}_i$. The time of acceleration would be inversely proportional to the maximum acceleration the system can stand. Consequently, it may be infered that the structure of the control is a constant initial acceleration at u_{min} followed by a constant deceleration at u_{max}, fig (2.10). The constraints are those stated in § 2.4.3. The optimization parameter becomes the time of initial acceleration, t_s.

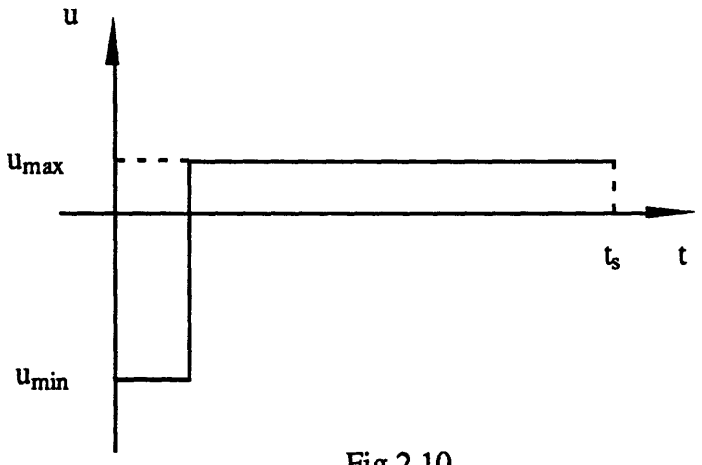

Fig 2.10

This acceleration must be large enough to enable the sub-satellite to reach a distance to the orbiter of L_f = 10 m. However, the final length rate must be higher than -.5 $m.s^{-1}$.

Thus $t_{smin} \le t_s \le t_{smax}$ with:

$$t_{smin} = \sqrt{\frac{\left(\frac{\dot{L}_{fmax}}{u_{max}}\right)^2 + \frac{2}{u_{max}}(L_0 - L_f)}{\left(\frac{u_{min}}{u_{max}}\right)^2 - \frac{u_{min}}{u_{max}}}} \quad \text{and} \quad t_{smax} = \sqrt{\frac{\frac{2}{u_{max}}(L_0 - L_f)}{\left(\frac{u_{min}}{u_{max}}\right)^2 - \frac{u_{min}}{u_{max}}}} \qquad (2.22)$$

The stopping condition is $L(t) = L_f = 10$ m. For an optimal t_s, the total time of retrieval t_f, is given by:

$$t_f = t_s - \frac{u_{min}}{u_{max}} t_s - \sqrt{\left[\left(\frac{u_{min}}{u_{max}}\right)^2 - \frac{u_{min}}{u_{max}}\right] t_s^2 - \frac{2}{u_{max}}(L_0 - L_f)}, \qquad (2.23)$$

and the impact velocity:

$$\dot{L}_f = - u_{max} \sqrt{\left[\left(\frac{u_{min}}{u_{max}}\right)^2 - \frac{u_{min}}{u_{max}}\right] t_s^2 - \frac{2}{u_{max}}(L_0 - L_f)}. \qquad (2.24)$$

For the considered system:

$u_{min} = -.1$ m.s^{-2},

$u_{max} = 3.10^{-5}$ m.s^{-2} so as to respect the tension constraint,

$L_i = 2000$ m,

$L_f = 10$ m. (2.24.1)

Thus, 3.5 s $\le t_s \le$ 6.1 s and 3,600 s $\le t_f \le$ 11,500 s or .57 orb $\le t_f \le$ 1.83 orb.

For $\theta(0) = .3$ rad and $\dot{\theta}(0) = .1\ \omega$ rad.s^{-1}, the minimum cost J is equal to 1.36 for an optimal time of acceleration $t_s = 3.8367$ s. The final retrieval time $t_f = 7{,}300$ s = 1.15 orb. These results are identical to those of the numerical solution of § 2.4.3 as expected. The optimal solution in different coordinates is given by fig 2.11. Fig 2.11.1 and 2.11.2 show that the sub-satellite does one period of oscillation before following the final retrieval path starting at $\theta \approx 1$ rad. This final retrieval path has the same characteristics as in § 2.4.1.

The final path leaves the "splitting line" too late to be able to reach the point (0,0) in the phase plane. In this case, $\theta_f = -.20$ rad and $\dot{\theta}_f = -4.44\ 10^{-5}$ rad.s^{-1} with $\dot{L}_f = -1.67\ 10^{-1}$ s^{-1}. It turns out that the optimal problem as stated does not enable us to reach our target point (0,0).

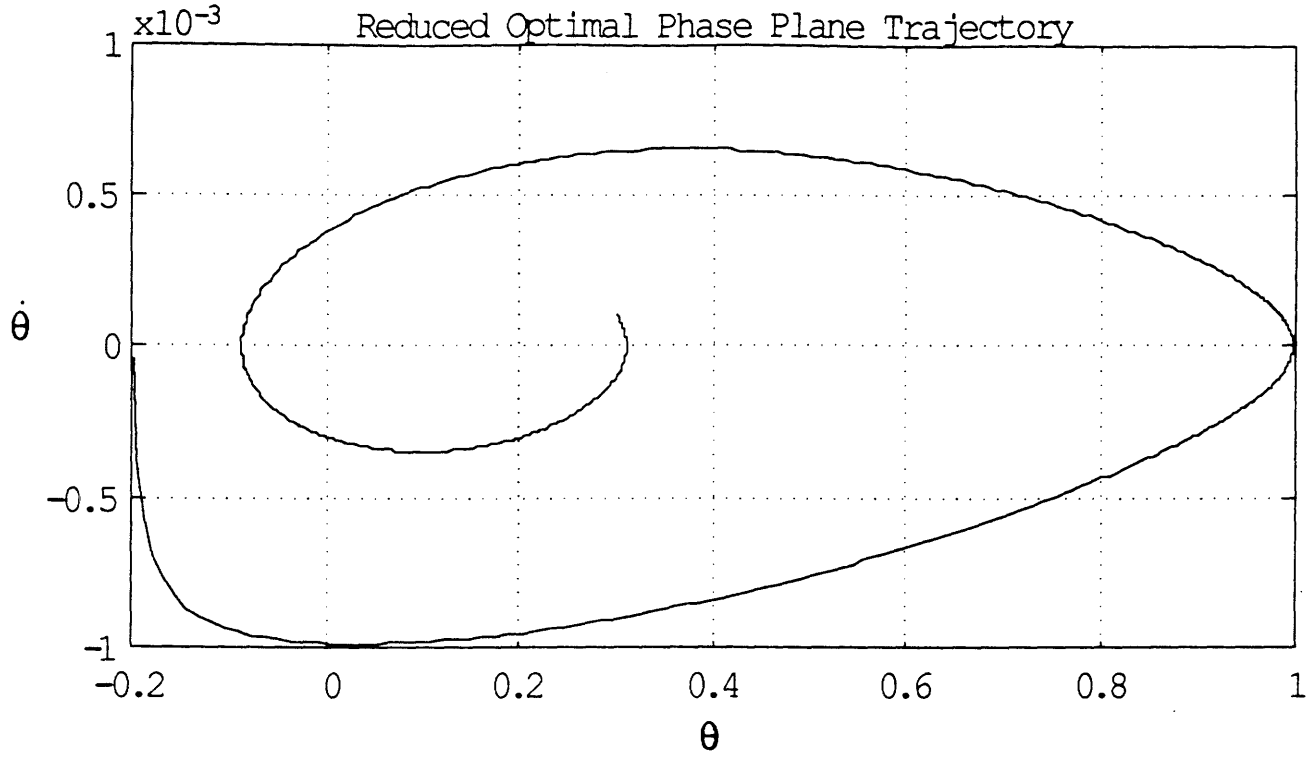

fig 2.11.1: Reduced optimal phase plane trajectory.

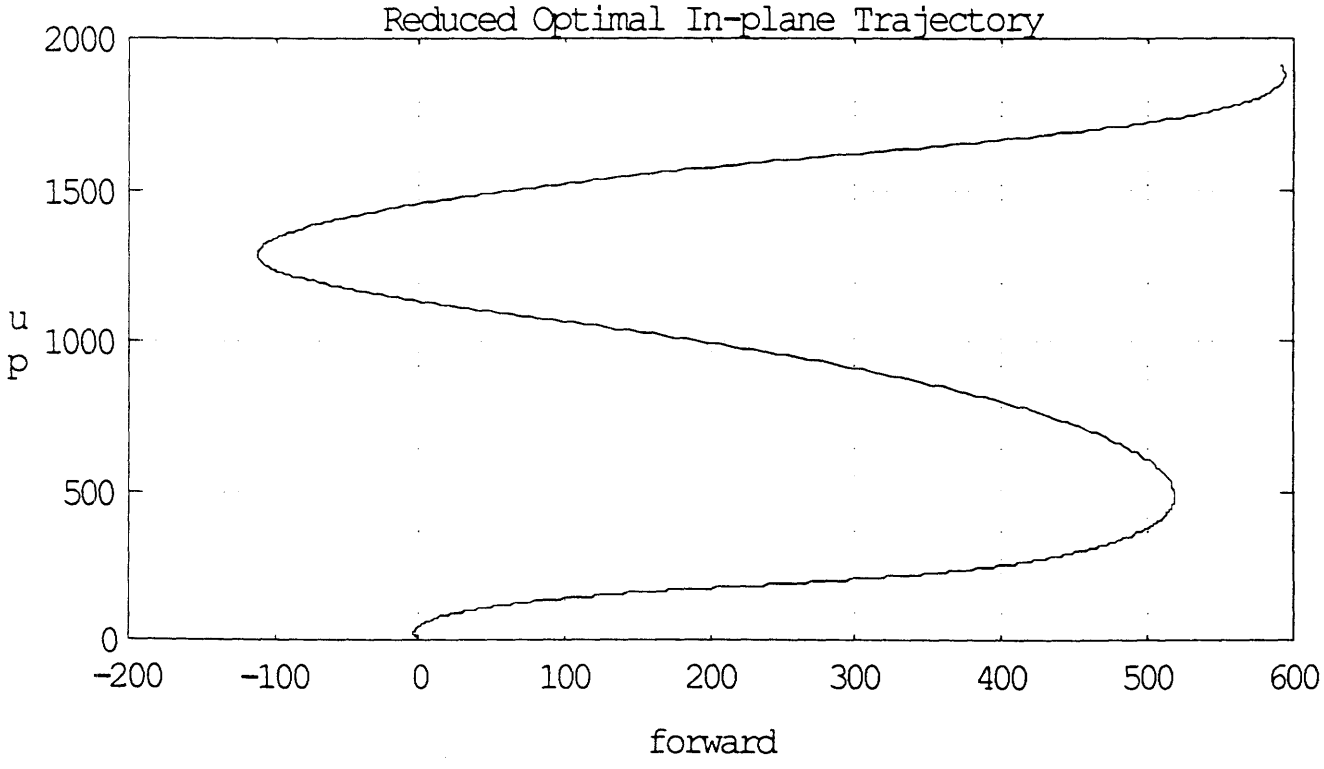

fig 2.11.2: Reduced optimal in-plane trajectory.

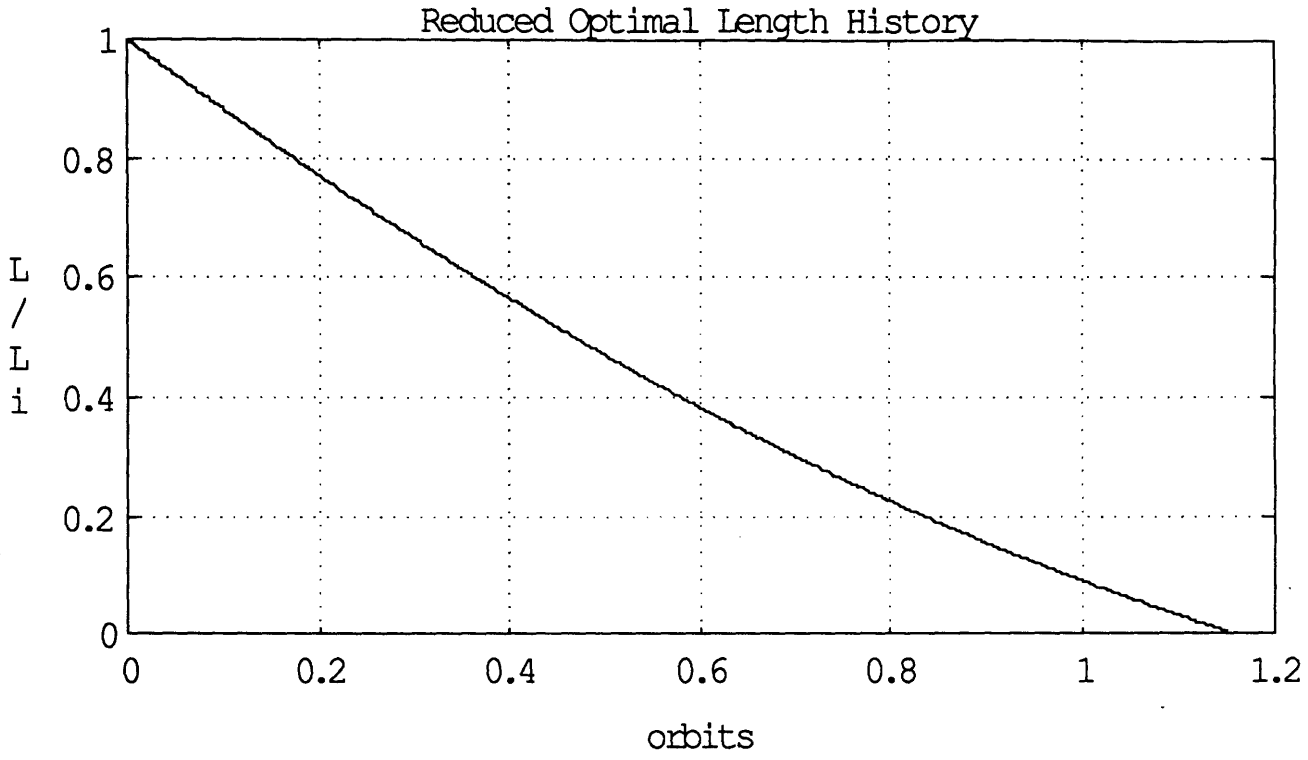

fig 2.11.3: Length history along the reduced optimal trajectory.

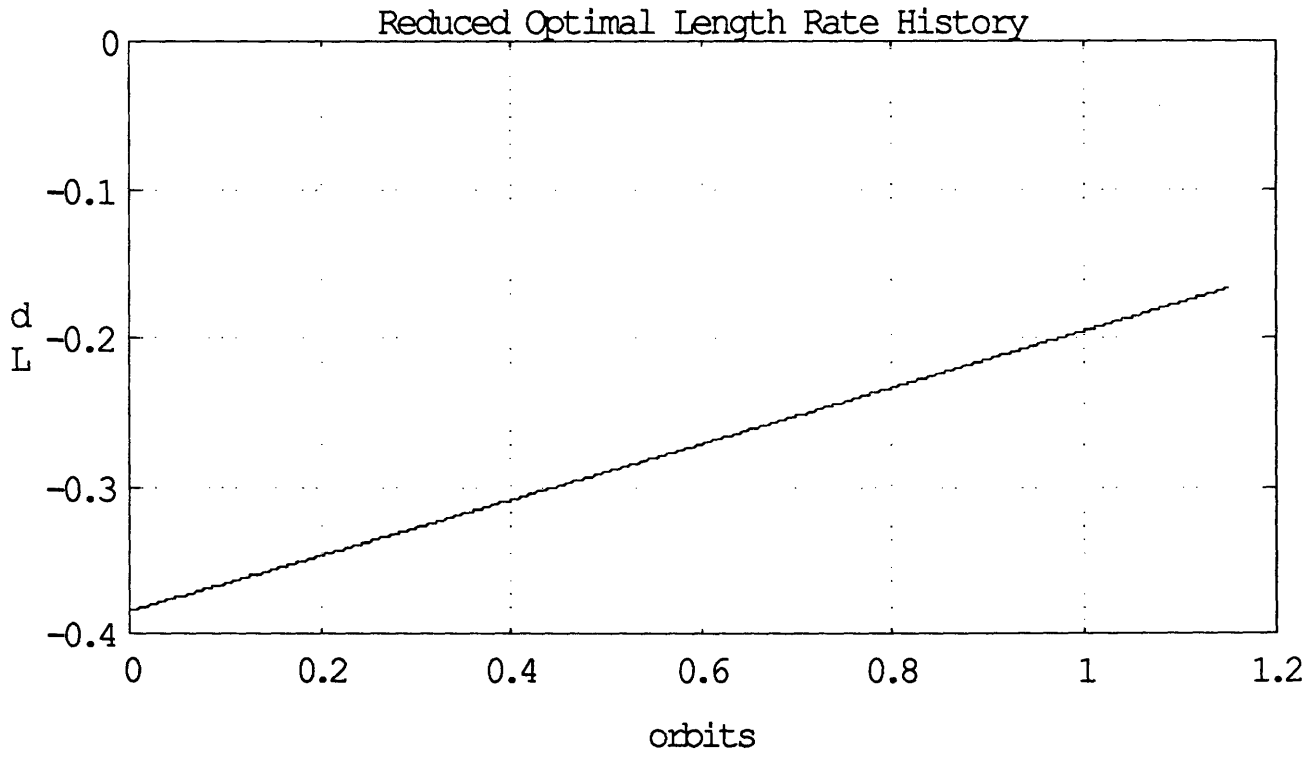

fig 2.11.4: Length rate history along the reduced optimal trajectory.

2.4.4.2 Sensitivity Issue.

The unstable nature of the system results in a high sensitivity of the cost to parameter variations. The plot of the cost function versus the time of acceleration fig 2.12 appears to be similar to that of fig 2.5. However, it only shows the first valley since the maximum deceleration was directly taken high enough. Fig 2.13 gives a zoom of fig 2.12 in the minimum region. In $\frac{4}{100}$ s the cost is multiplied by a factor of 1000. Consequently, the tolerance interval of t_s is unrealistically small. In fact, fig 2.13 shows the presence of two local minima. For t_s = 3.808 s, the retrieval path leaves the splitting line too late fig 2.14, whereas between the two local minima, t_s = 3.825 s fig 2.15, the retrieval trajectory diverges towards negative pitch rate.

To have a reasonable margin of tolerated error on t_s, it would be attractive to be able to flatten the cost function in the area of small cost. Very high cost, over 10^4, corresponds to divergent retrieval path. In this case, the path follows an expanding spiral in the phase plane (fig 2.2), which directly diverges instead of going through the premisses of the point (1, 0). Near the two minima, the cost depends on where the path actually leaves the splitting line before following a quickly divergent path in terms of pitch rate, (fig 15). If the splitting line is left too early, θ will diverge before the final length is reached. On the other hand, if the splitting line is left too late, the final point will eventually be far from the target point so that the cost will be also high.

The cost function might be flattened by stopping the retrieval algorithm before the path gets onto the splitting line in order to avoid the effect of the final divergence. Then the sub-satellite will be retrieve up to docking along an arbitrary nominal trajectory, like an exponential one, using a proper feedback to stabilize the system about this nominal trajectory. In this approach, the retrieval is only partially optimized.

Keeping the second order system analogy, the stopping condition becomes:

$$\delta = \frac{\dot{L}(t)}{\sqrt{3}\,\omega\, L(t)} = -1 \qquad (2.25)$$

In order to have the necessary initial energy to reach the state $\delta = -1$, t_s must meet the following condition:

$$t_s \geq \sqrt{\frac{\frac{2\,L_0}{u_{max}} - \frac{1}{3\,\omega^2}}{\left(\frac{u_{min}}{u_{max}}\right)^2 - \frac{u_{min}}{u_{max}}}}$$

Fig 2.16.2 shows that the cost is actually flattened in the region of the minima leading to a tolerance interval of $\frac{1}{10}$ s for a cost variation of 3.3.

To summarize, an optimal trajectory for a one parameter optimization problem meeting the specified initial conditions and constraints was found. The resulting final retrieval time is equal to 1.15 orbits for the initial conditions (2.20) and the values (2.24.1) of the maximum allowed controls The pitch rate and pitch angle do not diverge during the retrieval and reach reasonable final values equal to $\theta_f = -.23$ rad and $\dot{\theta}_f = -.6\ 10^{-4}$ rad.s^{-1}.

By stopping the optimized retrieval scheme before the end ($\delta = -1$), the sensitivity of the optimal solution is reduced. This second solution relies on the existence of an appropriate feedback to complete the retrieval up to docking, the same feedback as the one used to stabilize the sub-satellite about the optimal retrieval trajectory.

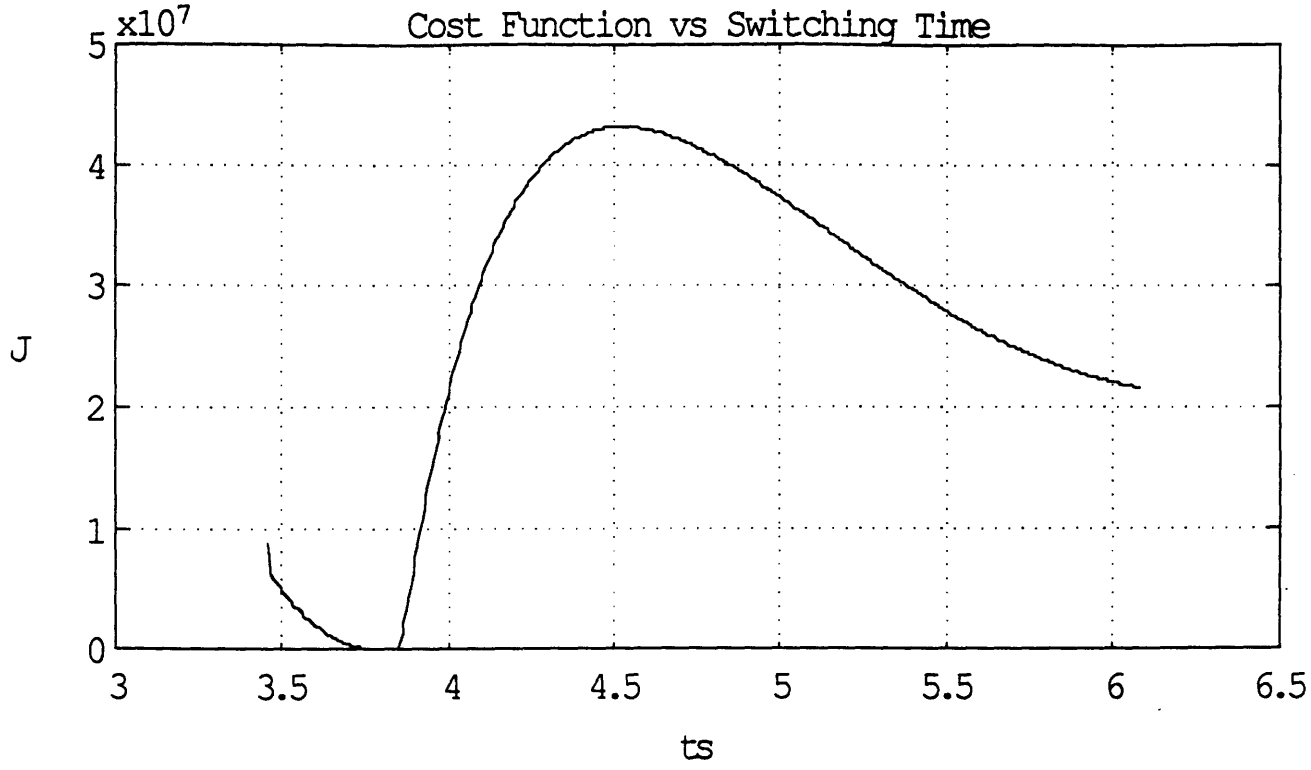

fig 2.12: Cost function vs switching time t_s for initial conditions $(\theta,\dot{\theta})_i = (.3,.1\omega)$.

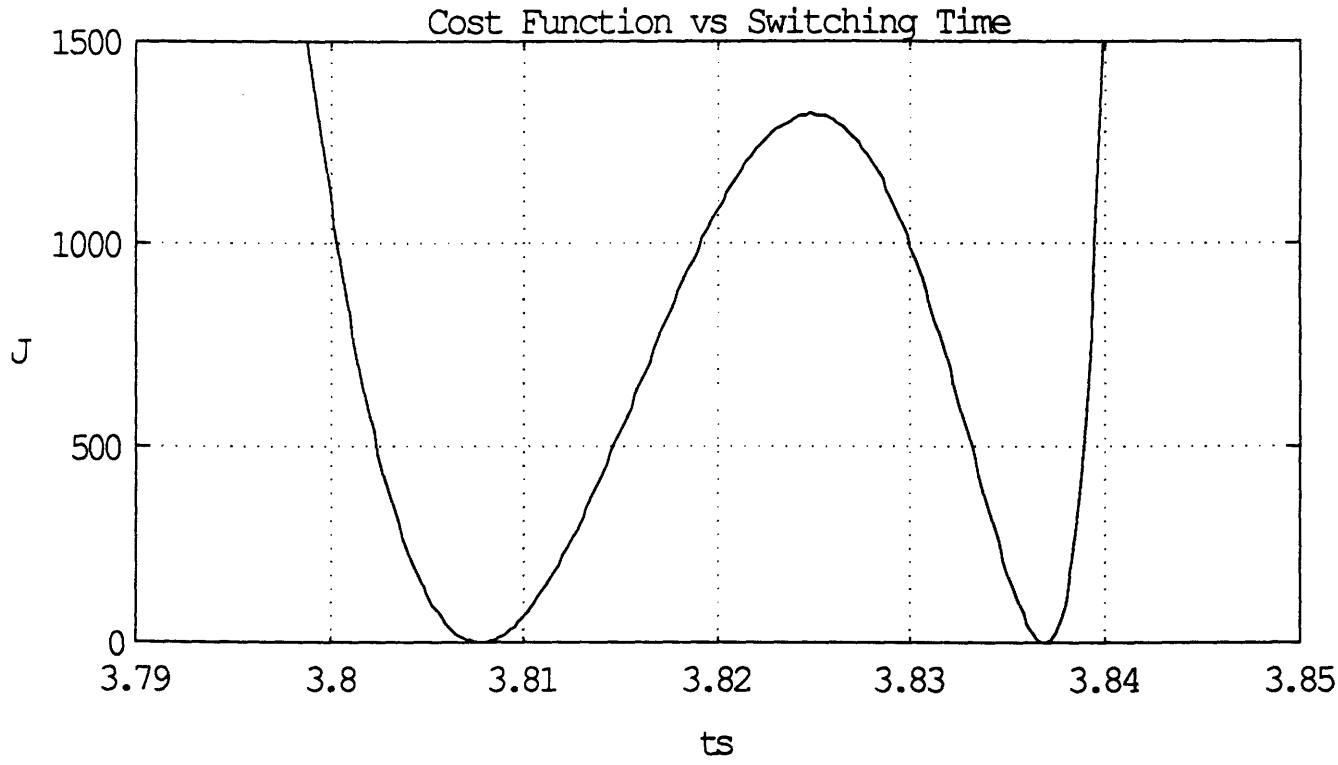

fig 2.13: Cost function vs switching time in the region of minima.

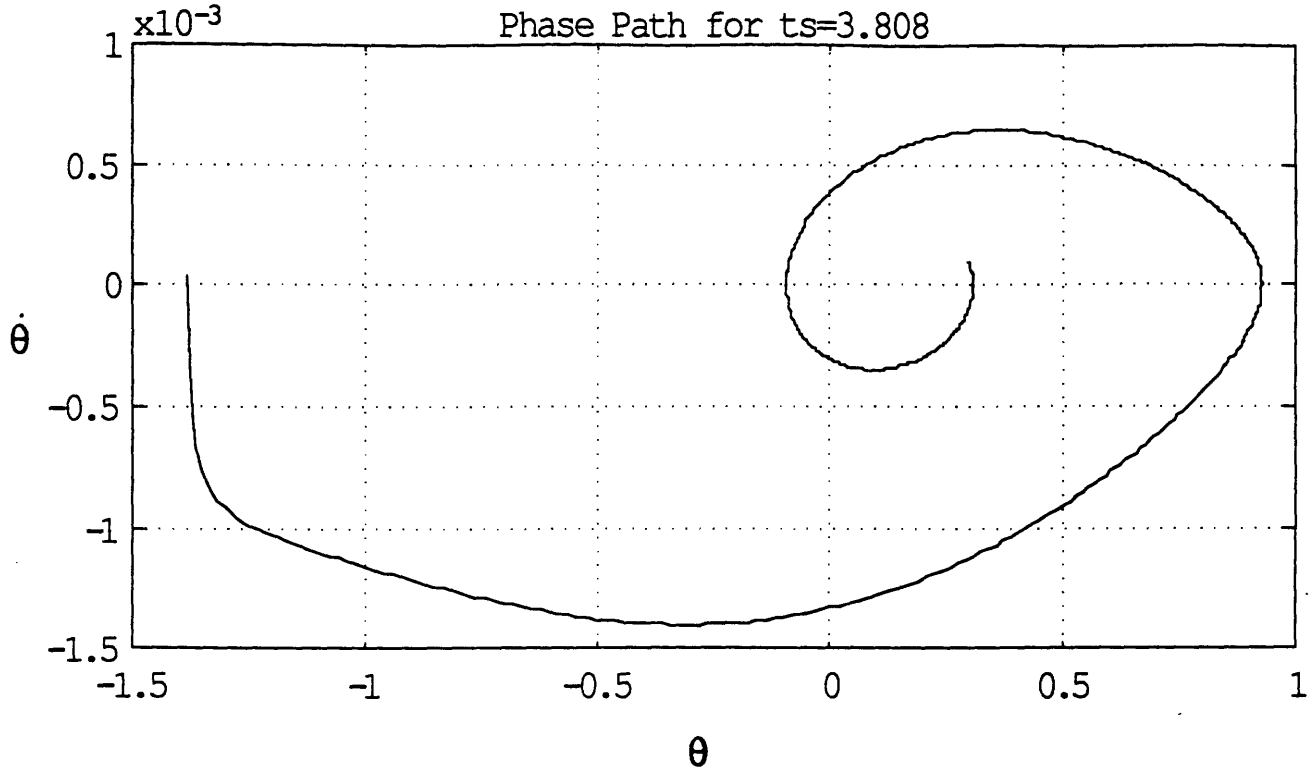

fig 2.14: Phase plane trajectory corresponding to the second minimum.

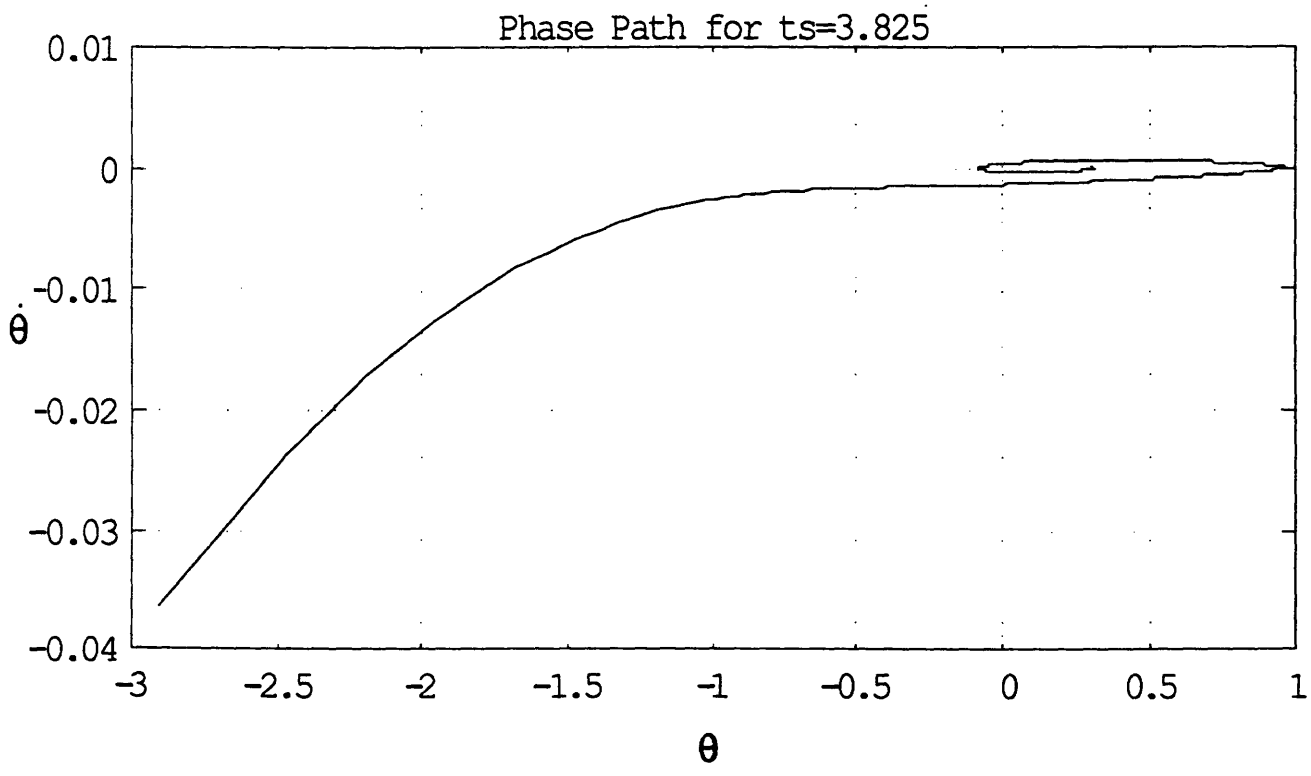

fig 2.15: Phase plane trajectory between the two minima of the cost function.

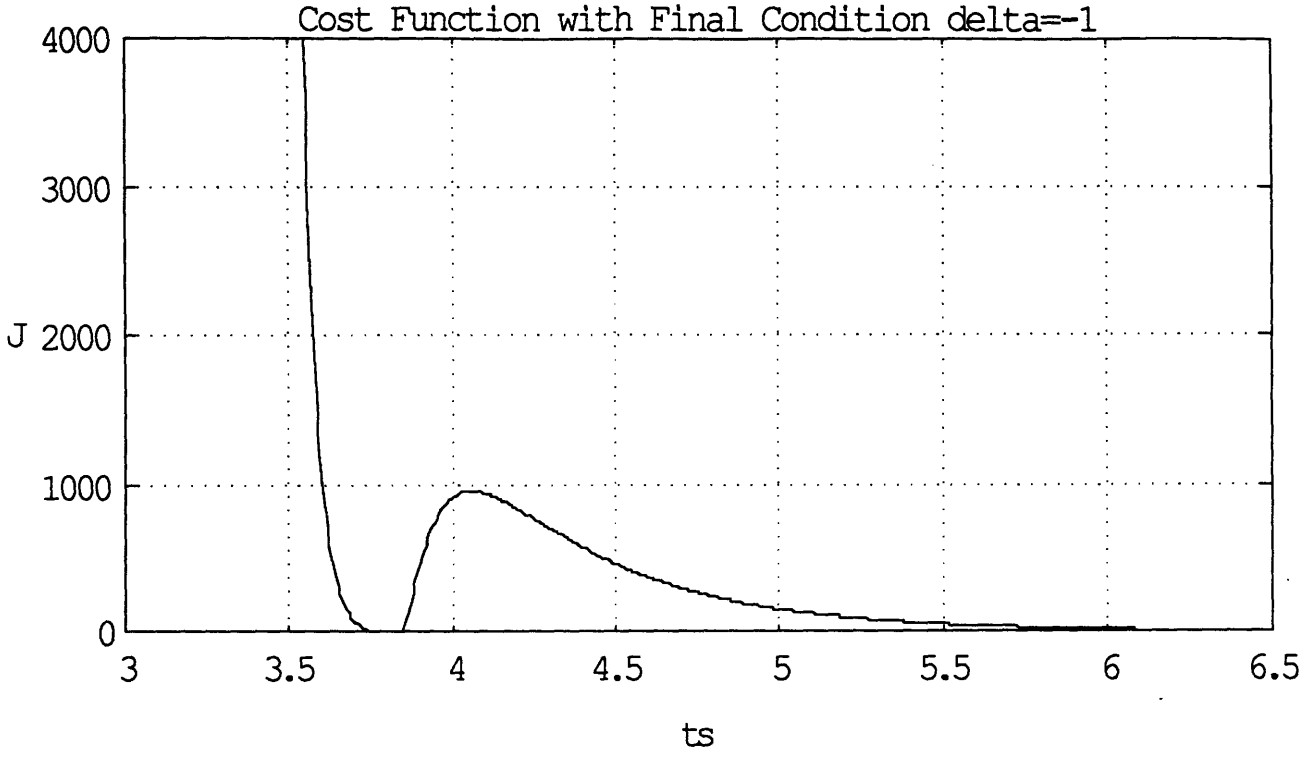

fig 2.16.1: Cost function vs switching time with final condition $\delta = -1$.

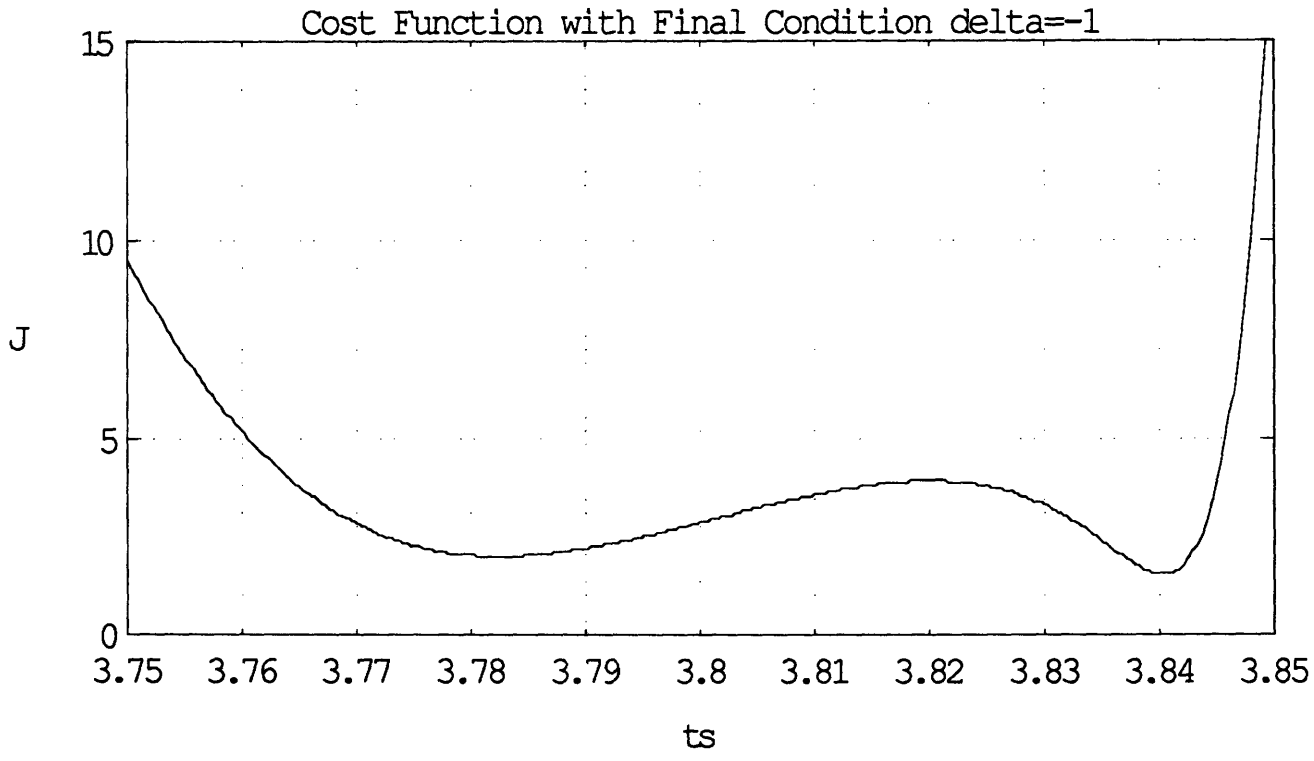

fig 2.16.2: Cost function with final condition $\delta = -1$ in the minimum region.

2.5 A Proposed Sub-optimal Retrieval Scheme.

2.5.1 Analysis.

The structure of the cost function J leads to a trade-off between minimizing the total retrieval time t_f and minimizing the final pitch angle and pitch rate. It would be interesting to reach at t_f the point (0,0) in the phase plane. One solution would be to state $\theta_f = 0$ and $\dot{\theta}_f = 0$ as additional constraints. But in this case, does our problem have a solution for constant deceleration retrieval after an initial acceleration?

The variation of t_s corresponds in fact to a variation of the final impact velocity. The actual initial and final conditions are fairly strict since on one state variable, the length, both final and initial conditions are fixed. It may be interesting to determine the area of permissible initial conditions θ_0 and $\dot{\theta}_0$ versus $\dot{L}_f$ for all constant acceleration retrieval trajectories with final conditions $(\theta,\dot{\theta})_f = (0,0)$. Fig 2.17.1. Since it is one parameter scanning, this area is a line of points in the phase plane. Therefore, if the initial conditions in the phase plane are not on this line, the new optimal problem with $(\theta,\dot{\theta})_f = (0,0)$ and the specified structure of the control, has no solution.

The minimum retrieval time corresponds to a maximum impact velocity. This maximum allowed impact velocity is, in fact, the hardest constraint on the minimization of the time of retrieval. With the experience acquired so far, it is reasonable to think that the final switch for the bang-bang control will be a switch from a constant acceleration to constant deceleration. The line on fig 2.17 splits the phase plane into two regions. To get to the final point (0,0), this line must be reached at L = 2000 m. So if the initial conditions are inside the line in the phase plane, the retrieval path will have to expand to reach a point on the line at L = 2000m. It is a natural behavior since § 2.3.1 shows that as long as θ_{eq} exists, the phase trajectory is a kind of expanding spiral. On the other hand, if the initial conditions are outside the line, the system will

have to loose energy. So the control will switch several times since without using any thrusters, the remaining way to loose energy is pumping. In both cases, to get to the required position in the phase plane is time consuming.

The new idea would be to use the thrusters at the beginning to reach the necessary entry point of the trajectory which ends at the point (0,0) in the phase plane, before starting to retrieve. The necessary fire time would be very small and the advantage would be a high reduction of the total retrieval time.

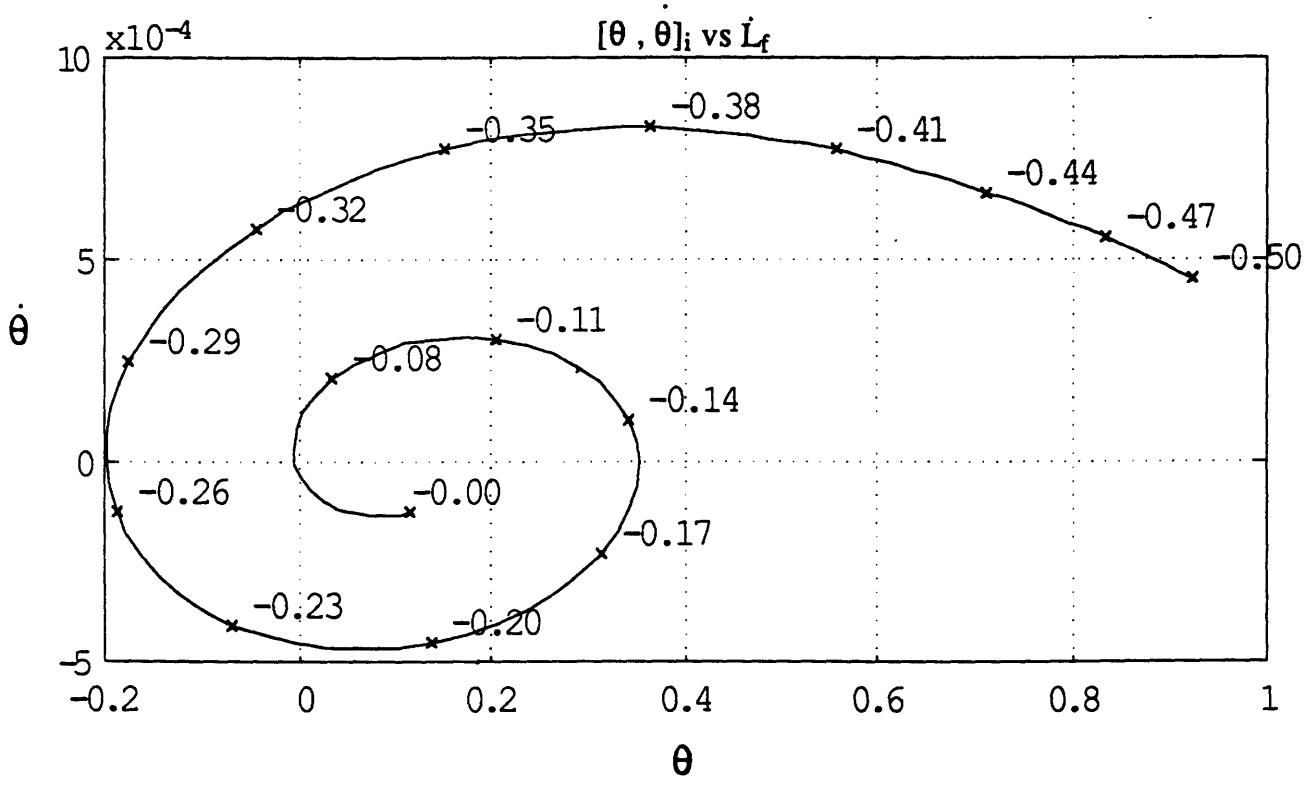

fig 2.17: Initial points in the phase plane vs final impact velocity for retrieval trajectories with L_i = 2000m and final pitch angle and pitch rate equal to zero.

2.5.2 Retrieval Scheme Statement.

The thrusters can be on and off, giving an impulse of acceleration. The resulting trajectories in the phase plane are a set of very steep parabola, almost vertical. Consequently, the following retrieval scheme may be envisioned: first, fire the tether-normal thrusters and coast at constant length to get to the entry point. Then retrieve with a constant acceleration followed by a constant deceleration. It is still a one parameter optimization problem since $\dot{L}_f$ is free, which corresponds to a free t_s and also to a free point on the previous set of starting point. This scheme may vary depending on the initial conditions in the phase plane. The period of the coasting part decreases with the diameter of the coasting path in the phase plane (cf § 2.3.1) and the retrieval time increases when $|\dot{L}_f|$ decreases. However the retrieval time increases faster than the period of coasting. Fig 2.18 shows the total retrieval time, ie firing, coasting and retrieval, versus the optimization parameter $\dot{L}_f$ for the initial conditions $\theta(0) = .3$ rad, $\dot{\theta}(0) = .1\ \omega$ rad.s^{-1}, $L(0) = 2000$ m and $\dot{L}(0) = 0$ m.s^{-1}.

The minimum time retrieval scheme is fire first, then coast with constant length and finally retrieve with a maximum final impact speed. The "entry point" for starting retrieval for all initial conditions is $\theta_0 = .9$ rad and $\dot{\theta}_0 = 4.5$ rad.s^{-1}. There is a firing trajectory going through this point in the phase plane, called line A. The complete retrieval scheme is the following: for $\theta_0 \in$ [-.9945 .9228] rad, fire thrusters to get to the coasting trajectory going through the entry point, coast and then retrieve. For $\theta_0 <$ -.9945 rad, coast until $\theta_0 =$ -.9945 rad, then fire thruster to get to the coasting trajectory, coast and then retrieve. For $\theta_0 >$ .9928 rad, coast up to line A, fire thruster along line A and then retrieve. Consequently, this scheme enables us to retrieve the satellite whatever the initial conditions are. For $\theta_0 \in$ [-.9945 .9228], the total retrieval time is included in the interval [.5723 .9572] orbits. Fig 2.19.

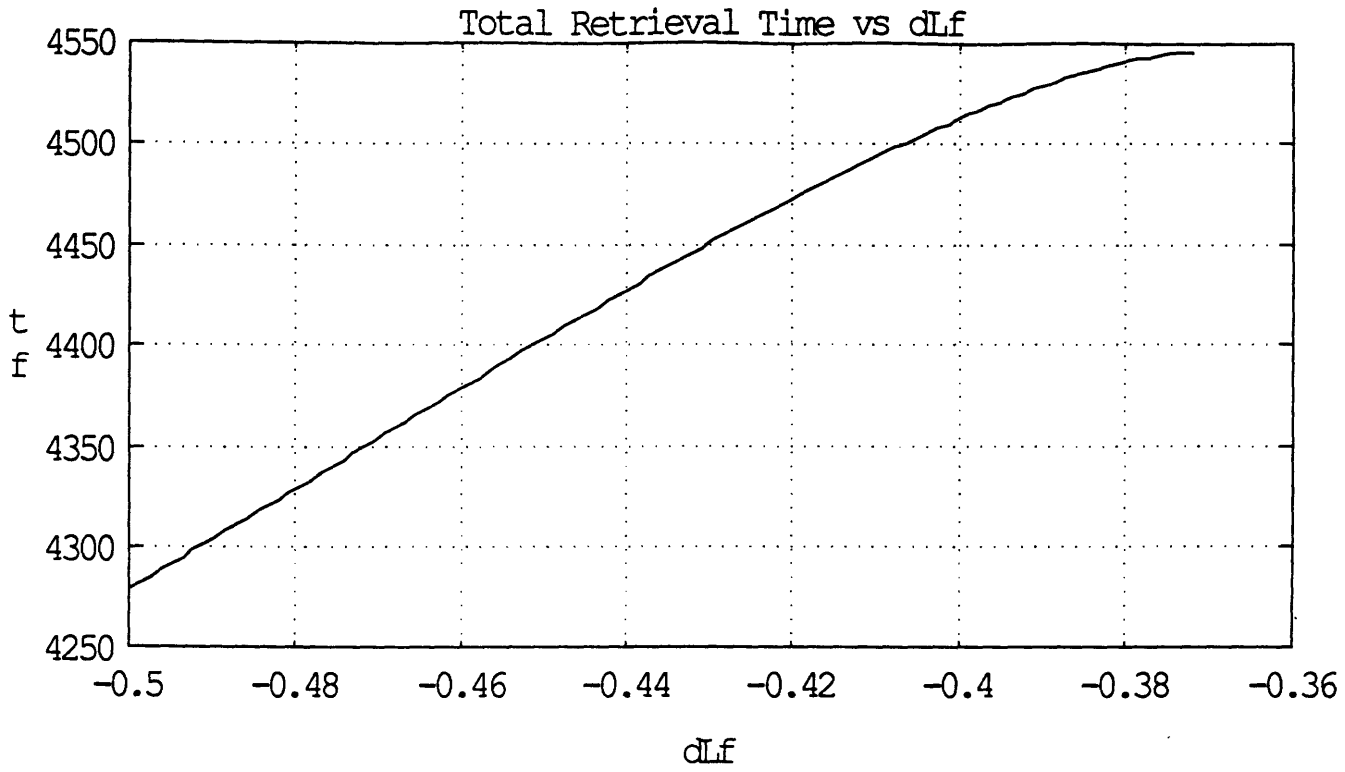

fig 2.18: Total retrieval time, thrusting, coasting and retrieving, vs final impact velocity.

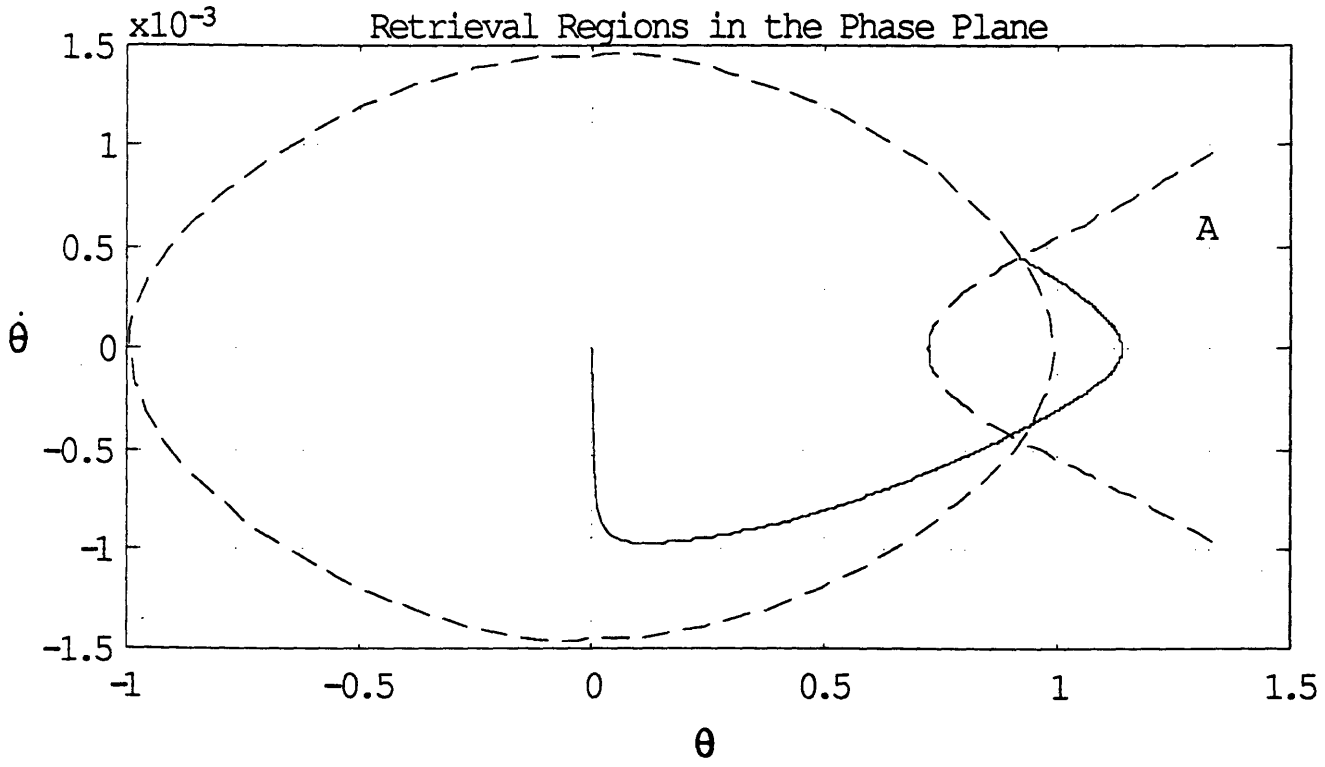

fig 2.19: Limits of regions of retrieval.

2.5.3 Example of Retrieval.

To reach the coasting trajectory which gets to the entry point, two thruster systems are available. An on-satellite thruster system delivers a thrust level resulting in a maximum angular acceleration of 4.10^{-3} rad.s^{-2} when the primary attitude control system of the orbiter leads to a maximum angular acceleration of 77.10^{-3} rad.s^{-2}.

Fig 2.20 shows an example of retrieval for $(\theta,\dot{\theta}/\omega) = (.3,.1)$ with $L_i = 2000$ m and $\dot{L}_i = 0$ m.s^{-1}. Using on-satellite thrusters, the firing time is equal to 884s for a coasting time equal to 256 s. The reel-in part takes .57 orbits and the whole retrieval takes .75 orbits. On the other hand, with on orbiter thrusters, the firing time is reduced to 33 s and the coasting time to 650 s leading to a total retrieval time equal to .68 orbits. In the on-satellite thruster solution, the gravity gradient is non-negligeable with respect to the angular acceleration given by the thrusters and therefore slows down the satellite motion. The fuel consumption in m.s^{-1} is given by:

$$C = \int_{t_0}^{t_f} L(\tau)\, u_\theta(\tau)\, d\tau$$

With on-satellite thrusters, the consumption is $C_s = 3.54$ m.s^{-1} whereas the consumption with orbiter thrusters is $C_s = 2.54$ m.s^{-1}. Consequently, the orbiter thrusters seem to be more appropriate for this part of the mission.

Overall, this sub-optimal retrieval scheme leads to a significant improvement of the time of retrieval of .47 orbits with respect to the solution of § 2.4, at the expense of a fuel consumption of 2.54 m.s^{-1}.

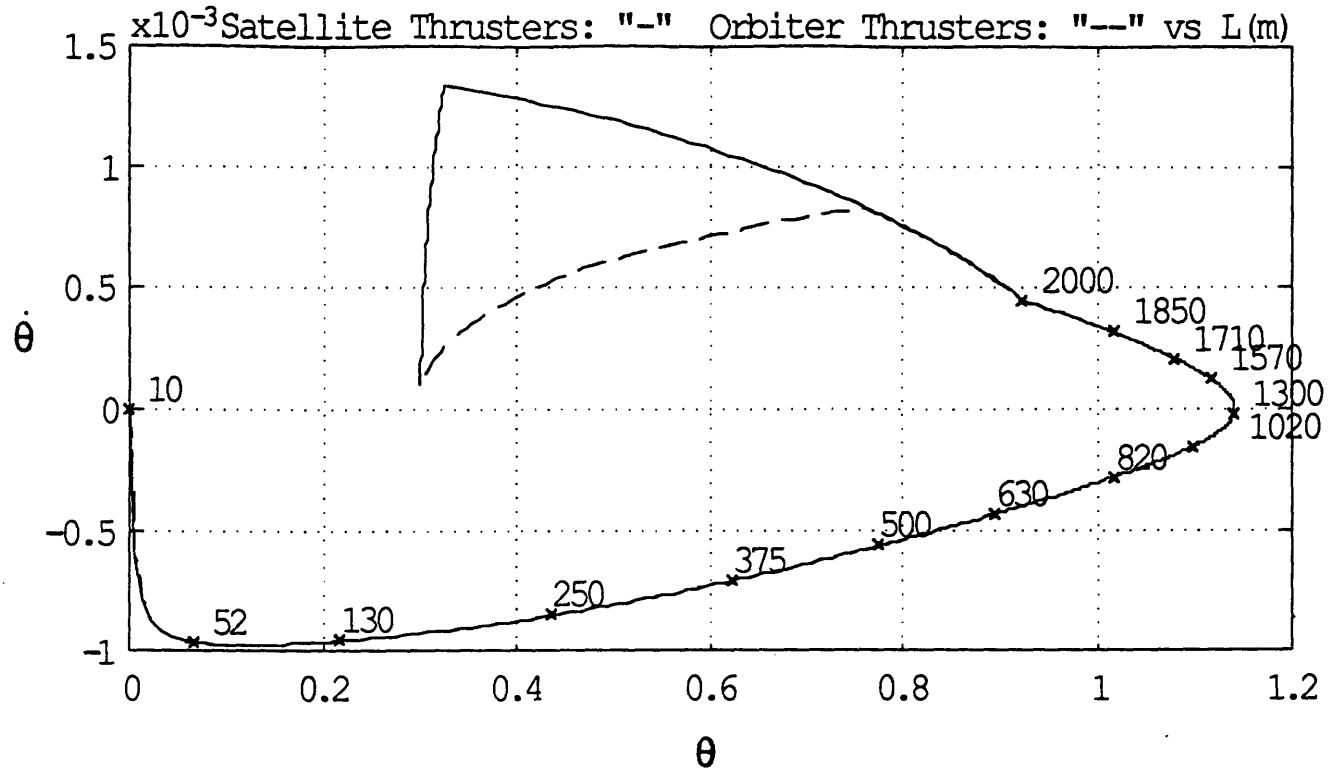

fig 2.20: Example of retrieval in the phase plane with $(\theta,\dot{\theta})_i = (.3,.1\omega)$.

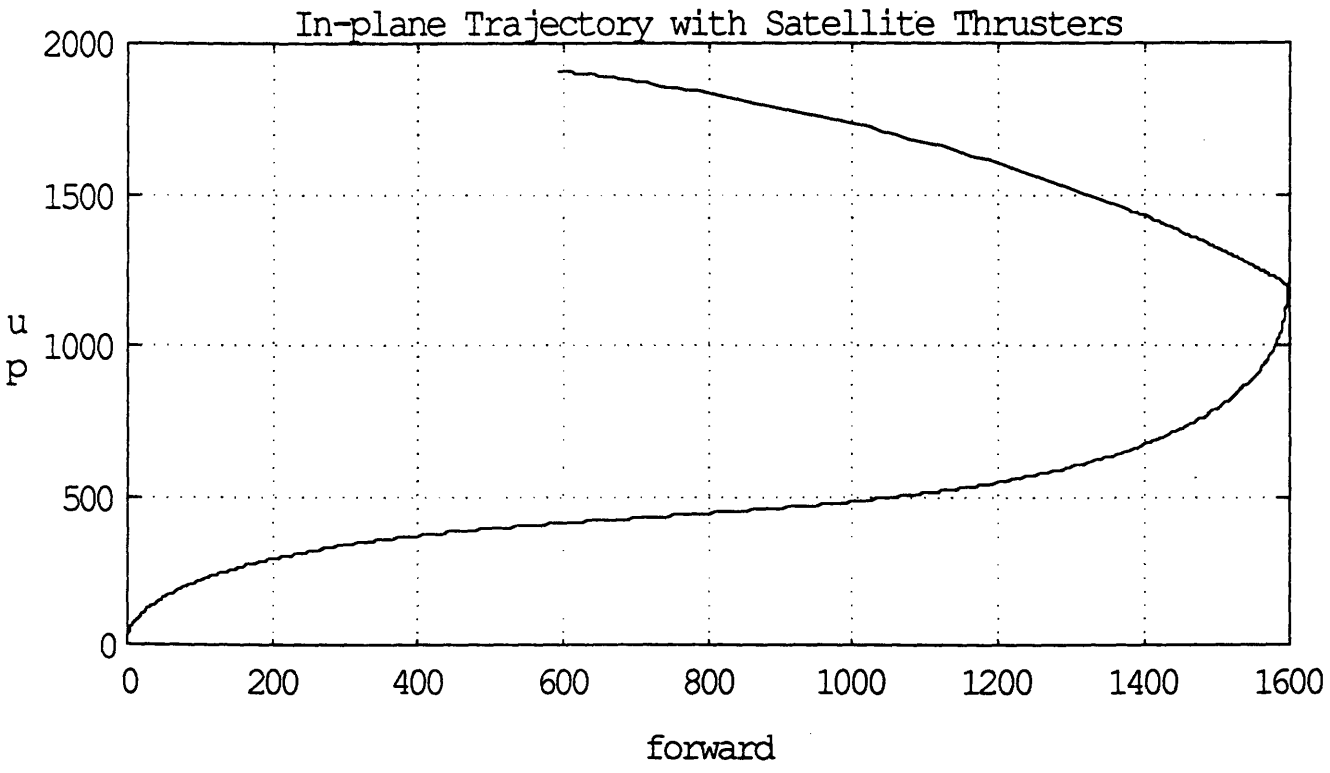

fig 2.21: Example of retrieval in the in-plane LVLH with $(\theta,\dot{\theta})_i = (.3,.1\omega)$.

2.6 Conclusion and Future Work.

The sub-optimal algorithm described in § 2.5.2 enables to retrieve the sub-satellite in less than one orbit at the expenses of a small fuel consumption. It proposes to fire the in plane thruster and to coast at a constant length in order to position the sub-satellite at a specific point in the phase plane. Then reel-in part of the retrieval can start with an initial acceleration on the length followed by a constant deceleration. This last part of the retrieval takes 0.57 orbits. The coasting part takes a maximum of .33 orbits and the firing part a maximum of 38 s. Consequently, the whole retrieval time is included in the interval [0.57 0.91] orbits.

Formally, the sub-satellite can be retrieved without using the thrusters. Cf § 2.4.2 and [22]. However, the solution is very sensitive to the parameter of optimization. So far, only an open loop analysis was performed without taking into account model error and natural disturbances. But in any case, we cannot avoid using the thrusters since a realistic implementation requires the use of a feedback loop, using thrusters as actuators, in order to keep the system on the optimal or sub-optimal trajectory we designed. Consequently using the thrusters to design a retrieval trajectory is a very realistic approach. But if the decision is made to use them, a good design still implies to minimize the consumption of fuel. Therefore, the optimization problem may be restated by aiming at minimizing a new cost:

$$J = \int_0^{t_f} 1 + \eta\, u_\theta^2\, dt$$

where u_θ is the thruster and η a pondering factor. Such a cost leads to a trade-off between minimizing the retrieval time and the fuel consumption, a trade-off which can be adjusted with η. However it has the advantages of getting rid of the bang-bang solution since it is no more a linear optimization problem. This new constrained problem can be solved using the algorithm described in § 2.4.1 since on the constraint, the two necessary equations are available:

$C(x,u)=0$ and $H_u = 0$ to determine u and μ. This is a very interesting new direction of investigation for future work, using both pitch and roll dynamics for a complete study.

CHAPTER 3:
A FEEDFORWARD/FEEDBACK DESIGN

3.1. The Feedforward/feedback Loop Structure.

3.1.1. Introduction.

In the preceding chapter, a nominal trajectory was computed and the resulting necessary length acceleration history was derived. Using directly this length acceleration as the control would mean to command the TSS in open loop, which is unrealistic. The control would be unable to recover any disturbance and model errors would certainly drive the sub-satellite on a divergent trajectory. Therefore, the possibility of designing a feedback control stabilizing this naturally unstable system about the nominal trajectory is investigated.

The closed loop structure must be fast enough to be able to drive the sub-satellite back to the nominal trajectory in a reasonable period of time, lower than one third of the total retrieval time, after the occurrence of a disturbance. Otherwise, the benefit of performing the retrieval along this nominal trajectory would be lost. The critical is the pitch. To remove excess angular momentum, the open loop structure only relies on the gravity gradient which becomes weak after 2000m. This observation justifies the use of thrusters installed either on the sub-satellite or on the orbiter, in order to have better control authority. Since these additional controls were not included in the design of the nominal trajectory, they will be fired only if the system is driven away from its nominal path. Otherwise, the system is left under the control of the tether control system. This approach should result in a minimum fuel consumption unless the modeling error are too important. In this worst case, the thruster would be required to be fired all along the retrieval.

3.1.2. The Actuators.

Two systems of thrust are available. Gas jets can be directly installed on the sub-satellite with the disadvantage of increasing its total mass. Another possibility is to use the primary control system of the orbiter (PRCS).

Gas jets on the sub-satellite give a constant thrust of 2 N. For a total mass m = 500 kg, the resulting acceleration is 4.10^{-3} $m.s^{-2}$. The time granularity of this on-off system is 80 ms leading to a thrust granularity of $3.2\ 10^{-4}$ $m.s^{-1}$. On the other hand, the two primary jets of the orbiter give a thrust of 7700 N. For a total mass of 10^5 kg, the resulting acceleration is .077 $m.s^{-2}$ with the same firing time error of 80 ms. Thus, the thrust granularity is $6.2\ 10^{-3}$ $m.s^{-1}$.

Both solutions are attractive. Using the orbiter PRCS would give more control and also would avoid having to fire a thruster from another spacecraft close to the shuttle. However, because of the inertia of the orbiter, this solution would lead to a greater fuel consumption. The discomfort of the crew submitted to these on-off accelerations can also be imagined. On the other hand, a sub-satellite thruster configuration requires the implementation of a yaw control system in order to keep the thrust in the in-plane direction. But this solution is more fuel efficient compared with thrusting from the orbiter and therefore is retained.

For the purpose of the regulator design, it would be convenient to be able to order a continuously varying level of thrust. The available thrusters for the TSS are on-off devices. But continuous thrust level may be approximated by fast pulsing with pulse width modulation. The pulsing period ΔT must be short compared with the system characteristic time constant so as to reasonably approximate the effect of continuous thrusting. If $T_\theta(t)$ is the continuous thrust

level commanded by the regulator and T_s, the constant thrust level available, the time of firing Δt on a pulsing period is given by:

$$\Delta t = \frac{1}{T_s}\int_0^{\Delta T} T_\theta(t)\,dt = \frac{\overline{T}_{req}}{T_s}\Delta T \quad \text{where} \quad \overline{T}_{req} = \frac{1}{\Delta T}\int_0^{\Delta T} T_\theta(t)\,dt \tag{3.1}$$

In other words, the integrals of thrusting with constant thrust level and with continuous level must be equivalent. Since Δt is lower than ΔT, the average value of requested thrusting $\overline{T}_{req}$ must always be lower than the available constant thrust level.

For a time incertitude of 80 ms on the on-off system and a pulsing period of 1 s,

$$\overline{T}_{real} = \overline{T}_{req} \pm T_s \times 80.10^{-2} \tag{3.2}$$

The second actuator is the reel-in acceleration which directly controls the length dynamics. Some variations about the nominal acceleration are necessary in order to recover any disturbance. With a no-pushing constraint at 3.10^{-5} m.s^{-2}, the control authority is very small. If an amplitude of control δu_L is allowed, the nominal trajectory will have to be recomputed with a maximum deceleration of 3.10^{-5} m.s^{-2} - δu_L, increasing the nominal time of retrieval. Therefore, there will be a trade-off between good control authority and optimized time of retrieval. The tethered-aligned thruster fired at 2N avoids this trade-off. For a total mass of the sub-satellite equal to 500 kg, it moves the tension constraint back to 4.10^{-3} m.s^{-2} which results in an acceptable control authority on the length dynamics.

3.1.3. The Sensors.

The best closed loop performances are usually given by full state feedback. The pitch angle is measured from the orbiter with a Ku band radar, the measurement of which is then added to the attitude of the orbiter given by its Inertial Navigation System (INS). The resolution of the radar is $\pm 2^o$ and that of the INS, $\pm$ 20 arcsec, resulting in a pitch resolution of $\pm$ 2.0056°.

A tether is not a rigid body and therefore, the sub-satellite can rotate on itself at the end of the tether. In such a configuration, the pitch rate can not be measured by a rate gyro. The simplest alternative would be to estimate it with an observer which would also filter the noisy measurement of the pitch angle. Because of the non-linear nature of the dynamics involved, the solution of an extended Kalman filter is retained.

The length is measured with a measurement wheel and the length rate with a tachometer.

3.1.4. The Specifications.

The goal of the closed loop structure is to bring good rejection properties of model error and external disturbances, to the control mechanism. Only the rigid body motion was included in the model. Vibrations [19] propagated along the tether may drive the system away from the nominal trajectory. Some modes of the tether may also be excited by the vibrations resulting from the limit cycle nature of the PRCS [5]. In addition, the coupling between roll and pitch dynamics was also ignored although it exists when the roll angle and roll rate are being driven to zero by the out-of-plane control mechanism.

Several disturbances are expected to act on the TSS, ranging from thermal effects to gravitational anomalies and interactions with the surrounding space plasma for conductive tether. For a sub-satellite deployed downward, an important external force is applied on the TSS in addition to gravity gradient. It is the atmospheric drag which contains an oscillatory component for polar orbits. The atmospheric force $\mathbf{f_a}$ is given by:

$$\mathbf{f_a} = f_{a\,stat}\,(1 + \frac{1}{4}\sin 2\omega t^2) \quad \text{with} \quad f_{a\,stat} = \frac{1}{2}\rho\, u^2\, C_D\, A\, L \qquad (3.3)$$

The orbiter velocity u is approximately equal to 7.10^3 $m.s^{-1}$, the atmospheric density ρ to 10^{-9} $kg.m^{-3}$, the aerodynamic coefficient and the surface of the sub-satellite orthogonal to the

orbital plane respectively to 2 and 2 m^2. $f_{a\ stat} = 9.8.10^{-2}$ L N resulting in a static atmospheric torque equal to $\frac{1.96.10^{-4}}{L}$ which is not negligible compared with a maximum thrust of 4.10^{-3} $m.s^{-2}$, and must be taken into account in the loop structure. The equilibrium pitch angle for constant length is given by

$$\sin 2\theta_{eq} = \frac{2\ f_{a\ stat}}{3\ \omega^2\ m\ L^2} \qquad (3.4)$$

resulting in a $\theta_{eq} = 1°.86$ for a length of 2000 m. This atmospheric bias torque becomes significant only for small length.

The sub-satellite is also submitted to the self-gravity of the orbiter approximately equal to $f_g = \frac{3.10^{-3}}{L^2}$ N. Self-gravity overpowers gravity gradient for L lower than 1.31 m. Thus its effect during the retrieval is negligible.

Because of the thruster granularity and sensor noise, an initial error on the states at the entry point of the reel-in part of the retrieval is expected. The closed-loop system should be able to correct a one percent error of the maximum value of every state on the retrieval path in a period of time not exceeding one-third of the total retrieval time (≈ 1000 s) without thruster saturation. The bandwidth of the system is mainly fixed by the maximum level of actuators, which is 4.10^{-3} $m.s^{-2}$ for the in-plane thrusters and 4.10^{-3} $m.s^{-2}$ for the length acceleration. However, to prevent the tether from being excited by the shuttle attitude control system, the bandwidth of the closed loop should not exceed 1/10 Hz. In accordance with this specification, the bandwidth of the observer should be one decade above, ie 1 Hz.

3.1.5. The Closed Loop Structure.

The whole closed loop structure is the following: the measurements Y of the Ku band radar, the length measurement wheel and the tachometer are filtered by the observer, and the

pitch rate is reconstructed from the three previous measurements. Thus, the output of the observer is a vector $\hat{X}$ of the four state estimates. These estimates are compared to the nominal states X_0 steming from the optimal trajectory previously stored in the digital computer. The state error $\delta\hat{X}$ is fed into the regulator which then computes a correction control term δu to be added to the nominal control u_0. This nominal control is reconstructed from the optimal length acceleration history stored with the nominal states, taking into account the constant disturbances and the length dynamics. Then the required control, addition of the nominal control u_0 and the correction term δu is applied on the plant (fig 3.1).

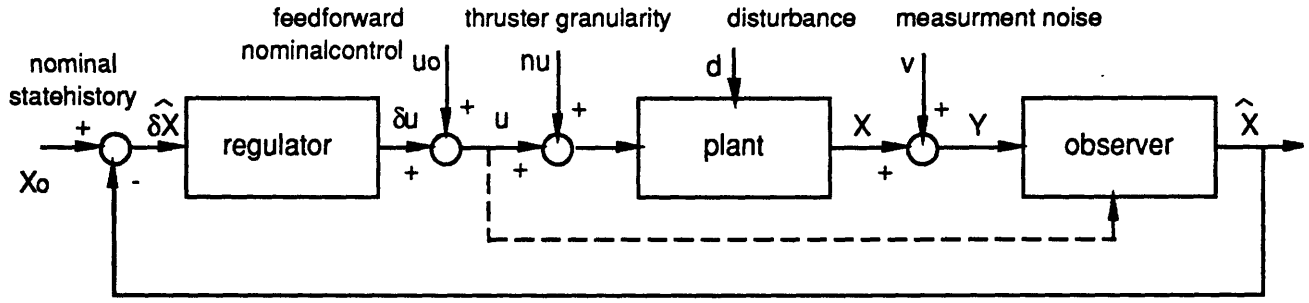

fig 3.1 : a feedforward /feedback scheme

The whole design consists in finding the appropriate feedback gain G and observer gain H. For this purpose, linear theories are used by linearizing the system at each step about the estimated position in the state space. In this case, this tracking system is brought back to the classical problem of regulating the new states $\delta X = X - X_0$ to zero. Finding the appropriate gains G and H is the purpose of the next study.

3.2. The System Analysis.

3.2.1. Linearization.

In the optimal trajectory design, the assumption was made that the length acceleration was directly controllable. Here, the effect of the gravity gradient and the Coriolis acceleration are included. The in-plane rigid body dynamics are described by the two following equations resulting from (2.4) and (2.6):

$$\ddot{\theta} + 2\frac{\dot{L}}{L}(\dot{\theta} + \omega) + 3\,\omega^2 \sin\theta \cos\theta + \frac{T_\theta}{L} + \frac{f_a}{L}$$

$$\ddot{L} = L\left[(\dot{\theta} + \omega)^2 + 3\,\omega^2 \cos^2\theta - \omega^2\right] + u_{Lc} \qquad (3.5)$$

where T_θ corresponds to the acceleration due to the thrusters and u_{Lc}, the length acceleration due to the length control effort. f_a will now be ignored since the true control can be directly reconstituted by adding f_a to the computed control.

The tension T is given by:

$$\frac{T}{m} = L\left[(\dot{\theta} + \omega)^2 + 3\,\omega^2 \cos^2\theta - \omega^2\right] + \frac{2N}{m} - \ddot{L} = \frac{2N}{m} - u_{Lc} > 0 \qquad (3.6)$$

So the new upper limit of the control u_{Lmax} for a sub-satellite mass equal to 500 kg is 4.10^{-3} $m.s^{-2}$.

At each step, the system can be linearized either about the nominal trajectory or about the real estimated states where the system is. But the position of the system needs to be estimated on its real trajectory. Therefore, in order to keep the property of separation between the dynamics of the observer and that of the closed loop feedback, the system is linearized about its estimated position to compute both the feedback and the observer gains. From a regulator point of view, both linearization are equivalent at the first order.

$$f(x,u) = f(x_0,u_0) + \text{grad } f_{x_0,u_0}\,(x-x_0) + \frac{\partial f}{\partial u}_{x_0,u_0}\,(u-u_0) + o(\varepsilon^2)$$

$$\Rightarrow (\dot{x}-\dot{x}_0) = f(x,u) - f(x_0,u_0) = \text{grad } f_{x_0,u_0}\,(x-x_0) + \frac{\partial f}{\partial u}_{x_0,u_0}\,(u-u_0)$$

or
$$f(x_0,u_0) = f(x,u) - \text{grad } f_{x,u}\,(x-x_0) - \frac{\partial f}{\partial u}_{x,u}\,(u-u_0) + o(-\varepsilon^2)$$

$$\Rightarrow (\dot{x}-\dot{x}_0) = f(x,u) - f(x_0,u_0) = \text{grad } f_{x,u}\,(x-x_0) + \frac{\partial f}{\partial u}_{x,u}\,(u-u_0)$$

The following non-dimentionalization is performed:

$$Z = T_x X \quad \text{with} \quad T_x = \begin{bmatrix} 1 & 0 & 0 & 0 \\ 0 & \frac{1}{\omega} & 0 & 0 \\ 0 & 0 & \frac{1}{L_i} & 0 \\ 0 & 0 & 0 & \frac{1}{\omega L_i} \end{bmatrix}$$

$$u^T = [u_\theta\ u_L]^T = [\ T_\theta\ \ u_{Lc}\ ]^T T_u \quad \text{with} \quad T_u = \begin{bmatrix} \frac{1}{T_s} & 0 \\ 0 & \frac{1}{u_{max}} \end{bmatrix} \qquad (3.7)$$

The state representation becomes:

$$\begin{aligned} \dot{z}_1 &= \omega z_2 \\ \dot{z}_2 &= -2\omega\frac{z_4}{z_3}(z_2+1) - \frac{3}{2}\omega \sin 2z_1 + \frac{T_s}{\omega L_i z_3} u_\theta \\ \dot{z}_3 &= \omega z_4 \\ \dot{z}_4 &= \omega z_3\left[(z_2+1)^2 + 3\cos^2 z_1 - 1\right] + \frac{u_{max}}{\omega L_i} u_L \end{aligned} \qquad (3.8)$$

The resulting time variant system is $\delta\dot{Z} = A(Z)\,\delta Z + B(Z)\,\delta u$ with $\delta Z = Z - Z_0$ and

$$A(Z) = \begin{bmatrix} 0 & \omega & 0 & 0 \\ -3\omega\cos 2z_1 & -2\omega\frac{z_4}{z_3} & 2\omega\frac{z_4}{z_3^2}(z_2+1) & -2\omega\frac{(z_2+1)}{z_3} \\ 0 & 0 & 0 & \omega \\ -3\omega z_3 \sin 2z_1 & 2\omega z_3(z_2+1) & \omega\left[(z_2+1)^2 + 3\cos^2 z_1 - 1\right] & 0 \end{bmatrix}$$

$$B(Z) = \begin{bmatrix} 0 & 0 \\ \frac{2\omega}{z_3} & 0 \\ 0 & 0 \\ 0 & 2\omega \end{bmatrix}$$

$$\text{and } y = C\,Z \text{ with } C = \begin{bmatrix} 1 & 0 & 0 & 0 \\ 0 & 0 & 1 & 0 \\ 0 & 0 & 0 & 1 \end{bmatrix}. \qquad (3.9)$$

Fig 3.2 through 3.4 give the variations of each coefficient of matrix A along the retrieval path. On the first 90% of the retrieval, these coefficients remain in the range of 10^{-3}. The coefficients reflecting the coupling of the pitch with the length, a_{41} and a_{42}, decrease with L. On the other hand, those reflecting the coupling of the length with the pitch dynamics,a_{23} and a_{24}, remain fairly constant. Both sets of coupling coefficients are in the same range as the other coefficients. In the last 10% of the retrieval, a22 and a24 which depend on $\frac{1}{L}$ and a23 in $\frac{1}{L2}$ start to diverge. When the coupling of the pitch with the length disappears, the coupling of the length with the pitch dynamics sharply increases. Consequently, a constant feedback which does not retain the time varying nature of the system is unlikely to be satisfactory. There is a risk that the system becomes unstable during the last 10% of the retrieval, even if the same gains would give good results in the first 90%. The divergence of the coefficients of the A matrix during the final 10% of the retrieval could be a matter of concern with respect to the ability of the feedback to track this final part of the trajectory. However, in any case, the available amount of control does not make the system fast enough to recover any disturbances even in the range of a 1% error, in the remaining period of time before docking. One must only make sure that the system remains stable up to the final docking.

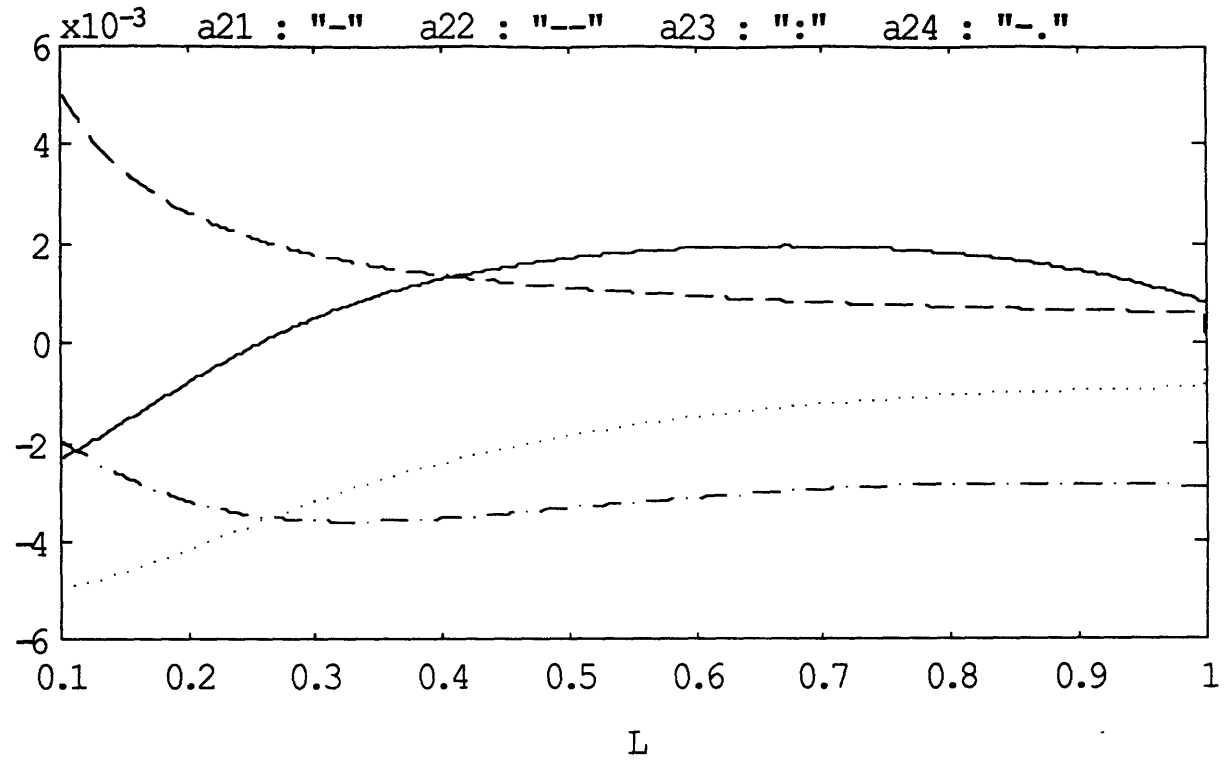

fig 3.2: Variations of the coefficients a_{2i} of A along the nominal retrieval trajectory for L>10%.

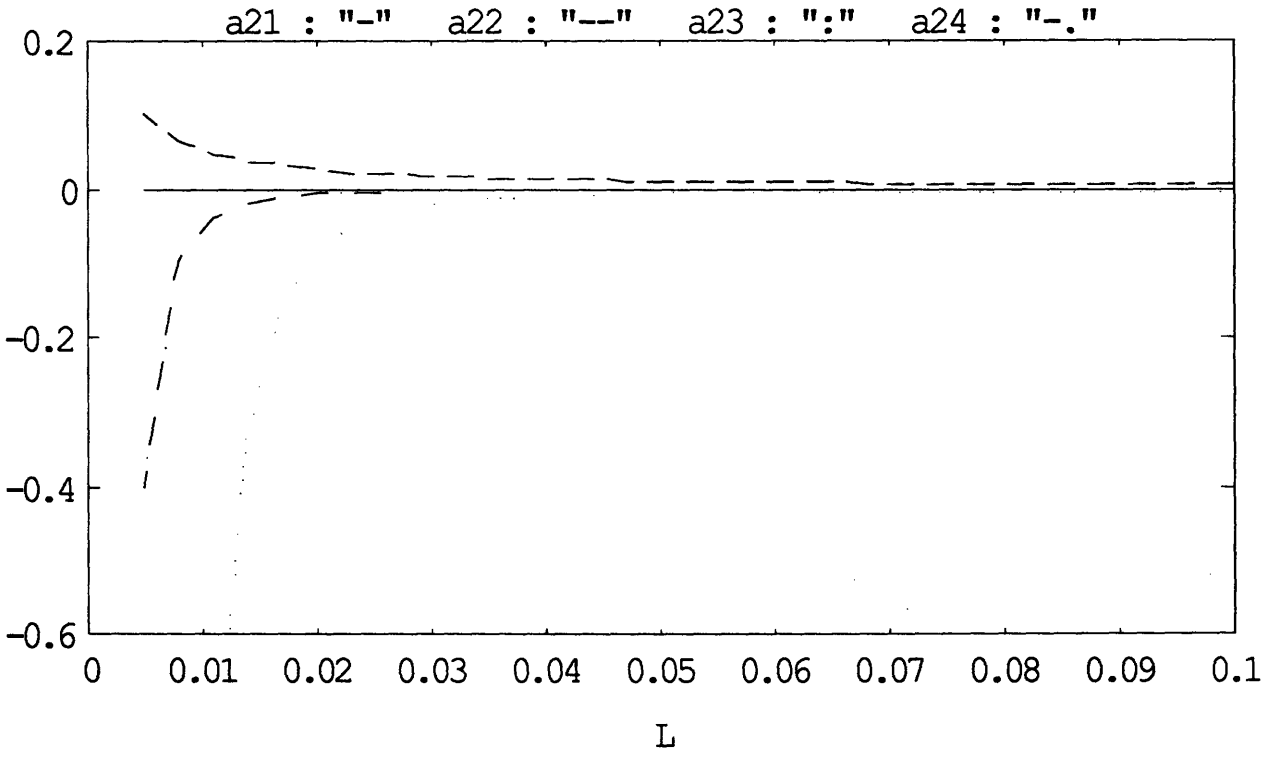

fig 3.3: Variations of the coefficients a_{2i} of A along the nominal retrieval trajectory for L<10%.

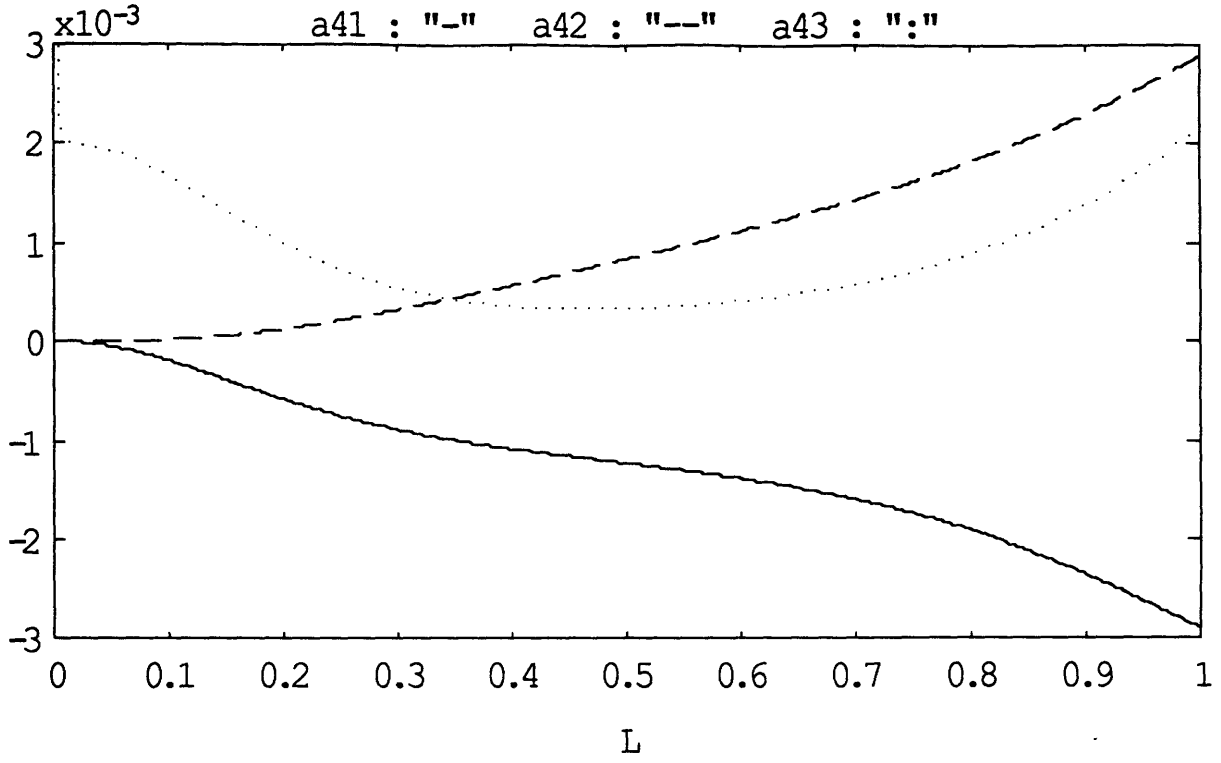

fig 3.4: Variations of the coefficients a_{4i} of A along the nominal retrieval trajectory

3.2.2. The Open Loop Dynamics.

3.2.2.1. Open Loop Poles.

The pole structure of the system significantly changes along the retrieval path. Two poles λ_1 and λ_2 are oscillatory during 90% of the trajectory, becoming unstable after 50% of the retrieval. λ_3 always is unstable and diverges in the last 10% of the retrieval whereas λ_4 remains stable, being close to an integrator in the first 30% of the retrieval fig 3.5 through 3.7.

The eigen structure is computed at two characteristic points L = 90% and L = 5 % which corresponds to the beginning of the divergence.

L = 90%

$$\lambda_1 = .95\ 10^{-3} \qquad v_1 = \begin{bmatrix} 1 \\ .95 \\ .33 \\ .31 \end{bmatrix}$$

$$\lambda_2 = -.04\ 10^{-3} \qquad v_2 = \begin{bmatrix} .57 \\ -.02 \\ 1 \\ -.04 \end{bmatrix}$$

$$\lambda_{3,4} = -.12\ 10^{-3} \pm i\ 1.98\ 10^{-3} \qquad v_{3,4} = \begin{bmatrix} .50\ e^{\pm 1.63\ i} \\ 1 \\ .50\ e^{\pm 2.77\ i} \\ .99\ e^{\pm 1.13\ i} \end{bmatrix}$$

L = 5%

$$\lambda_1 = 9.79\ 10^{-3} \qquad v_1 = \begin{bmatrix} .10 \\ 1 \\ 0 \\ 0 \end{bmatrix}$$

$$\lambda_2 = -1.39\ 10^{-3} \qquad v_2 = \begin{bmatrix} .18 \\ -.25 \\ -.72 \\ 1 \end{bmatrix}$$

$$\lambda_3 = 1.37\ 10^{-3} \qquad v_3 = \begin{bmatrix} .65 \\ .90 \\ .73 \\ 1 \end{bmatrix}$$

$$\lambda_4 = .30\ 10^{-3} \qquad v_4 = \begin{bmatrix} 1 \\ .31 \\ .02 \\ .01 \end{bmatrix} \qquad (3.10)$$

Because of the non negligible coupling terms, the two dynamics are mixed together at the beginning of the retrieval. When the length decreases, the pitch is decoupled from the length dynamics so that the remaining coupling terms does not impair the eigen structure.

The length dynamics are given by equation (3.5). The Coriolis acceleration and the pitch rate increase the tension and the acceleration of the length, like for a pendulum. This effect is given by the term $(\dot{\theta} + \omega)^2$. On the other hand, the gravity gradient, the magnitude of which increases with the pitch, has a stabilizing effect. This effect is reflected by the term - ω^2 (1 -

$3\cos^2\theta$). The length dynamics are oscillatory stable if the contribution of the gravity gradient to the tension overpowers that of the Coriolis acceleration; otherwise, they are exponentially unstable. Since the tracked trajectory is the result of a minimum time optimization, the retrieval is fast and then, the contribution of the gravity gradient is always overpowered by that of the Coriolis acceleration. Therefore, the length dynamics are unstable. This is given by λ_3 for L = 5%. This same balance between gravity gradient and Coriolis acceleration also applies on the pitch dynamics, § 2.1, as shown by V_3 and also V_4 when the two dynamics are coupled. For L = 90%, the coupling effect transforms this exponentially divergent mode into an oscillatory one and even stabilizes it at the beginning of the retrieval. λ_2 is the corresponding eigen value of λ_3 in the left half plane for the length dynamics. It does not concern the pitch as shown by V_2. The coupling effect moves this eigen value close to a pure integrator, mainly reflecting the integral of the length rate, but also that of the pitch angle, as shown by V_2.

λ_1 and λ_4 both correspond to the pitch dynamics, cf V_1 and V_4 for L = 5%. Since the length rate is negative during the retrieval, the pitch dynamics are unstable. this is reflected by λ_1. This eigen value always is real, therefore the pitch never is in the spiral mode, cf § 2.3.1. Because of the coupling coefficients, the other eigen value becomes oscillatory. Even without the coupling effect, the gravity gradient may drive the second pole of the pitch dynamics into the left half plane. Without coupling, the pitch eigen values are given by $\lambda^2 + 2\omega\frac{z_4}{z_3}\lambda + 3\omega^2\cos 2z_1 = 0$. If $\left(\frac{z_4}{z_3}\right)^2 < 3\cos 2z_1$ and $\frac{\pi}{4} < z_1 < \frac{3\pi}{4}$ which is the case for 75% of the retrieval, the gravity torque which increases with the pitch, overpowers the destabilizing Coriolis momentum, and stabilize one of the modes of the pitch dynamics. That is why λ_3 and λ_4 are stable on 55% of the retrieval, fig 3.7. The coupling effect destabilizes this mode earlier than without coupling.

The variation of the eigen structure enlightens the time varying nature of the TSS. It reinforces the need for a gain scheduling solution.

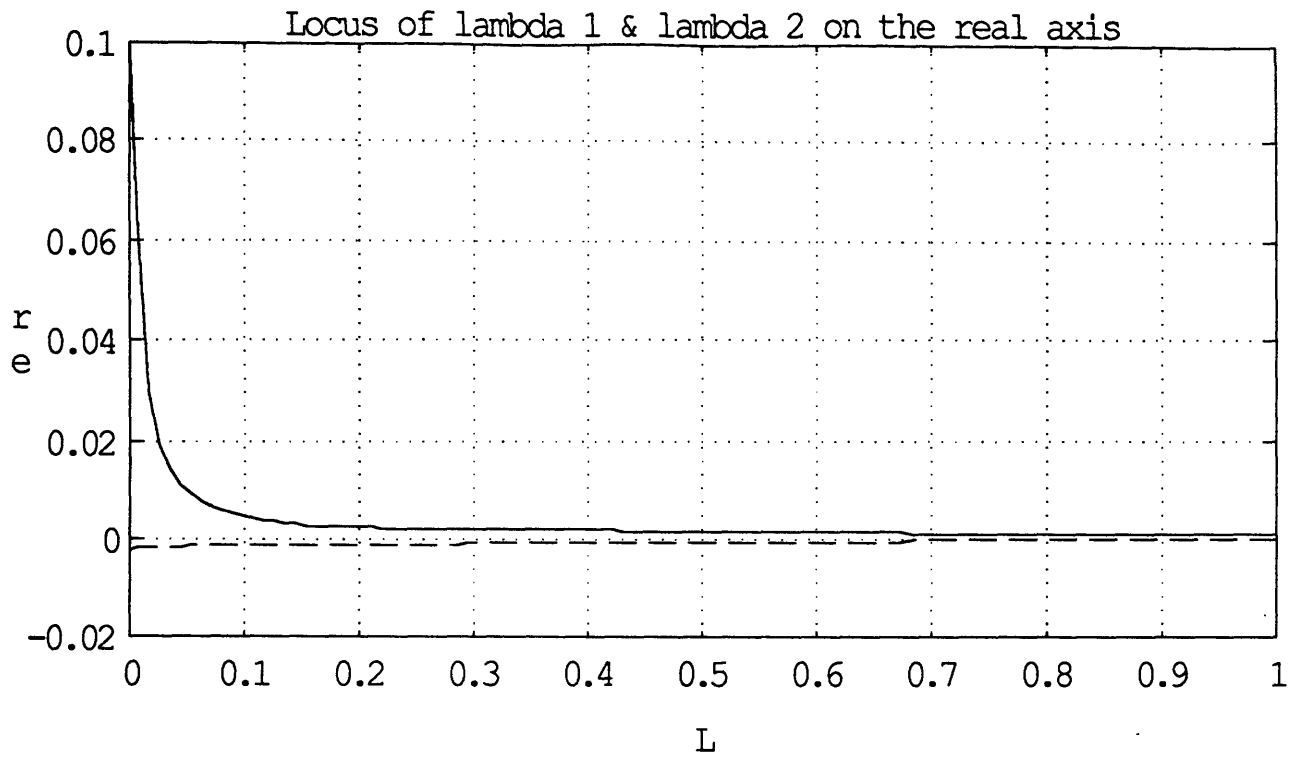

fig 3.5: Real part of λ_1 and λ_2 along the nominal retrieval trajectory

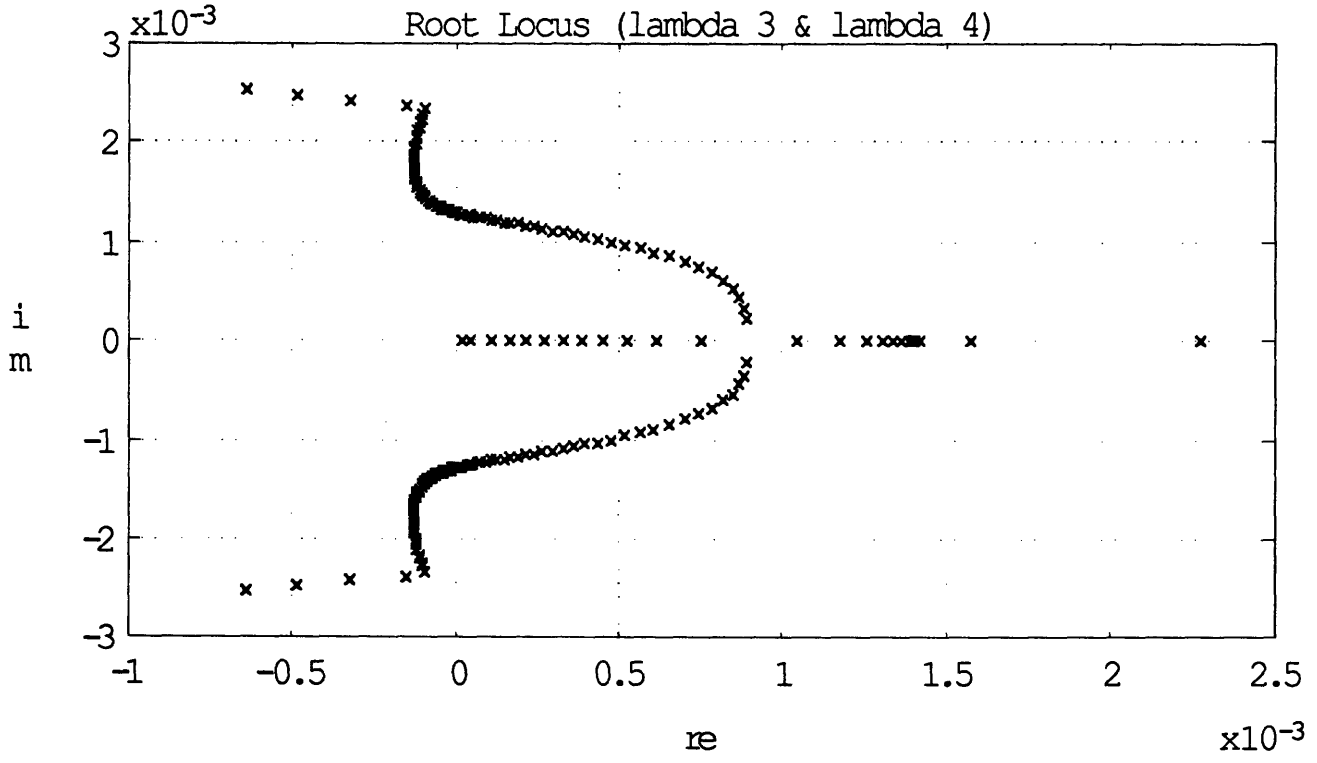

fig 3.6: Root locus of λ_3 and λ_4 along the nominal retrieval trajectory

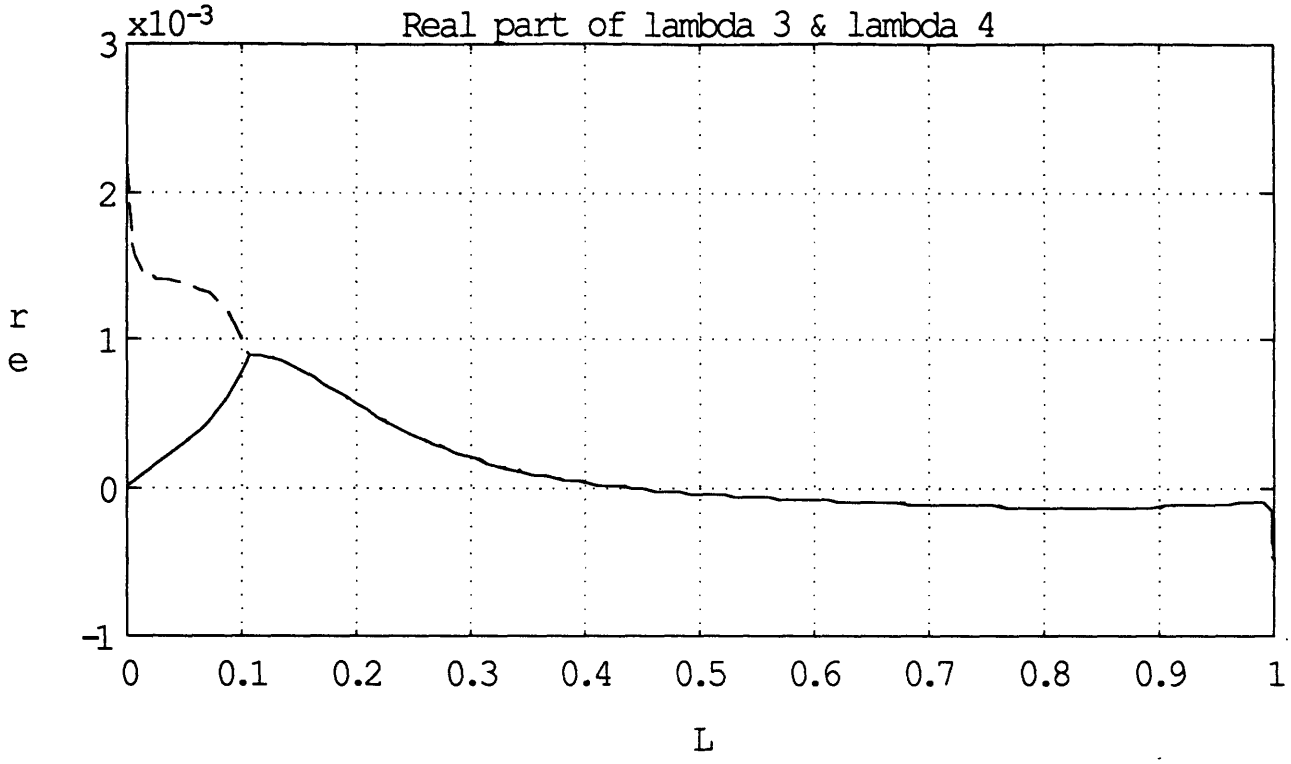

fig 3.7: Real part of λ_3 and λ_4 along the nominal retrieval trajectory

3.2.2.2. Observability, Controllability, Modal Decomposition.

Because the system is time varying, a rigorous way of verifying the controllability and observability is to compute the two grammians. However, this tracking problem may be decomposed into a set of regulation problems where at each step, a regulator for the LTI system must be designed to drive the error states back to zero. Therefore, at each step, the controllability and observability properties of the TSS can be evaluated by computing the rank of the Kalman matrices [B AB A^2B A^3B] and [C^T A^TC^T $A^{T2}C^T$ $A^{T3}C^T$]. The rank of both matrices are equal to four all along the retrieval trajectory; thus the TSS is controllable and observable with the two controls u_θ and u_L and the three measurements.

With the coupling terms, the pitch and length dynamics are controllable from the two controls. A feedback based on a decoupling of both dynamics would not take advantage of this coupling. A modal decomposition performed at the two characteristics steps of the retrieval enables to evaluate the degree of controllability of the modes by each control. In the steady state,

$$X(t) = \sum_{i=1}^{4} V_i \sum_{k=1}^{2} W_i^T b_k \int_0^t e^{\lambda_i (t-\tau)} u_k(\tau)\, d\tau \qquad (3.11)$$

where V_i and W_i are the right and left eigen vectors respectively of the open loop system associated with the ith eigen value λ_i , and b_k, the kth column of the B matrix associated with the kth control.

L = 90%

$$X(t) = \int_0^t - \begin{bmatrix} 1 \\ .95 \\ .33 \\ .31 \end{bmatrix} e^{.95\ 10^{-3}(t-\tau)}\ 10^{-3}\ (\ .21\ u_\theta(\tau) + 1.44\ u_L(\tau)\ )\ d\tau$$

$$+ \int_0^t \begin{bmatrix} .57 \\ -.02 \\ 1 \\ -.04 \end{bmatrix} e^{-.04\ 10^{-3}(t-\tau)}\ 10^{-3}\ (\ 1.39\ u_\theta(\tau) + .73 u_L(\tau)\ )\ d\tau$$

$$+ \int_0^t 2\ 10^{-3}\ e^{-.12\ 10^{-3}(t-\tau)}\ (\ 1.32 \begin{bmatrix} .50\cos[1.98\ 10^{-3}(t-\tau)-1.63-.38] \\ 1\cos[1.98\ 10^{-3}(t-\tau)-.38] \\ .50\cos[1.98\ 10^{-3}(t-\tau)-2.77-.38] \\ .99\cos[1.98\ 10^{-3}(t-\tau)-1.13-.38] \end{bmatrix} u_\theta(\tau)$$

$$+ 1.26 \begin{bmatrix} .50\cos[1.98\ 10^{-3}(t-\tau)-1.63-.99] \\ 1\cos[1.98\ 10^{-3}(t-\tau)-.99] \\ .50\cos[1.98\ 10^{-3}(t-\tau)-2.77-.99] \\ .99\cos[1.98\ 10^{-3}(t-\tau)-1.13-.99] \end{bmatrix} u_L(\tau)\ )\ d\tau$$

L = 5%

$$X(t) = \int_0^t \begin{bmatrix} .1 \\ 1 \\ 0 \\ 0 \end{bmatrix} e^{9.79\,10^{-3}(t-\tau)}\, 10^{-3}\,(\,.1\,u_\theta(\tau) + 1.01\,u_L(\tau)\,)\,d\tau$$

$$+ \int_0^t \begin{bmatrix} .18 \\ -.25 \\ -.72 \\ 1 \end{bmatrix} e^{-1.39\,10^{-3}(t-\tau)}\, 10^{-3}\,(\,.054\,u_\theta(\tau) + u_L(\tau)\,)\,d\tau$$

$$- \int_0^t \begin{bmatrix} .65 \\ -.90 \\ -.73 \\ 1 \end{bmatrix} e^{1.37\,10^{-3}(t-\tau)}\, 10^{-3}\,(\,4.25\,u_\theta(\tau) + .80\,u_L(\tau)\,)\,d\tau$$

$$+ \int_0^t \begin{bmatrix} 1 \\ .31 \\ .02 \\ .01 \end{bmatrix} e^{.30\,10^{-3}(t-\tau)}\, 10^{-3}\,(\,41.12\,u_\theta(\tau) + .41\,u_L(\tau)\,)\,d\tau \qquad (3.12)$$

The coupling of the two dynamics introduces some interesting "cross-control" effects which predicts the structure of an optimal feedback gain using multivariable techniques like linear quadratic regulators. For instance, the first mode is part of the pitch dynamics, as shown by V_1. However, because of the important value of a_{23} in the A matrix, this mode is more controllable with the length control than with the pitch control. This comparison can be done since the controls also have been non-dimentionalized. Consequently, it is very likely that the gains g_{21} and g_{22} of the LQR gain matrix will be non negligible, in opposition to a decoupled feedback where they would be equal to zero. In addition, because of the important value of a_{23}, an error on the length will induce a non negligible error on the pitch. To prevent this, the feedback will certainly anticipate the error on the pitch by ordering the firing of the in-plane thruster. Therefore g_{13} will certainly also be non negligible in an LQR solution.

λ_{34} is equally controllable by u_θ and u_L, as predicted by V_{34}. For L = 5%, the second mode of the pitch dynamics λ_4 is predominantly controllable with u_θ, and λ_2, the second mode of the length dynamics mainly is controllable with u_L.

The computation of W^TB gives the controllability of each mode with the different controls. Unless the modes are fully decoupled with respect to the states, it does not directly give the controllability of each states by the controls. However, except for the first mode because of the divergence of a_{34}, it seems that the controllability of each mode by u_θ or u_L is proportional to the contribution of this same mode to the pitch or length dynamics respectively. This could suggest that from the states point of view, the controls are decoupled. Such an information can be deduced from the singular value decomposition.

3.2.2.3. Frequency Domain, Singular Value Decomposition.

A singular value decomposition of $(sI-A)^{-1}B$ is performed at L = 90% and L = 5% for $\omega = 10^{-2}$ rad.s^{-1}. Since the open loop dynamics are in the range of 10^{-3} rad.s^{-1}, it seems reasonable to expect a closed loop system performing one decade faster.

If $v_{ki} = |v_{ki}| e^{i \varphi_{ki}}$ is the component of the ith right singular value vector corresponding to the kth control u_k, and $u_{li} = |u_{li}| e^{i \psi_{ki}}$ is the component of the ith left singular value vector corresponding to the lth output x_l, then for $u_{ki}(t) = |v_{ki}| \sin(\omega t+\varphi_{ki})$, $x_{li}(t) = |u_{li}| \sigma_i \sin(\omega t+\psi_{li})$ where σ_i is the ith singular value.

For L = 90%, $\sigma_{max} = .34$ and $\sigma_{min} = .19$,

$$V_{max} = \begin{bmatrix} .92 \\ .38\ e^{i\ -1.54} \end{bmatrix} \qquad V_{min} = \begin{bmatrix} -.38 \\ .92\ e^{i\ -1.54} \end{bmatrix}$$

$$U_{max} = \begin{bmatrix} .09\ e^{i\ 3.08} \\ .93\ e^{i\ -1.63} \\ .03\ e^{i\ 1.61} \\ .34\ e^{i\ -3.11} \end{bmatrix} \qquad U_{min} = \begin{bmatrix} .03\ e^{i\text{-}.06} \\ .93\ e^{i\ 1.63} \\ .03\ e^{i\ 1.60} \\ .34\ e^{i\ -3.11} \end{bmatrix}$$

For L = 5%, $\sigma_{max} = 2.86$ and $\sigma_{min} = .2$,

$$V_{max} = \begin{bmatrix} 1 \\ 0 \end{bmatrix} \qquad V_{min} = \begin{bmatrix} 0 \\ 1\ e^{i\,-1.1} \end{bmatrix}$$

$$U_{max} = \begin{bmatrix} .10\ e^{i\,2.34} \\ .99\ e^{i\,-2.37} \\ 0 \\ 0 \end{bmatrix} \qquad U_{min} = \begin{bmatrix} 0 \\ 0 \\ .10\ e^{i\,2.04} \\ .99\ e^{i\,-2.68} \end{bmatrix} \qquad (3.13)$$

The two remaining U vectors correspond to the integration of the pitch and length rate. The maximum amplification mainly occurs in the pitch rate and is obtained almost with u_θ only for L = 90%. The minimum amplification is obtained with u_L and mainly occurs in the length rate. For L = 5% where the length dynamics are nearly decoupled from the pitch one, the controls are orthogonal and u_θ only controls the pitch and u_θ the length. Therefore, a feedback design based on the decoupling of the pitch and the length dynamics is likely to give good results.

Fig 3.8 shows that the difference of amplification between the two controls decreases for high frequencies. The peak corresponds to the oscillatory mode. For small length, this difference remains after the roll-off because of the decoupling, fig 3.9. The amplification for the length remains constant with L and sharply decreases when L is very small whereas the maximum singular value, amplification gain for the pitch steadily increases,fig 3.10.

These results seem consistent with the frequency representation.

L = 90%

$$z_1 = \frac{2.21\ 10^{-6}(s-1.18\ 10^{-3})(s+1.18\ 10^{-3})u_\theta - 5.67\ 10^{-9}(s+.33\ 10^{-3})u_L}{(s+.12\ 10^{-3}\pm 1.98\ 10^{-3}i)(s-.95\ 10^{-3})(s+.04\ 10^{-3})}$$

$$z_2 = \frac{2.21\ 10^{-3}s(s-1.18\ 10^{-3})(s+1.18\ 10^{-3})u_\theta - 5.67\ 10^{-6}s(s+.33\ 10^{-3})u_L}{(s+.12\ 10^{-3}\pm 1.98\ 10^{-3}i)(s-.95\ 10^{-3})(s+.04\ 10^{-3})}$$

$$z_3 = \frac{5.11\ 10^{-9}(s-1.02\ 10^{-3})u_\theta + 2\ 10^{-6}(s+.92\ 10^{-3})(s-1.59\ 10^{-3})u_L}{(s+.12\ 10^{-3}\pm 1.98\ 10^{-3}i)(s-.95\ 10^{-3})(s+.04\ 10^{-3})}$$

$$z_4 = \frac{5.11\ 10^{-6}s(s-1.02\ 10^{-3})u_\theta + 2\ 10^{-3}s(s+.92\ 10^{-3})(s-1.59\ 10^{-3})u_L}{(s+.12\ 10^{-3}\pm 1.98\ 10^{-3}i)(s-.95\ 10^{-3})(s+.04\ 10^{-3})}$$

L = 5%

$$z_1 = \frac{4\ 10^{-5}(s-1.39\ 10^{-3})(s+1.39\ 10^{-3})u_\theta - 2.55\ 10^{-9}(s+5.04\ 10^{-3})u_L}{(s+1.39\ 10^{-3})(s-.31\ 10^{-3})(s-1.37\ 10^{-3})(s-9.79\ 10^{-3})}$$

$$z_2 = \frac{4\ 10^{-2}s(s-1.39\ 10^{-3})(s+1.39\ 10^{-3})u_\theta - 2.55\ 10^{-6}s(s+5.04\ 10^{-3})u_L}{(s+1.39\ 10^{-3})(s-.31\ 10^{-3})(s-1.37\ 10^{-3})(s-9.79\ 10^{-3})}$$

$$z_3 = \frac{1.28\ 10^{-10}(s-14.76\ 10^{-3})u_\theta + 2\ 10^{-6}(s-9.79\ 10^{-3})(s-.29\ 10^{-3})u_L}{(s+1.39\ 10^{-3})(s-.31\ 10^{-3})(s-1.37\ 10^{-3})(s-9.79\ 10^{-3})}$$

$$z_4 = \frac{1.28\ 10^{-7}s(s-14.76\ 10^{-3})u_\theta + 2\ 10^{-3}s(s-9.79\ 10^{-3})(s-.29\ 10^{-3})u_L}{(s+1.39\ 10^{-3})(s-.31\ 10^{-3})(s-1.37\ 10^{-3})(s-9.79\ 10^{-3})} \quad (3.14)$$

The system is non-square. To have a transmission zero, there should be a direction of control and a frequency for which all the output channels would be equal to zero, which is not the case for the TSS. Since there is no integrator in the pole structure, the pitch and length rate are the derivative of the length and pitch angle.

The gain values for each channel confirm the results of the singular value decomposition. Therefore, it seems reasonable to try to design a feedback based on a decoupling of controls.

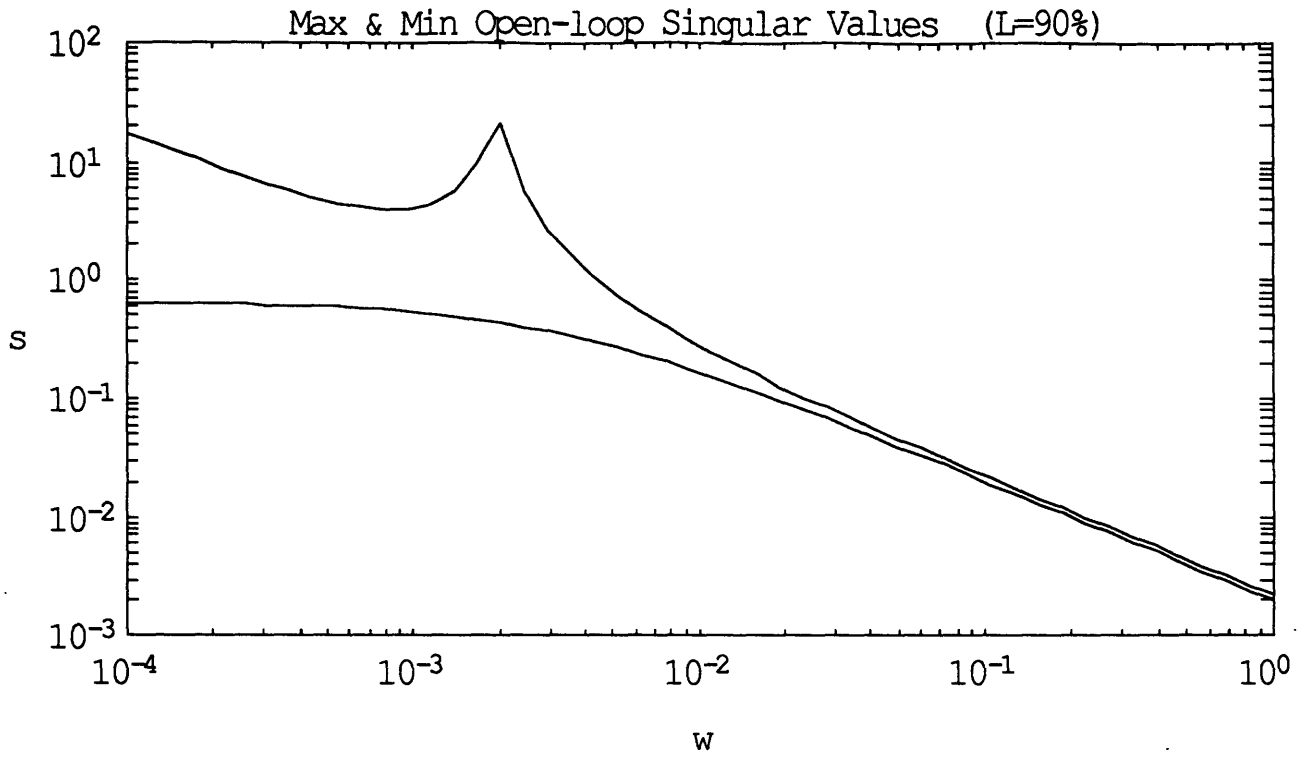

fig 3.8: Singular value decomposition vs pulsation for L=90%

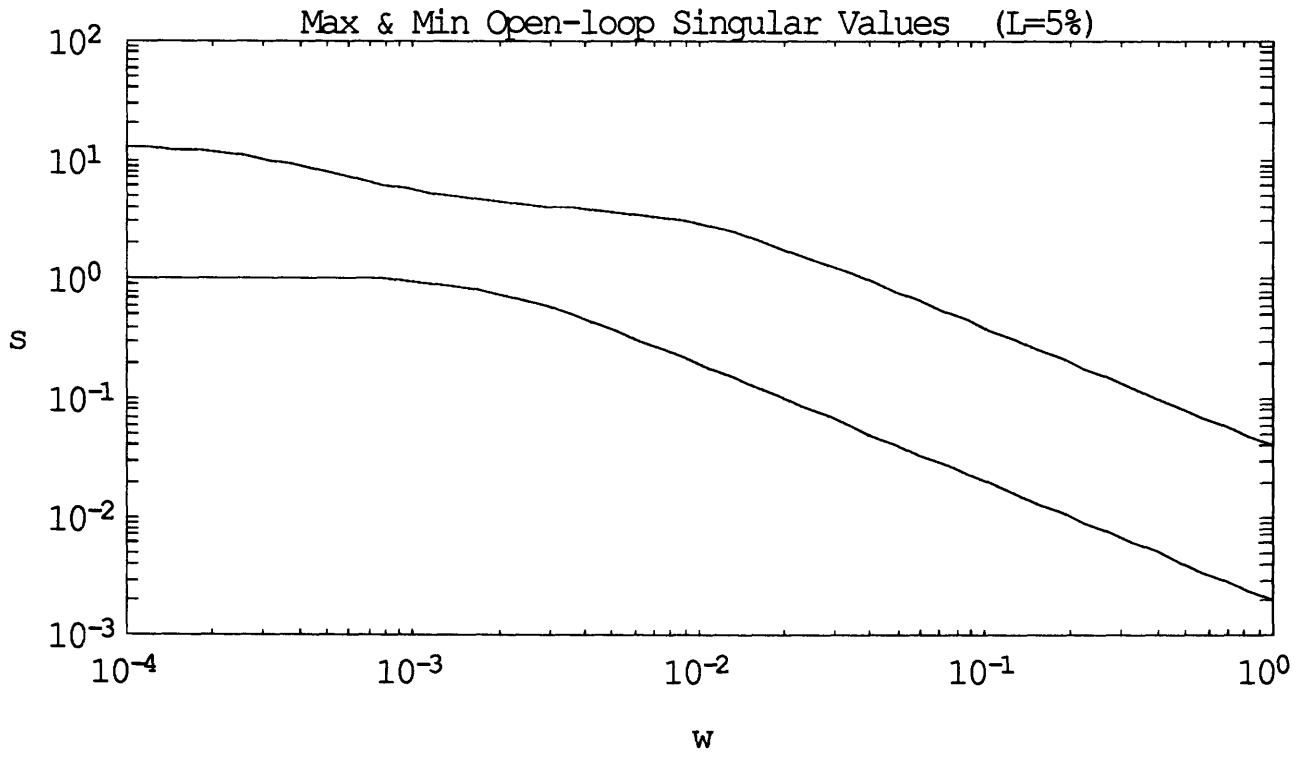

fig 3.9: Singular value decomposition vs pulsation for L=5%

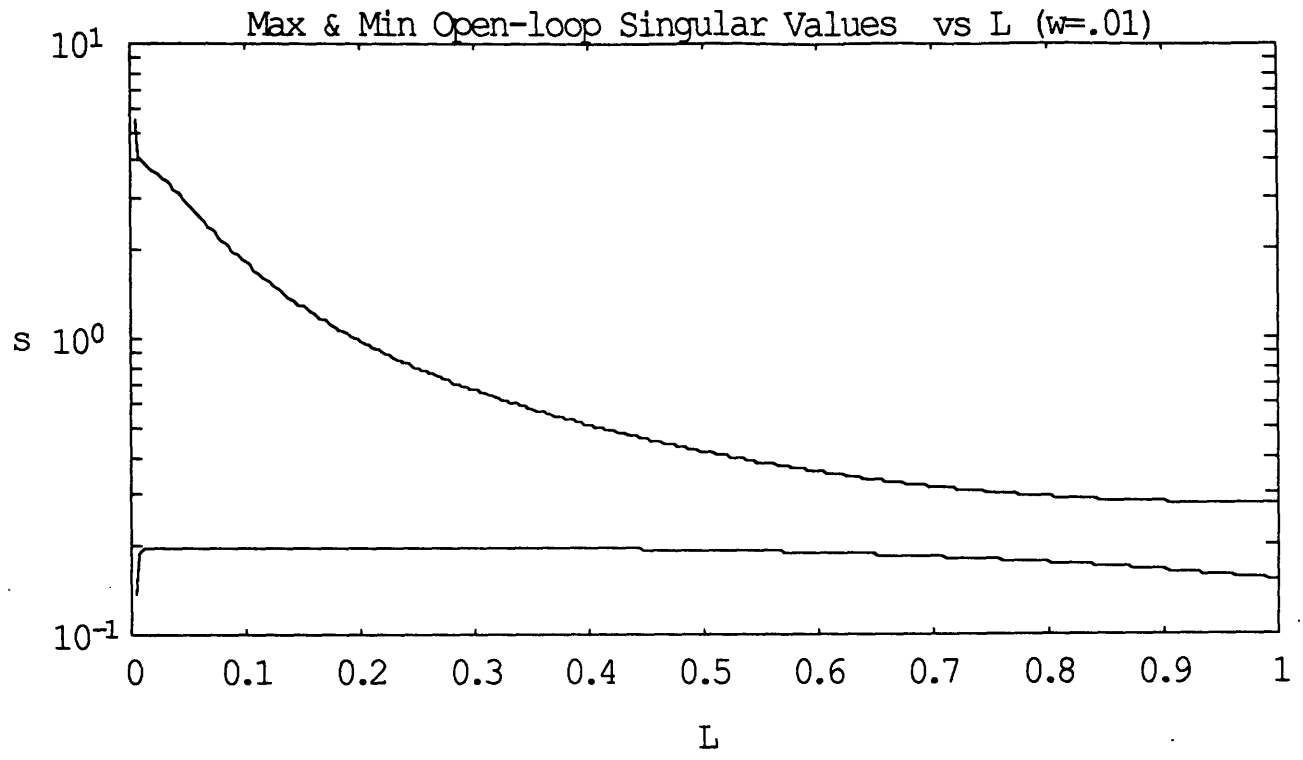

fig 3.10: Singular value decomposition vs length for ω=.1 rad.s^{-1}

3.3. The Feedback Design.

3.3.1. A Decoupling of Controls: Pole Placement.

All the modes of the system approximately have the same velocity with a time constant in the range of 10^3 s.rad^{-1}. Therefore, the pitch and the length loops must be closed together. However, because of the characteristics enlightened by the singular value decomposition, it can be considered that u_θ only controls the pitch and u_L, the length. If G is the feedback gain matrix, g_{13}, g_{14}, g_{21} and g_{22} are set to zero.

3.3.1.1. The Pitch Dynamics

The pitch dynamics may be expressed in a state-space representation as follow:

$$\begin{bmatrix} \delta\dot{z}_1 \\ \delta\dot{z}_2 \end{bmatrix} = \begin{bmatrix} 0 & \omega \\ -3\omega\cos 2z_1 & -2\omega\frac{z_4}{z_3} \end{bmatrix} \begin{bmatrix} \delta z_1 \\ \delta z_2 \end{bmatrix} + \begin{bmatrix} 0 \\ \frac{2\omega}{z_3} \end{bmatrix} \delta u_\theta + A_{\theta L} \begin{bmatrix} \delta z_3 \\ \delta z_4 \end{bmatrix}$$

$$\Rightarrow \delta\dot{Z}_\theta = A_\theta \delta Z_\theta + B_\theta \delta u_\theta + A_{\theta L}\delta Z_L \qquad (3.15)$$

z_3 and z_4 are here considered as disturbances. If $\delta u_\theta = - G_\theta \delta Z_\theta$ with $G_\theta = [g_{\theta p}\ g_{\theta d}]$, then the closed loop dynamics are given by:

$$\delta\dot{Z}_\theta = (A_\theta - B_\theta G_\theta)\delta Z_\theta + A_{\theta L}\delta Z_L \qquad (3.16)$$

The characteristic equation is given by:

$$D_\theta(\lambda) = \lambda^2 + 2\omega\left(\frac{z_4}{z_3} + \frac{g_{\theta d}}{z_3}\right)\lambda + \omega^2\left(3\cos 2z_1 + 2\frac{g_{\theta p}}{z_3}\right) \qquad (3.17)$$

which is identified with $\lambda^2 + 2\delta\omega_n\lambda + \omega_n^2$.

For a critical damping, δ is set to .7 . The cross-over frequency is given by

$$\omega_{c\theta} = \omega_n\left(1-2\delta^2+\sqrt{2-4\delta^2+4\delta^4}\right)^{1/2} = 1.01\omega_n.$$

and is adjusted so as to be able to recover a 1% initial error without saturation.

$$g_{\theta p} = \frac{z_3}{2}\left[\left(\frac{\omega_{c\theta}}{\omega}\right)^2 \frac{1}{1.01^2} - 3\cos 2z_1\right]$$

$$g_{\theta d} = z_3\left[\delta\frac{\omega_{c\theta}}{\omega}\frac{1}{1.01} - \frac{z_4}{z_3}\right] \qquad (3.18)$$

The feedback gains will decrease with the length. $\omega_{c\theta} = 10^{-2}$ rad.s^{-1} is used as an initial guess.

3.3.1.2. The Length Dynamics.

In the same way, the state space representation of the pitch dynamics may be rewritten as follow:

$$\begin{bmatrix} \delta\dot{z}_3 \\ \delta\dot{z}_4 \end{bmatrix} = \begin{bmatrix} 0 & \omega \\ \omega[(z_2+1)^2+3\cos^2 z_1-1] & 0 \end{bmatrix} \begin{bmatrix} \delta z_3 \\ \delta z_4 \end{bmatrix} + \begin{bmatrix} 0 \\ 2\omega \end{bmatrix} \delta u_L + A_{L\theta} \begin{bmatrix} \delta z_1 \\ \delta z_2 \end{bmatrix}$$

$$\Rightarrow \delta\dot{Z}_L = A_L\delta Z_L + B_L\delta u_L + A_{L\theta}\delta Z_\theta \qquad (3.19)$$

z_1 and z_2 are here considered as disturbances. If $\delta u_L = - G_L\delta Z_L$ with $G_L = [g_{Lp}\ g_{Ld}]$, then the closed loop dynamics are described by:

$$\delta\dot{Z}_L = (A_L - B_L G_L)\delta Z_L + A_{L\theta}\delta Z_\theta \qquad (3.20)$$

The characteristic equation is given by :

$$D_L(\lambda) = \lambda^2 + 2\omega g_{Ld}\lambda + 2\omega^2 g_{Lp} - \omega^2[(z_1+1)^2+3\cos^2 z_1-\omega^2] \qquad (3.21)$$

The damping coefficient is still set to .7.

$$g_{Lp} = \frac{1}{2}\left[\left(\frac{\omega_{cL}}{\omega}\right)^2 \frac{1}{1.01^2} + [(z_2+1)^2+3\cos^2 z_1-1]\right]$$

$$g_{Ld} = \frac{\omega_{cL}}{\omega}\frac{1}{1.01} \qquad (3.22)$$

The cross-over frequency is adjusted in order to be able to recover an initial 1% error on the states without thruster saturation.

3.3.1.3. LTI Simulation.

$\omega_{c\theta}$ and ω_{cL} are adjusted by performing a time simulation using the whole linearized dynamics at the entry point of the retrieval trajectory with a 1% error on every state.

$$\delta\dot{Z} = A(Z)\delta Z + B(Z)\delta u \quad \text{with} \quad \delta u = -G\delta Z \quad \text{and} \quad G = \begin{bmatrix} G_\theta & 0 \\ 0 & G_L \end{bmatrix} \tag{3.23}$$

$\omega_{c\theta}$ and ω_{cL} are adjusted to 10^{-2} rad.s^{-1} and 1.3 10^{-2} rad.s^{-1} respectively.

$$G = \begin{bmatrix} 50 & 7 & 0 & 0 \\ 0 & 0 & 84 & 9 \end{bmatrix}$$

Since the integral of a state usually is slower than the state itself, the gains on the pitch angle and on the length are higher in order to have the same time of recovery for the states and their integral. The variations of the gains along the nominal trajectory are given by fig 3.11. Since the linearized state space representation depends on the four states, the feedback gains also depend on the same four states at the point of linearization. However this plot suggests that the gains could be approximated by a gain scheduling law depending only on L, which would simplify the computation.

$$G(z_3) = \begin{bmatrix} 49.5z_3+.46 & 6.95z_3+.35 & 0 & 0 \\ 0 & 0 & 83.5 & 9.01 \end{bmatrix}$$

An LTI simulation for the system linearized at the entry point is given by fig 3.12 and 3.13. The state histories are given in the non-dimentionalized representation. The recovery is performed in approximately 1000s to be compared with 3596 s of the total retrieval time.

The loop transfer function is $G(sI-A)^{-1}B$. A plot of the singular value decomposition vs the frequency ω is given by fig 3.14. The maximum singular value crosses over at $\omega_{cmax} = 2.12$ 10^{-2} rad.s^{-1} whereas the minimum one crosses over at $\omega_{cmin} = 1.43$ 10^{-2} rad.s^{-1}. According to the singular value analysis, § 3.2.2.3, it approximately gives the cross-over frequency of the closed loop pitch dynamics and that of the length dynamics respectively. A sensitivity plot is given by fig 3.15. It shows in particular, that the amplitude of a disturbance, the frequency of which would be equal to two times the orbital rate like the atmospheric torque, would be divided by ten. Fig 3.16 shows a small amplification in closed loop for frequency in the range of 10^{-2} rad.s^{-1}.

For L = 5%, the recovery is performed in 800 s, fig 3.18, so the bandwidth of the closed loop system is increased but not enough to drive the system back on the nominal path in the

180 remaining seconds. Fig 3.17 also shows that the bandwidth of the pitch dynamics could be improved since the maximum level of control is far from being reached. Since for small length, the pitch and length dynamics are decoupled, the crossover frequency of both dynamics can directly be reached on the Bode plot of the maximum and minimum singular values, cf § 3.2.2.3. It shows that $\omega_{cmax} = 2.13\ 10^{-2}$ rad.s^{-1} and $\omega_{cmin} = 1.99\ 10^{-2}$ rad.s^{-1}. The difference between the two singular value is reduced, which was expected fig 3.30. The poles are placed by specifying approximately the same crossover frequency, making the assumption that both dynamics are decoupled, which becomes almost the case at this length.

The pole locations are given by fig 3.19 along the retrieval path. This plot enlightens the time varying nature of the system.

Overall, the feedback gain makes the system ten times faster.

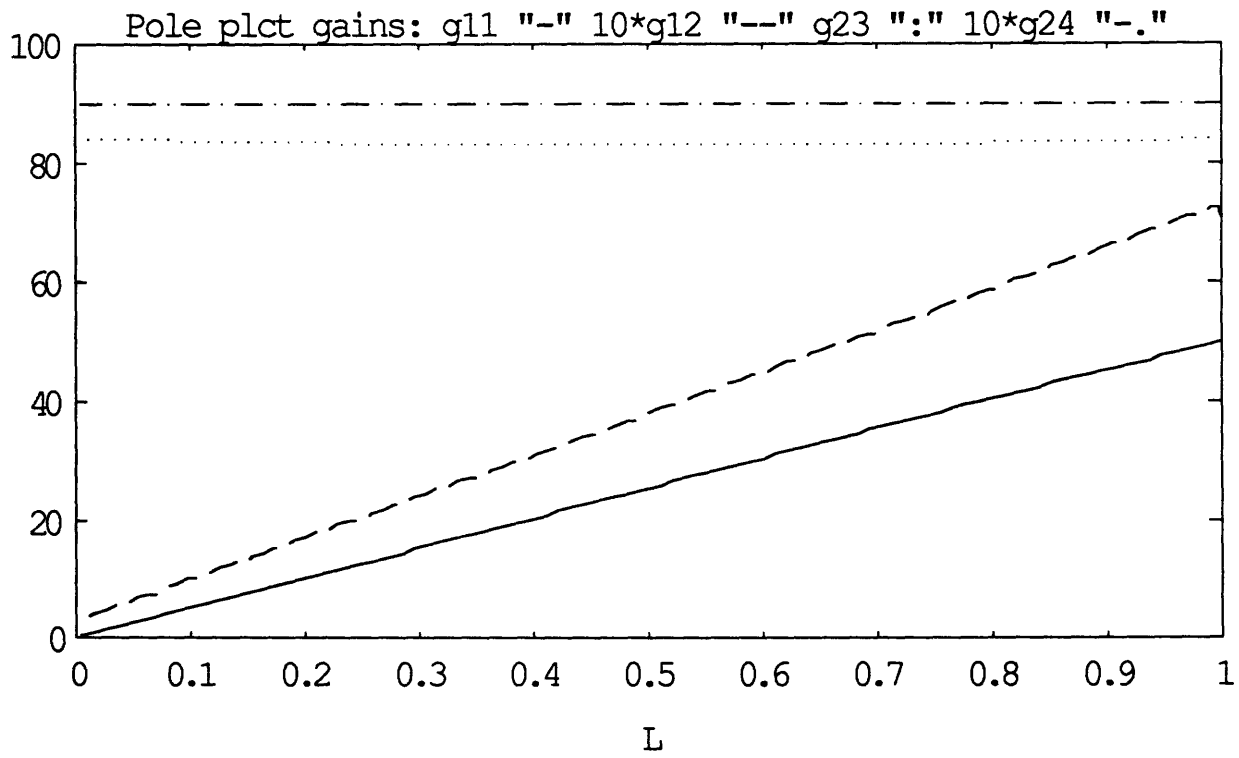

fig 3.11: Variations of the feedback gains vs nominal length, pole placement solution.

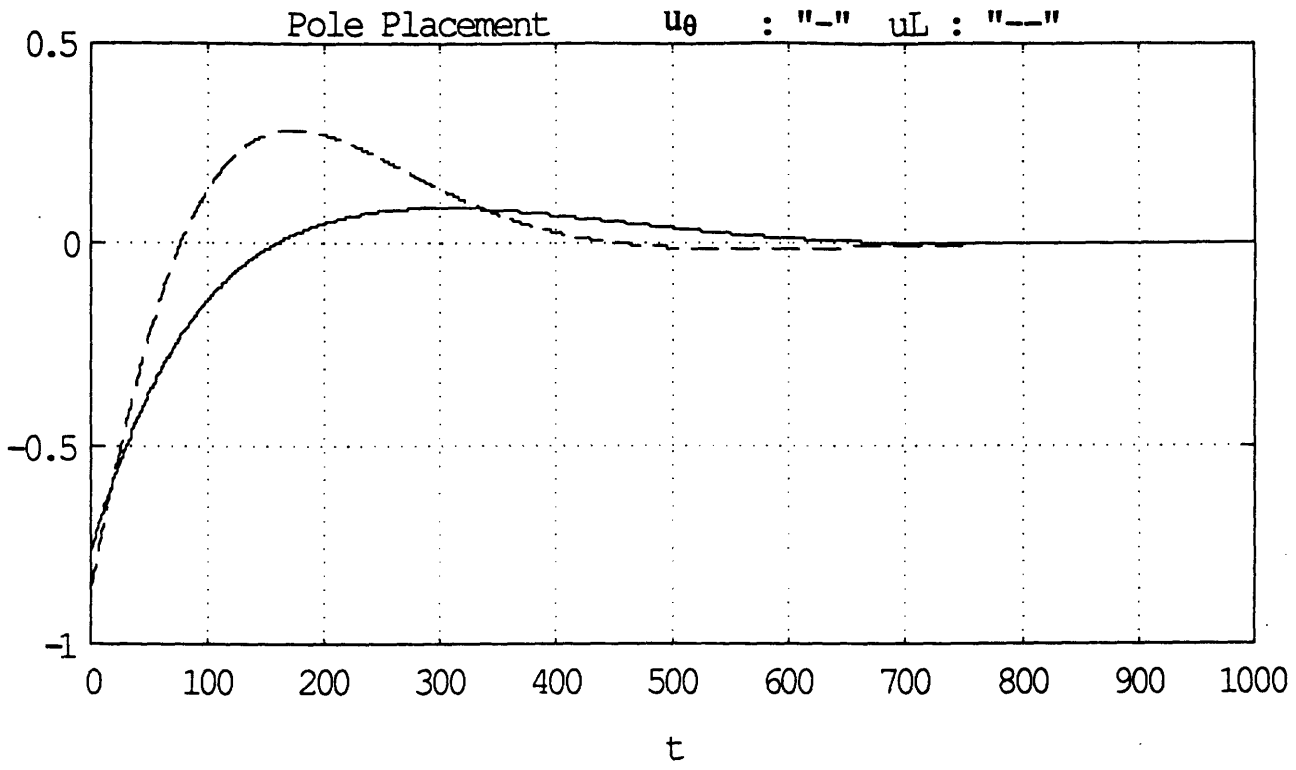

fig 3.12: Control history for a 1% error recovery. Pole placement Solution, L=0%

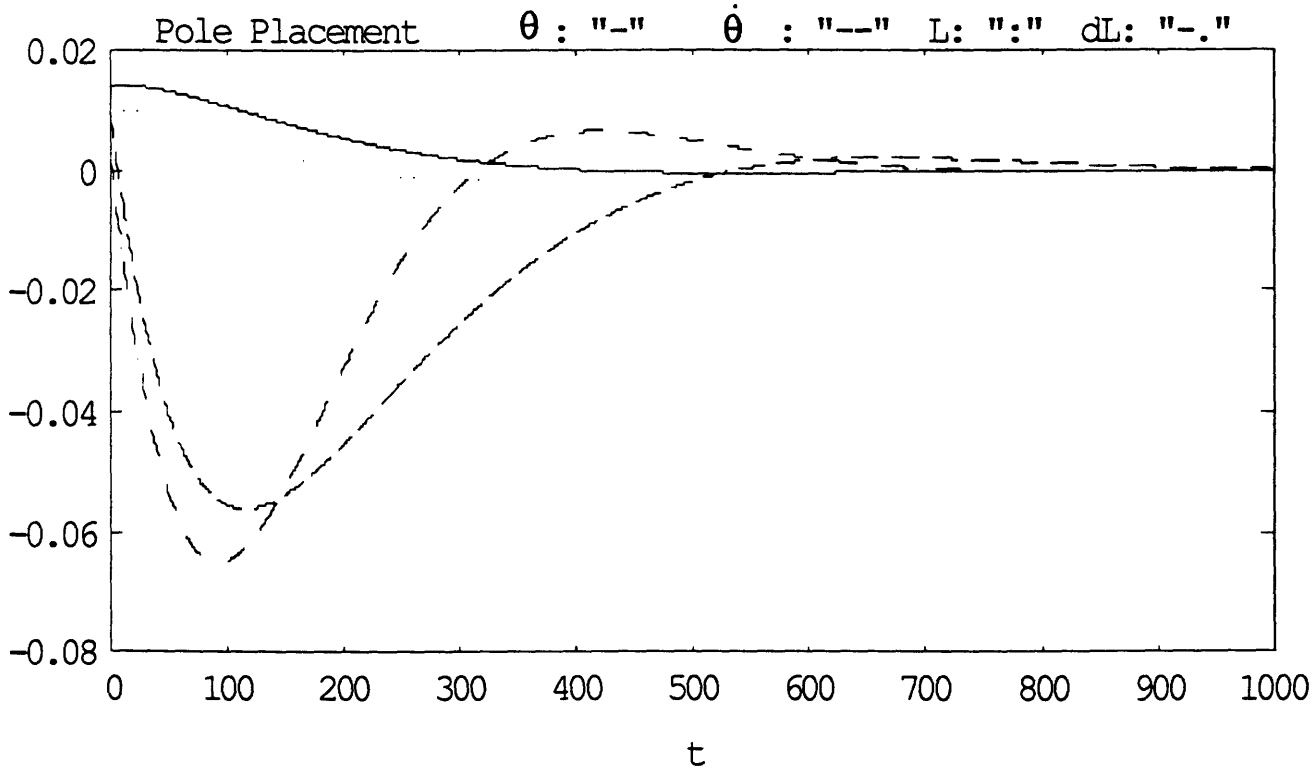

fig 3.13: Response to a 1%. Pole placement Solution, L=0%

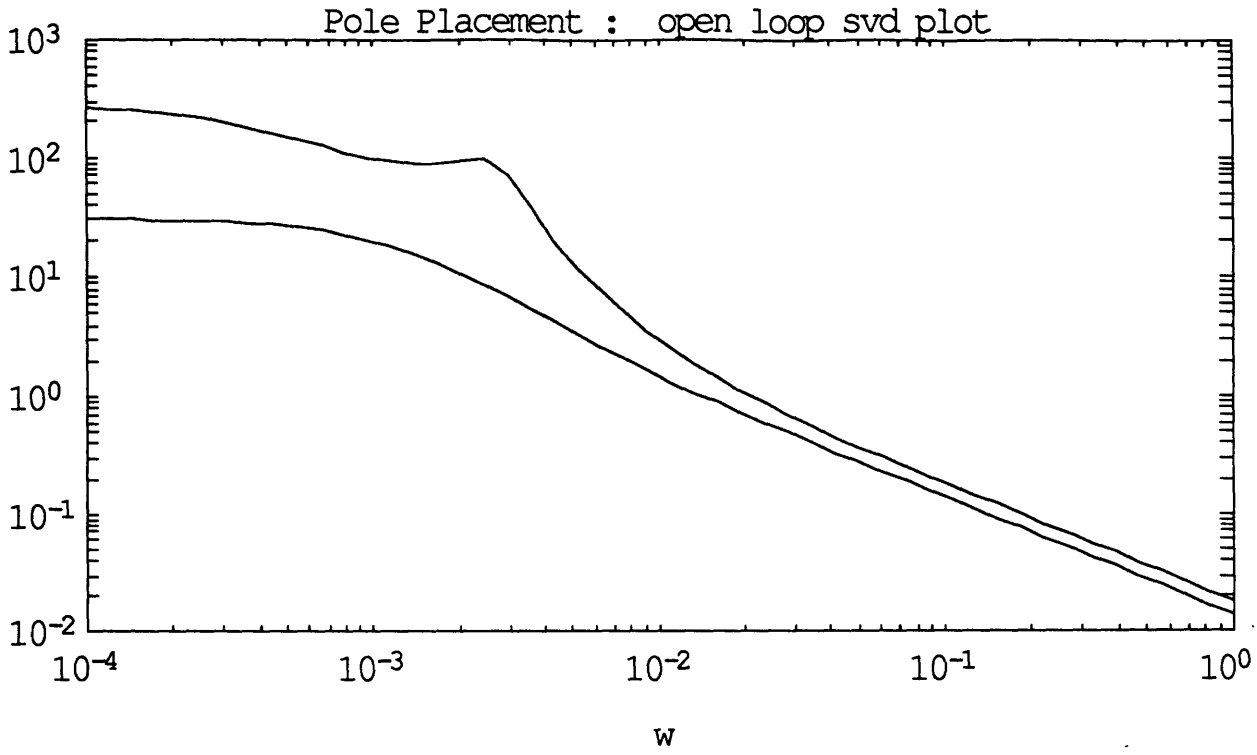

fig 3.14: Singular value decomposition of the loop transfer function, pole placement

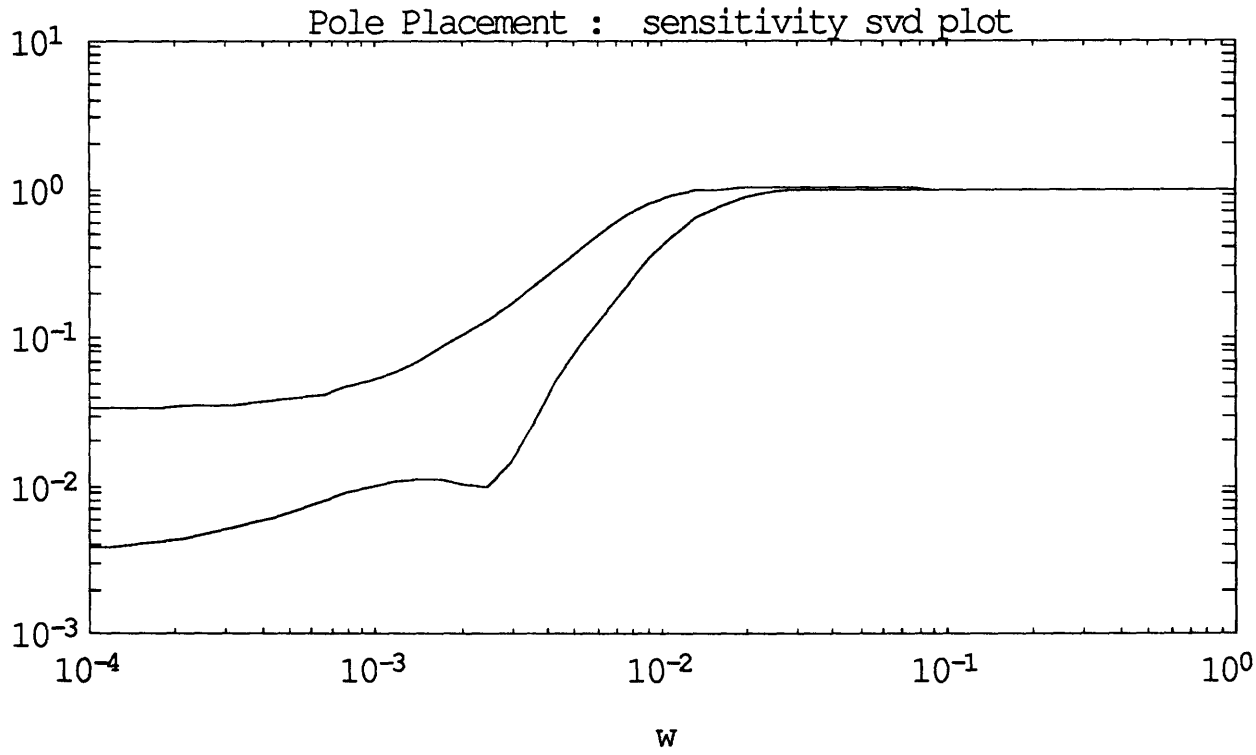

fig 3.15: Singular value decomposition of the sensitivity transfer function, pole placement

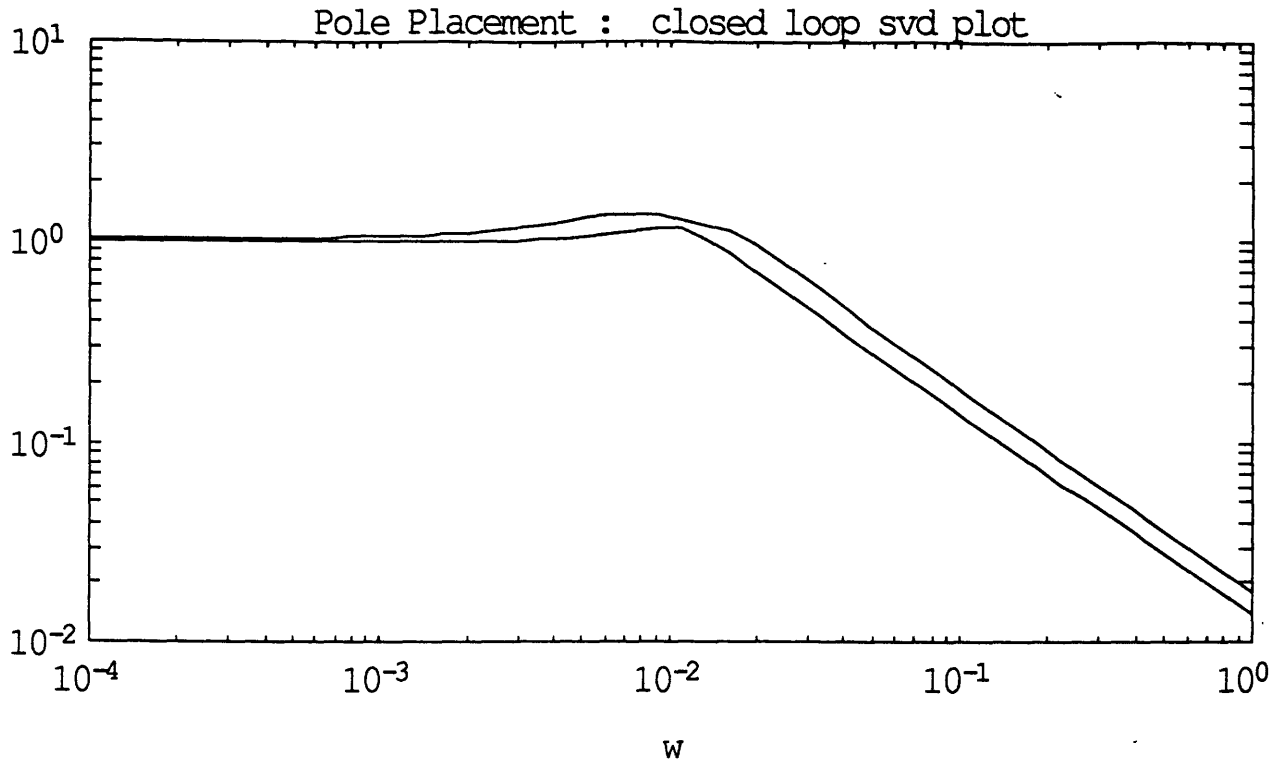

fig 3.16: Singular value decomposition of the closed loop transfer function, pole placement

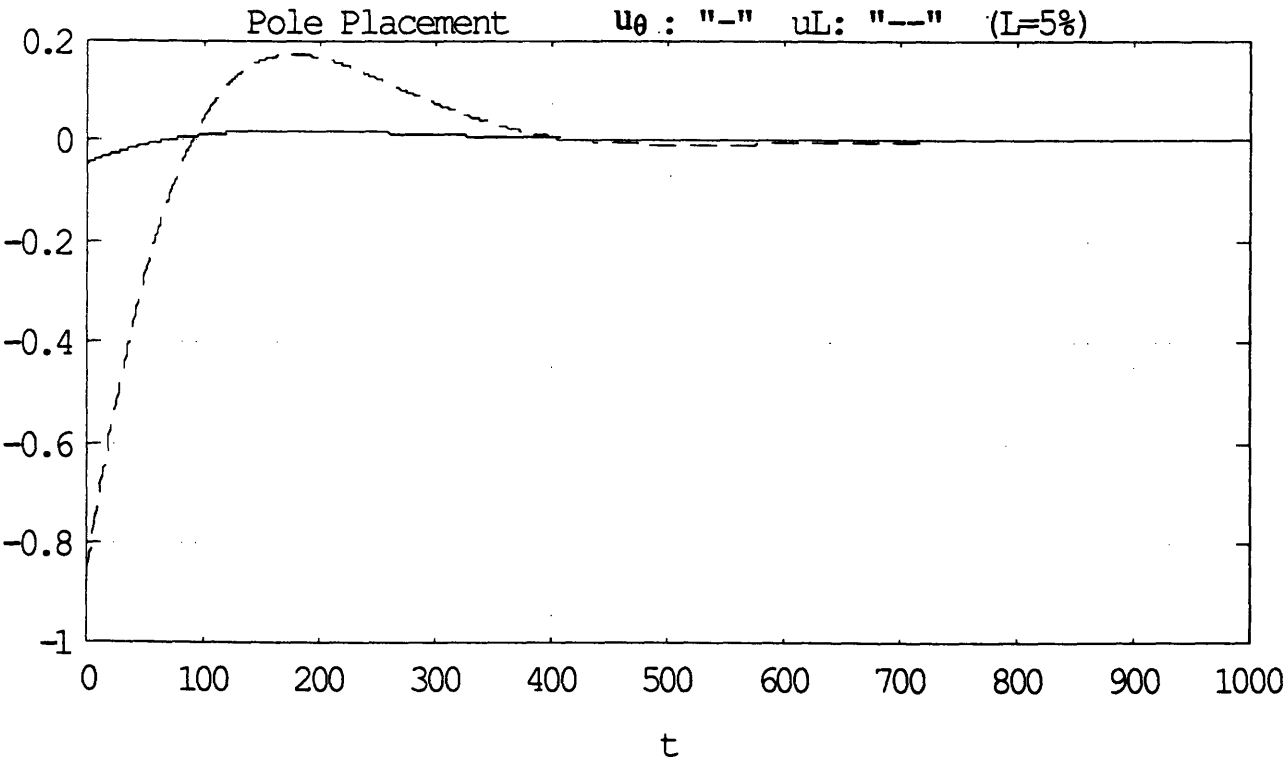

fig 3.17: Control history for a 1% error recovery, pole placement L=5%

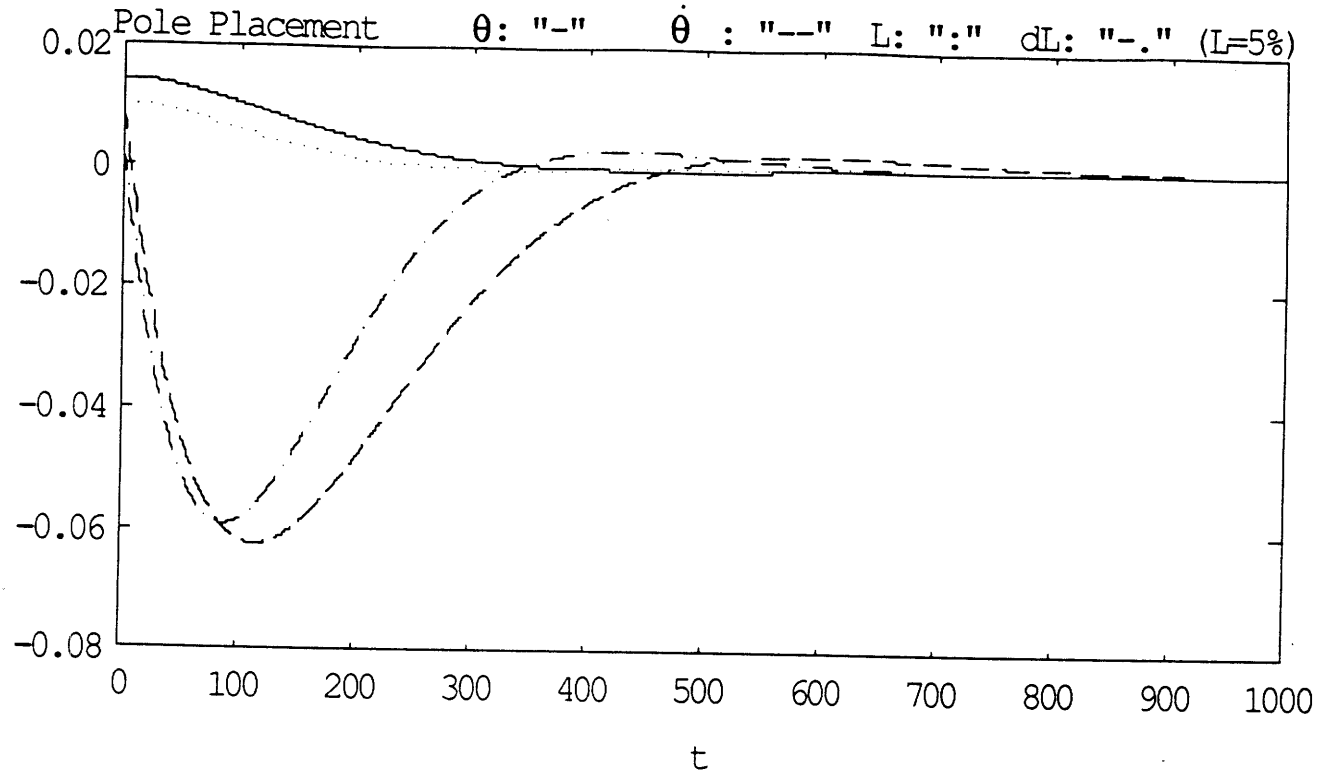

fig 3.18: Response to a 1% error, pole placement L=5%

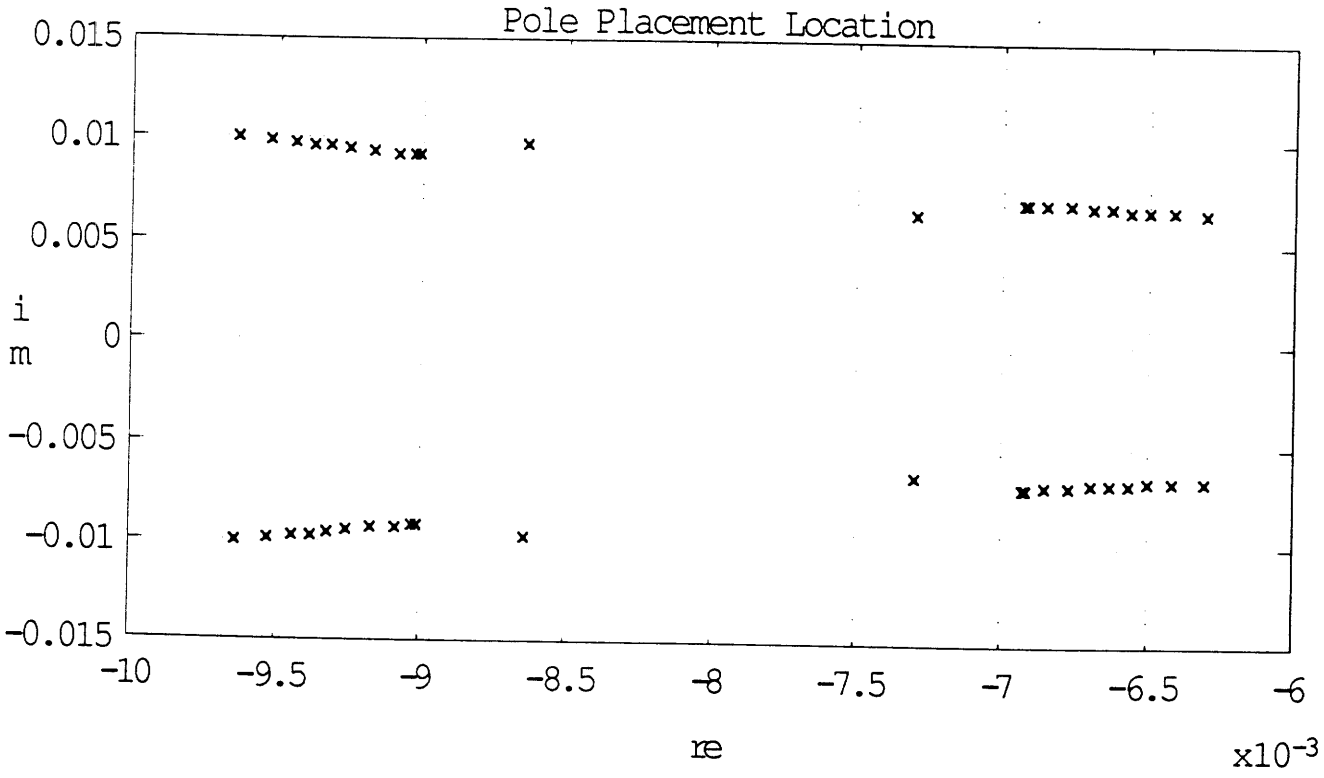

fig 3.19: Pole location along the nominal retrieval trajectory, pole placement

3.3.2. LQR compensator, a Multivariable Feedback Design.

LQR compensators are known to give smoother results than pole placement. In addition, the LQR solution takes advantage of the multicontrol nature of the system. The most difficult part of this design is to find the proper weighting matrices Q and R in the cost function J:

$$J = \int_0^{t_f} \delta Z^T Q \delta Z + \delta u^T R \delta u \, dt \tag{3.24}$$

An initial guess is given by the Bryson's rule. The purpose of the design is to be able to recover a one percent error Δz_i on every state with the maximum level of control available:

$$J = \int_0^{t_f} \sum_{i=1}^{4} \left(\frac{\delta Z_i}{\Delta Z_i} \right)^2 + \sum_{i=k}^{2} \left(\frac{\delta u_k}{u_{max}} \right)^2 dt \tag{3.25}$$

The weights on the integral of states usually are higher than those on the same states. After several adjustments, a good design is given by:

$$Q = \begin{bmatrix} 7.09 & 0 & 0 & 0 \\ 0 & 1.03\ 10^{-2} & 0 & 0 \\ 0 & 0 & 40 & 0 \\ 0 & 0 & 0 & .6 \end{bmatrix} \quad \text{and} \quad R = 4\ 10^{-3} I \tag{3.26}$$

For L = 0%,

$$G = \begin{bmatrix} 42.25 & 6.84 & 12.46 & .71 \\ -6.71 & .71 & 100.32 & 15.74 \end{bmatrix}$$

g_{21} and g_{22} converge toward zero as the length decreases since the pitch decouples from the length dynamics, fig 3.20. On the other hand, g_{13} and g_{14} tend toward zero and then diverge because of the cross term a_{23} in the A matrix.

Like for the pole placement design, fig 3.20 and 3.21 suggest that the gains could be approximated with a polynomial extrapolation vs the length. The final divergence of g_{13} and

g_{14} can be neglected since in any case, the closed loop is not fast enough to recover a disturbance occurring at this final point of the retrieval, providing this approximation does not drive the system unstable.

The pole location, fig 3.22, clearly enlightens the time varying nature of the TSS. The open loop unstable poles are matched in the left half plane by stable closed loop poles. The open loop structure is kept: two oscillatory poles ending on the real axis and two poles always remaining on the real axis. The oscillatory poles split, one diverging towards $-\infty$ and one converging to -.026. Of the two remaining poles, one remains steady at -.0088 whereas the last one approximately remains about -.02.

The response of the system to a one percent error is given by fig 3.23 through 3.24. The LQR solution makes a much better use of the controls compared with the previous solution, resulting in a smoother and faster recovery. The crossover frequency of the maximum and minimum singular value are respectively $\omega_{cmax} = 3.27\ 10^{-2}$ rad.s^{-1} and $\omega_{cmin} = 1.45\ 10^{-2}$ rad.s^{-1}, fig 3.25 through 3.27.

The advantage of the LQR algorithm is demonstrated by the results of the time simulation at L = 5% fig 3.28 and 3.29. Only the weighting matrices are fixed in this design and therefore, the bandwidth of the system is optimized at each step. Therefore, full use of the available control is made resulting in a faster closed loop system than the previous solution, fig 3.30, with better disturbance rejection properties, fig 3.31. $\omega_{cmax} = 8.54\ 10^{-2}$ rad.s^{-1} and $\omega_{cmin} = 3.25\ 10^{-2}$ rad.s^{-1}.

Because of its inherent qualities, this LQR design is retained over the previous one.

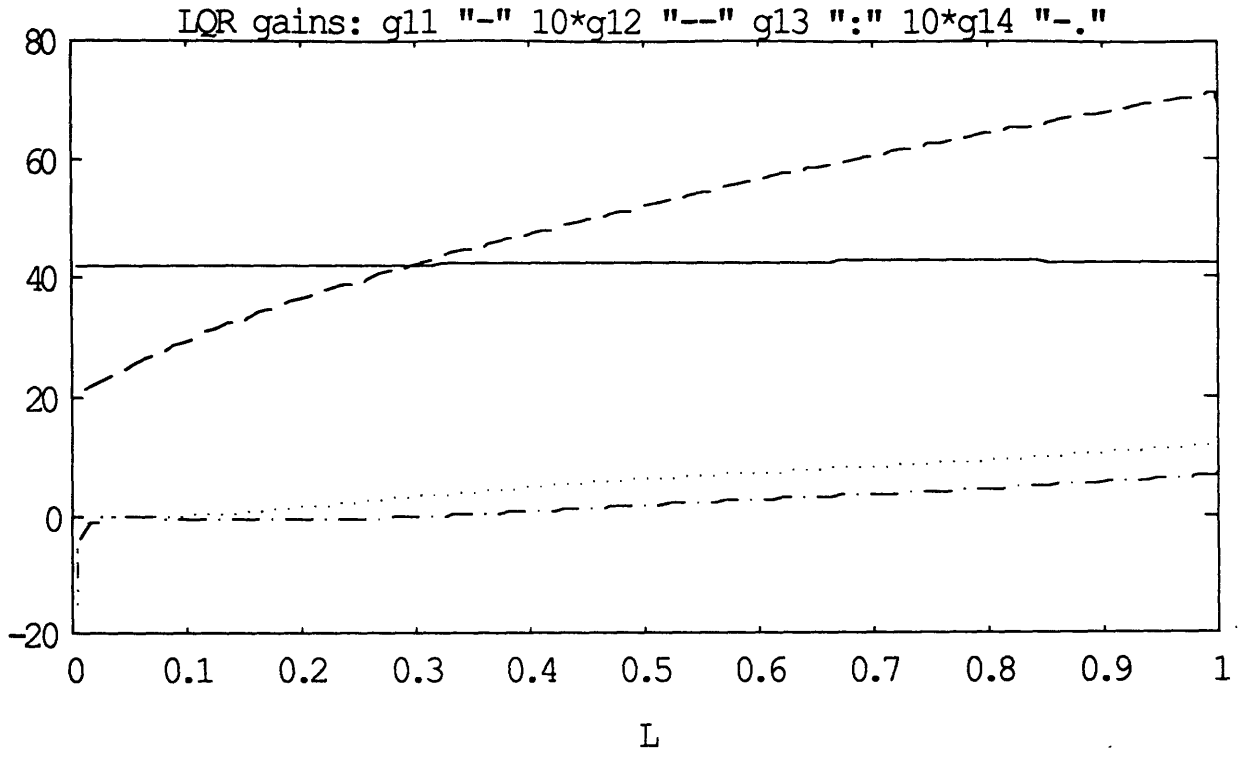

fig 3.20: Variations of the LQR feedback gains of the pitch control along the nominal retrieval

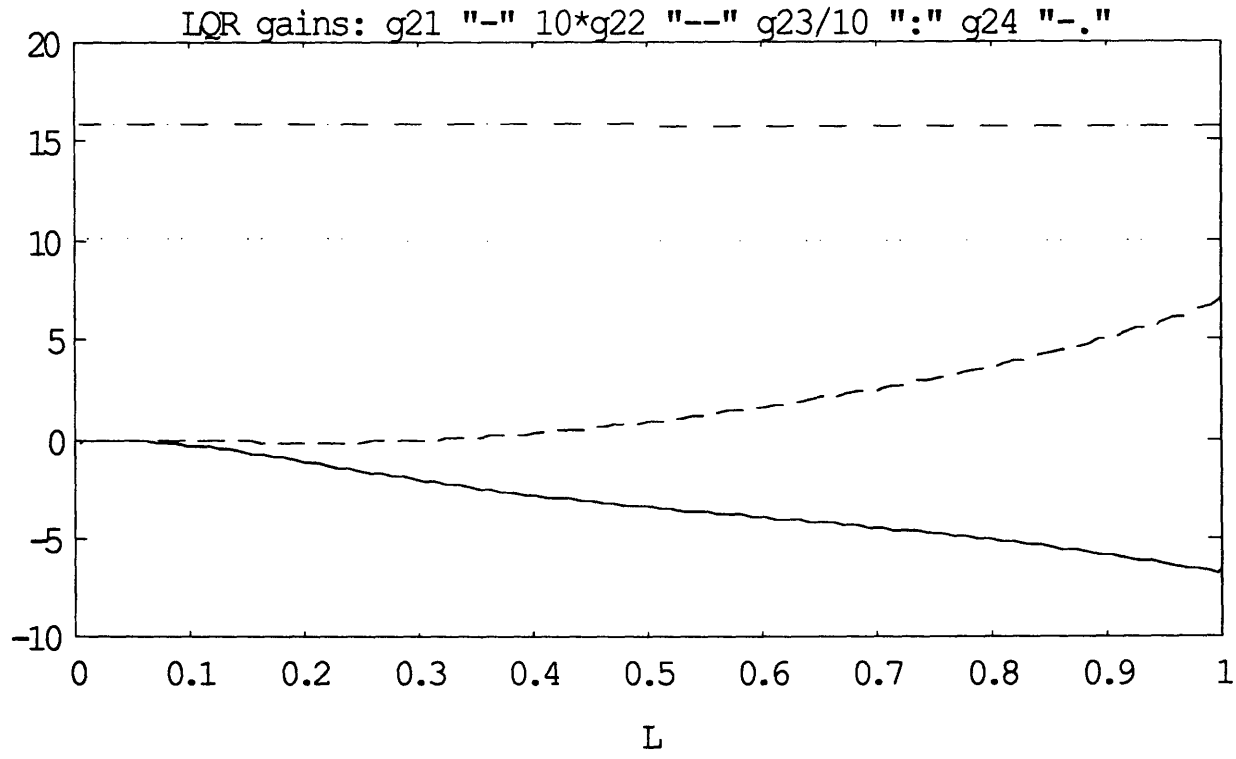

fig 3.21: Variations of the LQR feedback gains of the length control along the nominal retrieval

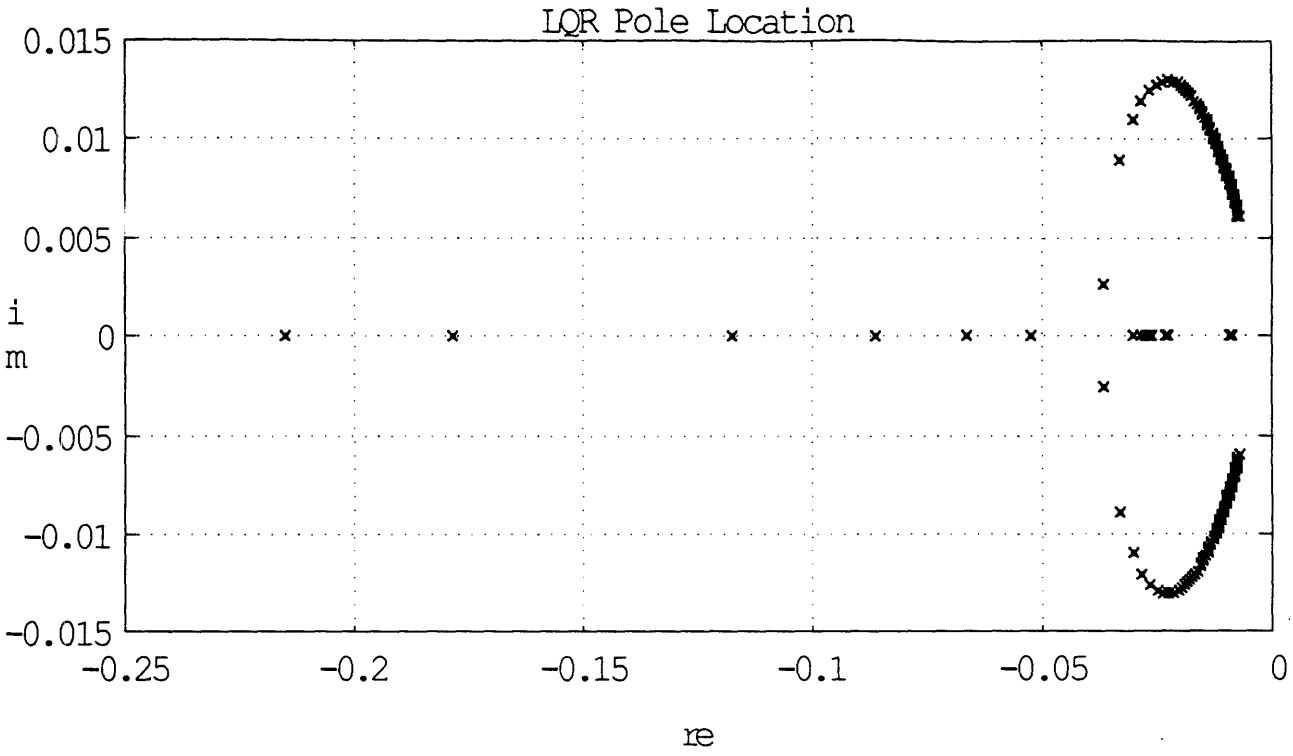

fig 3.22: Root locus of the LQR closed loop system along the nominal retrieval

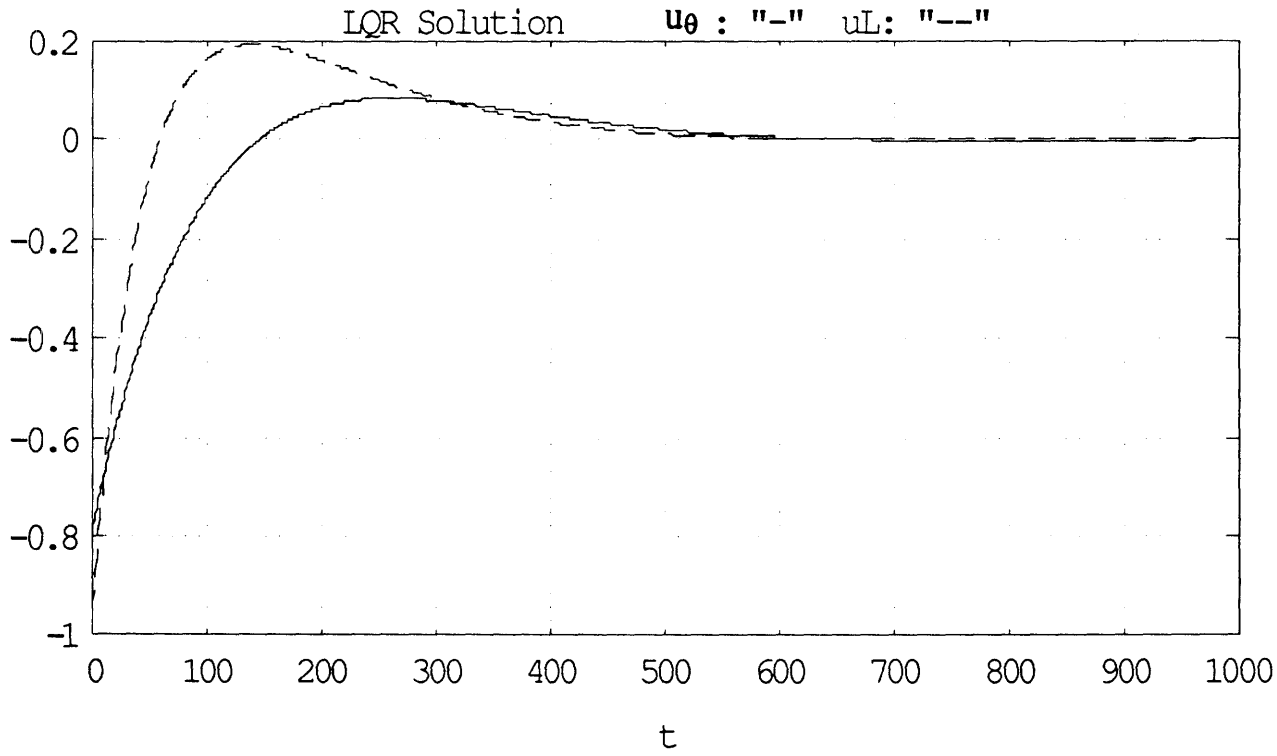

fig 3.23: LQR control history for a 1% error recovery L=0%

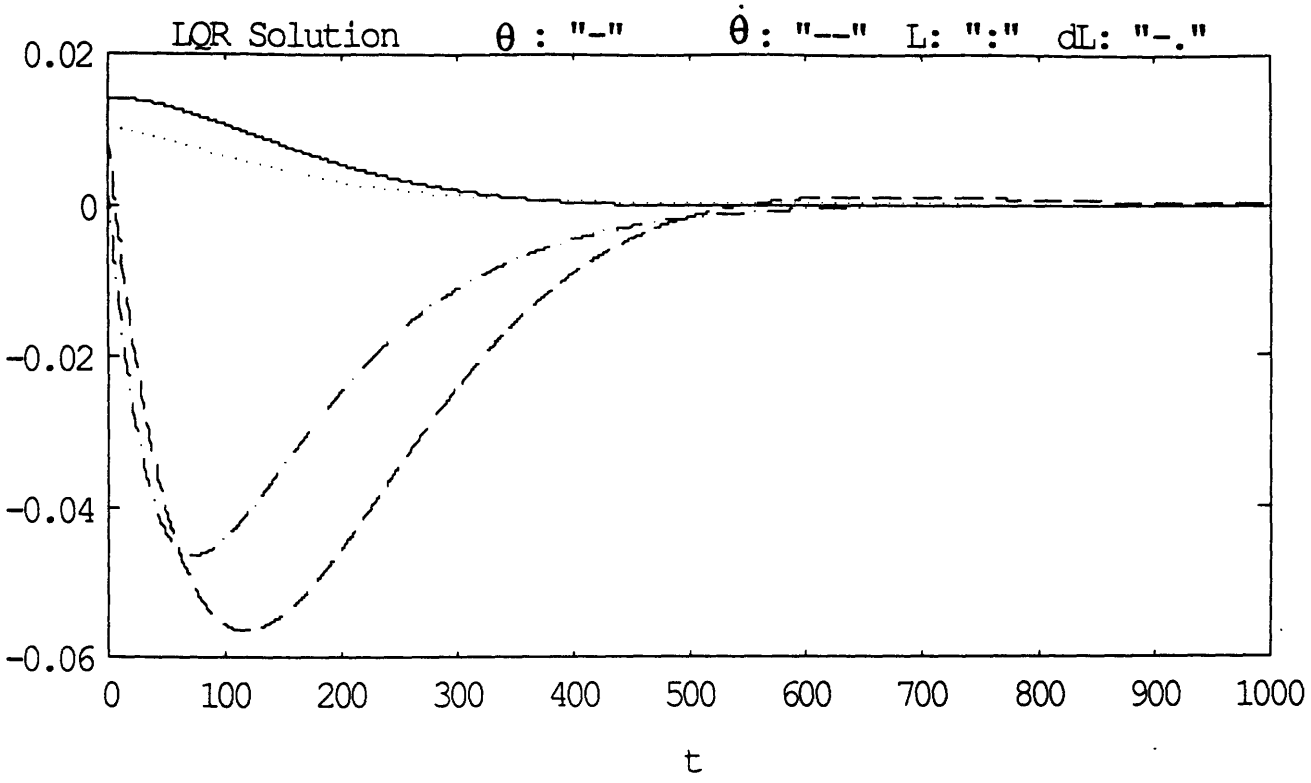

fig 3.24: LQR response of the system to a 1% error, L=0%

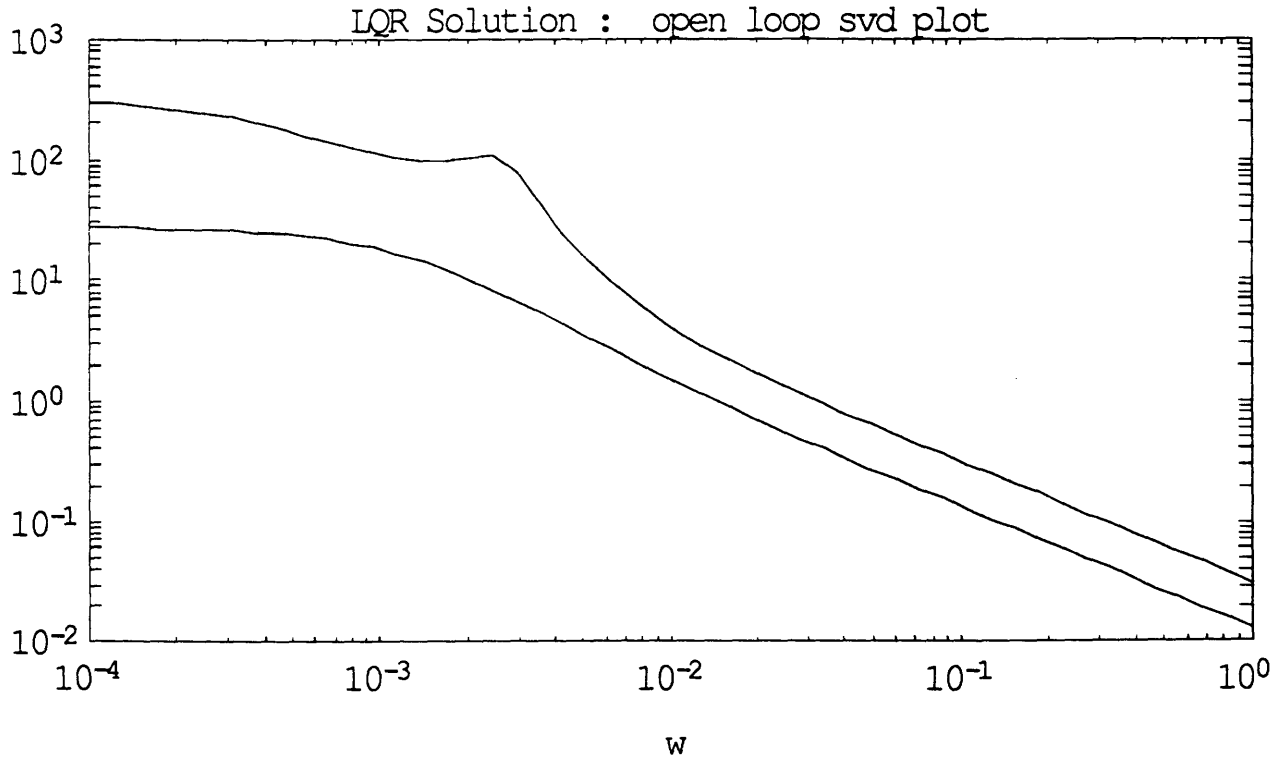

fig 3.25: Singular value decomposition of the LQR loop transfer function

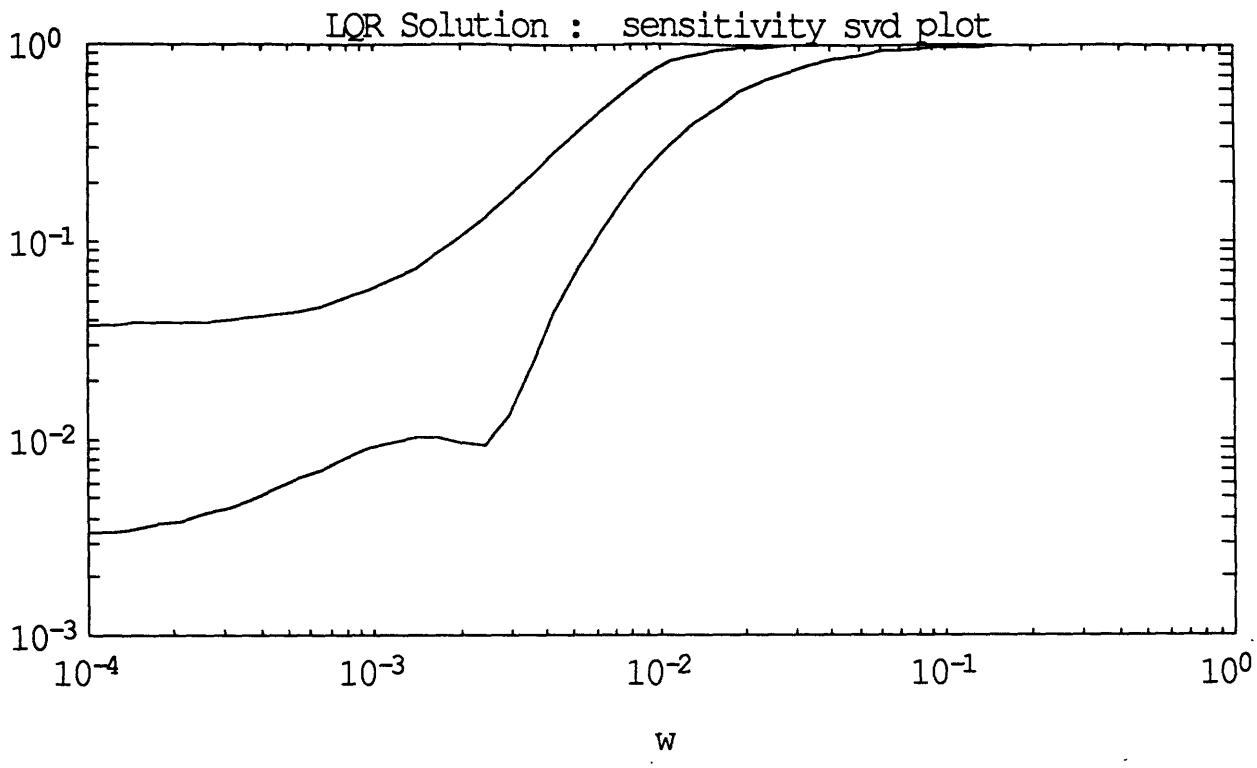

fig 3.26: Singular value decomposition of the LQR sensitivity transfer function

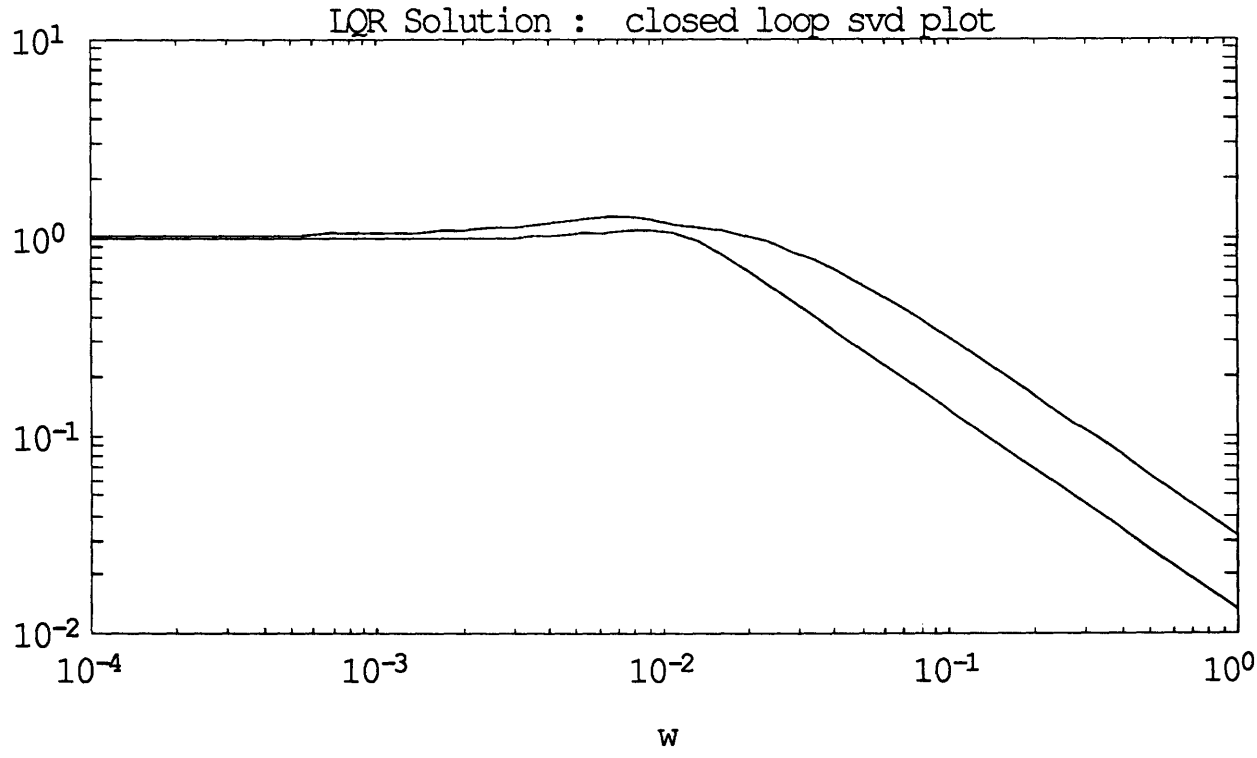

fig 3.27: Singular value decomposition of the LQR closed loop transfer function

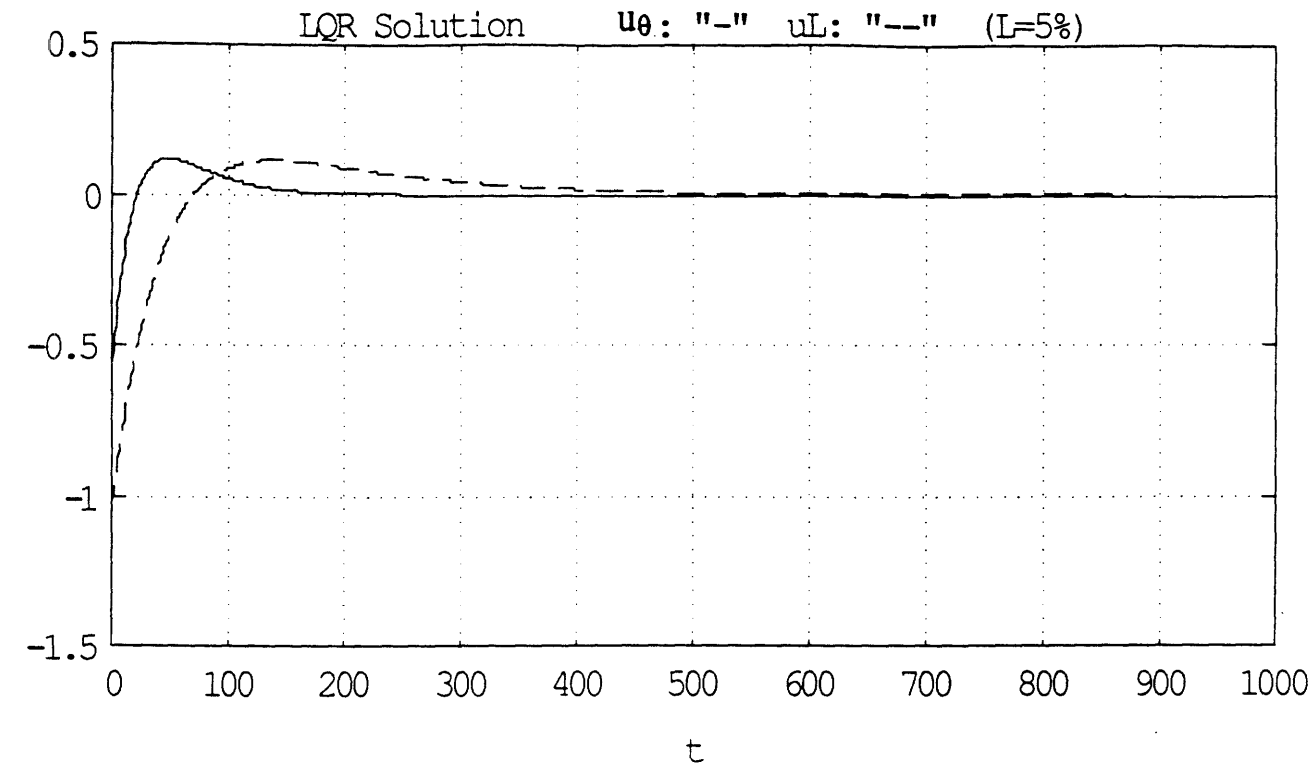

fig 3.28: LQR control history for a 1% error recovery, L=5%

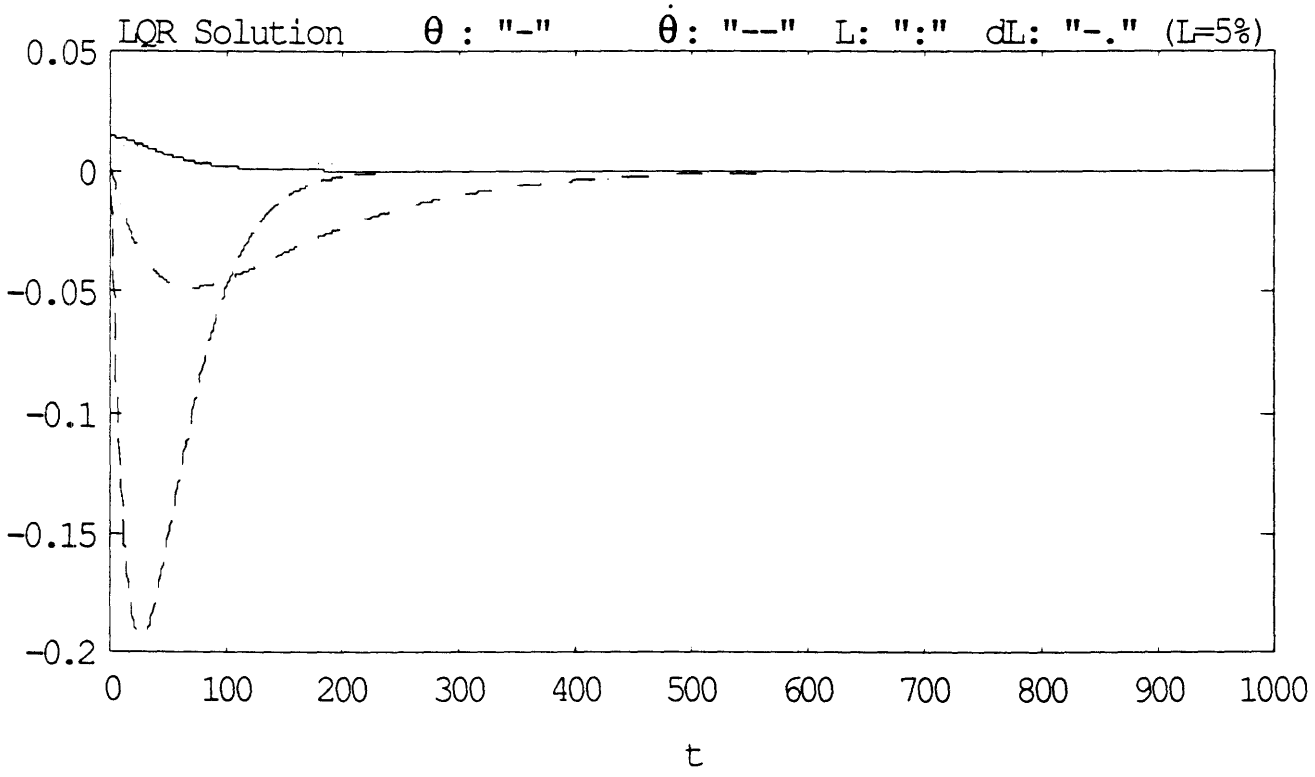

fig 3.29: LQR response of the system to a 1% error, L=5%

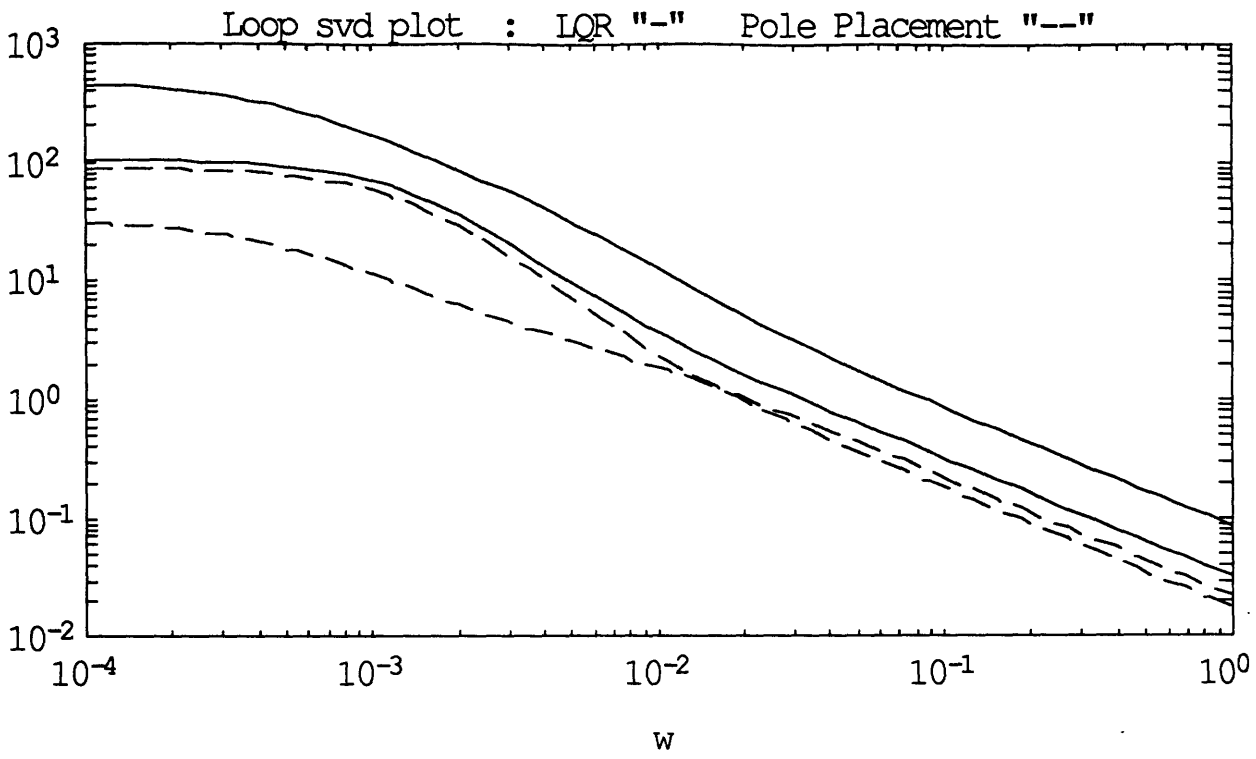

fig 3.30: Singular value decomposition of the loop transfer function, LQR & pole plct, L=5%

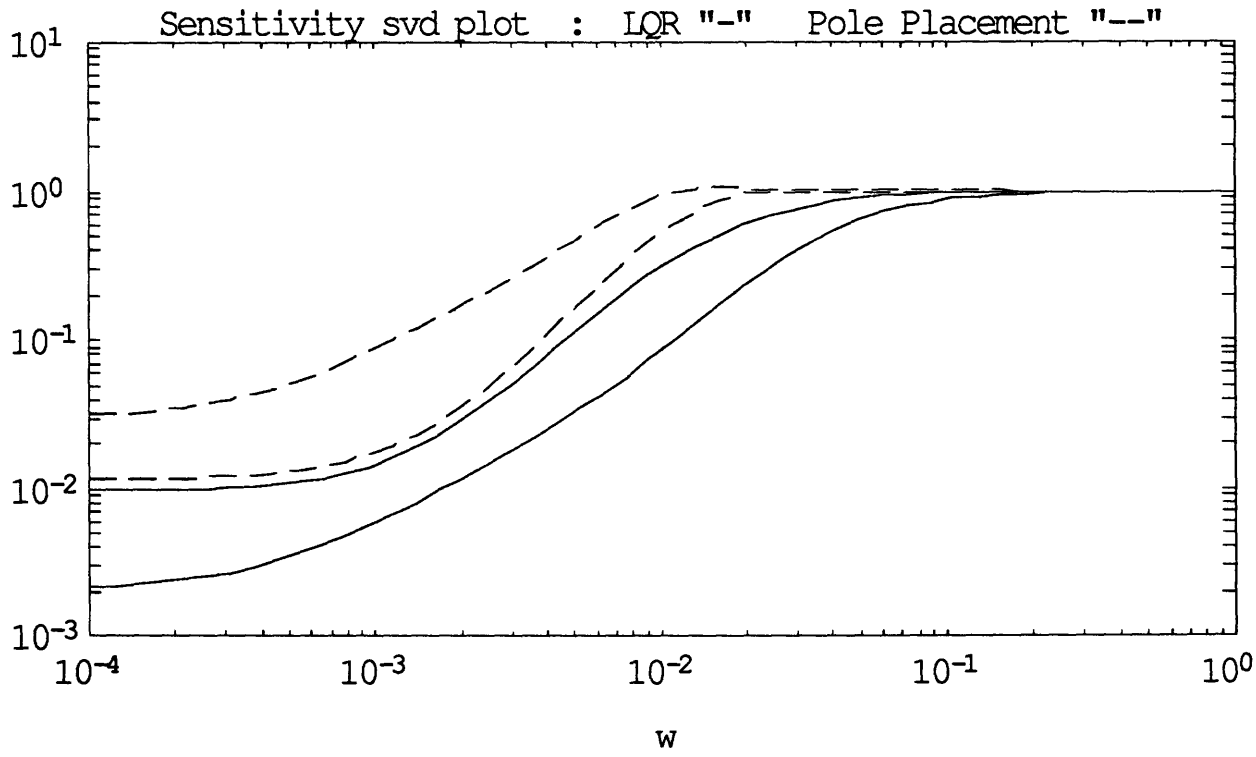

fig 3.31: Singular value decomposition of the sensitivity transfer function, LQR & pole plct, L=5%

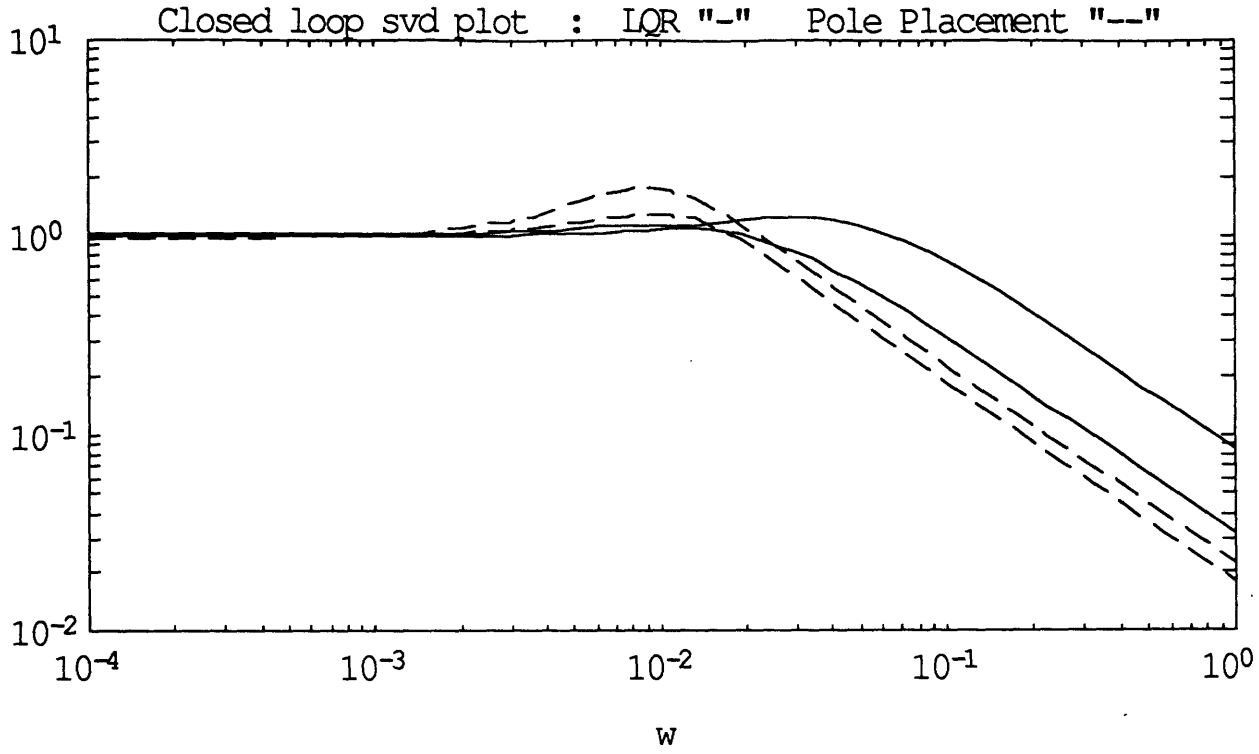

fig 3.32: Singular value decomposition of the closed loop transfer function, LQR & pole plct, L=5%

3.4. The Estimator Design.

The estimator must meet two objectives: estimate the pitch rate which can not be directly measured because of the many degrees of freedom introduced by the flexible tether, and estimate the pitch angle, the length and the length rate by filtering the noisy measurements resulting from sensor noises. The true states can already be considered as random processes because of thruster granularity and modeling error.

Because of these random processes involved, the retained estimator is an extended Kalman filter which takes into account the non-linear nature of the process in the propagation of the estimate. At each step during the retrieval, the state representation $\dot{Z} = f(Z,u)$ is linearized at the

first order about the estimated state in order to compute the Kalman filter gain. The additional precision obtained with a second order gaussian Kalman filter would not really justify the amount of computation required, considering the purpose of the mission.

The available specification on the Ku band radar is a precision of ±2°. For the purpose of the Kalman filter design, this precision must be converted into a white gaussian noise. for such a gaussian noise y of standard deviation σ, the probability P that the variation of y from its mean $\bar{y}$ be lower than 2.58σ is equal to 99%.

$$P(|y - \bar{y}| < 2.58\sigma) = .99$$

Therefore a precision of Δy_i on the measurement y_i is approximated with a white gaussian noise, the standard deviation of which is given by $\sigma_i = \frac{\Delta y_i}{2.58}$.

To the precision of the Ku band radar must be added the precision of 20 arcsec of the estimate of the orbiter attitude. The length and length rate measurements are arbitrary considered to have a precision of 1%, in the absence of reliable technical data. Therefore,

$$\sigma_\theta = \frac{2.0056}{2.58}\frac{\pi}{180} = 1.36\ 10^{-2},\ \sigma_L = \frac{20}{2.58L_i} = 3.88\ 10^{-3} \text{ and } \sigma_{\dot{L}} = \frac{6.08\ 10^{-3}}{2.58\omega L_i} = 1.18\ 10^{-3}$$

and the covariance matrix V of the sensor noises is equal to:

$$V = E[vv^T] = \begin{bmatrix} \sigma_\theta^2 & 0 & 0 \\ 0 & \sigma_L^2 & 0 \\ 0 & 0 & \sigma_{\dot{L}}^2 \end{bmatrix} \quad \text{with } y = CZ + v \tag{3.27}$$

The plant noise w represents modeling errors like the different modes of vibration of the tether or the modes introduced by the orbiter control system, which were not taken into account. In a first simplification, only the plant noise introduced by the thruster granularity will be taken into account. This thruster granularity introduces a precision of $8\ 10^{-2}$ rad.s^{-1}, § 3.1.2., on the non dimensionalized requested level of thrust u_θ. Therefore, the linearized dynamics can be represented as follow:

$$\delta\dot{Z} = A(Z)\delta Z + B(Z)\delta u + L(Z)w$$

$$\text{with } L(Z) = [0\ \frac{2\omega}{z_3}\ 0\ 0]^T \text{ and } W = E[ww^T] = \left(\frac{8\ 10^{-2}}{2.58}\right)^2. \qquad (3.28)$$

An approximated optimal estimate of the states is given by:

$$\dot{\hat{Z}} = f(\hat{Z},u) + H\left(Y - C\hat{Z}\right) \quad \text{with} \quad H = \Sigma C^T V^{-1} \qquad (3.29)$$

where Σ is solution of $A\Sigma + \Sigma A^T + LWL^T - \Sigma C^T V^{-1} C\Sigma = 0$.

The estimator is supposed to be run for a while before starting the retrieval. Thus only the steady state solution of the Kalman filter algorithm is retained.

For L = 0%,

$$H = 10^{-3}\begin{bmatrix} 1.98 & -.16 & 4.85 \\ 2.05 & -.37 & 49.21 \\ -.01 & .30 & 1.00 \\ .04 & .09 & 16.32 \end{bmatrix}$$

These gains remain fairly constant in the range of .1 10^{-3} to finally diverge at the end of the retrieval in order to follow the final increase of velocity of the system, fig 3.35 to 3.37. The high gains on the measurement of the length rate are due to the fact that this measurement is less noisy than the others. The low gains on the measurements of the pitch reflect the low quality of these measurements.

The singular value decomposition of the loop transfer function $C(sI-A)^{-1}$ reveals this same difference of quality between the measurements with an important gap between the maximum and the minimum singular value fig 3.33.

For L = 0%, the poles are:

$$\lambda_{12} = -8.66\ 10^{-3} \pm i\ 9.00\ 10^{-3}$$

$$\lambda_3 = -.98\ 10^{-3}$$

$$\lambda_4 = -.31\ 10^{-3}$$

The dynamics of this estimator are in the range of that of the pole placement feedback and slower than that of the LQR feedback, fig 3.19, 3.22 and 3.34. It means that the estimator almost only relies on the prediction of the estimates to reconstruct the states. This is due to the fact that plant noises are small compared with sensor noises. However, because of a lack of information, only thruster granularity was retained in the plant noise model. This model ignores non-rigid body motion, out-of-plane coupling, orbiter-tether coupling.

The pole locations along the nominal trajectory are given by fig 3.34. Two poles, starting oscillatory at $-8.66\ 10^{-3} \pm 9.00\ 10^{-3}$ split into one diverging towards $-\infty$ and the other one converging to -.01. The two others, starting from $-.98\ 10^{-3}$ and $-.31\ 10^{-3}$, remains real to eventually converge to $-1.65\ 10^{-3} \pm i\ .25\ 10^{-3}$.

A good design should lead to an estimator crossover frequency one decade above that of the feedback. The estimator would rely less on the approximated model to build the estimates of the states, using the measurements to update the prediction. Such a bandwidth can be adjusted by making guesses on the value of the plant noise covariance matrix W. z_1 and z_3 being only the integral of the non-dimentionalized states z_2 and z_4, W may be written as:

$$W = \varpi\, I(2) \quad \text{with} \quad L = \begin{bmatrix} 0 & 1 & 0 & 0 \\ 0 & 0 & 0 & 1 \end{bmatrix}^T$$

For $\varpi = 10^{-3}$, the estimator closed-loop poles are:

$$\lambda_{12} = -2.16\ 10^{-1} \pm i\ 2.16\ 10^{-1}$$

$$\lambda_3 = -.98\ 10^{-3}$$

$$\lambda_4 = -.31\ 10^{-3}$$

Another approach would be to use the covariance matrix of the plant noise and that of the sensor noise to adjust the bandwidth of the estimator, using singular value matching theory. If $V = \mu\, I$, $W = I$ and $L = C^T(CC^T)^{-1}$, then the bandwidth of the estimator can be directly adjusted to 10^{-1} rad.s^{-1} by taking μ equal to 10^2 fig 3.38. This approach gives a fast estimator;

however, because of the singular value matching, it supposes that all the measurements are equally noisy. Therefore, such a design would give good results in the transient but would very badly filter the sensor noises in the steady state.

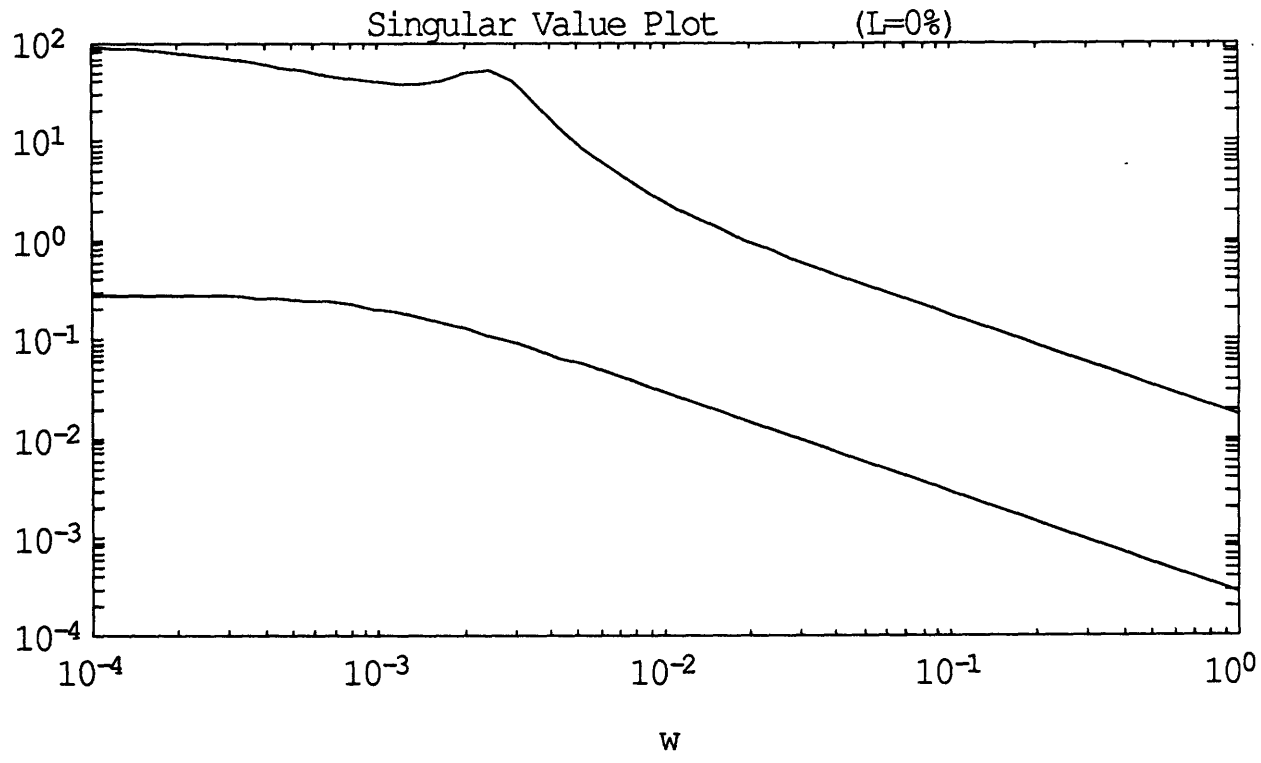

fig 3.33: Singular value decomposition of the estimator loop transfer function, L=0%

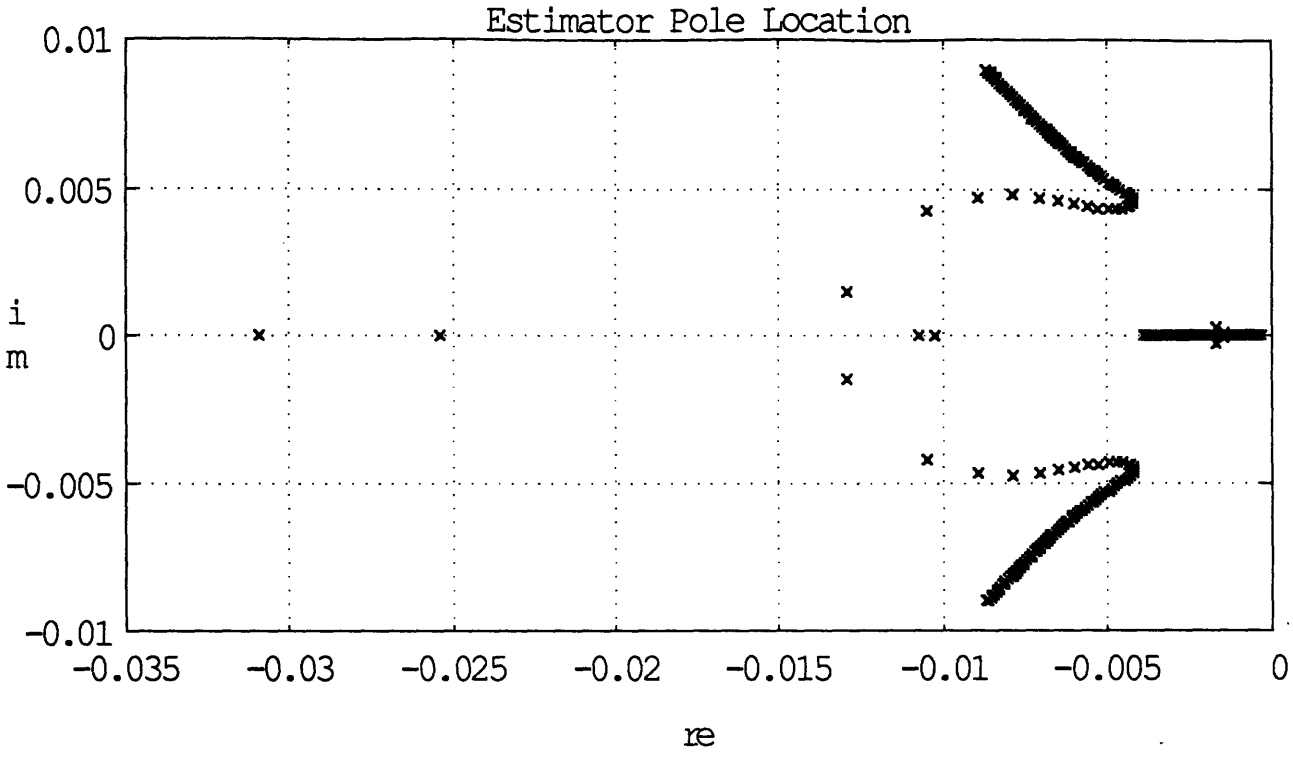

fig 3.34: Root locus of the estimator along the nominal retrieval

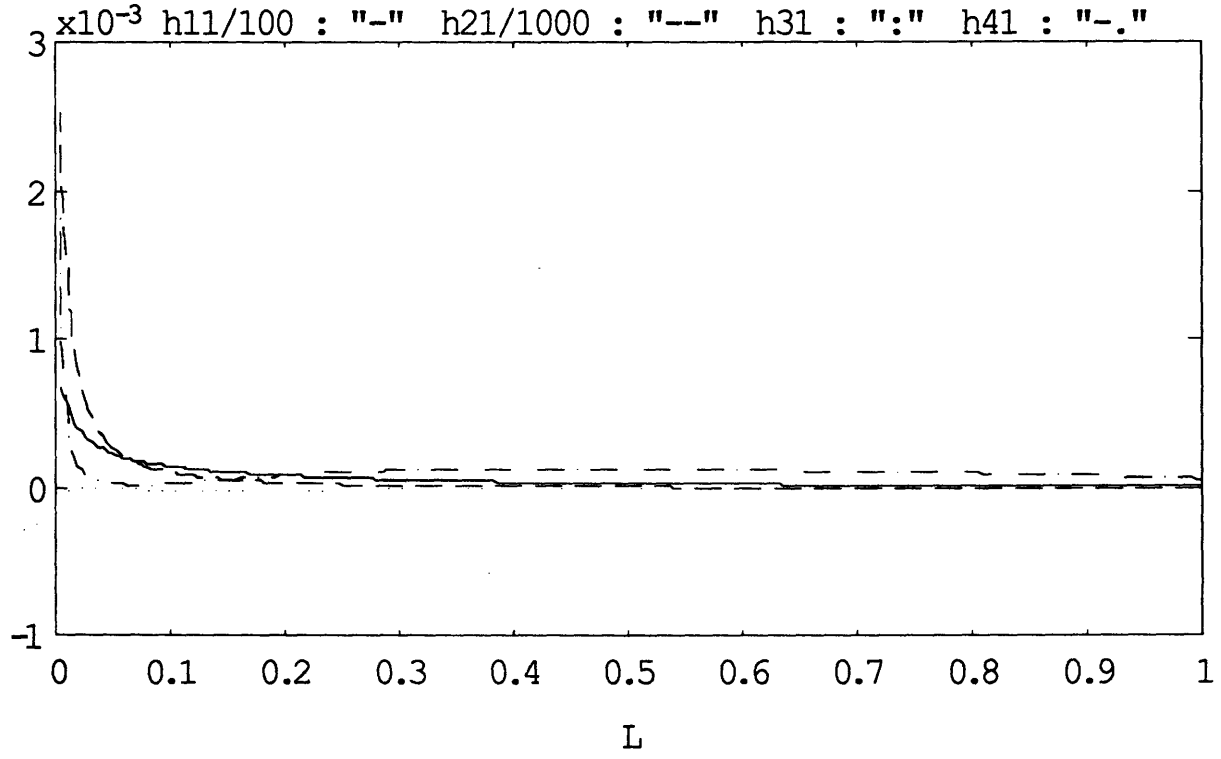

fig 3.35: Variation of the estimator gains on the pitch measurement along the nominal retrieval

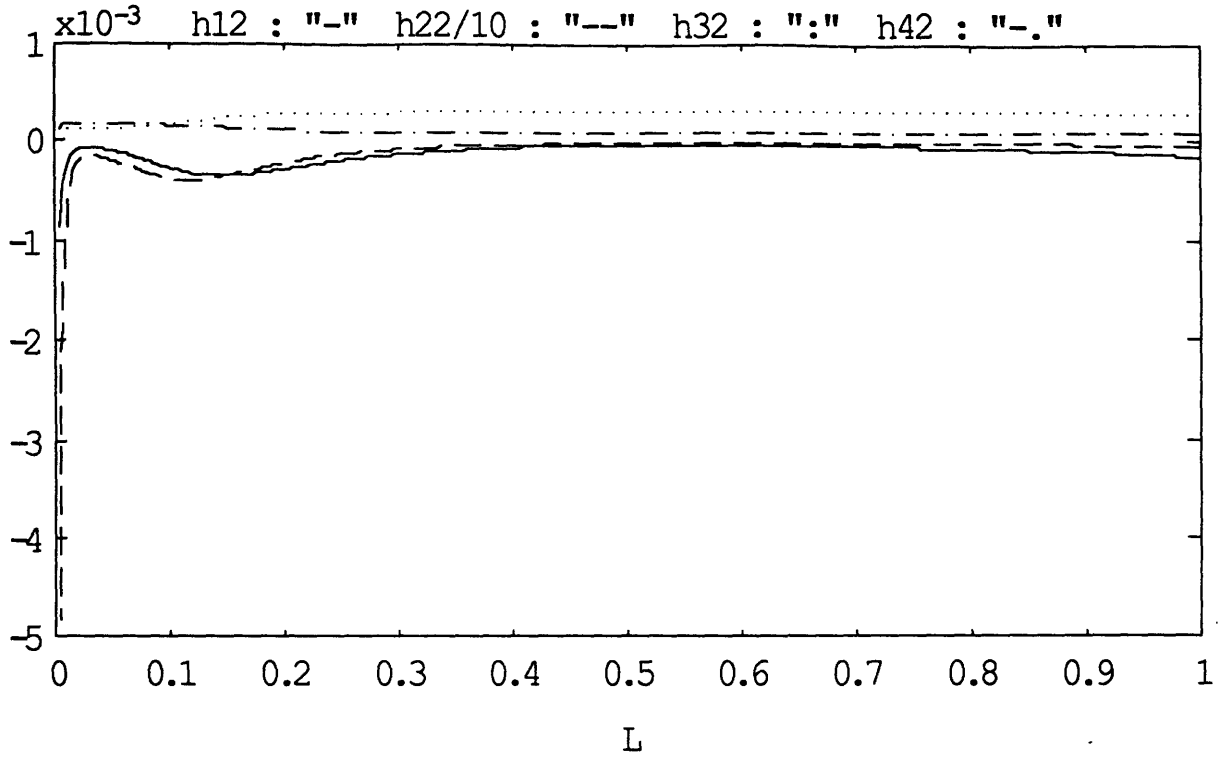

fig 3.36: Variation of the estimator gains on the length measurement along the nominal retrieval

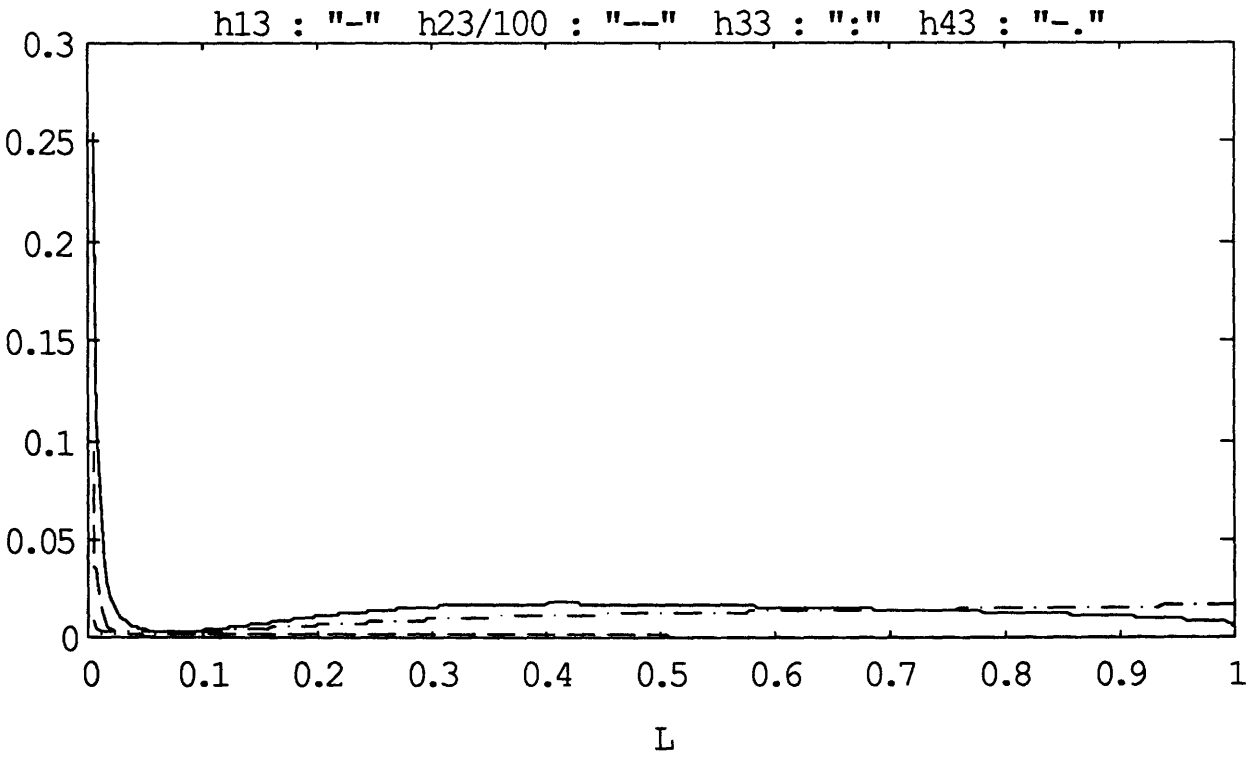

fig 3.37: Variation of the estimator gains on the length rate measurement along the nominal retrieval

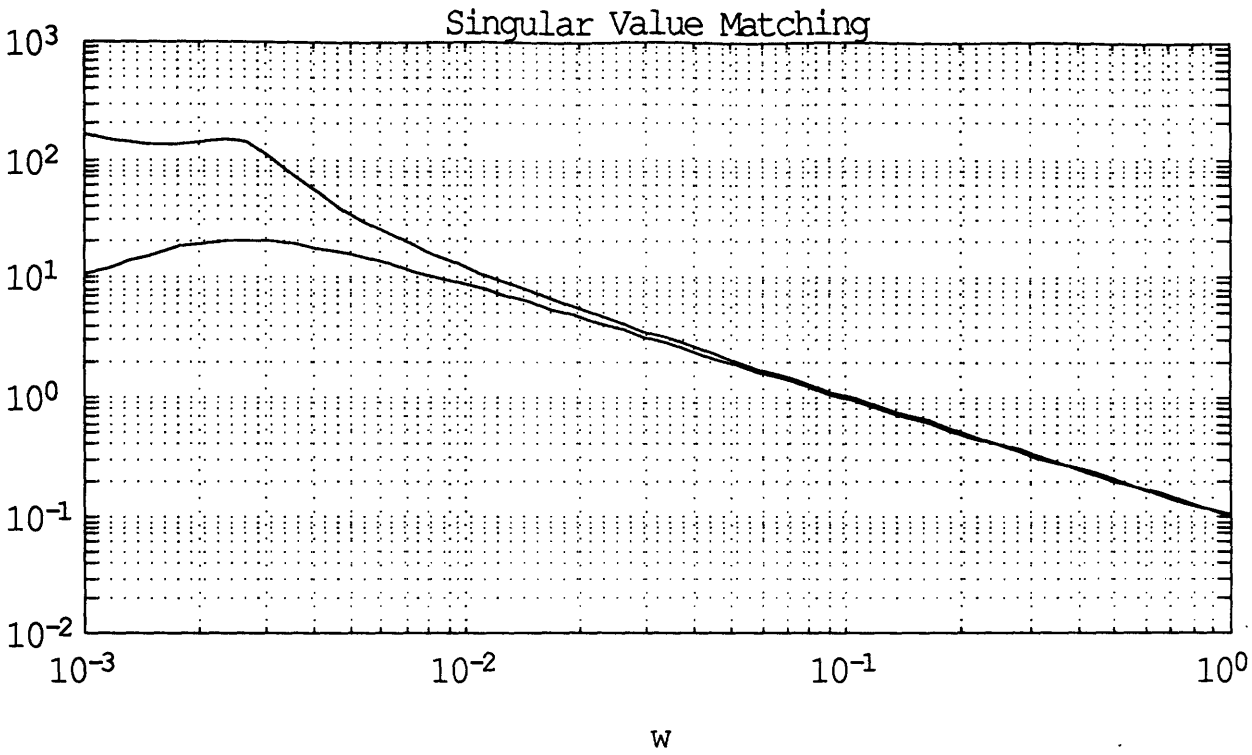

fig 3.38: Estimator singular value matching design.

3.5. LQG Simulation of the Linearized System.

In order to assess the quality of the whole design, an LQG simulation of the system linearized at the entry point is performed. The results of the LQG response for a one percent error on every state are compared with the response of the system driven by the LQR compensator with the same noises.

The linearized system is given by:

$$\delta\dot{Z} = A\delta Z + B\delta u + Lw \tag{3.30}$$

The estimates of the states are given by:

$$\delta\dot{\hat{Z}} = A\delta\hat{Z} + B\delta u + H(\delta Y - C\delta\hat{Z}) \quad \text{with} \quad \delta Y = C\delta Z + v \tag{3.31}$$

and the control $\delta u = - G\hat{Z}$.

Therefore,

$$\begin{bmatrix} \delta\dot{Z} \\ \delta\dot{\hat{Z}} \end{bmatrix} = \begin{bmatrix} A & -BG \\ HC & A-BG-HC \end{bmatrix} \begin{bmatrix} \delta\dot{Z} \\ \delta\dot{\hat{Z}} \end{bmatrix} + \begin{bmatrix} L & 0 \\ 0 & H \end{bmatrix} \begin{bmatrix} w \\ v \end{bmatrix} \qquad (3.32)$$

In the case of an LQR regulator, $\delta u = - G(\delta X + v)$. There is a direct transmission of the measurement noises whereas with an LQG scheme, the estimator filters them. For the purpose of the LQG/LQR comparison, the pitch rate is supposed to be measured with a 1% precision.

Fig 3.39 shows the random oscillations of the pitch control resulting from the thruster granularity and from the random nature of the states. The length and length rate responses are hardly impaired by the presence of noisy measurements fig 3.43 and 3.44. On the other hand, the pitch rate randomly oscillates about the reference response without noise fig 3.42, with a maximum amplitude of oscillation equal to $3\ 10^{-3}$ fig 3.45. The error on the pitch angle included in the interval $\pm 7\ 10^{-4}$ whereas its measurement has a precision of $\pm 3\ 10^{-3}$ in the non-dimentionalized representation. However this error is the addition of the error resulting from the noisy measurements and the integration of the error on the pitch rate by the system fig 3.45. Therefore, this error increases. This suggests the implementation of a feedback including the integral of the pitch. Such a structure would detect the increase of the error on the pitch angle in the steady state and correct it.

Fig 3.46 shows that the error in the length rate and length with respect to the reference response without noise is included in the interval $\pm\ 5\ 10^{-3}$ and $\pm\ 10^{-4}$ respectively on two-third of the total time of the retrieval. The error on the length also increases because of the integration of the error on the length rate by the system. A feedback gain on the integral of the length error would also remedy this inconvenience.

A degradation of the performances of the estimator can be observed for L = 5% at the beginning of the final divergence. When at L = 0%, the conjunction of thruster granularity and

noisy measurements resulted in a random oscillation of the pitch control of a maximum amplitude equal to .1, for L = 5%, the amplitude of these oscillations are equal to .2 in the non-dimentionalized representation, fig 3.47. Fig 3.48 and 3.49 shows the degradation of the pitch angle and the pitch rate. In particular, fig 3.48 demonstrates that an integral feedback on the pitch angle is necessary. The advantage of such a structure would be clearly seen during the final part of the retrieval. The length rate and length responses are not significantly impaired by the degradation of the estimator fig 3.50 and 3.51. This suggests that only the estimate of the pitch is degraded at the end of the retrieval.

The error on the pitch angle with respect to the reference response without noise is included in the interval $\pm 6\ 10^{-3}$ and the pitch rate in $\pm .14$, fig 3.52.1. For the length and length rate, the error is included in the interval $\pm 7\ 10^{-5}$ and $\pm 3\ 10^{-3}$ respectively, fig 3.52.2. Thus, only the estimates of the pitch and pitch rate are degraded in the final part of the retrieval.

The recovery to a 1% initial error with the fast estimator where the plant covariance matrix is equal to 10^{-3} I(2), is given by fig 3.53.1 and 3.53.2 for the pitch angle and pitch rate respectively. It shows that the random oscillations are higher than the initial error amplitude, .8 rad or 3.4° for the pitch and $.8\omega$ rad.s^{-1} for the pitch rate. Therefore, a 1% initial error cannot be recovered since it is included in the dead-band of the estimator. In addition, the random pitch oscillations have an amplitude higher than the pitch sensor precision. Thus, the performances of this estimator are very poor .

There is here a fundamental nonsense in the specifications of the system. To benefit from the optimization trajectory design, it seemed reasonable to aim at retrieving an initial error in one-third of the total retrieval time. However, the available level of thrust limits the amplitude of initial error the feedback loop can retrieve without thruster saturation, to 1% of the maximum amplitude of the states along the nominal retrieval trajectory. For the pitch angle, it limits the initial error to .6°. Therefore, the Ku band radar having a precision of 2°, the sensors can not detect such an error.

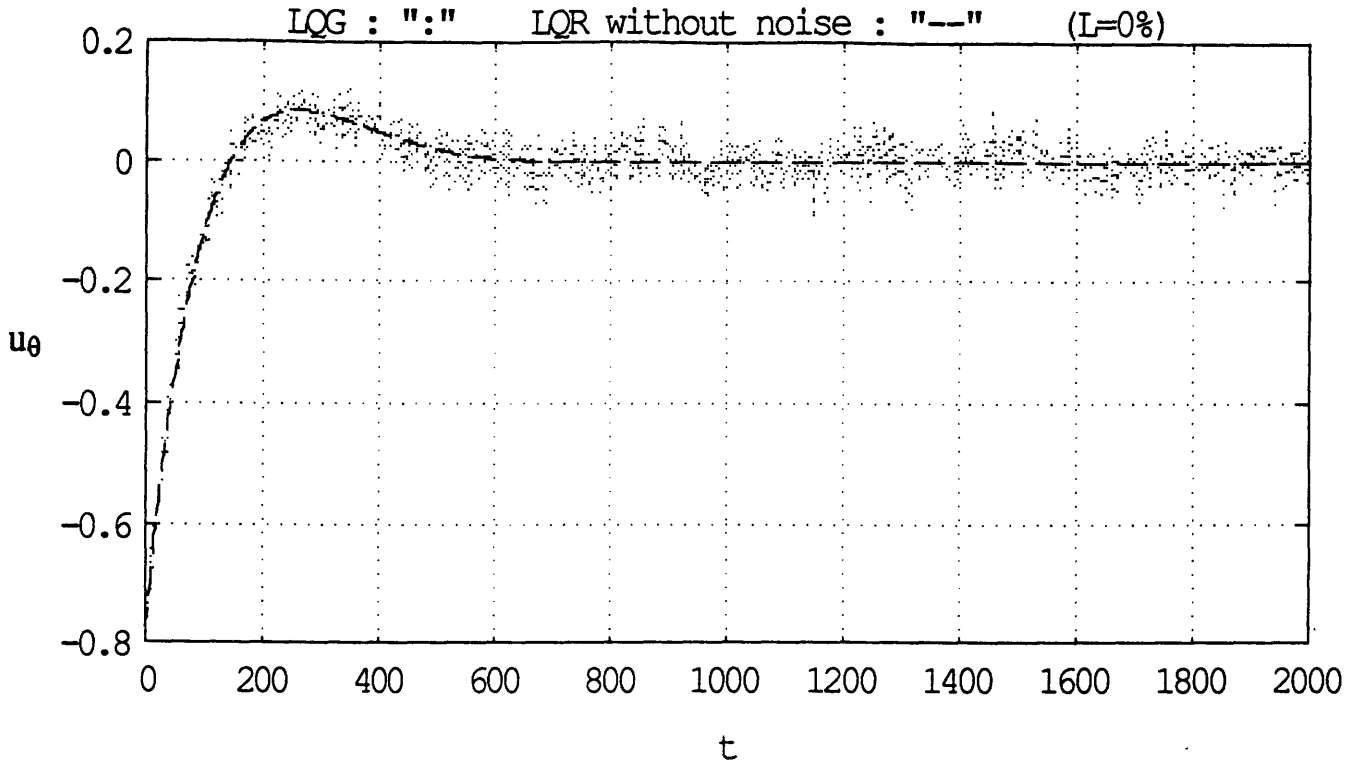

fig 3.39: LQG pitch control history for a 1% initial error recovery, L=0%

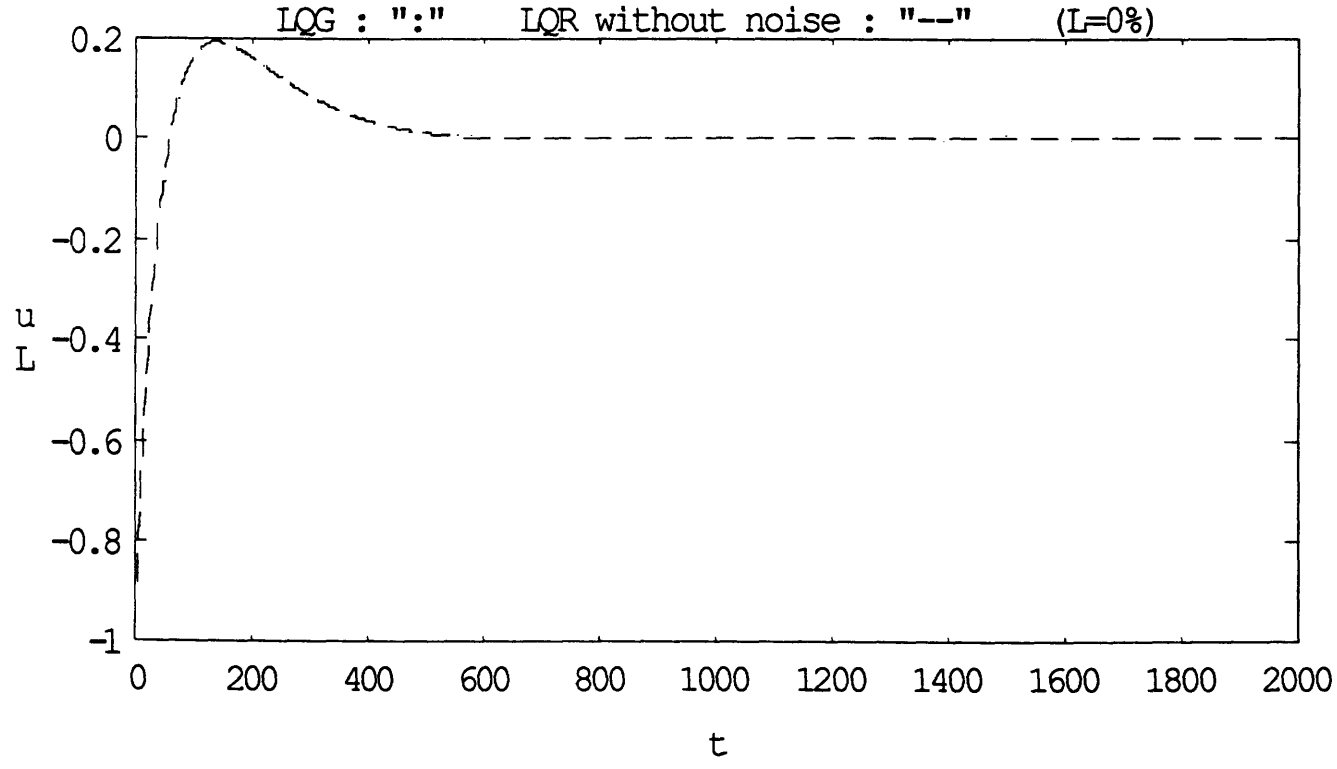

fig 3.40: LQG length control history for a 1% initial error recovery, L=0%

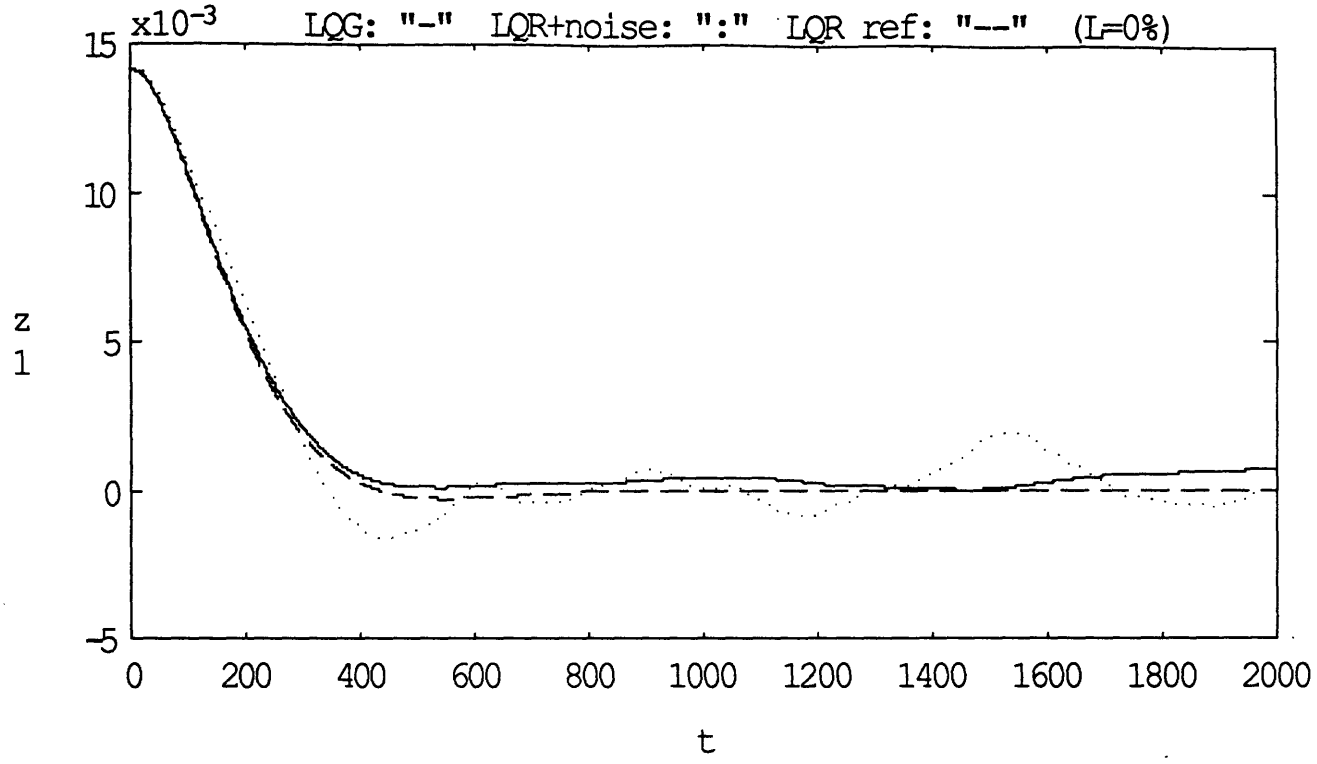

fig 3.41: LQG pitch response to a 1% initial error, L=0%

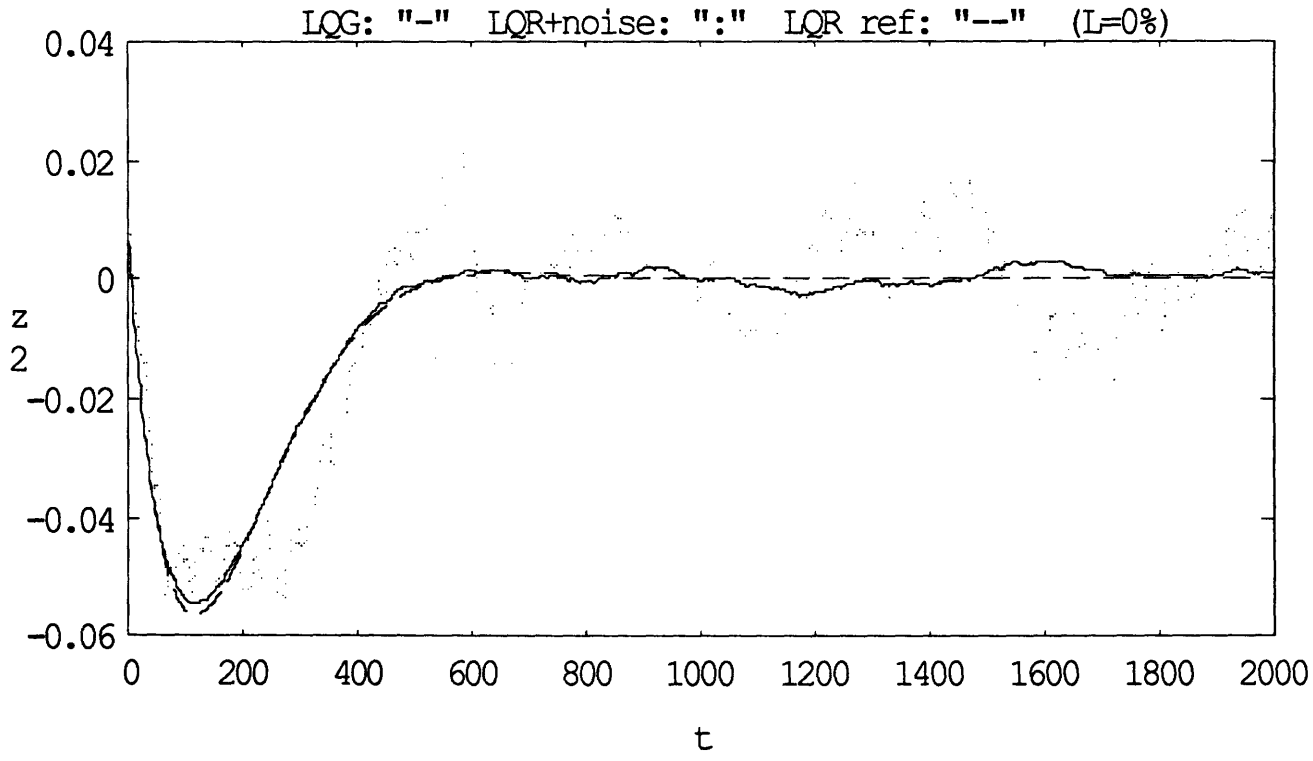

fig 3.42: LQG pitch rate response to a 1% initial error, L=0%

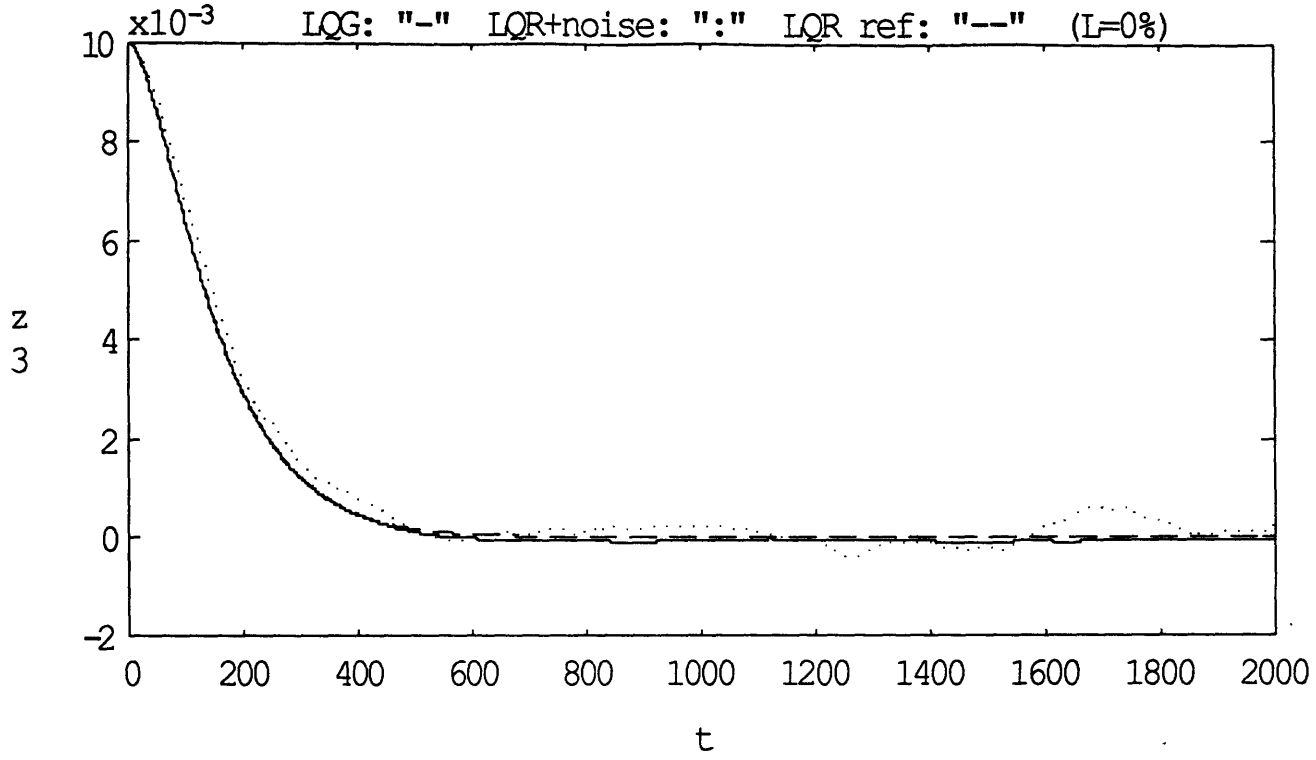

fig 3.43: LQG length response to a 1% initial error, L=0%

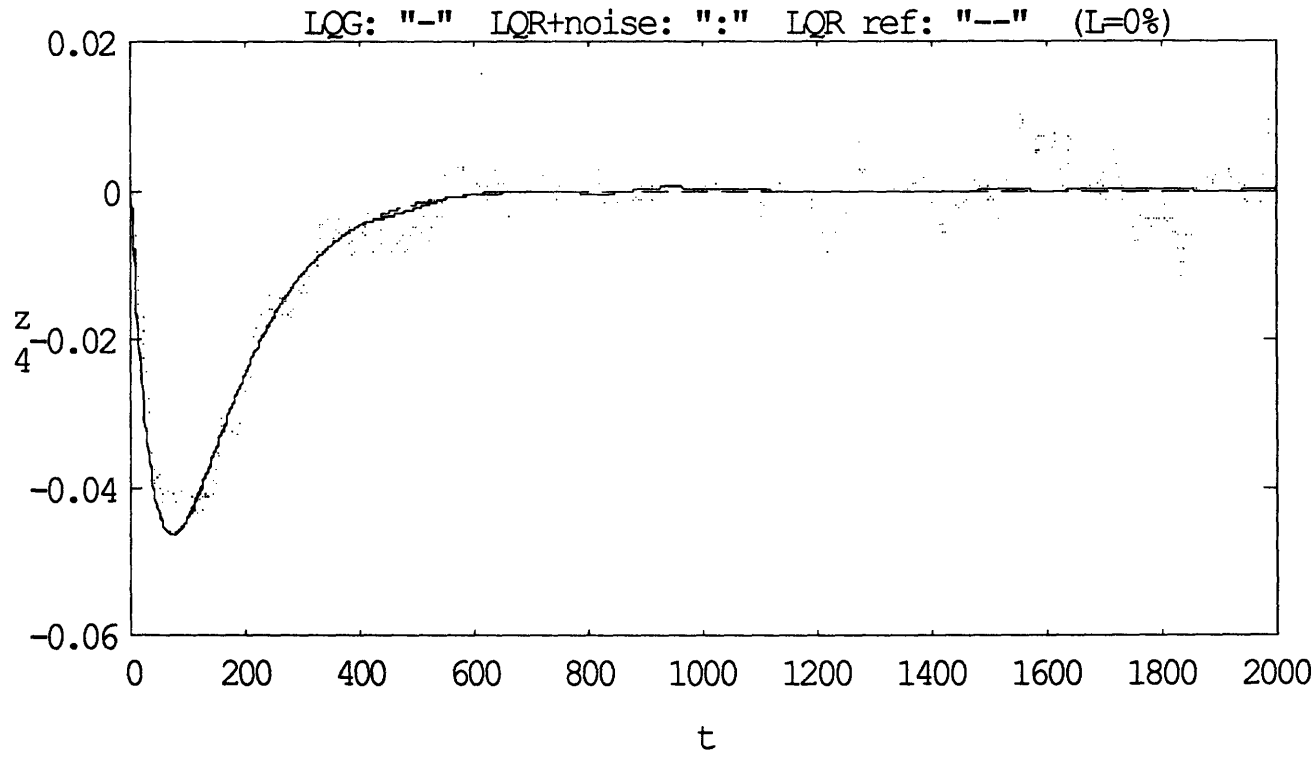

fig 3.44: LQG length rate response to a 1% initial error, L=0%

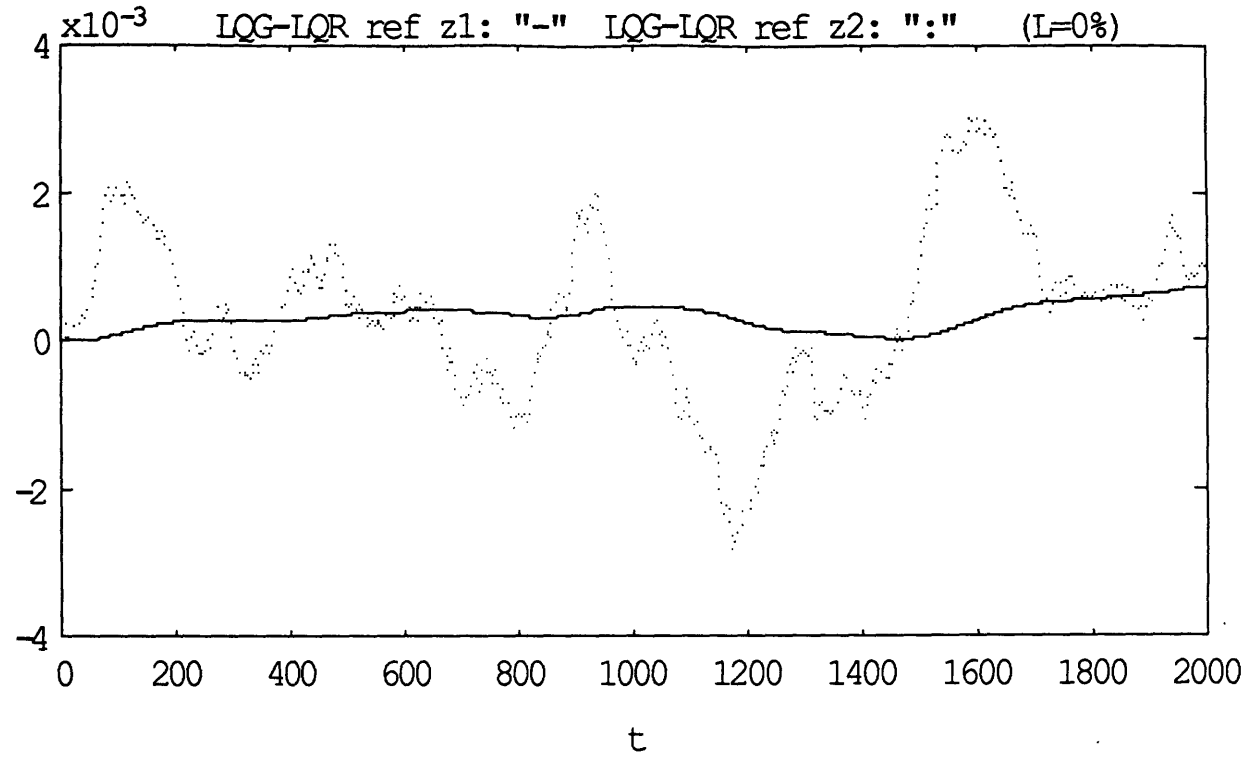

fig 3.45: Pitch angle and pitch rate error evolution with respect to the LQR reference response

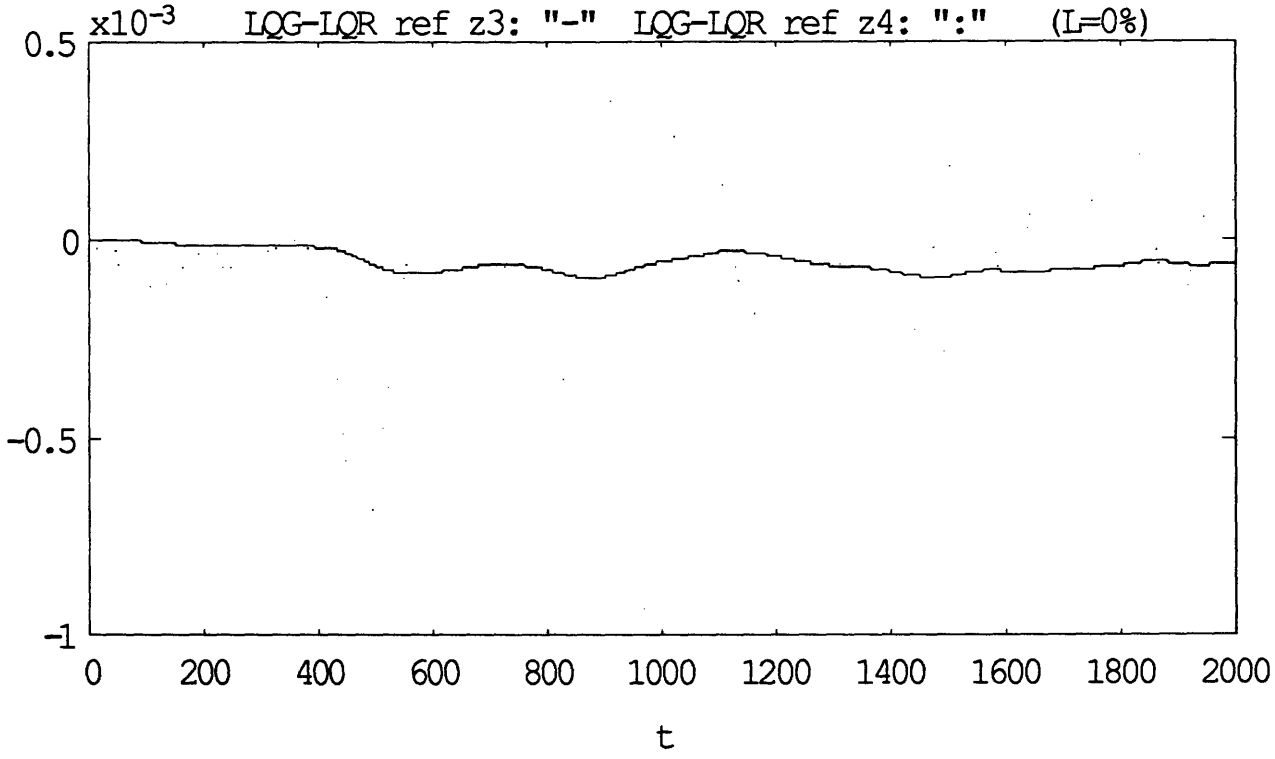

fig 3.46: length and length rate error evolution with respect to the LQR reference response

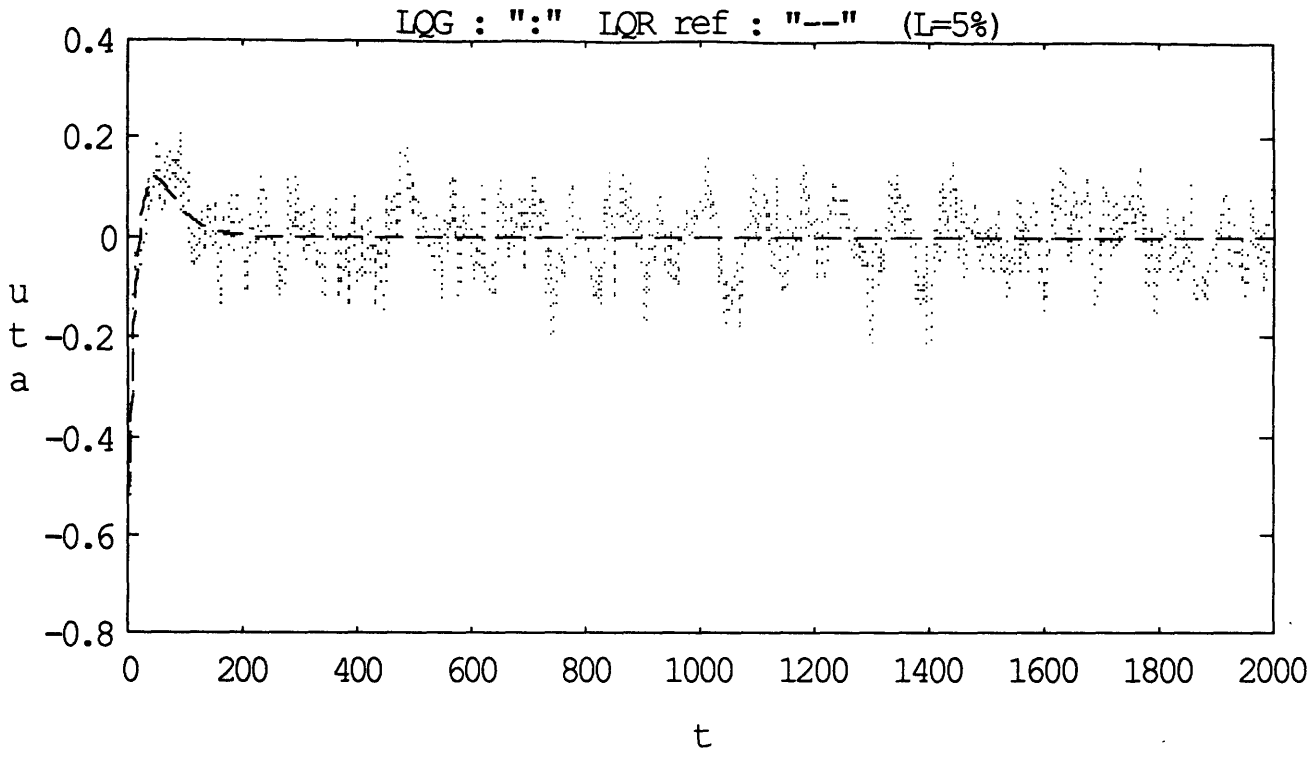

fig 3.47: LQG pitch control history for a 1% initial error recovery, L=5%

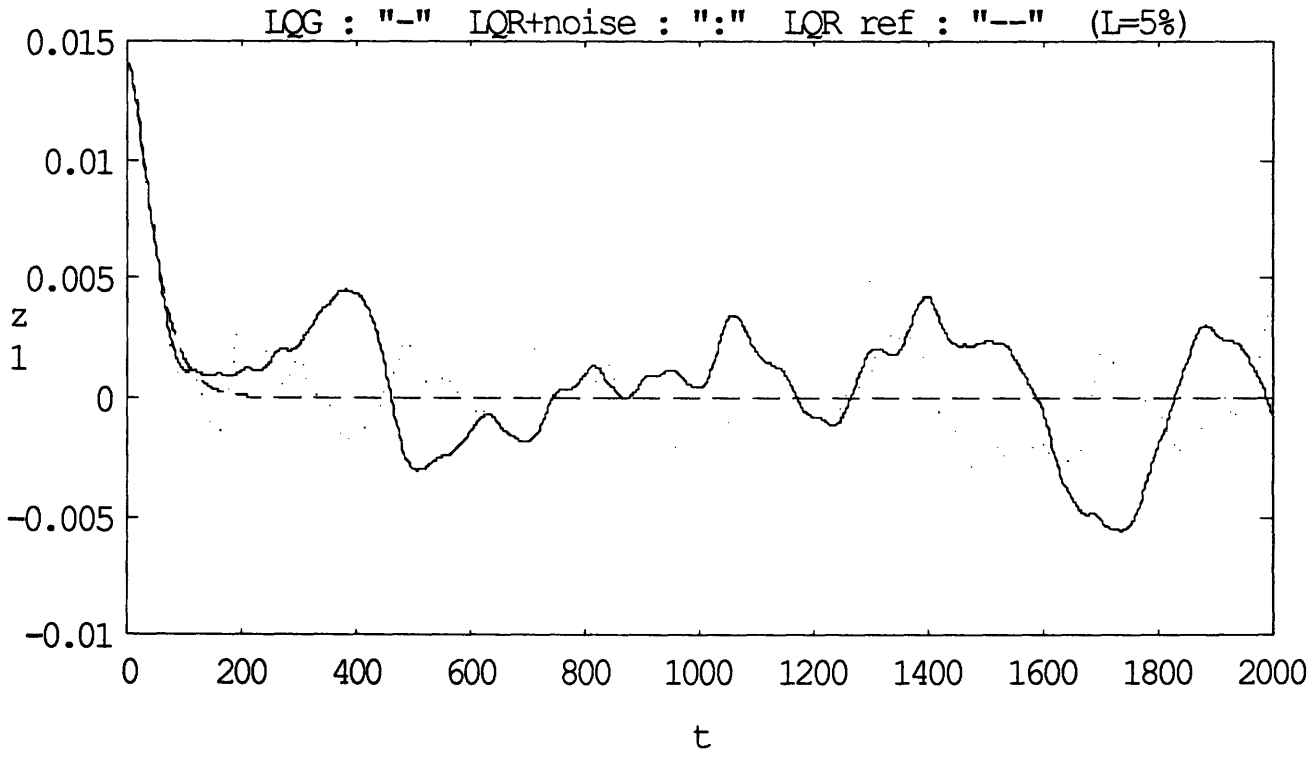

fig 3.48: LQG pitch response to a 1% initial error, L=5%

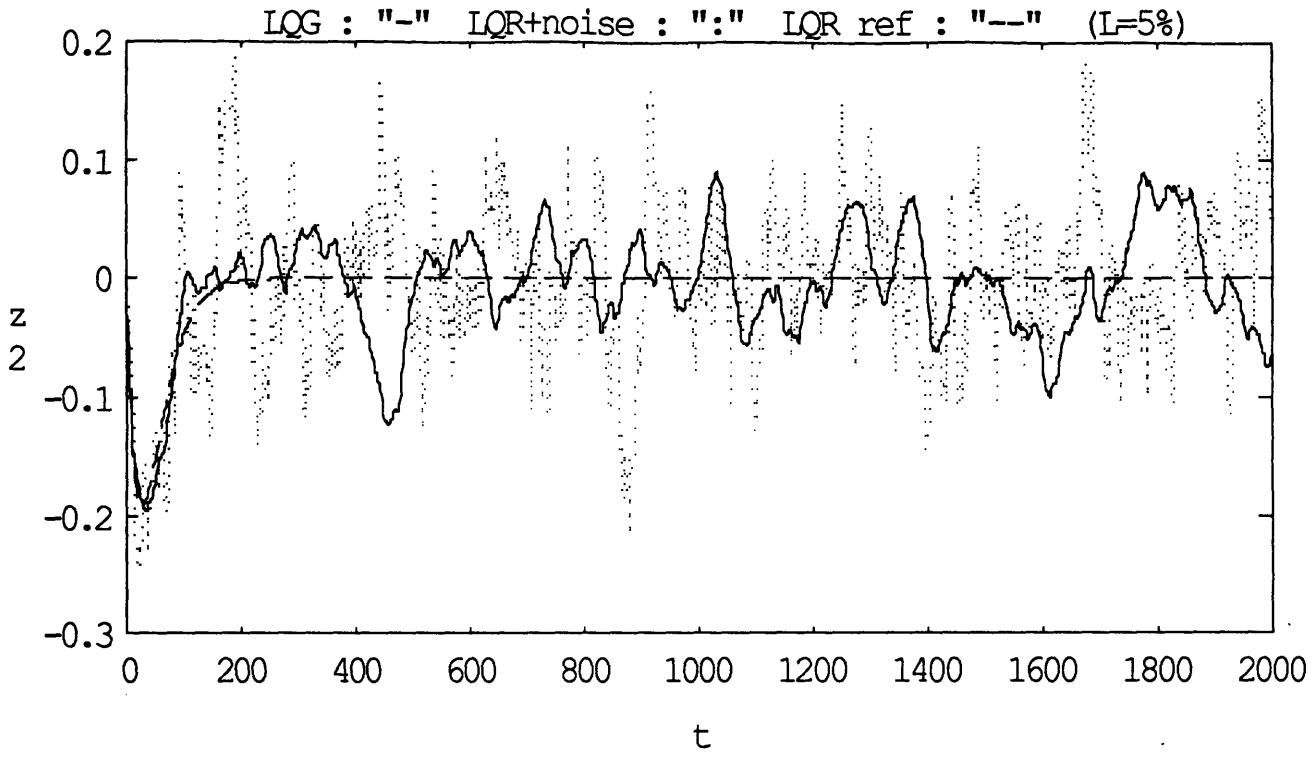

fig 3.49: LQG pitch rate response to a 1% initial error, L=5%

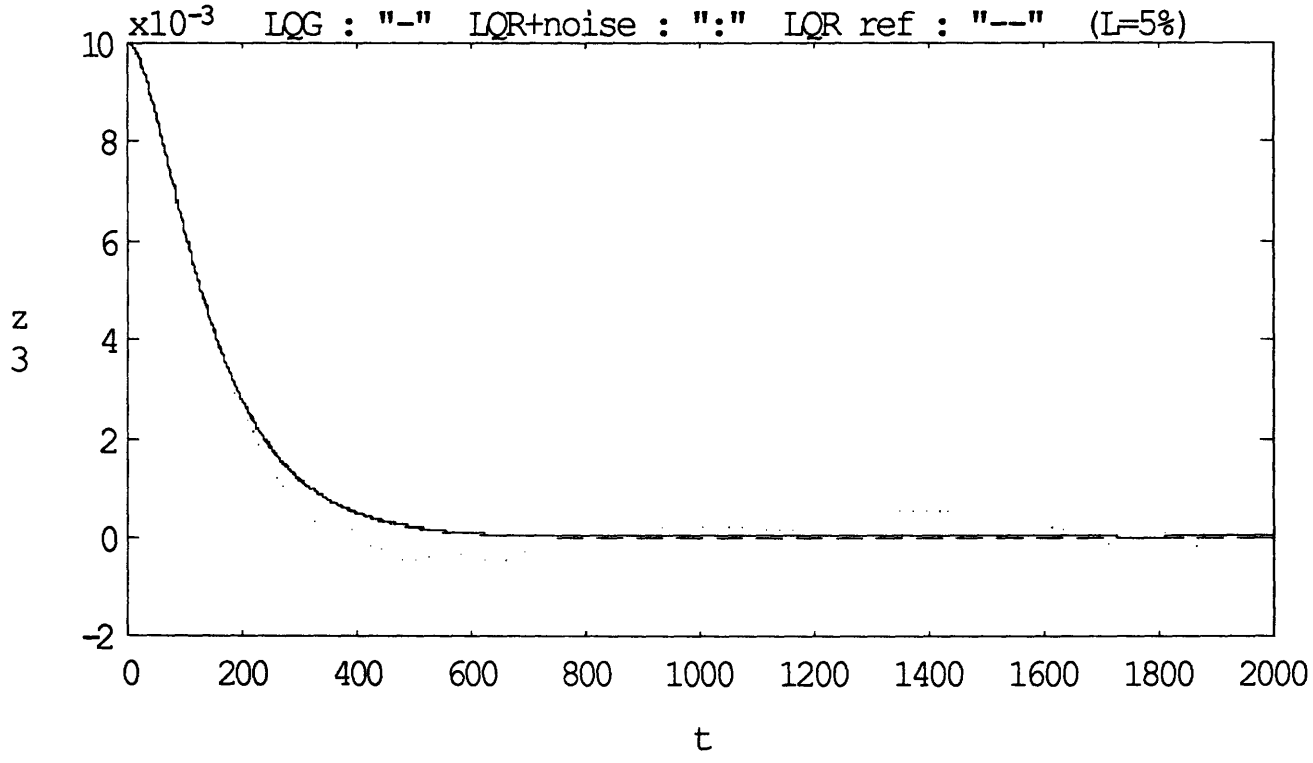

fig 3.50: LQG length response to a 1% initial error, L=5%

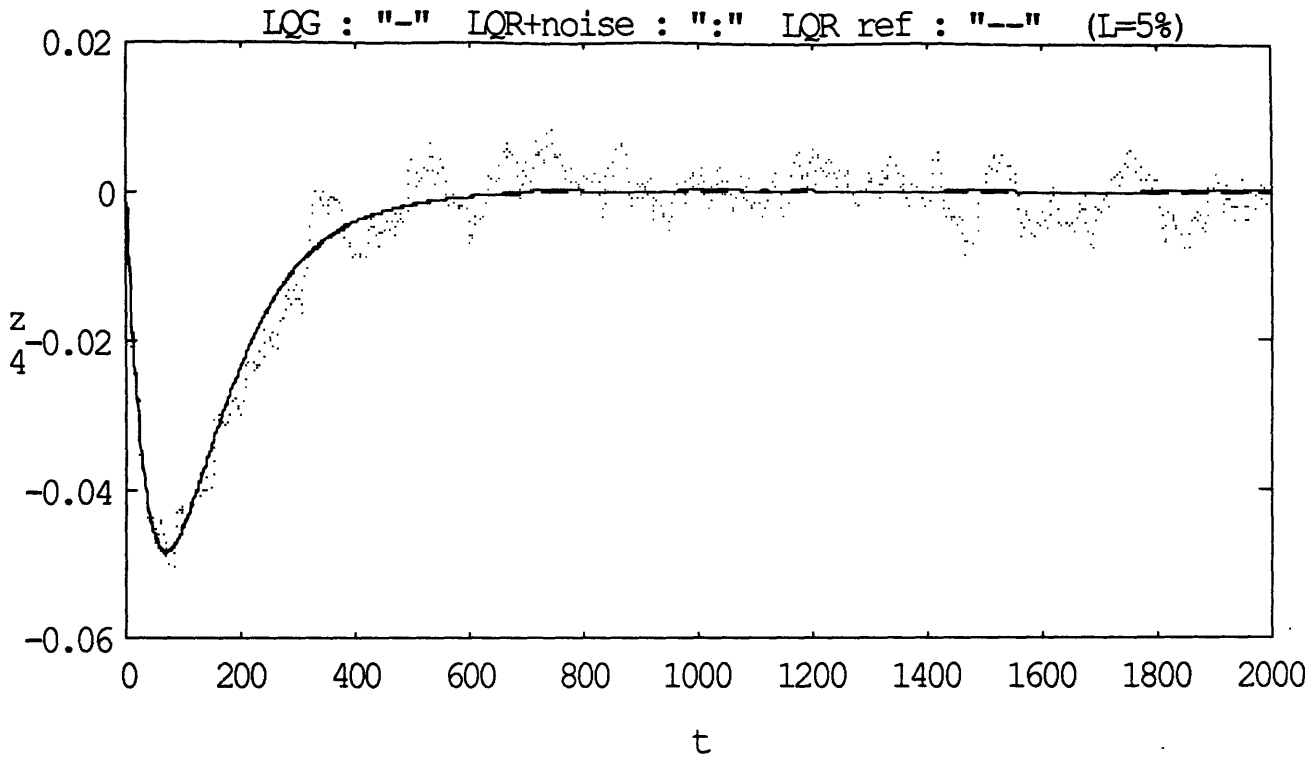

fig 3.51: LQG length rate response to a 1% initial error, L=5%

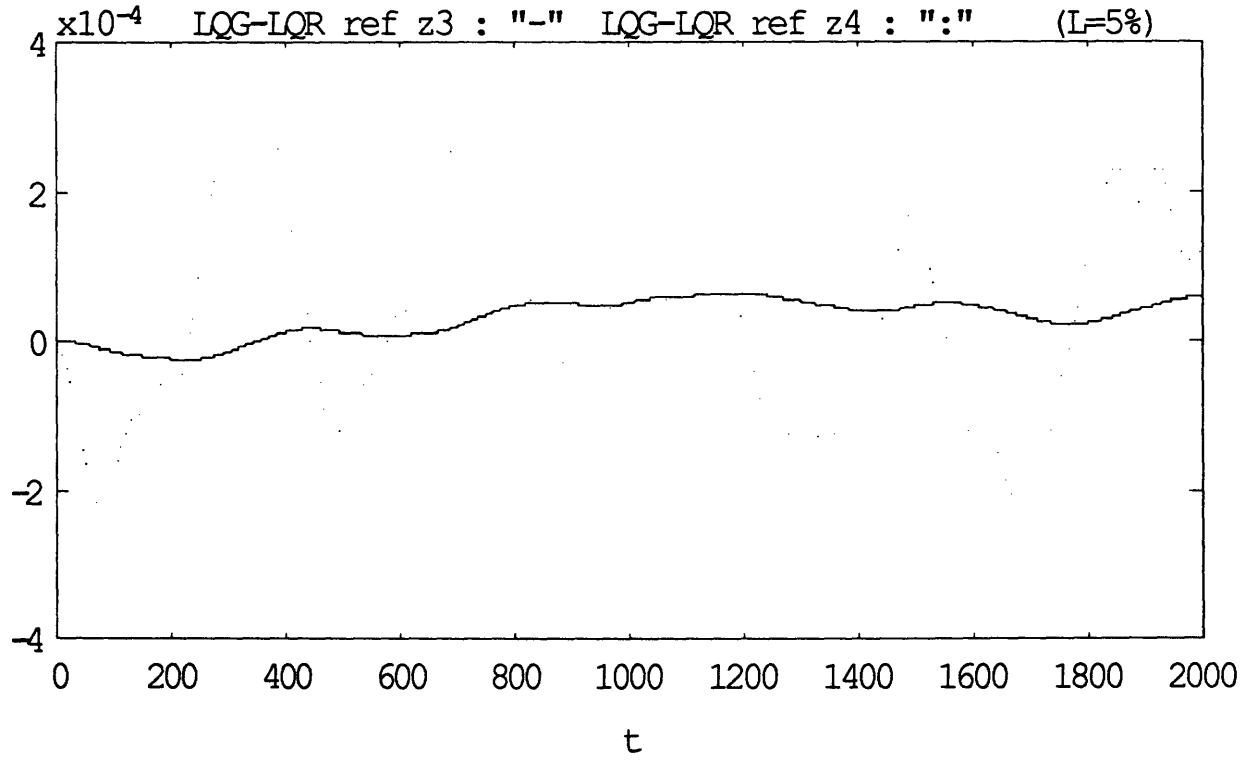

fig 3.52.1: Pitch angle and pitch rate error evolution with respect to the LQR reference response

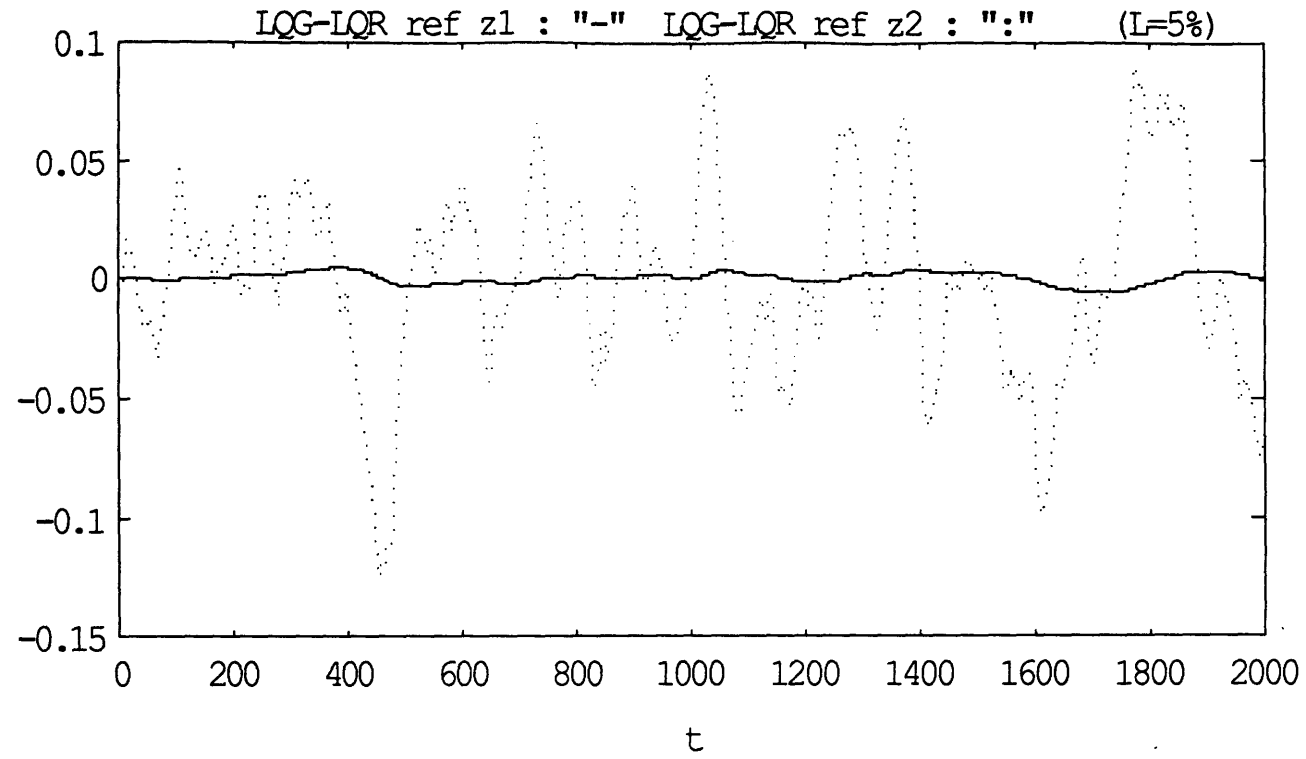

fig 3.52.2: Length and length rate error evolution with respect to the LQR reference response

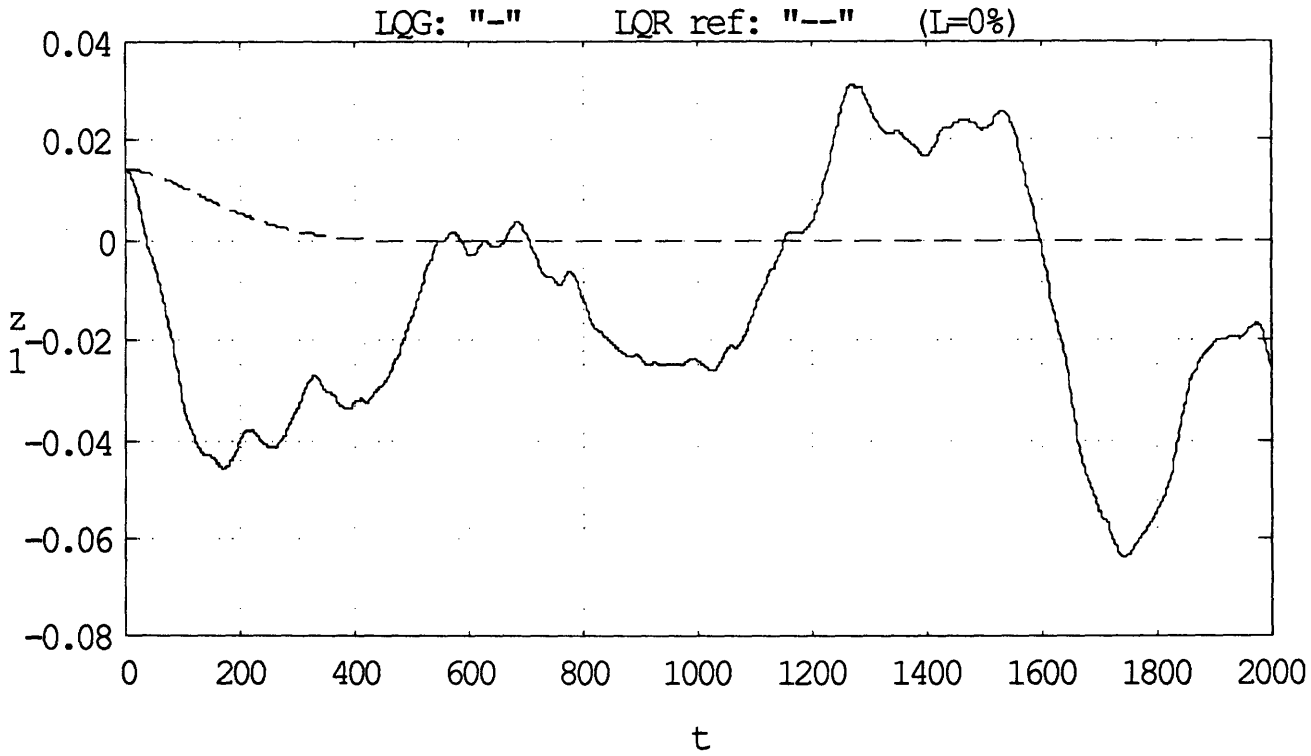

fig 3.53.1: LQG pitch response to a 1% initial error with fast estimator

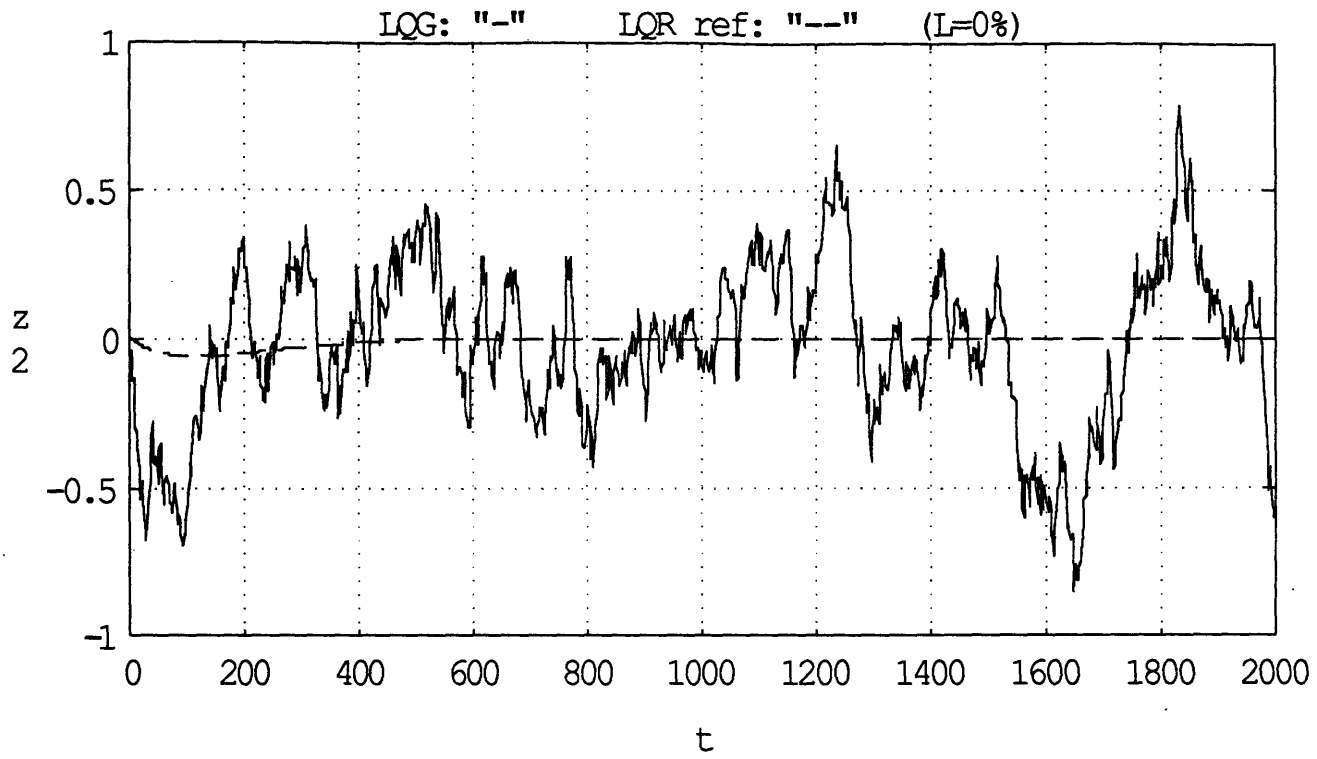

fig 3.53.2: LQG pitch rate response to a 1% initial error with fast estimator

3.6. Non-Linear Numerical Simulation.

3.6.1. The Algorithm.

The structure described by fig 3.1 § 3.1.5 is implemented. Th real feedback and estimator gains are given by:

$$G(X) = T_u^{-1}G(Z)T \quad \text{and} \quad H(X) = T^{-1}G(Z)T_3 \tag{3.33}$$

where T_3 is the reduction of T to the pitch, the length and length rate. Both gains are computed at each step with the estimates of the states.

The nominal control history was designed assuming the the length acceleration was directly controllable. In order to take into account the length dynamics,

$$u_{Lo} = \dot{L}_o - L_o\left[(\dot{\theta}_o + \omega)^2 + 3\omega^2\cos^2\theta_o - \omega^2\right] \qquad (3.34)$$

The nominal pitch control is equal to zero in the nominal trajectory design. Taking into account the atmospheric torque, the nominal control becomes:

$$u_{\theta o} = - f_a \qquad (3.35)$$

The plant dynamics are described by equation (3.5) equivalent to $\dot{X} = f(X,u)$. The whole system is described by the following representation:

$$\dot{X} = f(X,u)$$
$$\dot{\hat{X}} = f(\hat{X},u_o + \delta u) + H(\hat{X})\,(Y - C\hat{X})$$
$$Y = CX + v$$
$$\delta u = - G(\hat{X})\,(\hat{X} - X_o)$$
$$u = u_o + \delta u + nu \qquad (3.36)$$

where nu represents the thruster granularity.

This simulation is performed for an initial length of 2000m with initial conditions equal to $X_o + dX_o$ with

$$X_o = [.92 \;\; 4.5\;10^{-4} \;\; 2000 \;\; 0]$$
$$dX_o = [.141 \;\; 9.71\;10^{-6} \;\; 20 \;\; 6.03\;10^{-3}]$$

For L higher that 4000 m, the maximum real part of the eigen values of the system is lower than $2\;10^{-3}$ resulting in a time constant higher than 500 s. The step size of integration must be lower than 50s. For the first 6 s of the initial acceleration, the step size is taken equal to 1 s and during the deceleration for length higher than 400 m, to 10 s. For L lower than 400 m, the real part of the eigen values is lower than .1 resulting in a time constant higher than 10 s. Thus the step size of integration is taken equal to 1 s.

3.6.2. Results.

The LQR and Pole Placement feedback loop both recover and track the nominal trajectory appropriately, fig 3.54 to 3.61. As stated in § 3.2.1, the last 10% of the retrieval are critical because of the divergence of one of the unstable pole of the plant. Despite sensor and plant noises, the extended LQG feedback loop keeps the sub-satellite on the nominal trajectory up to the end, fig 3.63. The variations of the states with respect to the nominal reference are ten times lower than the prediction given by the linear simulation of § 3.5., fig 3.66 to 3.69. The effect of the final divergence of one of the unstable pole of the plant can be observed on fig 3.67. The relative error of the pitch rate with respect to the nominal rate increases from an average lower than .01ω to .03ω rad.s^{-1}, but remains acceptable.

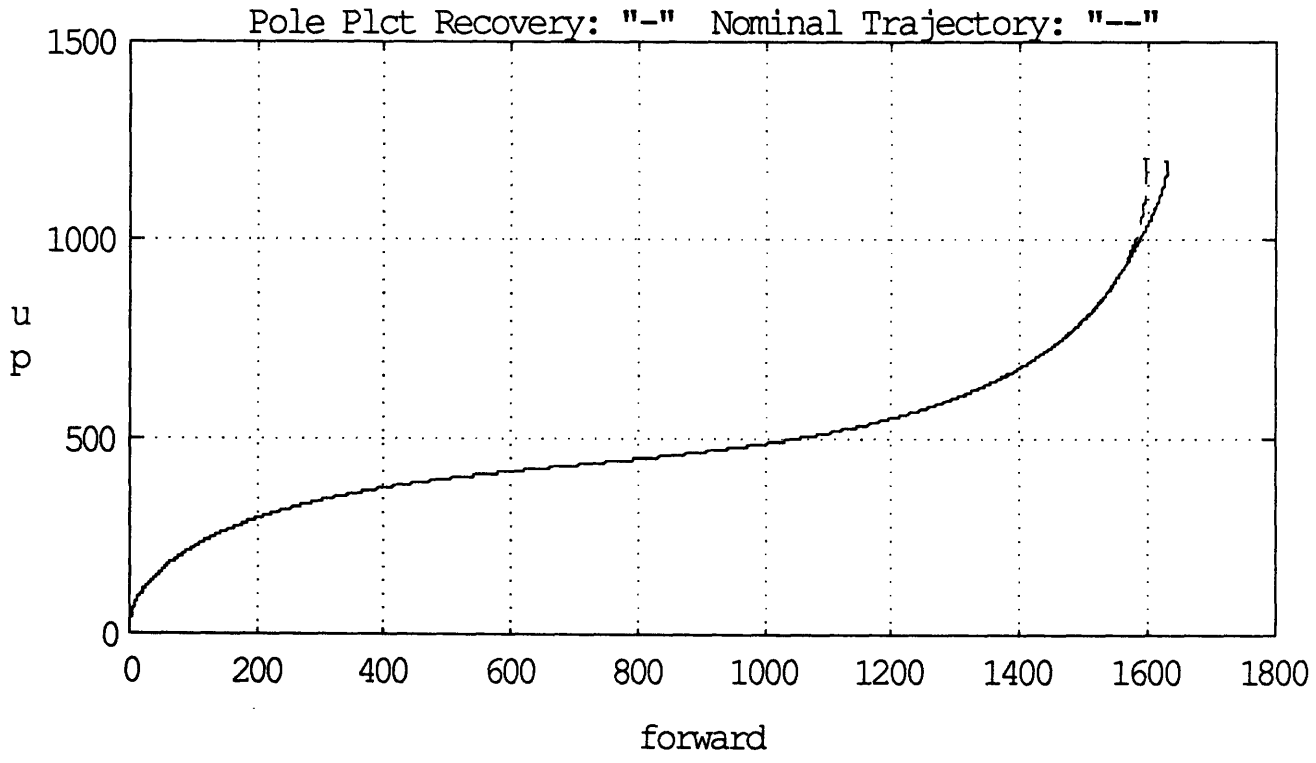

fig 3.54: In-plane trajectory for a 1% initial error, pole placement solution.

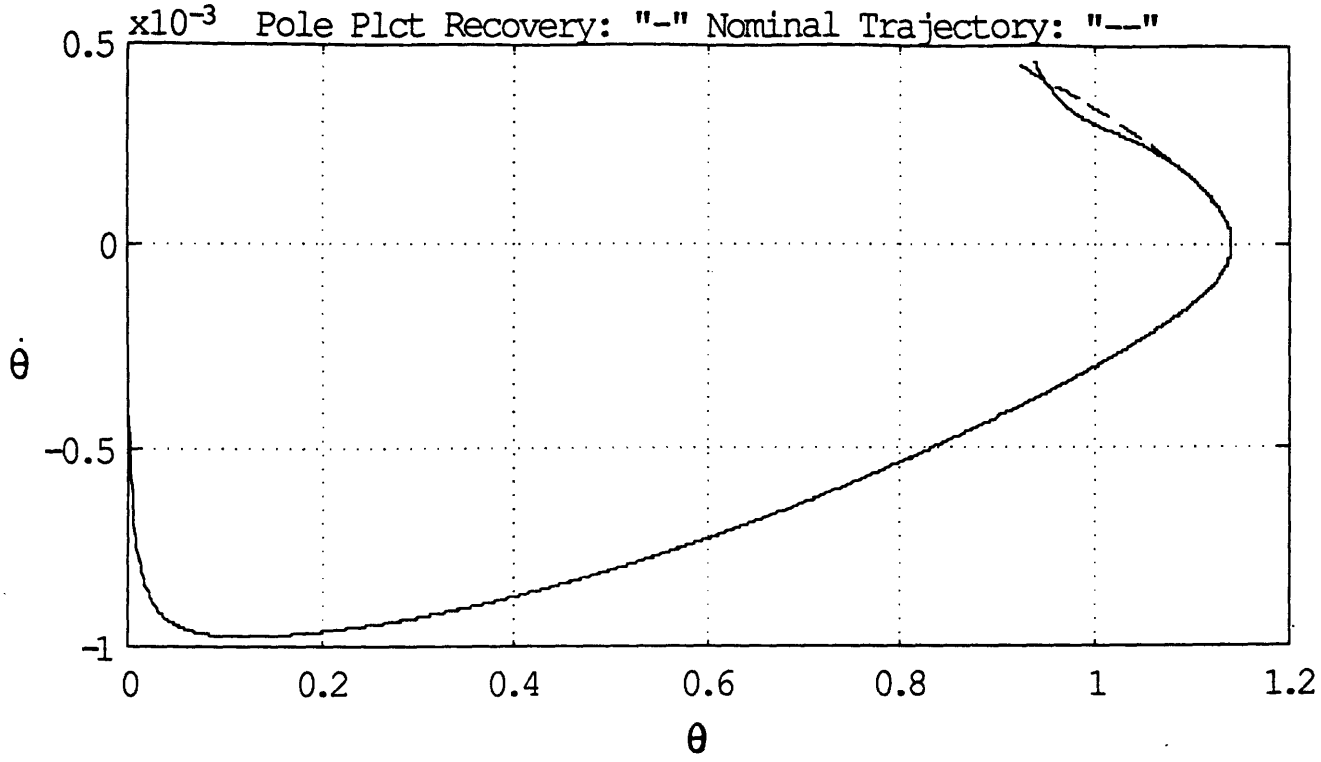

fig 3.55: Phase plane trajectory for a 1% initial error, pole placement solution.

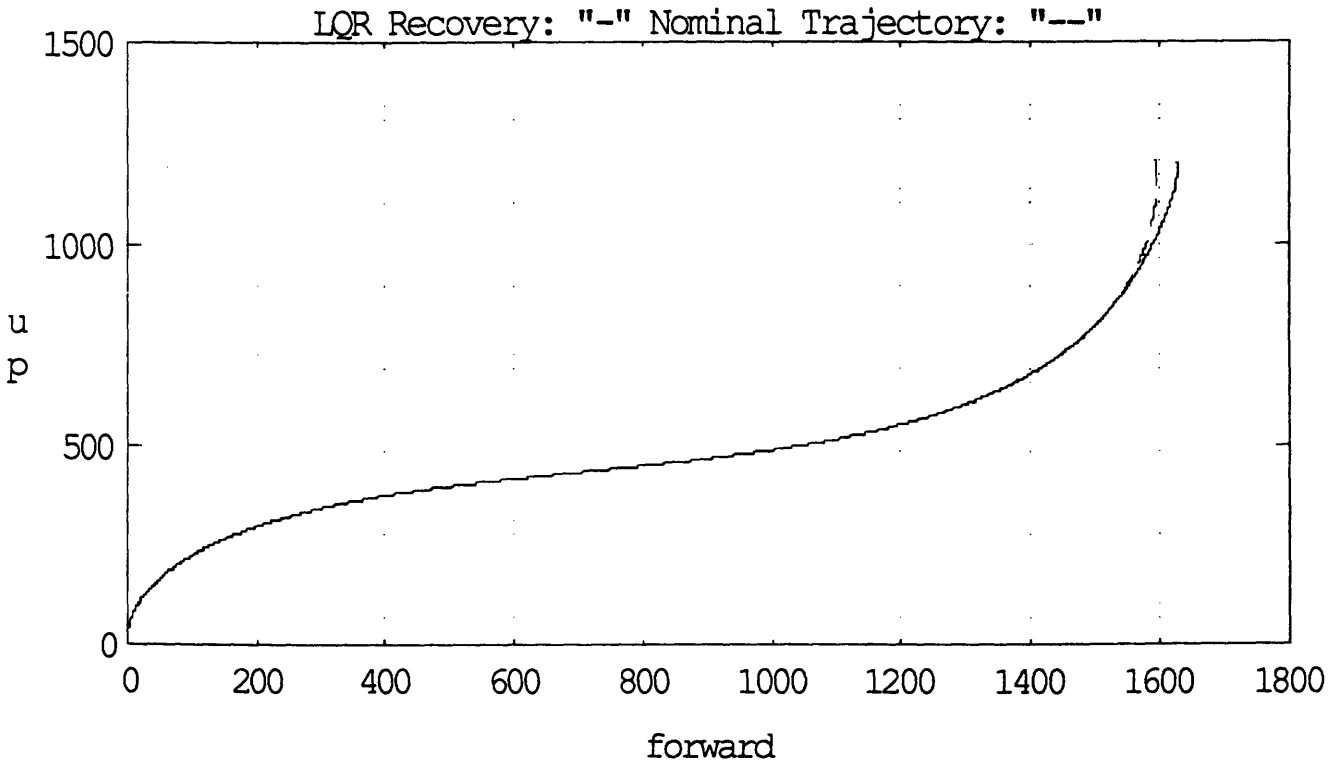

fig 3.56: In-plane trajectory for a 1% initial error, LQR solution.

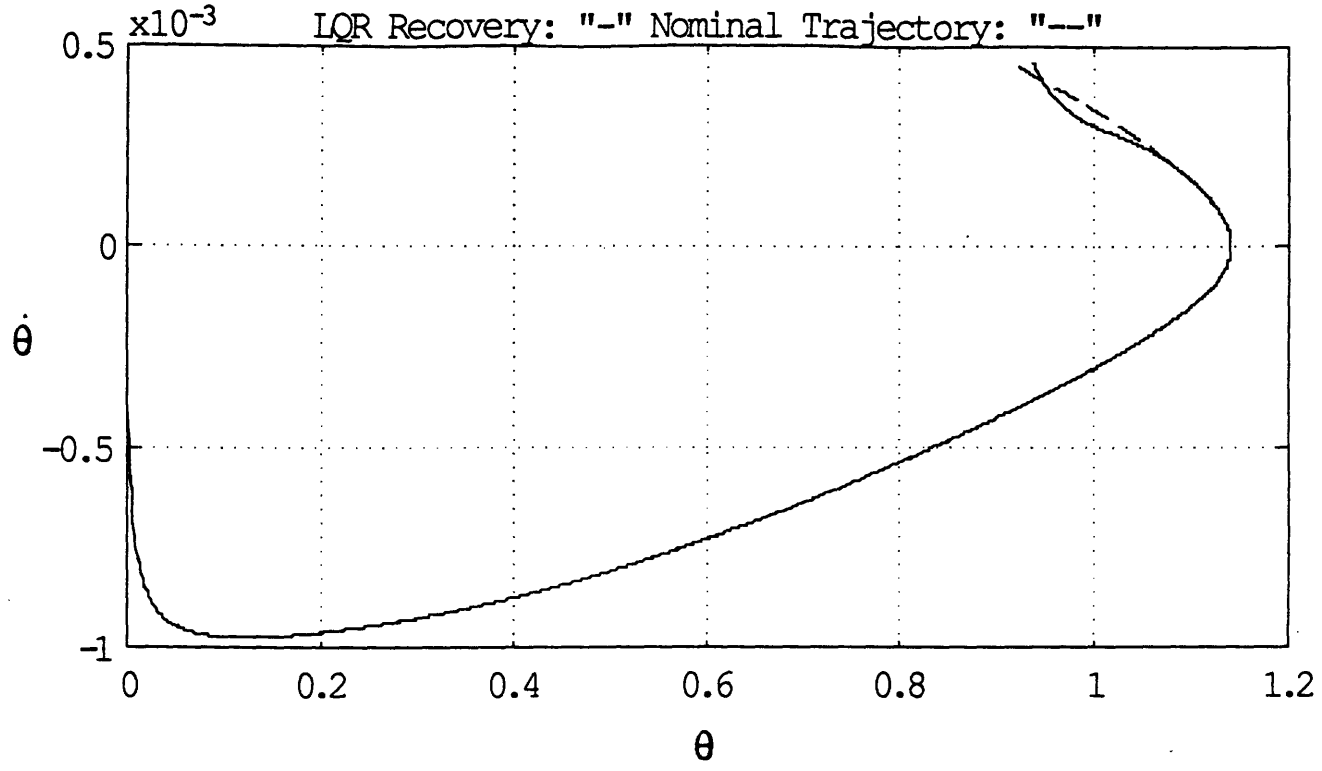

fig 3.57: Phase plane trajectory for a 1% initial error, LQR solution.

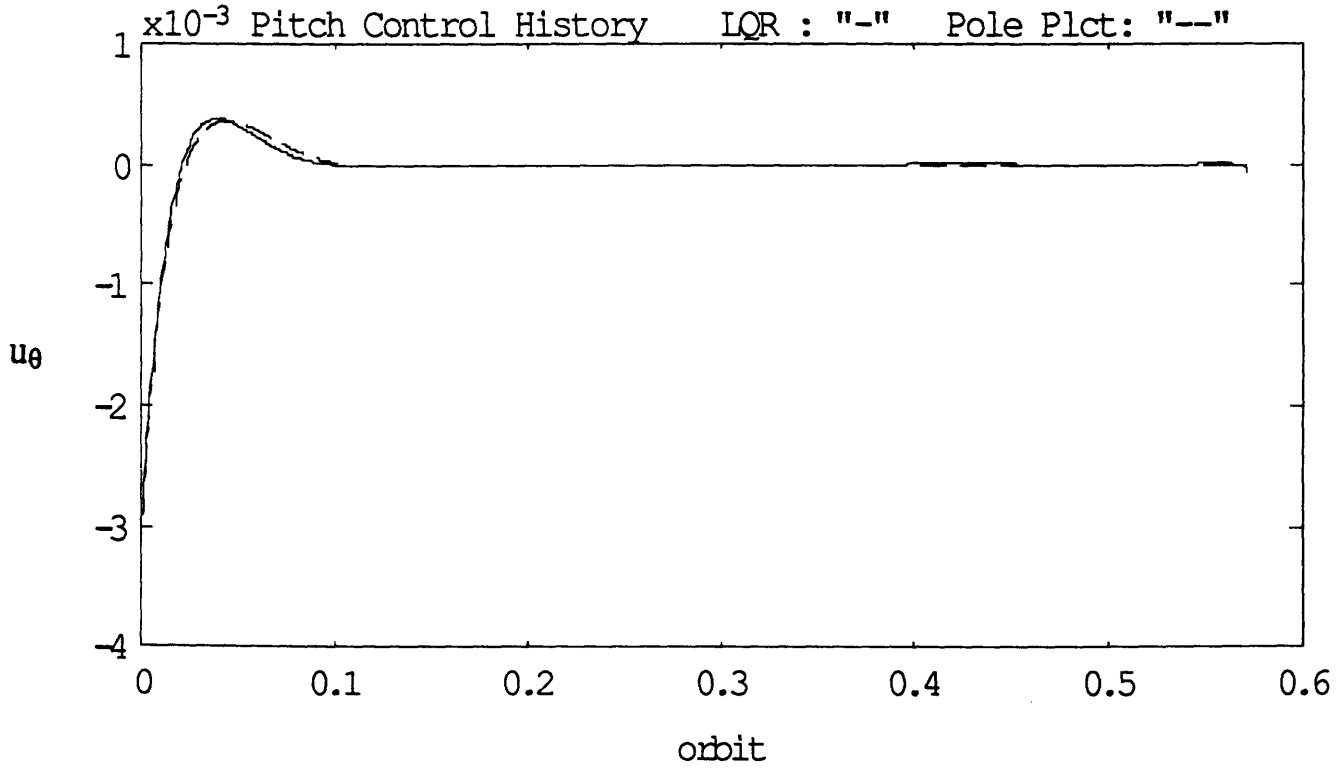

fig 3.58: Pitch control history along the retrieval, LQR & Pole Placement solution.

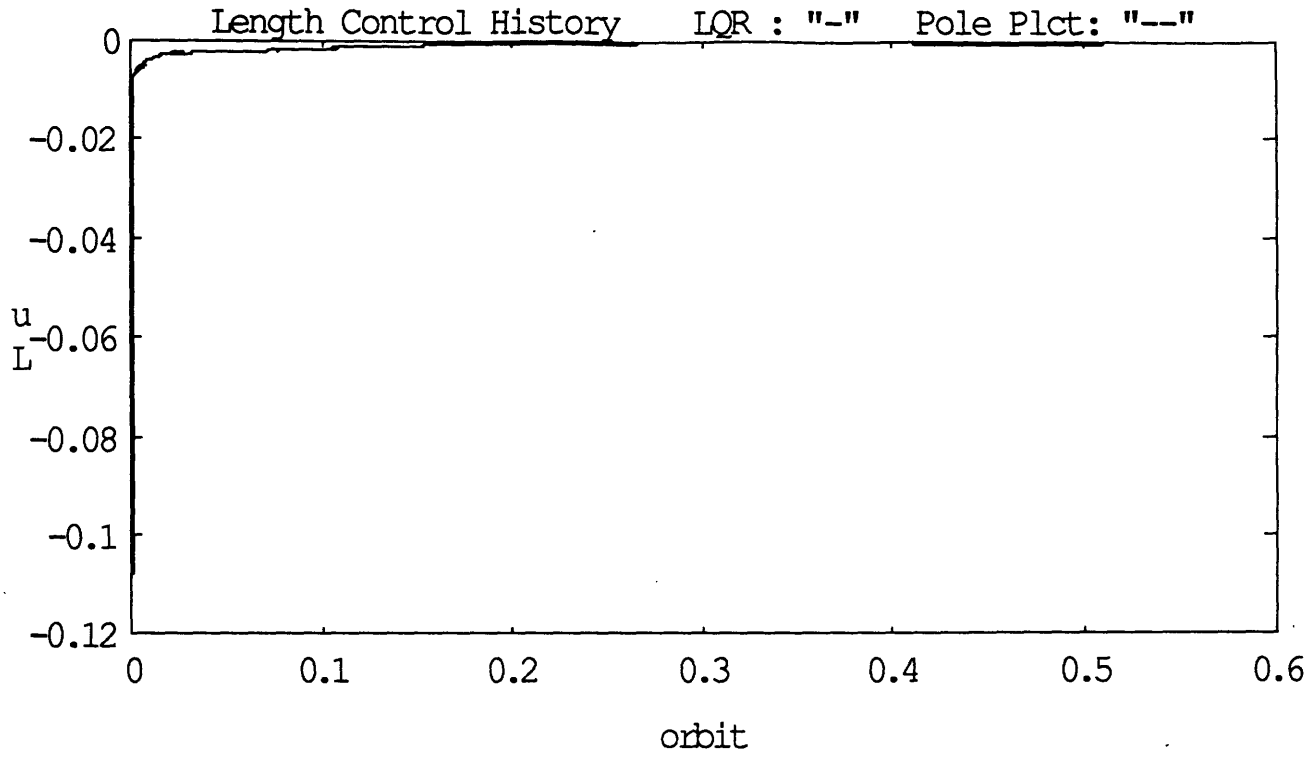

fig 3.59: Length control history along the retrieval, LQR & Pole Placement solution.

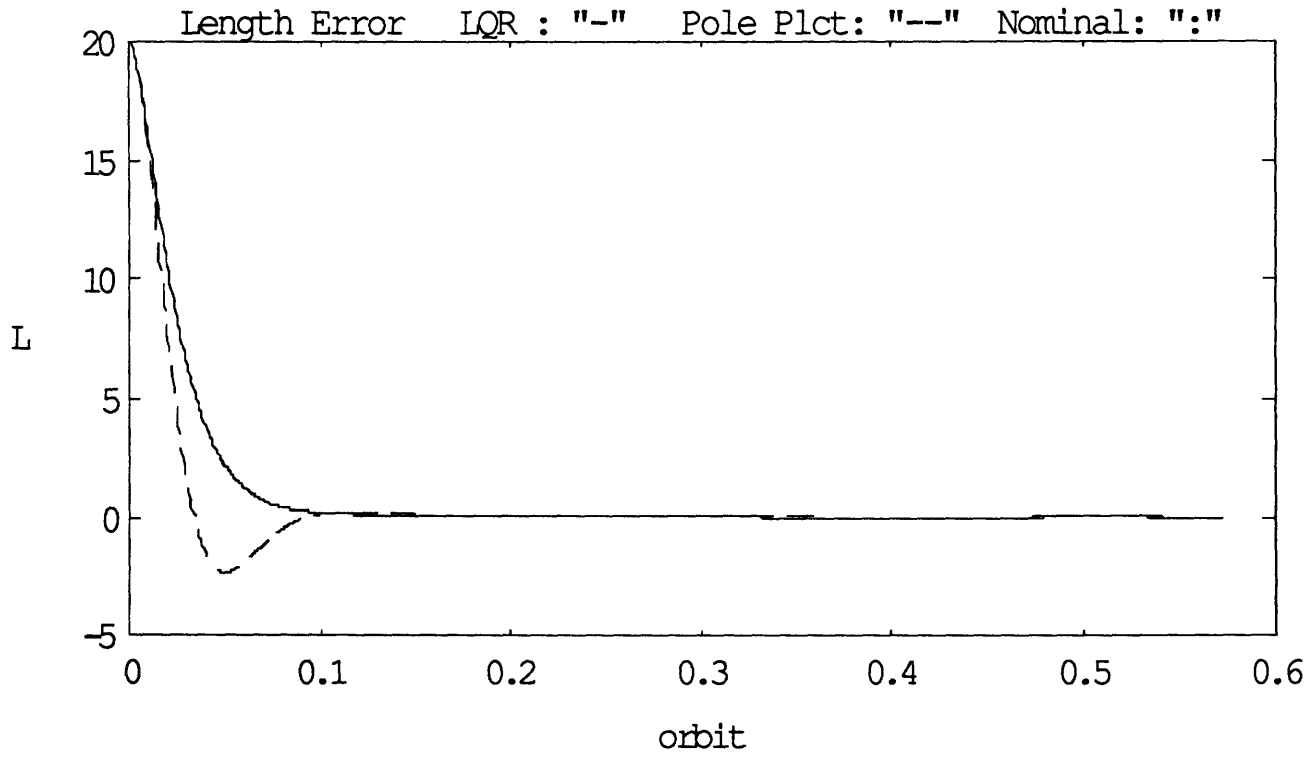

fig 3.60: Length error with respect to the nominal trajectory, LQR & Pole Placement solution.

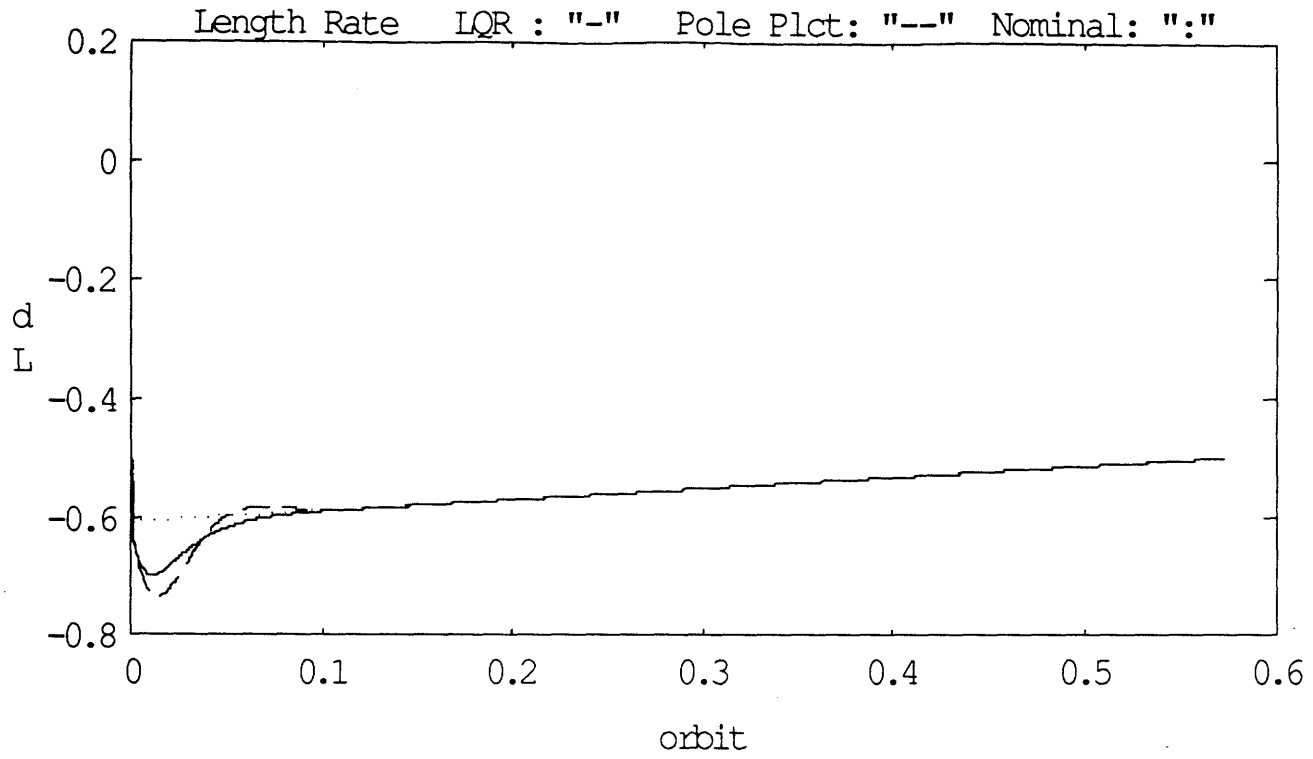

fig 3.61: Length rate history along the retrieval, LQR & Pole Placement solution.

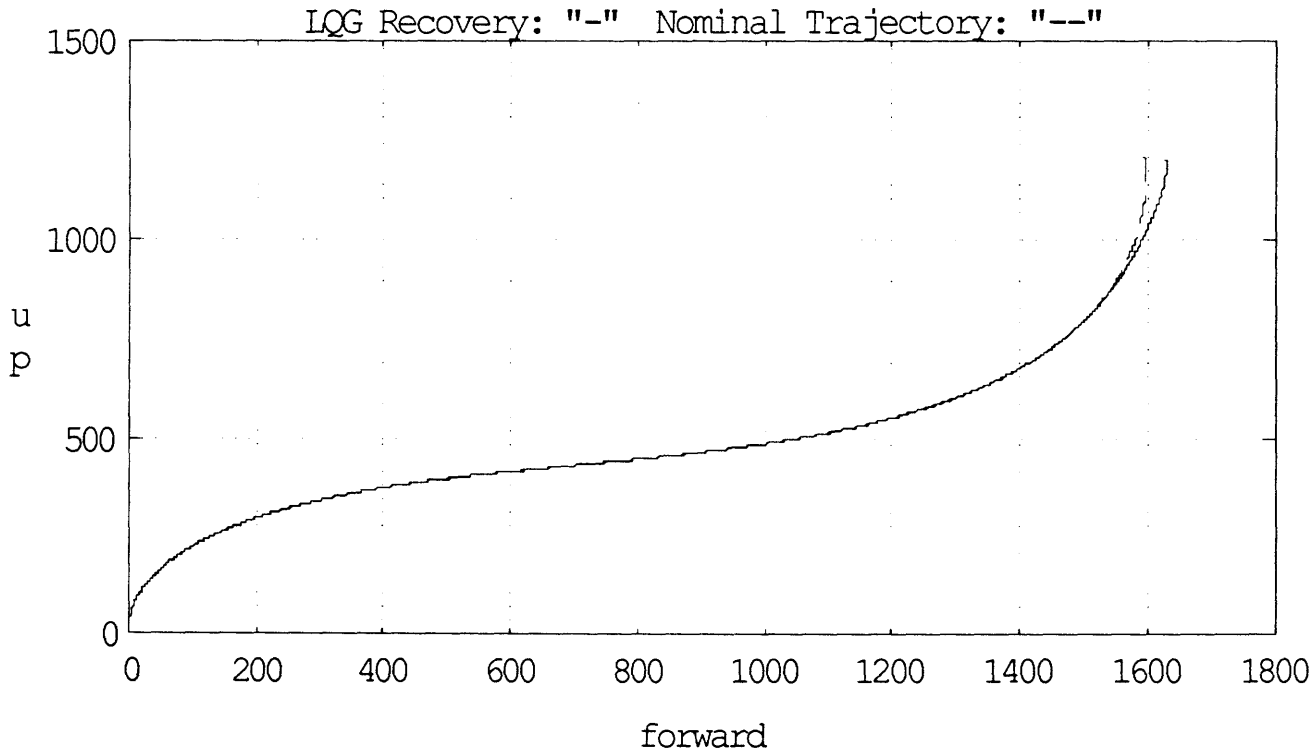

fig 3.62: In-plane trajectory for a 1% initial error, LQG solution.

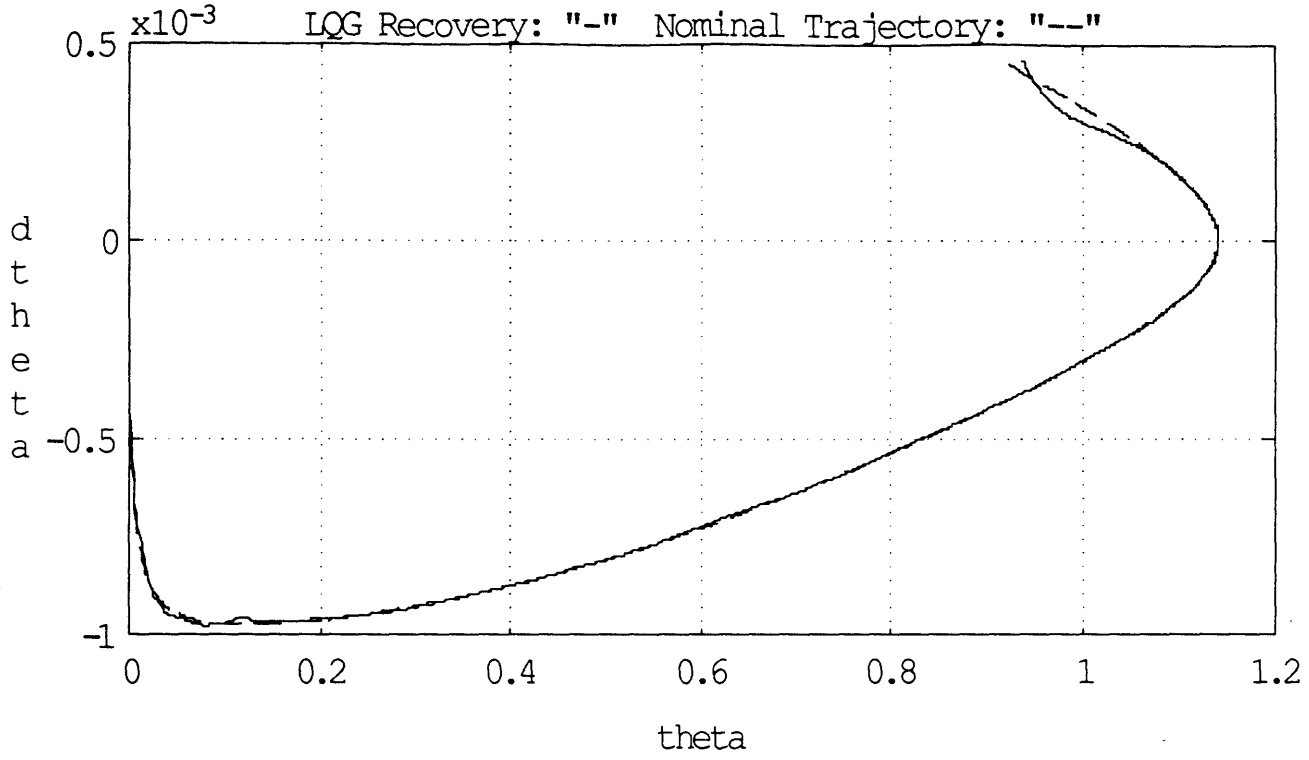

fig 3.63: Phase plane trajectory for a 1% initial error, LQG solution.

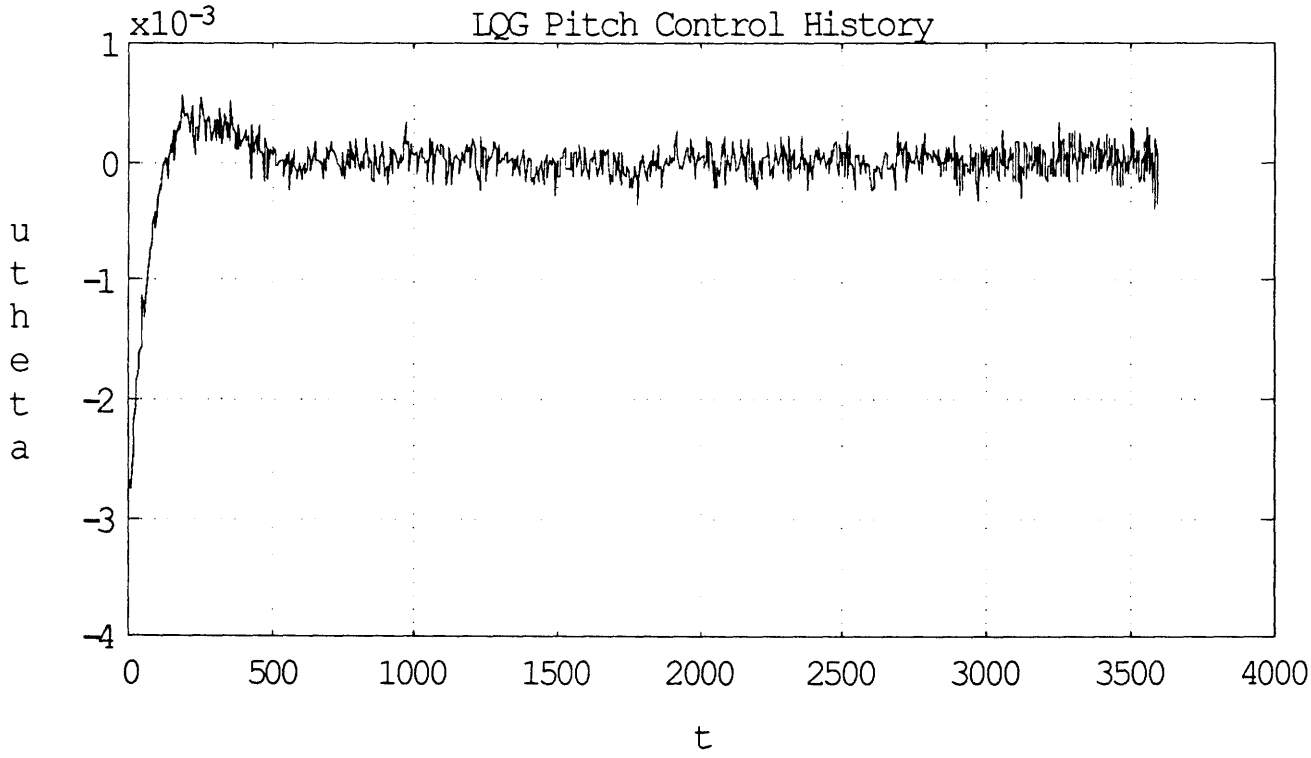

fig 3.64: Pitch control history along the retrieval, LQG solution.

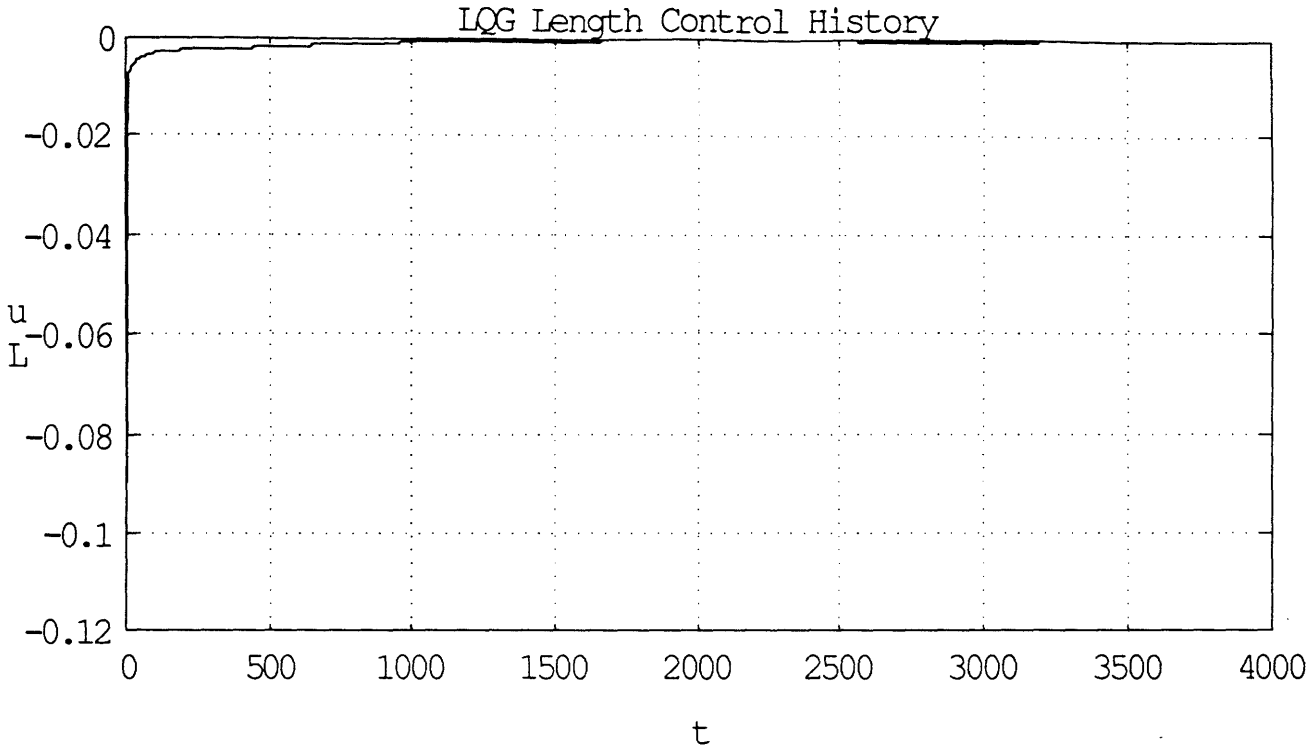

fig 3.65: Length control history along the retrieval, LQG solution.

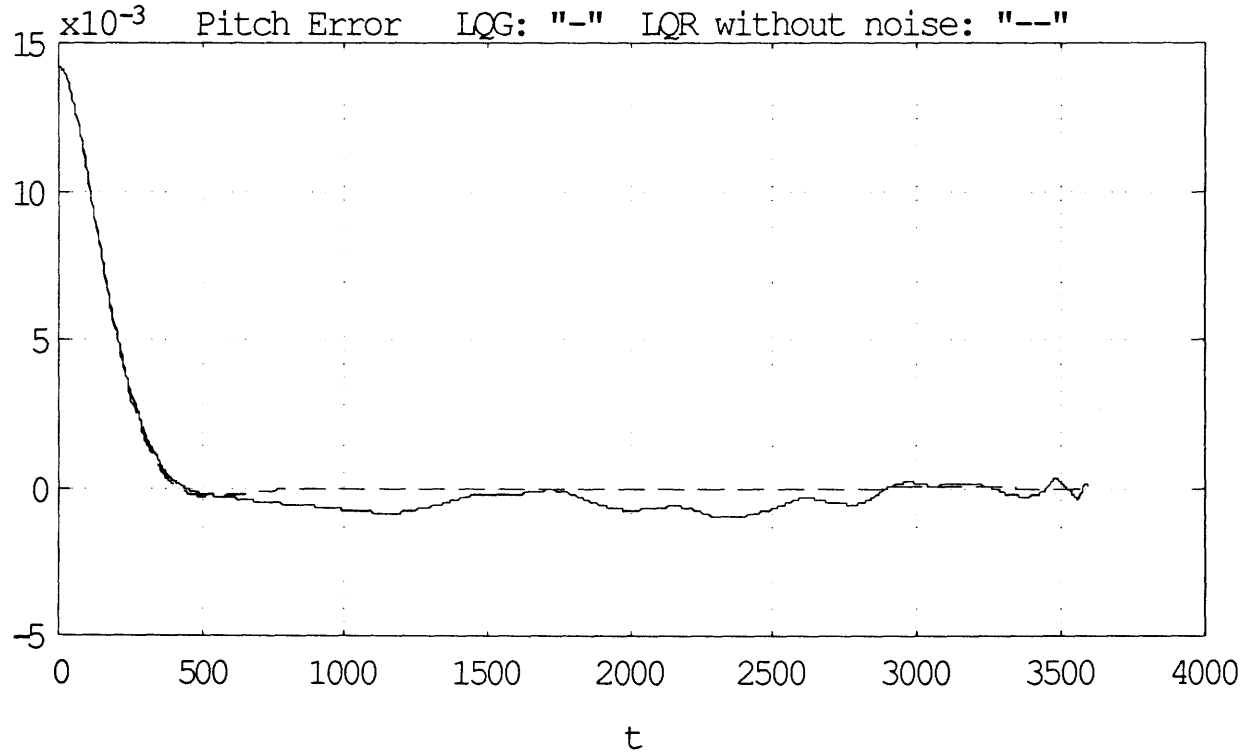

fig 3.66: Pitch error with respect to the nominal trajectory, LQG solution.

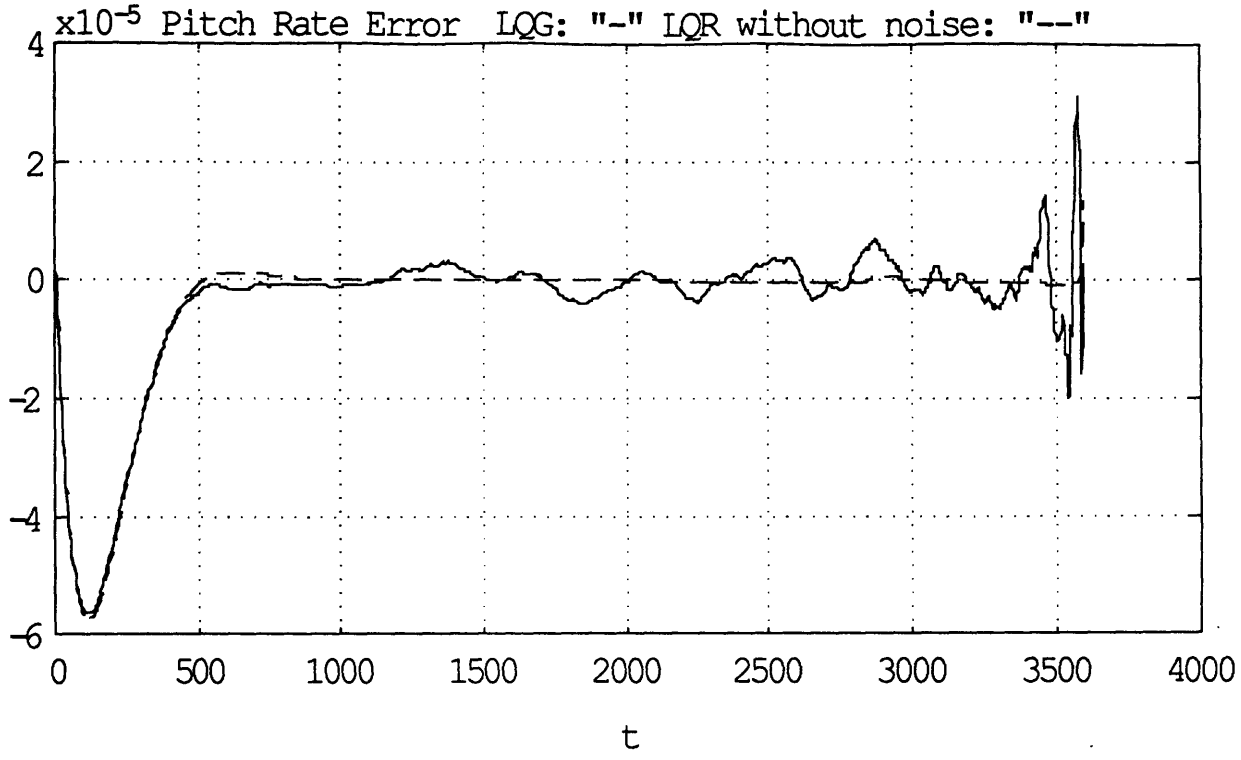

fig 3.67: Pitch rate error with respect to the nominal trajectory, LQG solution.

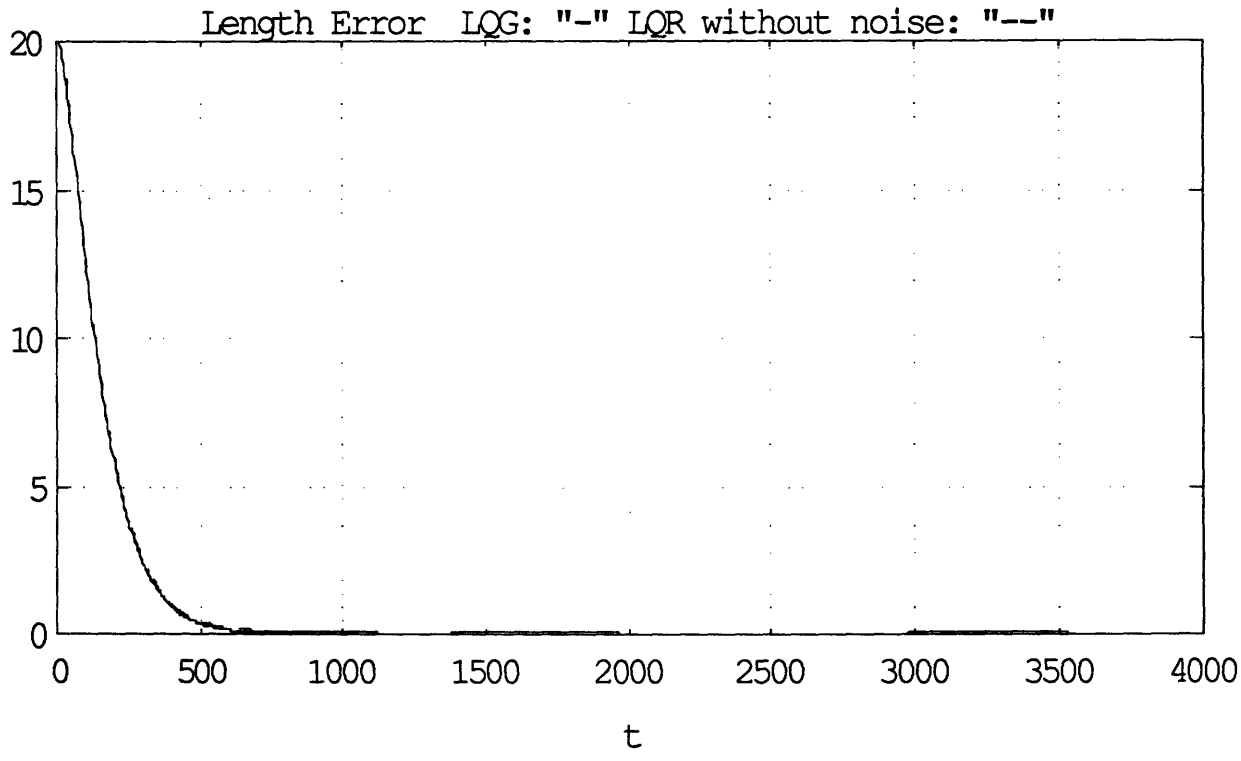

fig 3.68: Length error with respect to the nominal trajectory, LQG solution.

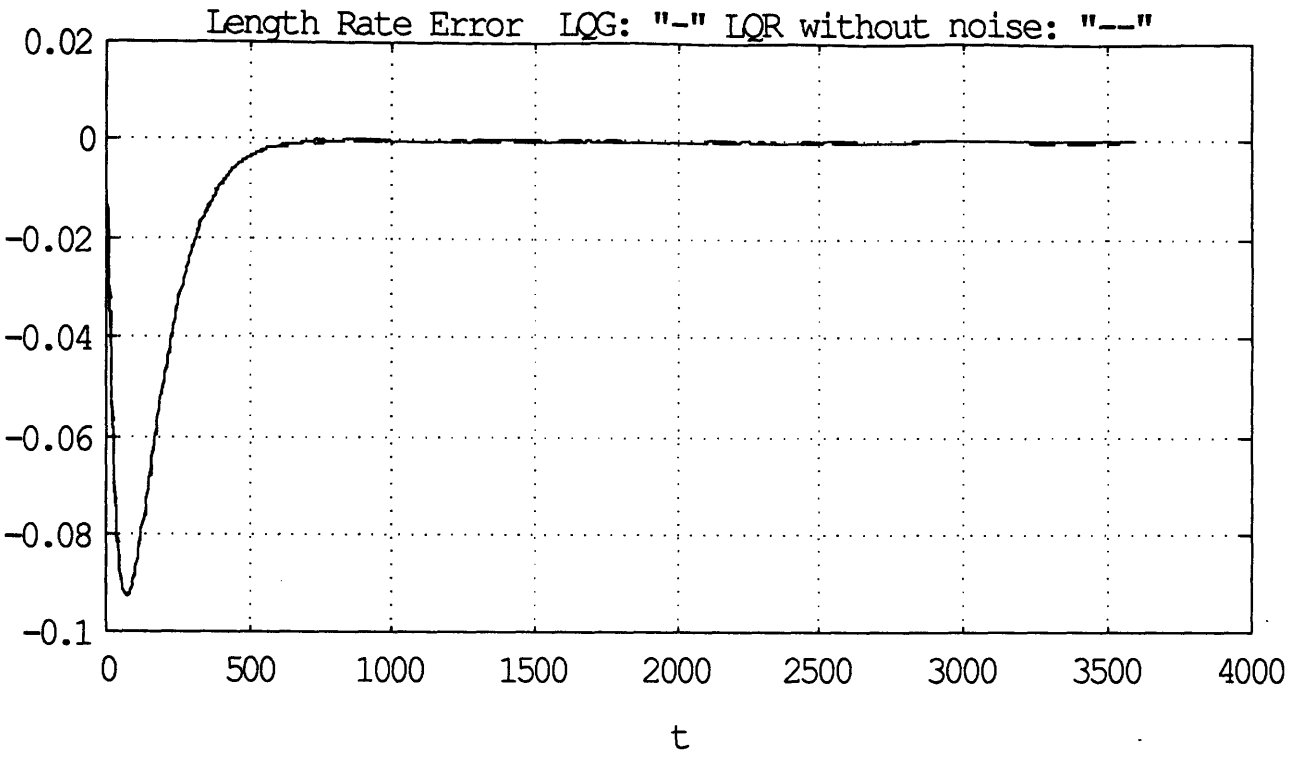

fig 3.69: Length rate error with respect to the nominal trajectory, LQG solution.

CHAPTER 4:
CONCLUSION AND FUTURE WORK

4.1. Trajectory Design and Feedforward.

This study showed that for reasonable initial pitch angle and pitch rate, there exists a retrieval trajectory which enables to retrieve the sub-satellite in about 1.15 orbits with reasonable final pitch angle and pitch rate, § 2.4.3. This solution only relies on the gravity gradient to remove excess angular momentum. The control, ie the length acceleration, is bang-bang and, for initial conditions $(\theta_0,\dot{\theta}_0/\omega)$ in the range of (.3,.1), its structure can be simplified by one initial acceleration followed by a constant deceleration, § 2.4.4.

In the formulation of § 2.2.1 of this optimization problem, the tension constraint may appear as a limiting factor to the optimization of the total retrieval time, by limiting the final deceleration. This constraint can be eased by installing a tether-aligned thruster fired at 2N on the sub-satellite, resulting in a maximum deceleration of $4\ 10^{-3}$ m.s^{-2}. A full investigation of the variations of the optimal solution with respect to the maximum deceleration remains to be done in order to get quantitative data. However, from the results of § 2.3.1, we know that to reach the origin in the phase plane, the retrieval path has to remain on the splitting line, which is an unstable equilibrium. If use of tether-normal thrusters are excluded, only the gravity gradient removes the excess angular momentum to keep the retrieval trajectory on the splitting line, and therefore limits the velocity of retrieval. Consequently, an increase of the maximum deceleration is unlikely to significantly improve the time of retrieval. However, it will certainly result in an increase of the number of switches of the bang-bang length control.

The final pitch angle and pitch rate were only constrained by being included in the cost function. Such a formulation leads to a trade-off between the minimization of the time of

retrieval and that of the final pitch angle and pitch rate. An increase of the maximum deceleration will undoubtedly result in a degradation of these final states. Therefore the optimization problem should be reformulated, considering final pitch angle and pitch rate equal to zero as final conditions, so as to only focus on the minimization of the time of retrieval.

For a given maximum deceleration and a structure of bang-bang control of one switch, the final impact velocity also appears to be a limiting factor. From this observation, a sub-optimal retrieval scheme was derived, § 2.5.2, which enables to retrieve the sub-satellite in a maximum of .9 orbits, with the final pitch angle and pitch rate equal to zero. However, it implies to fire thrusters for a maximum time of .37 s in order to reach the entry point of this trajectory, whatever the initial pitch conditions are.

The results of this chapter 2 should be used as initial guesses for solving a revised optimization problem where final pitch angle and pitch rate equal to zero would be imposed as final conditions. The positive tension constraint being eased thanks to the tether-aligned thruster, the variations of the optimal solution with respect to the maximum deceleration should be derived, enabling retrieval of the sub-satellite for all initial conditions without turning to in-plane thrusters. After an oscillatory part in the spiral region depending on the initial conditions, all retrieval paths will join the splitting line in the neighborhood of the point $(\theta,\dot{\theta}) = (1,0)$ in the phase plane. A small variation from this splitting line will lead to a trajectory exponentially divergent, § 2.3.1. Staying on this splitting line appears to be the critical part of the retrieval, even if most of the length is retrieved before, fig 2.20. The system becomes highly unstable, one of the unstable poles starting to diverge toward $+\infty$. Therefore any feedback system aiming at stabilizing the system about the retrieval trajectory must have accurate sensors to detect any variations away from the splitting line, and high bandwidh with respect to that of the open-loop system along the retrieval path in order to recover any disturbance without loosing the benefit of the optimized trajectory.

4.2. Feedback Control.

The design of a feedback loop with pitch rate estimator was investigated in chapter 3. From a control point of view, pitch and length dynamics are nearly decoupled. Therefore a feedback based on this decoupling gives a good approximation of an LQR design, § 3.3.1 and § 3.3.2. However, the bandwidth of the closed loop system is limited by the maximum thrust level available, if the constraint is imposed that the control should not saturate with an initial condition error of 1%. With on satellite thrusters, the bandwidth of the closed loop system is thus limited to the range of 10^{-2} rad.s^{-1} if a one percent initial error is imposed to be recovered without thruster saturation.

This recovery is also limited by the ability of the estimator to give accurate estimates of the states. A sensible design would lead to an estimator ten times faster than that of the feedback loop. The Kalman filter state estimator designed in chapter 3, however, is based upon our best estimates of sensor noise and plant noise. The pitch sensor, a Ku band radar measuring line of sight from the orbiter, drives the design most strongly. Our information is that this pitch sensor has a resolution of two degrees. This specification was converted into an equivalent noise intensity, leading to the low estimator bandwidth. The estimation is thus practically open loop, ignoring the sensor almost completely. Therefore the estimator masks any state error under the range of the state oscillations. Moreover, these noisy estimates would lead to a high fuel consumption since the thrusters would be required to be fired continuously. The resulting oscillations lead to a total fuel consumption of 680 m.s^{-1}. A remedy might be to implement a dead-band in the algorithm of control.

In chapter 3, plant and sensor noises were approximated by white noises. However, high frequency modes are not retained in the rigid body description. Therefore, the plant noise should be approximated by a white noise through a high pass shaping filter with a cross over frequency before the first mode of libration of the system, tab 1 [12]. The continuous Kalman filter should also be replaced by discrete updating of the estimate.

Therefore, the critical issue for the implementation of the proposed feedforward/feedback scheme is the precision of the sensors. Given the Ku band radar of a precision of 2°, the estimator is unable to detect errors which are in the range of what the feedback loop is able to recover with the available maximum thrust level. Moreover, the lack of precision on the states leads to a high fuel consumption which voids the benefits of the optimization trajectory design. Consequently, if an optimal retrieval strategy is retained, new sensors should be implemented.

The purpose of this study was to investigate the possibility of retrieving a tethered sub-satellite while attempting to minimize both total retrieval time and fuel consumption. This investigation revealed that precise sensors is the key issue in the fuel consumption minimization. The possibility of using precise linear thrusters instead of constant thrust level pulsing would also contribute to the optimization of fuel use as well as adjusting the bandwidth of the feedback loop. High bandwidth leads to fast initial error and disturbance recovery but requires a large maximum constant thrust level. On the other hand, a low bandwidth would result in a long recovery leading to an important time of thrusting. Therefore a minimum fuel use versus bandwidth should exist. A quantification of this minimum remains to be done.

REFERENCES

[1]: M. Athans, "The Role and Use of Stochastic Linear Quadratic Gaussian Problem in Control System Design", IEEE Transaction on Automatic Control, vol. ac 16, nº 6, Dec 1971.

[2]: P. M. Bainum and V. K. Kumar, "Shuttle-Tethered Sub-satellite System", Acta Astronautica, Vol 7, 1980, page 1333-1348.

[3]: A. K. Banerjee and T. R. Kane, "Tethered Satellite Retrieval with Thruster Augmented Control", Journal of Guidance, Control and Dynamics, Vol 7, nº 1, 1984, page 45-50.

[4]: V. V. Beletsky and Y. M. Levin, "Dynamics of Space Tether Systems", Nauka 1990, Moscow, The USSR Academy of Sciences, CK 90-50/104.

[5]: E. V. Bergmann, "Interaction of the Space Shuttle On-orbit Autopilot with Tether Dynamics", Draper Laboratory Memo under contract NAS8-36602 with NASA George C. Marshall Space Flight Center.

[6]: A. H. Boschitsh, O. O. Bendikson, "Non-linear Control Laws for Tethered Satellites", 1986 Tethers in Space Conference, Arlington, VA. Advances in the Astronautical Sciences,Vol. 62, page 257-276. AAS Paper 86-219.

[7]: A. H. Boschitsh, "The Controlled Retrieval of a Tethered Satellite", PhD Thesis, Department of Mechanical and Aerospace Engineering, Princeton University, 1990.

[8]: A. E. Bryson and Ho, "Applied Optimal Control", Hemisphere Publishing Corporation.

[9]: D. S. Crouch and M. M. Vignoli, "Shuttle Tethered Satellite System Development Program", AIAA Journal of Guidance 1984. AIAA Paper 84-1106.

[10]: W. F. Denham, A. E. Bryson, "Optimal Programming Problem with Inequality Constraints", AIAA Journal, January 1964, vol. 2, nº 1.

[11]: E. J. Fleurisson, "Optimization of the Maximum Range of a Glider after Engine Failure", Thesis for Engineer in Aeronautics and DEA in System Control from Sup'Aero, 1989, Toulouse, France.

[12]: A. H. von Flotow, "Some Approximations for the Dynamics of Spacecraft Tethers", AIAA Journal of Guidance, Control and Dynamics, Vol. 11, nº 4, July-August 1988, page 357-364.

[13]: A. H. von Flotow and P. R. Williamson, "Deployment of a Tethered Plasma Diagnostics Satellite into Low Earth Orbit", Journal of the Astronautical Sciences, Vol 34, January-March 1986, page 65.

[14]: P. C. Hughes, "Spacecraft Attitude Dynamics", Wiley Press, Page 299.

[15]: L. G. Lemke, J. D. Powell and X. He, "Attitude Control of Tethered Spacecraft", Journal of the Asronautical Sciences, Vol 35, January-March 1987, page 41-56.

[16]: A. K. Misra and G. S. Diamond, "Dynamics of a Sub-satellite System Supported by Two Tethers", AIAA Journal of Guidance, Control and Dynamics, Vol. 9, nº 1, January-February 1986, page 12-16.

[17]: A. K. Misra and V. J. Modi, "A Survey on the Dynamics and Control of Tethered Satellite Systems", Advances in Astronautical Sciences, Vol 62, 1986, AAS Paper 86-247.

[18]: A.K. Misra and V.J. Modi, "A General Dynamical Model for the Space Shuttle Based Tethered Sub-satellite System", Advances in the Astonautical Sciences, Vol 40, Part II, 1979, page 537-557.

[19]: A.K. Misra, D. M. Xu and V.J. Modi, "On Vibrations of Orbiting Tethers", Acta Astronautica, Vol 13, nº 10, 1986, page 587-596.

[20]: A.K. Misra and V.J. Modi, "Frequencies of Longitudinal Oscillations of Tethered Satellite Systems", AIAA Paper 86-2274, August 1986.

[21]: H. J. Oberle, W. Grimm, "BNDSCO, A Program for the Numerical Solution of Optimal Control Problems". Institute for Applied Mathematics, University of Hamburg.

[22]: D. J. Pines, E. J. Fleurisson, A. H. von Flotow, "An Optimal Guidance Approach to Retrieval of a Tethered Sub-satellite", 1990 AIAA Dynamics Specialists Conference, Long Beach, CA, April 5-6, 1990. AIAA Paper 90-1196.

[23]: D. J. Pines, A. H. von Flotow, D. C. Redding, "Two Non-linear Control Approaches for Retrieval of a Thrusting Tethered Sub-Satellite". AIAA Journal of Guidance, Control and Dynamics, Vol 13, nº 4, July-August 1990, page 651-658.

[24]: W. H. Press, B. P. Flannery, S. A. Teukolsky, W. T. Vetterling, "Numerical Recipes", Cambridge University Press.

[25]: C. Rupp, "A Tether Tension Control Law for Tethered Sub-satellites Deployed Along The Local the Local Vertical", NASA TMX-64963, September 1975.

[26]: Seales, "Introduction to Non-linear Optimization", Spring-verlag New York Inc.

[27]: S. R. Valadi and E. S. Kim, "Feedback Control of Tethered Satellites using Liapunov Stability Theory", 1990 AIAA Dynamics Specialists Conference,Long Beach, CA, April 5-6, 1990. AIAA Paper 90-1197.

[28]: D. M. Xu and A. K. Misra, "Thruster Augmented Active Control of a Tethered Sub-satellite during its retrieval", Journal of Guidance and Control, Vol 9, nº 6, November-December 1986, page 663-672.

[29]: D. M. Xu, A. K. Modi and V. J. Modi, "Three Dimensional Control of the Shuttle Supported Tethered Satellite System During Retrieval", Proceedings of the 3rd VPI & SU/AIAA Symposium, Blackburg, VA, June 15-17, 1981, page 453-469.

APPENDIX A:
LIST OF FIGURES

fig 1.1:	Tethered electrodynamic satellite system	11
fig 1.2:	Downward tethered satellite system	11
fig 1.3:	The TSS system	13
fig 1.4:	A feedforward/feedback scheme	17
fig 2.0:	Angle convention	19
fig 2.1:	Example of divergent retrieval trajectory in the LVLH plane	22
fig 2.2:	Example of divergent retrieval trajectory in the phase plane	23
fig 2.3:	Periods of coasting oscillations	28
fig 2.4.1:	Phase plane trajectories for $\delta = 0$	30
fig 2.4.2:	Phase plane trajectories for $\delta = -.1$	30
fig 2.4.3:	Phase plane trajectories for $\delta = -.28$	31
fig 2.4.4:	Phase plane trajectories for $\delta = -.43$	31
fig 2.4.5:	Phase plane trajectories for $\delta = -.7$	32
fig 2.4.6:	Phase plane trajectories for $\delta = -.1$	32
fig 2.5.1:	Feasible Region in the $(\dot{L}_i,\dot{L}_f)$ plane for constant acceleration retrieval	34
fig 2.5.2:	Cost function for constant acceleration retrieval, $(\theta,\dot{\theta})_i = (.3,.1\omega)$	34
fig 2.6.1:	Cost function for constant velocity retrieval $(\theta,\dot{\theta}) = (.3,.1\omega)$	35
fig 2.6.2:	In-plane retrieval trajectory for different vallaies	35
fig 2.7:	Optimal retrieval acceleration, numerical solution	43
fig 2.8:	Costate λ_4 history along the optimal retrieval	43
fig 2.9.1:	Optimal retrieval phase trajectory	44
fig 2.9.2:	Optimal in-plane retrieval trajectory	44

fig 2.10: Bang-bang structure control 45

fig 2.11.1: Reduced optimal phase plane trajectory 47

fig 2.11.2: Reduced optimal in-plane trajectory 47

fig 2.11.3: Length history along the reduced optimal trajectory 48

fig 2.11.4: Length rate history along the reduced optimal trajectory 48

fig 2.12: Cost function vs switching time t_s for initial conditions $(\theta,\dot{\theta})_i = (.3,.1\omega)$ 51

fig 2.13: Cost function vs switching time in the region of minima 51

fig 2.14: Phase plane trajectory corresponding to the second minimum 52

fig 2.15: Phase plane trajectory between the two minima of the cost function 52

fig 2.16.1: Cost function vs switching time with final condition $\delta = -1$ 53

fig 2.16.2: Cost function with final condition $\delta = -1$ in the minimum region 53

fig 2.17: Initial points in the phase plan vs final impact velocity for retrieval trajectories with $L_i = 2000$m and $(\theta,\dot{\theta})_f = (0,0)$ 55

fig 2.18: Total retrieval time, thrusting, coasting and retrieving, vs final impact velocity 57

fig 2.19: Limits of regions of retrieval 57

fig 2.20: Example of retrieval in the phase plane with $(\theta,\dot{\theta})_i = (.3,.1\omega)$ 59

fig 2.21: Example of retrieval in the in-plane LVLH with $(\theta,\dot{\theta})_i = (.3,.1\omega)$ 59

fig 3.1: A feedforward/feedback scheme 67

fig 3.2: Variations of the coefficients a_{2i} of A along the nominal retrieval trajectory for L>10% 71

fig 3.3: Variations of the coefficients a_{2i} of A along the nominal retrieval trajectory for L<10% 71

fig 3.4: Variations of the coefficients a_{4i} of A along the retrieval trajectory 72

fig 3.5: Real part of λ_1 and λ_2 along the nominal retrieval trajectory 75

fig 3.6:	Root locus of λ_3 and λ_4 along the nominal retrieval trajectory	75
fig 3.7:	Real part of λ_3 and λ_4 along the nominal retrieval trajectory	76
fig 3.8:	Singular value decomposition vs pulsation for L=90%	82
fig 3.9:	Singular value decomposition vs pulsation for L=5%	82
fig 3.10:	Singular value decomposition vs length for ω=.1 rad.s^{-1}	83
fig 3.11:	Variations of the feedback gains vs nominal length, pole plct sol.	87
fig 3.12:	Control history for a 1% error recovery. Pole plct Solution, L=0%	88
fig 3.13:	Response to a 1%. Pole placement Solution, L=0%	88
fig 3.14:	Singular value decomposition of the loop transfer function, pole placement	89
fig 3.15:	Singular value decomposition of the sensitivity transfer function, pole placement	89
fig 3.16:	Singular value decomposition of the closed loop transfer function, pole placement	90
fig 3.17:	Control history for a 1% error recovery, pole placement L=5%	90
fig 3.18:	Response to a 1% error, pole placement L=5%	91
fig 3.19:	Pole location along the nominal retrieval trajectory, pole placement	91
fig 3.20:	Variations of the LQR feedback gains of the pitch control along the nominal retrieval	94
fig 3.21:	Variations of the LQR feedback gains of the length control along the nominal retrieval	94
fig 3.22:	Root locus of the LQR closed loop system along the nominal retrieval	95
fig 3.23:	LQR control history for a 1% error recovery L=0%	95
fig 3.24:	LQR response of the system to a 1% error, L=0%	96
fig 3.25:	Singular value decomposition of the LQR loop transfer function	96
fig 3.26:	Singular value decomposition of the LQR sensitivity transfer fct	97
fig 3.27:	Singular value decomposition of the LQR closed loop transfer fct	97

fig 3.28:	LQR control history for a 1% error recovery, L=5%	98
fig 3.29:	LQR response of the system to a 1% error, L=5%	98
fig 3.30:	Singular value decomposition of the loop transfer function, LQR & pole plct, L=5%	99
fig 3.31:	Singular value decomposition of the sensitivity transfer function, LQR & pole plct, L=5%	99
fig 3.32:	Singular value decomposition of the closed loop transfer function, LQR & pole plct, L=5%	100
fig 3.33:	Singular value decomposition of the estimator loop transfer function, L=0%	104
fig 3.34:	Root locus of the estimator along the nominal retrieval	105
fig 3.35:	Variation of the estimator gains on the pitch measurement along the nominal retrieval	105
fig 3.36:	Variation of the estimator gains on the length measurement along the nominal retrieval	106
fig 3.37:	Variation of the estimator gains on the length rate measurement along the nominal retrieval	106
fig 3.38:	Estimator singular value matching design	107
fig 3.39:	LQG pitch control history for a 1% initial error recovery, L=0%	110
fig 3.40:	LQG length control history for a 1% initial error recovery, L=0%	110
fig 3.41:	LQG pitch response to a 1% initial error, L=0%	111
fig 3.42:	LQG pitch rate response to a 1% initial error, L=0%	111
fig 3.43:	LQG length response to a 1% initial error, L=0%	112
fig 3.44:	LQG length rate response to a 1% initial error, L=0%	112
fig 3.45:	Pitch angle and pitch rate error evolution with respect to the LQR reference response	113

fig 3.46: Length and length rate error evolution with respect to the LQR reference response 113
fig 3.47: LQG pitch control history for a 1% initial error recovery, L=5% 114
fig 3.48: LQG pitch response to a 1% initial error, L=5% 114
fig 3.49: LQG pitch rate response to a 1% initial error, L=5% 115
fig 3.50: LQG length response to a 1% initial error, L=5% 115
fig 3.51: LQG length rate response to a 1% initial error, L=5% 116
fig 3.52.1: Pitch angle and pitch rate error evolution with respect to the LQR reference response 116
fig 3.52.2: length and length rate error evolution with respect to the LQR reference response 117
fig 3.53.1: LQG pitch response to a 1% initial error with fast estimator 117
fig 3.53.2: LQG pitch rate response to a 1% initial error with fast estimator 118
fig 3.54: In-plane trajectory for a 1% initial error, pole placement solution 120
fig 3.55: Phase plane trajectory for a 1% initial error, pole placement solution 121
fig 3.56: In-plane trajectory for a 1% initial error, LQR solution 121
fig 3.57: Phase plane trajectory for a 1% initial error, LQR solution 122
fig 3.58: Pitch control history along the retrieval, LQR & Pole Placement sol. 122
fig 3.59: Length control history along the retrieval, LQR & Pole Plct sol. 123
fig 3.60: Length error with respect to the nominal trajectory, LQR & Pole Plct 123
fig 3.61: Length rate history along the retrieval, LQR & Pole Placement sol. 124
fig 3.62: In-plane trajectory for a 1% initial error, LQG solution 124
fig 3.63: Phase plane trajectory for a 1% initial error, LQG solution 125
fig 3.64: Pitch control history along the retrieval, LQG solution 125
fig 3.65: Length control history along the retrieval, LQG solution 126
fig 3.66: Pitch error with respect to the nominal trajectory, LQG solution 126
fig 3.67: Pitch rate error with respect to the nominal trajectory, LQG solution 127

fig 3.68: Length error with respect to the nominal trajectory, LQG solution 127

fig 3.69: Length rate error with respect to the nominal trajectory, LQG solution 128

APPENDIX B: LIST OF SYMBOLS

C_u:	Derivative of C with respect to u
cte:	constant
g:	gravitational acceleration
$\underline{f}$:	gravitational force
f(x,u):	First derivative of the states
f_u:	Derivative of f with respect to u
H:	Hamiltonian
$\underline{H}_{o'}$:	Kinetic momentum of the sub-satellite with respect to 0'
H_u:	Derivative of H with respect to u
J:	Cost function
J^*:	Modified control cost
L:	Length of the tether
$\dot{L}$:	Length rate of the tether
$\ddot{L}$:	Length acceleration of the tether
m:	mass of the sub-satellite
M:	gravity center of the tethered sub-satellite
$\underline{M}_{o'}$:	Gravitational torque applied on the sub-satellite with respect to O'
O:	center of the Earth
O':	gravity center of the orbiter
r	Distance tethered sub-satellite, center of the Earth
R:	Distance orbiter center of the Earth
t_s:	Switching time

t_{smin}: Minimum allowed ts

t_{smax}: Maximum allowed ts

t_f: Final time, total retrieval time

T: Tension - Period of the coasting oscillations

u: Control

u_{max}: Maximum level of control

u_{min}: Minimum level of control

x_0: State x at the initial time

x_f: State a at the final time

x_i: ith state

$\underline{z}$: Unitary vector orthogonal to the orbital plan

α: Angle O'OM - Penalty coefficient in the cost function

ϕ: Roll angle

λ_i: Vector of costates

μ: Kune-Tucker coefficient of C in the Hamiltonian

ν: Kune-Tucker coefficient for final constraints

θ: Pitch angle

θ_{eq}: Pitch angle at the equilibrium

$\dot{\theta}$: Pitch rate

ω: Orbital rate

δ: Damping factor in the second order system analogy